The synthesis and characterisation of novel Sn(II), Zn(II) and Cu(II) compounds for anti-bacterial evaluation

Wright, Philip

Award date:
1999

Awarding institution:
University of Bath

THE SYNTHESIS AND CHARACTERISATION OF NOVEL Sn(II), Zn(II) AND Cu(II) COMPOUNDS FOR ANTI-BACTERIAL EVALUATION

Submitted by Philip Wright

for the degree PhD

of the University of Bath

1999.

COPYRIGHT NOTICE

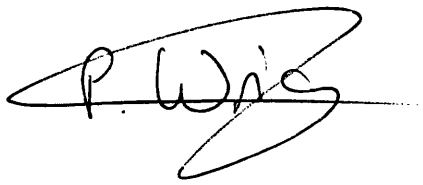

Philip Wright

ProQuest LLC
789 East Eisenhower Parkway
P.O. Box 1346
Ann Arbor, MI 48106-1346

ABSTRACT

The work described in this thesis has been divided into two main sections. Chapter 1 contains the Introduction and Background to the work, with the remaining three chapters detailing the preparation, characterisation and anti-bacterial testing of the materials produced.

Chapter 1 provides a background to the problems associated with the build-up of plaque and the methods which have been adopted in its removal and prevention of its regrowth. The anti-bacterial agents covered include triclosan and metal salts such as Sn(II), Zn(II) and Cu(II). As well as the anti-bacterial activity of such compounds, this chapter looks at the bonding and other structural aspects of the chemistry of three metals, and methods of characterisation including ^{119m}Sn Mössbauer and ^{119}Sn NMR.

Chapter 2 describes in detail the synthesis and characterisation of a series of M(II) sugar phosphates and carboxylates. The stability of the oxidatively unstable Sn(II) compounds was evaluated both as a pure compound and also in a toothpaste using ^{119m}Sn Mössbauer. This chapter also introduces an assay known as pH Stat which allows the evaluation of potentially anti-bacterially active compounds.

Chapter 3 describes the synthesis and characterisation of a number of compounds derived from triclosan. This chapter introduces another assay known as the Biofilm assay which also allows evaluation of potentially active compounds. The crystal structure of a new compound, triclosan phosphate, is also presented.

Chapter 4 describes the synthesis and characterisation of M(II) derivatives of maltol and hinokitiol (a natural product with known anti-bacterial properties). This chapter details results from both anti-bacterial assays as well as three crystal structures, Zn(II) maltolate, Cu(II) hinokitiol and tris(maltolato)monhydroxotin(IV). The work detailed in this chapter has been used in the successful filing of a Unilever patent, after *in vivo* evaluations carried out at Unilever confirmed the original findings detailed in this chapter.

ACKNOWLEDGEMENTS

I owe a huge debt of gratitude to Mum and Dad for all their support during the last twenty seven years and giving me the chance to achieve this PhD.

I would especially like to thank Dr Kieran Molloy for everything he has done over the last three years, and for his continuing support throughout the research work and during the writing up of this thesis.

My thanks go to Dr Mary Mahon for the crystallography work, Alan Carver for all the microanalyses, Dave and Harry for the NMR work, and Robert, Ahmed and Sheila for all their help over the last three years.

I would like to thank Phil Waterfield, Jon Creeth, Jenny Simmons and Craig Boniface for all their help and support during my placement periods at Unilever, and everyone else in the Unilever dental labs for all their help and for making the placements so enjoyable.

Special thanks must go to Dave "smudge" Smith and John McGinlay for introducing me to the delights of Claverton Academicals football, and the ensuing injuries!

Chris "prof." Rainford, Mike Maxwell, Jo "blondie" Stanley, Mike Hill, Tim Paget, Rob Harker and Sean Beckett for making Lab 2.10 the place it was, and anyone else who has worked with me over the last three years.

Finally I would like to thank all of my colleagues at work for the support and patience during the writing of the thesis, with a special thanks to Julia.

Financial support for this project from Unilever Research Port Sunlight Laboratories is gratefully acknowledged.

CONTENTS

PAGE

APPENDICES

ABBREVIATIONS

^{t}Bu	Tertiary butyl
^{t}BuOH	Tertiary butanol
d	Doublet
dd	Doublet of doublets
Ether	Diethyl ether
EtOH	Ethanol
αG1P	α-D-glucose-1-phosphate
αG6P	α-D-glucose-6-phosphate
βG6P	β-D-glucose-6-phosphate
HAP	Hydroxyapatite
IR	Infra-red spectroscopy
m	Multiplet
Me	Methyl
MeOH	Methanol
NMR	Nuclear Magnetic Resonance spectroscopy
^{i}Pr	Iso-propyl
q	Quartet
s	Singlet
S. mutans	*Streptococcus mutans*
t	Triplet
THF	Tetrahydrofuran
ZCT	Zinc citrate trihydrate

"Work expands so as to fill the time available for its completion."

Parkinson's law.

CHAPTER 1

INTRODUCTION

1. CHAPTER 1 - INTRODUCTION

1.1. Background

Stannous fluoride (SnF_2) has been used for many years as an anti-bacterial agent in toothpastes and mouthrinses. The efficacy of SnF_2 is known to be due to a combination of the activity of the fluoride and the stannous ions. It is also known that stannous ions are unstable with respect to oxidation to stannic ions (Sn^{4+}), which exhibit no anti-bacterial activity. Stabilisation of the Sn^{2+} ions is thus a key factor in the production of new anti-bacterial agents. Detailed in this thesis is the synthesis, characterisation and anti-bacterial evaluation of a range of novel stannous compounds which may offer increased stability and hence increased activity.

Other metal ions are also known to exhibit anti-bacterial activity with Zn^{2+} and, to a much lesser extent Cu^{2+}, being the most commonly used in the dental industry. Zinc is most often used in the form of zinc citrate trihydrate (ZCT) an active agent which has been used for a number of years, especially combined with another anti-bacterial agent, triclosan (a non-ionic organic compound). This thesis details the synthesis, characterisation and anti-bacterial evaluation of a number of zinc and copper complexes, and a range of compounds based on triclosan.

The introduction to this thesis is written by way of a look at the early beginnings of dentistry, the oral environment, toothpaste technology and common oral health problems such as plaque. All of the metal complexes described in the results chapters are based on Sn^{2+}, Zn^{2+} and Cu^{2+} ions, and a review of the chemistry of these three elements is included. Finally an overview of the project objectives is detailed.

1.2. A Brief History of Dentistry[1]

Hippocrates (460-377 BC) referred to the deleterious effects on the gums and teeth of *pituita* or *calculus*, which "insinuates itself under the roots of the teeth." The Romans, concerned with personal grooming, developed instruments for scaling and polishing as important features of oral care, but it was the Arabian physician-surgeon Albucasis (963-1012 AD) who most clearly enunciated the relationship between calcified deposits and "corruption of the gums and suppuration around the teeth." Convinced of the need for meticulous removal of "rough and ugly scales", he designed a special set of 14 instruments - the forerunners of modern dental tools - and described in detail the process of removal.

Paracelcus, a Swiss-German physician and alchemist, introduced the term "*tartar*" in about 1535 as a designation of stone-like concretions that form in various organs. Until the middle of the 20th century, calculus (or tartar) was considered to be the primary cause of periodontal disease. This was before the importance of a complicated mixture of micro-organisms, otherwise known as *dental plaque*, was fully understood. The earliest written observations on the role of plaque can be credited to GV Black.[2] He observed that a soft, mucinous, water-insoluble deposit formed on the surface of the teeth shortly after cleaning had taken place.

1.3. The Dental Environment

The major components of the dental environment are teeth, gums, tongue and salivary glands. When food is put into the mouth the teeth act to break down the food into smaller fragments which can be swallowed. Without the teeth it would be difficult to get food into a suitable form for digestion and it is therefore imperative that the teeth and the gums which support them are kept in a healthy state. In practice this can now be achieved by simple brushing of the teeth with a suitable dental product.

Teeth consist of enamel, which is the hardest tissue to be found in the body. Approximately 96% of tooth enamel is mineral - primarily calcium carbonate and calcium hydroxyapatite, $Ca_5(PO_4)_3OH$, with the remaining 4% being organic matter and water. Dental enamel is built up of enamel rods or prisms, rod sheaths, and a cementing substance. The rod sheaths, as the name suggests, surround the enamel rods and are higher in organic matter and less calcified. The cementing substance holds the sheathed rods together. These rods are arranged at 90° to the surface and extend into the layer of softer tissue below. The teeth are firmly held to the jaw bone through their roots, and additionally secured by the soft gum tissue.

The salivary glands play an important part in the mouth as they produce saliva which constantly irrigates the teeth and gums. Saliva serves two major functions:

i) Digestion - Salivary amylase is a starch digesting enzyme which helps in the breakdown of food.

ii) Protection - Saliva acts as a pH buffer to help counter changes in acidity which occur in the mouth.

1.4. Bacterial aggregations and disease

1.4.1 Acquired Pellicle

The *acquired pellicle* is a sticky organic film which coats the surface of teeth. This film builds up within minutes of the teeth being cleaned, and dental enamel is, therefore, rarely in direct contact with the oral environment. The acquired pellicle consists primarily of proteins (which are laid down by the saliva which is constantly irrigating the teeth) and is found to be essentially bacteria-free. With the pellicle being proteinaceous in nature, this means it is easily stained by certain staining agents such as tannins in tea and coffee and nicotine from inhaled tobacco smoke.[3] Staining of the pellicle can also occur through other means, and a recent study found that intensive swimming (such as that undertaken by competitive swimmers) can cause discoloration.[4] The staining is believed to be a result of long-term contact with pool water which contains a mixture of chemicals to keep it clean.

As it is the pellicle which is in contact with the oral environment, this is where the bacteria will colonise to cause the build up of plaque and periodontal disease.

1.4.2. Dental Plaque

For a bacterium to adhere to a surface it must first come close enough. Kinetic forces, i.e. movement in saliva, enable oral bacteria to approach tooth surfaces.[5] At a certain distance, further approach is prevented since van der Waals attraction forces are exceeded by the repulsive forces exerted by similar types of surface charges. Such a potential barrier must be overcome for a more permanent adhesion to exist. If the surface charges are reduced and a much closer contact occurs, short-range attractive

forces such as hydrogen bonds may develop. Once bacteria have begun to adhere to a surface such as a tooth, colonisation soon follows.[6] In the oral cavity there are numerous species of bacteria which are able to colonise on the exposed tooth pellicle. Colonisation therefore leads to a complex mass of bacteria, which is known as dental plaque. The most common species of bacteria found in dental plaque are *Streptococcus mutans* and *Streptococcus sobrinus*.[7] The surface of dental plaque is composed predominantly of coccoid- and rod-shaped bacteria, and a few yeast cells.[8]

The earliest recorded observation on dental plaque[2] describes the formation of a soft, mucinous, water-insoluble deposit on the surface of teeth shortly after cleaning. In an early study it was found that these water-insoluble deposits were polysaccharides.[9] All of the plaque-forming cariogenic streptococci which were tested in this study were found to synthesise extracellular polysaccharides of the dextran and levan type, specifically from sucrose. It has been postulated that these gelatinous adhesive polymers are at least partially responsible for the ability of these organisms to form plaque, as bacteria producing these polysaccharides adhere to surfaces such as teeth.[10]

Once plaque is established it can rapidly become mineralised to form an ugly, hard deposit which is known as *dental calculus* or, more commonly, *tartar*. Tartar is most likely formed when calcium phosphate crystals grow within the plaque matrix, although the exact mechanism of this crystallisation is not yet known in detail. The calcium and phosphate required for this are both present in saliva. A build-up of tartar is problematic as it is very difficult to remove with brushing, and it is an ideal substrate for further colonisation of plaque-forming bacteria. Tartar generally builds-up at the gingival crevices (where the teeth and gums meet) and is therefore responsible for the gum disease known as gingivitis.

Plaque is the single major factor responsible for two of the most prevalent human oral diseases, namely dental caries and periodontal disease.

1.4.3. Dental Caries and Periodontal Disease

Dental caries is a disease which is caused primarily by plaque which leads to the physical decay and eventual loss of teeth. The major cause of dental caries is the generation of lactic acid by bacteria present in the plaque film as they metabolise carbohydrates from food. This acid penetrates the acquired pellicle and reacts with the mineral hydroxyapatite in the enamel. The acid is said to de-mineralise the tooth enamel leading to calcium deficient apatites. This de-mineralisation of the enamel surface causes it to weaken, leading to the formation of cavities and eventually the destruction of the whole tooth. The formation of cavities and the subsequent exposure of the nerves within the tooth is a cause of painful toothache.

Over the last two decades the prevalence of dental caries has significantly decreased due to a number of factors:[11]

i) The fluoridation of public water supplies.

ii) The widespread use of fluoride toothpastes.

iii) The use of fluoride tablets and gels.

iv) Dietary fluoride supplements.[12,13]

As well as the above factors, over the last twenty years there has been an increased dental awareness and a decrease in sugar consumption.

Periodontitis is an infectious disease associated with only a few of the several hundred bacterial species found in dental plaque at diseased sites. For example, *Campylobacter rectus*[14,15] and *Porphyromonas gingivalis*[16] have been linked with active periodontitis and their levels have been reported to increase at sites prior to clinical breakdown.[17]

The presence of periodontal disease is often indicated by inflammatory gingivitis, which shows as bleeding around the gingival margin during, and after, brushing. Most people suffer from mild periodontitis, and regular dental check-ups should prevent the disease becoming serious. When periodontitis does become more serious there is a gradual withdrawal of the gums from around the teeth, causing the teeth to loosen and eventually fall out. Prevention of full periodontitis can be achieved through early and effective removal of plaque from the teeth and gingival margin. The prevailing view is that tartar enhances gingival inflammation by promoting and retaining new plaque accumulations.[18] The presence of tartar limits natural self-cleaning mechanisms, makes oral hygiene difficult and reduces drainage from crevicular areas.

There is data to support the view that subgingival calculus contributes to the chronicity and progression of periodontal disease.[18] Clinical studies attest to the importance of frequent and thorough removal of root deposits by scaling and root planing to prevent attachment loss.[19]

There is another form of periodontitis, known as *early-onset periodontitis*, which affects children and young adults.[20-22] It is characterised by a rapid and progressive destruction of the periodontal attachment apparatus. There are three ways in which early-onset periodontitis can affect a person:[23,24]

i) In a localised form, where only molars and incisors are affected.

ii) In a generalised form, which affects more or most of the teeth.

iii) In an incidental form, where only one or a few teeth are affected.

The exact aetiology (cause) and pathogenesis (mode of development) of early-onset periodontitis is not well understood. In contrast with adult periodontitis, early-onset periodontitis is not thought to be associated with gingival inflammation or substantive calculus formation.[25]

1.5. Formulation of Commercial Toothpastes

Toothpastes, or dentifrices, appeared on the market around the turn of the century having evolved from toothsoaps (flavoured blocks of soap) and toothpowders (typically chalk mixed with flavour oil, sweetener and a little soap) both of which were sold in tins. Part of the demise of toothpowders was related to their uneconomical use (it would fall off the brush!) and their lack of hygiene (unless every member of the family had their own tin). The success of toothpastes, and indeed its physical form, owes much to the development of the collapsible metal tube (by Rand in 1841) which gave the consumer a handy, clean and hygienic dispenser.

The function of a toothpaste is twofold. It has a cosmetic function which is to clean and freshen the teeth (by removal of stain, food debris and plaque) and also a therapeutic function in delivering a range of therapeutic agents to control caries, plaque, gingivitis, tartar and sensitive teeth.

Toothpastes are designed to fulfil several objectives:

i) Upon application of the paste with suitably designed toothbrushes, the teeth and gums should be thoroughly cleansed.

ii) The paste should be formulated to deliver suitably chosen therapeutic agents to the sites of periodontal disease in the mouth, namely the teeth and gums.

iii) Contain a water-soluble fluoride source, as fluoride is a well documented anti-caries agent.

iv) To be accepted by the consumer by having the correct consistency, and being easy and pleasant to use on a daily basis.

The clinical effectiveness of therapeutic toothpastes is a great credit to both dental and formulation scientists given the harsh conditions prevailing during tooth brushing which are not conducive to the delivery and oral retention of therapeutic agents.

Commercial toothpaste formulations are generally quite similar and are usually based on the generic toothpaste formulation shown in Table 1.1.

Table 1.1. Basic Toothpaste Formulation.

COMPONENT	LEVEL (% w/w)	EXAMPLE
Water	1.0 - 28.0	
Humectant	27.0 - 70.0	Sorbitol
Detergent	1.5 - 3.0	Sodium Lauryl Sulphate
Flavour	1.0 - 1.5	Peppermint
Abrasive	4.0 - 55.0	Silica, Chalk
Thickener	0.6 - 1.5	Xanthan Gum
Stucturant	0 - 5.0	Polyethylene glycol
Therapeutic Agent(s)	0.1 - 5.0	Zinc/Tin(II) salts; Triclosan; Fluoride
Sweetener	0 - 1.0	Saccharin
Opacifier	0 - 2.0	Titanium Dioxide

As can be seen from Table 1.1., the quantities of each ingredient vary considerably depending on the desired properties of the completed paste. There are also other components which are sometimes incorporated into pastes such as colourants,

stabilisers, pH adjusters and preservatives. The role of the main ingredients will now be discussed in more detail.

The **water** is present to dissolve and disperse the therapeutic agents, sweetener, detergent and thickener and also to provide the toothpaste with the desired consistency.

The major role of the **humectant** is to lower water-activity in the product. This aids self-preservation and prevents the paste drying out, for example if the cap is left off.

The **detergent** or surfactant serves to dissolve and disperse water-insoluble flavours by the formation of micelles and aids cleaning of the teeth by helping remove food debris and plaque. It also creates foam which is important from a consumer point of view - 'a toothpaste which doesn't foam isn't working' is a common misconception of consumers.

Flavour is dominant in determining the sensory properties of the toothpaste and its characteristic taste. Peppermint is the common choice since it has the ability to deliver the sensation of freshness to a wide spectrum of consumer palates.

The roles of the **abrasive** are to aid cleaning of the teeth and to contribute to the viscosity of the toothpaste. Cleaning is achieved by the abrasion of stained pellicle from the tooth surface. Although a toothbrush and water will remove some food debris and plaque it will not remove the thin proteinous pellicle that picks up stain from our diet and smoking.

The major function of the **thickener** or binder is to prevent sedimentation of the abrasive and the consequent appearance of the clear liquid-phase of the product. It also provides the formulation with the characteristic rheological properties such as ribbon hold on the brush and ease of squeeze.

The **structurant** is used in addition to the thickener in some formulations and also as a solubiliser for both detergent and flavour.

The **therapeutic agent(s)** are chosen depending on the nature of the toothpaste and the desired market. The toothpaste can be marketed as either anti-caries, anti-tartar,

anti-sensitive tooth or anti-plaque depending on the active agent which is incorporated. Current toothpastes tend to offer a mixture of therapeutic agents to give better all-round activity. Anti-caries agents are generally fluorides such as NaF or SnF_2; anti-tartar agents are traditionally pyrophosphate salts ($P_2O_7^{2-}$); anti-sensitive tooth agents used to be $SrCl_2/Sr(OAc)_2$, but are now the analogous potassium salts; and anti-plaque agents include zinc/tin(II) salts, chlorhexidine and triclosan (I).

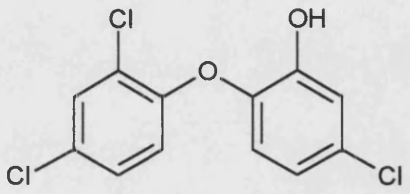

Triclosan (I)

The incorporation of a **sweetener** compliments the flavour in producing a consumer acceptable product. It also helps mask any bitterness from other components in the formulation.

In most white opaque formulations titanium dioxide (TiO_2) is used as an **opacifier** to improve the whiteness of the product.

1.6. Anti-bacterial Agents

Dental plaque is the major cause of gingivitis, caries and periodontal disease. It follows that improved dental health can be achieved by removal of plaque, and the prevention of further plaque growth using suitable anti-bacterial dental products. There are a number of ways to administer anti-bacterial agents into the oral cavity, the most common being toothpastes and mouthrinses. Anti-bacterial agents which are to be incorporated into a commercial product should have the following properties:

i) A broad spectrum of anti-bacterial activity.

ii) Non-toxic.

iii) Good oral substantivity.

iv) Good chemical stability.

Since the introduction of the first oral care products there have been a number widely varying classes of anti-bacterial agent which have been identified. These include phenols, peroxides, inorganic fluorides and metal salts. The class of agent which is utilised in a formulation depends on which market the product is aimed at, and what other components will be in the product. In the case of toothpastes, various chemical and physical interactions between the anti-bacterial agent and the other components limits the number of agents which can be used.

Stannous fluoride has been used in oral care products since the 1950's, and has been reported to be an effective agent for treating various oral conditions and diseases including plaque,[26-35] gingivitis[36] and dental caries.[36,37-39] Product stability has been an outstanding problem because stannous fluoride is unstable in water and readily forms stannic compounds, which is problematic as this oxidised form of tin is inactive towards bacteria. Historically, it was believed that the mechanism of action of SnF_2 was to interact with enamel to form a protective coat ($Sn_3F_3PO_4$) on the enamel surface.[40,41] Considerable evidence has accumulated over the past twenty years showing topical application of SnF_2 reduces levels of *S. mutans* in humans.[42]

Metal salts have been investigated over many years for their potential to inhibit plaque formation and thereby prevent dental caries and chronic gingivitis.[36] Particular interest has been shown in stannous and zinc salts and results have shown, when used alone or combined with anti-microbial agents, inhibition of the formation of both plaque and tartar.[43] Stannous fluoride is of interest, since the stannous moiety has the potential to inhibit plaque and prevent gingivitis,[27,28] and the fluoride moiety to prevent dental caries.[37] The major problem with stannous fluoride is hydrolysis and oxidation which causes precipitation in the presence of water. For this reason there was a lull in the

research into stannous fluoride toothpastes for a number of years as it was not possible to stabilise the stannous sufficiently to prevent hydrolysis and oxidation to Sn(IV). Recently, however, there has been a resurgence of interest into stannous fluoride products for which claims of stability for the stannous fluoride within the formulations have been made.[27,28] This work has led to a number of available stannous fluoride gels, toothpastes and, in combination with an amine fluoride, a mouthwash preparation.[44] This study detailed a stable amine/stannous fluoride mouthrinse which combined the anti-microbial effect of stannous fluoride with the caries-preventive potential of amine fluoride. Clinical studies on this mouthrinse have confirmed that daily use of the mouthrinse produces a clear-cut fall in pathogenic micro-organisms and a reduction in inflammation.[45] Interest and research in stannous fluoride products has centred largely upon their potential to prevent plaque accumulation and inhibit gingivitis. Early studies on stannous fluoride products supported efficacy against plaque accumulation and the development of gingivitis which appeared to be via an anti-microbial action. Stannous fluoride appears to be substantive to the tooth surface (i.e. it "sticks to it") in a manner similar to chlorhexidine, a common ingredient in mouthrinses, which may explain its plaque inhibitory effects.[46]

It is now known that the reason for the high efficacy of stannous fluoride is due to the presence of Sn^{2+} ions. The Sn^{2+} ions appear to inhibit the formation of acid by plaque bacteria and thus inhibit dental plaque formation. The reason for this inhibition is that the tin accumulates and is strongly bound in dental plaque,[30] suggesting an uptake of Sn^{2+} by plaque bacteria. It was originally believed that the tin was bound to the bacteria in an extracellular manner,[30] thus interfering with the surface potential of the bacteria. It is possible that the tin bound to the surfaces of the bacteria may block the passage of sucrose into the cell and hence inhibit the formation of acid. This early observation on the mode of action of tin appears to have been superseded by the belief that the tin is actually bound in an intracellular manner.[47] An electron-microscopy study, which was able to show if there was any tin present within the bacterial cell, was carried out, the results of which indicate that bacteria exposed to stannous fluoride do contain intracellular tin. The electron micrographs show that the bacteria exposed to stannous

fluoride contain electron dense areas and intracellular electronlucent holes as well as distorted cell shapes.

The damage to plaque bacteria caused by stannous fluoride would seem to suggest that it is possible to destroy plaque itself. Unfortunately, this is not the case as shown by a number of studies.[48,49] In these studies the efficacy of stannous fluoride was evaluated against existing plaque which was grown on stainless steel wire. The findings of both of these studies were the same, stating that pre-formed "plaques" exposed to stannous fluoride were still metabolically active after the treatment. The decreased effectiveness of stannous fluoride on pre-formed plaque was in agreement with the concept that a dense bacterial mass may inhibit penetration of anti-bacterial agents.[39]

It is significantly easier to manufacture tin(IV) compounds than tin(II), so this raises the question "why not use tin(IV) anti-bacterial agents?". The answer to this question is that tin(IV) compounds have been found to be inactive towards bacteria. For example, stannous fluoride is highly active but the corresponding stannic fluoride, SnF_4, is inactive under the same test conditions.[38] It is not known why the stannic ion offers no anti-bacterial activity, although the reducing nature of the stannous ion, which is obviously missing in stannic ions, may be important.

With the knowledge that tin(IV) ions are inactive, any toothpastes which have a tin(II) anti-bacterial agent (either SnF_2 or $Sn_2P_2O_7$) must offer stability to the stannous ion for the product to be effective. Tin(II) compounds are known to react with polyhydroxy compounds such as sorbitol and ethylene-glycol.[50] Since a large proportion of a toothpaste is sorbitol it is likely that a chemical interaction will occur between the hydroxyl groups of the sorbitol and the stannous ion. It is possible that this type of interaction provides stability to the stannous ion by co-ordinating it in such a way that it is surrounded by hydroxyls and thus resistant to oxidation. It is possible to stabilise the stannous ions by the addition of a specific stabilising agent. The choice of agent is important as it must be selective to Sn^{2+} ions and not chelate Ca^{2+} ions as this could lead to a demineralisation of the tooth, and eventually to dental caries.

A copolymer of maleic anhydride and methoxyethylene (**II**) with molecular weight around 30 000gmol^{-1} acts in a similar manner to sorbitol thus stabilising the tin(II).[51] A more recent approach to the stabilisation of stannous ions has come from the inclusion of an organic anti-oxidant in the formulation.[52] The compound in question is propyl gallate (**III**), an organic radical inhibitor:

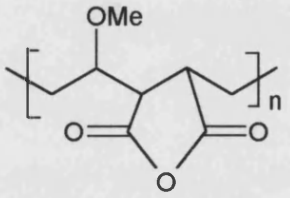

Methoxyethylene/Maleic Anhydride Copolymer (**II**)

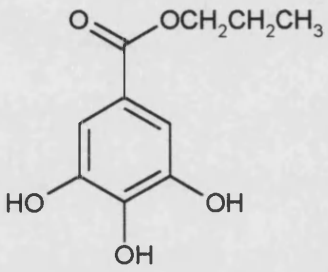

Propyl Gallate (**III**)

The tendency for stannous ions to oxidise is greatly reduced by incorporation of as little as 1% of this compound into a toothpaste. The results suggest that the presence of a radical inhibitor greatly restricts the major oxidation route of tin(II) to tin(IV).

Another major anti-bacterial agent which has been found to exhibit a broad spectrum of activity is the halogenated phenol, 2,4,4′-trichloro-2′-hydroxy diphenyl ether, more commonly known as triclosan (**I**). Triclosan is a particularly attractive non-ionic anti-bacterial compound because as well as the broad spectrum of activity, it is compatible with toothpaste components. The use of triclosan as an anti-bacterial agent was first reported in 1968[53] when it was called irgasan, and was used as a skin-degerming agent in toiletries, soaps, and cosmetics. Clinical studies using triclosan containing toothpastes have found that they are effective in reducing the accumulation of plaque[54] as well as the degree of gingival inflammation.[55]

The use of triclosan alone has only a moderate effect on the formation of plaque.[56] The low salivary levels of triclosan a short time after application indicate too

rapid a release from the oral binding sites to exert a prolonged anti-bacterial effect. A major determinant in the retention of a compound in the oral cavity is its water solubility, and it is here that triclosan is disadvantaged with a low solubility (ca. 1ppm @20°C). One way of improving the water solubility has been to emulsify the triclosan with a surfactant, such as sodium lauryl sulphate (SLS), to form a micellar phase. However, upon dilution in the mouth the surfactant concentration falls below the critical micelle concentration and triclosan is precipitated, rendering it biologically inactive.

An alternative method for improving the delivery of triclosan is to incorporate a lipophilic copolymer of methoxyethylene and maleic acid into the toothpaste. The addition of this carrier copolymer, which itself has no anti-bacterial activity, dramatically increases the intraoral bioavailability of triclosan and results in enhanced substantivity and therefore sustained anti-bacterial activity.[57]

There is another technique for enhancing the activity of triclosan by increasing its water solubility. This method involves reacting triclosan with phosphoryl chloride to produce triclosan phosphate:[58]

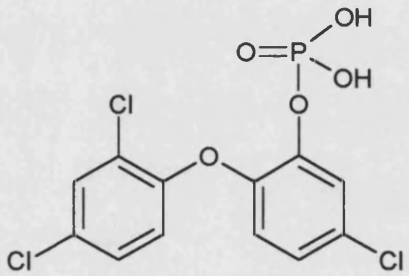

Triclosan phosphate

Triclosan phosphate is readily soluble in both water and toothpastes, and therefore acts as an ideal means of delivering triclosan. This derivatised triclosan has been found to be much more active than triclosan alone.[58] A possible explanation for this increased activity is that triclosan phosphate, being water soluble, can bind to phosphatases in saliva, bacterial cell walls and plaque fluids through its phosphate functional group. The triclosan phosphate is also able to diffuse into plaque deposits and

bind to phosphatases in gingival lesions and gingival fluid. Once bound to these specific sites within the oral cavity the triclosan phosphate liberates free triclosan via the action of phosphatase enzymes on the functional group.

Zinc ions, Zn^{2+}, are known to exhibit anti-bacterial properties when incorporated into dental formulations.[59-61] The zinc salt which is most commonly used is zinc citrate trihydrate (ZCT). The use of ZCT in a mouthrinse has been found to inhibit the production of lactic acid by dental plaque from external sugar.[62] Zinc has been found to exhibit a small effect on plaque regrowth on surfaces which had originally been clean, but had a greater effect on surfaces initially associated with moderate amounts of plaque.[63] This suggests that the major effect of the zinc is to reduce the rate of bacterial proliferation in existing plaque.

Most dental formulations which use ZCT also contain triclosan to achieve a synergistic effect of the two anti-bacterial agents, which have different modes of action. Triclosan has been found to have a large effect on surfaces which are clean, and no real effect on existing plaque. This suggests that triclosan may be adsorbed to the tooth surface and either prevents bacterial adhesion or inhibits growth of the colonising bacteria. The complementary action of these two agents, ZCT and triclosan, is advantageous for a toothpaste, as reported in a number clinical trials.[64-66]

1.7. The Chemistry of Tin

1.7.1. Introduction to Group 14

Tin belongs to Group 14 of the periodic table along with carbon, silicon, germanium and lead, and has the outer electronic configuration $5s^25p^2$. On descending Group 14 the metallic character of the elements increases: carbon is non-metallic; silicon is essentially non-metallic; germanium has some metallic properties; and tin and lead are metals. The greater tendency to form M^{2+} ions, due to a decrease in stability of the +IV oxidation state and an increase in stability of the +II state, is also notable on descending the group. Lead is the only member of the group where the lower oxidation state is favoured. This is true for inorganic compounds but not organometallic compounds, although this is outside the scope of this review. In the case of tin and germanium the higher valence state is favoured, which causes problems during the preparation of tin(II)/germanium(II) compounds.

1.7.2. Tin(II) Chemistry

As previously stated, the ground state of tin metal is $5s^25p^2$, and the element could form covalent bonds in the lower +2 oxidation state by using two unpaired $5p$ electrons. The resulting stereochemistry of the molecule formed will depend upon the type of hybridisation adopted by the valence shell electrons. If the hybridisation of the orbitals is p^2, the bond angles should be 90°. If the lone-pair s electrons are incorporated in sp^2 hybridisation, then the bond angles should approach 120°.

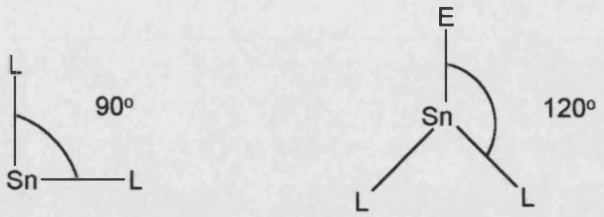

(i) p^2 (ii) sp^2

Where E = Stereochemically active lone pair

The bond angles will depend heavily on the extent of repulsion between the bonds formed and the highly repulsive effect of the lone-pair electrons leading to the prediction of a distorted geometry in covalent tin(II) compounds. Compounds of this type have an empty p_z orbital, set at right angles to the molecular plane, which is of similar energy to those used in bonding. Therefore, any tin(II) compound with an appreciable covalent character should act as a monofunctional acceptor towards suitable ligands. This will result in the formation of adducts of the type $SnX_2.n$(ligand).

The stannous ion, Sn^{2+}, having empty 5*p* and 5*d* orbitals can act as an acceptor toward certain ligands. As tin(II) species contain a stereochemically active lone-pair, it might be expected that they would behave as σ-donor ligands. The ability of a lone-pair to act as a donor generally decreases as the atomic weight increases, therefore the σ-donor strength of the 5*s* lone-pair orbital should be low making stannous species slightly Lewis acidic. Stannous compounds can actually act as both donors and acceptors, although the Lewis acidity is the more dominant behaviour.

Application of simple VSEPR theory predicts that bivalent tin will adopt an angular geometry, although this is rarely the case. In fact, this geometry is only observed for tin(II) halides in the gas phase[67] and for tin(II) derivatives where the steric bulk of the ligands precludes a higher coordination number at tin, e.g. $Sn(OC^tBu_3)_2$.[68]

Bivalent tin compounds wherever possible adopt structures in which the metal achieves coordination numbers higher than two, either by complexation, chelation, or by bridging. The basic unit is usually recognisable as a trigonal pyramid (**I**), but additional bonds or contacts are often present, leading to distorted pseudo-trigonal bipyramidal

(**II**), square-based pyramidal (**III**), octahedral (**IV**), distorted octahedral (**V**), or facially capped trigonal prismatic (**VI**). The most common geometries are **I**, **II** and **III**.

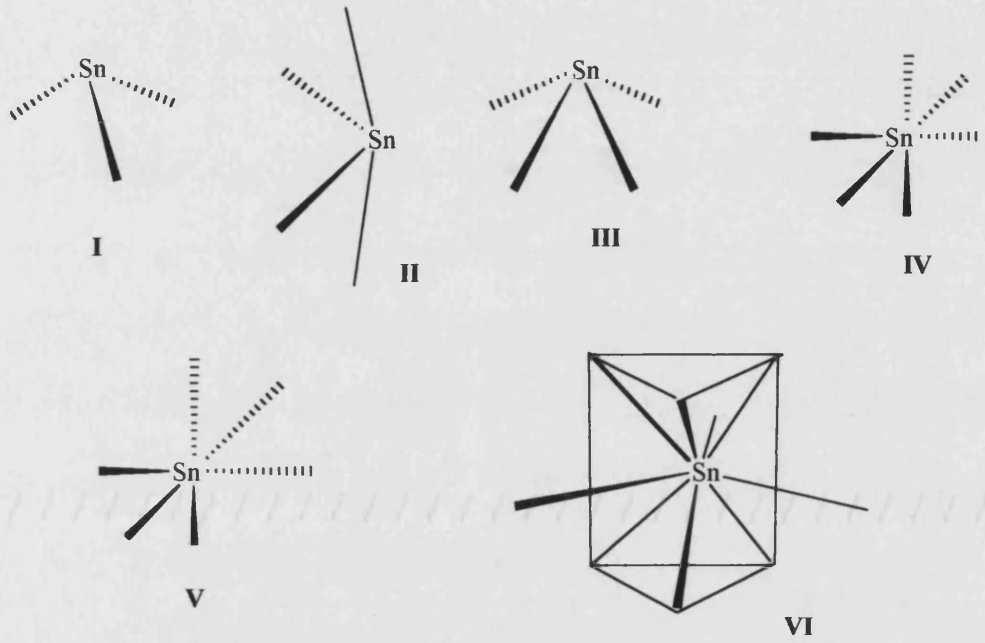

With stannous species adopting one of these geometries, the coordination number ranges from 2 - 9. The presence of the lone-pair of electrons now takes on major importance in that the ideal geometries mentioned are rarely encountered. It is usual to find distorted structures which can be difficult to distinguish, for example, four-coordinate square pyramidal and distorted pseudo-trigonal bipyramidal. In the majority of tin(II) compounds the lone-pair is stereochemically active, indicated by an apparent vacancy in the coordination sphere accompanied by the expected distortion of regular geometries. Table 1.2. summarises the possible coordination geometries exhibited by stannous compounds with specific examples.

Table 1.2. Sn(II) coordination geometries.

COORDINATION NUMBER	COORDINATION GEOMETRY	EXAMPLE	REF.
2	Angular	$Sn[CH(SiMe_3)_2]_2$	69
3	Trigonal planar	$(OC)_5Cr \cdot Sn[CH(SiMe_3)_2]_2$	70
3	Pyramidal	$SnSO_4$	71
		$SnHPO_4$	72
4	Square pyramidal	SnO	73
4	ψ-trigonal bipyramidal	$[EtO_2CHC(NH_2)CH_2S]_2Sn$	74
		SnClF	75
6	Octahedral	Cubic SnSe	76
9	Trifacially capped trigonal prismatic	$SnBr_2$	77

Angular coordination: The crystal structure of $Sn[CH(SiMe_3)_2]_2$ consists of a centrosymmetric dimer with a Sn-Sn bond length of 2.764Å, which is similar to that found in hexaphenylditin, and Sn-C bond lengths of 2.28Å. The stereochemistry around the tin is non-planar with a [C-Sn-C] angle of 112°.

Trigonal planar coordination: The structure of $(OC)_5Cr \cdot Sn[CH(SiMe_3)_2]_2$ consists of a three-coordinate tin with average Sn-C bond lengths of 2.185Å. The effect of the electron withdrawing $Cr(CO)_5$ group is to cause this shorter bond length. The [C-Sn-C] angle is ca. 98°, which is slightly distorted from the ideal planar arrangement.

Pyramidal coordination: $SnSO_4$ is an example of a pyramidal three-coordinate tin atom with one Sn-O bond length of 2.25Å, and two Sn-O bond lengths of 2.27Å. One of the pyramidal bond angles in this compound is 79.0°, with the other two angles

77.1°. This is a common coordination for tin(II) compounds,[72,76,78-81] with sp^3 hybridisation involving three covalent bonds to nearest-neighbour atoms and the fourth orbital occupied by a lone-pair.

Square pyramidal coordination: In SnO each oxygen atom is surrounded tetrahedrally by four tin atoms, with [Sn-O-Sn] angles of 118° and 105°. Each tin atom is bonded to four oxygen atoms which form a square to one side of it, i.e. the tin atom lies at the apex of the pyramid. This is consistent with four bonding orbitals being directed from the tin atom towards the four corners of the base, and a fifth orbital occupied by a stereochemically active lone-pair directed toward the apex. The average Sn-O bond length is 2.21Å, and a Sn-Sn distance of 3.70Å suggesting a tin-tin bond.

ψ-trigonal bipyramidal coordination: The structure of SnClF has been determined and has been shown to have ψ-trigonal pyramidal geometry with a stereochemically active lone-pair. The environment of the tin atom is somewhat distorted due to the presence of the lone-pair and consists of pyramids, linked to form an infinite $(SnClF)_n$ chain structure.

Octahedral coordination: Six coordinate tin compounds include cubic SnSe and SnTe,[76,82] both of which adopt the NaCl lattice. This implies that the tin will be covalently bonded to six neighbours using both lobes of each of the three *p*-orbitals. The average Sn-Se and Sn-Te bond lengths in these structures are 3.00 and 3.14Å respectively, which is in keeping with a bond order of one-half and is similar to that seen in interstitial compounds.[83]

Trifacially capped trigonal prismatic coordination: This coordination is exhibited by $Sn(NCS)_2$[84] and also by $SnBr_2$.[77] In both of these structures there are six atoms surrounding the tin at the apices of a trigonal prism, with the other three atoms lying outside the prism faces. The bond distances fall between 2.20Å and 3.74Å in $Sn(NCS)_2$, and between 2.81Å and 3.11Å for the nearest Sn-Br interactions.

1.8. The Chemistry of Copper and Zinc

1.8.1. Copper and Group 11

The metals in Group 11 (copper, silver and gold) have the highest electrical and thermal conductivities known. The atoms of these metals have one *s* electron in their outer orbital, but differ from Group 1 elements in that the penultimate shell has ten *d* electrons. The poor screening by the *d* electrons makes the atoms of Group 11 much smaller in size, and the ionisation energies consequently higher. The three elements each exhibit oxidation states +I, +II and +III, with silver most commonly being +I and gold +III.

Copper(II) is the most stable oxidation state of copper in aqueous solution. Having a d^9 electronic configuration with one unpaired electron, copper(II) compounds are coloured and paramagnetic. For example, $CuSO_4.5H_2O$ and many hydrated cupric salts are blue. The hydrated ion $[Cu(H_2O)_6]^{2+}$ is a blue complex and has a distorted octahedral geometry, with two long axial bonds and four short equatorial bonds:

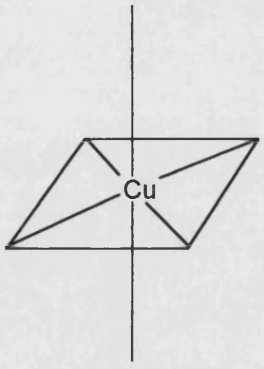

The distortion in this complex can be explained using crystal field arguments whereby the elongation of the two axial bonds reduces the repulsions between the ligand

electrons and the d_{z2} electrons of the metal. This distortion is known as the Jahn-Teller effect and is common among copper complexes.

The most common coordination numbers for copper(II) compounds are four, five and six. In each structure a variation from idealised geometries occurs through bond length and bond angle distortions.

Four coordinate copper(II) compounds: Four coordinate copper(II) complexes exhibit both square planar[85-89] and tetrahedral[90] geometries. In the structure of bis(tropolonato)copper(II)[85] the Cu-O bonds are equivalent, 1.913(3)Å and 1.915(3)Å, respectively, observations consistent with earlier work.[91]

Five coordinate copper(II) compounds: Five coordinate, square pyramidal, geometry is less common for copper(II). An example of this geometry is copper(II) 4-hydroxy-6-methyl-3-[3-dimethylaminoacryloyl]-2H-pyran-2-one.pyridine,[92] where the square plane is comprised of two of the bidentate ligands bonded to copper, with the pyridine in the axial position.

Six coordinate copper(II) compounds: Six coordinate copper(II) complexes often exhibit distorted tetragonal bipyramidal geometries.[93,94] From these examples it can be noted that bidentate ligands will be bonded to the copper(II) in the square plane with other ligands adopting axial positions. A Cu-Cu interaction (typically ca. 2.64Å, quite close to the distance found in metallic copper) is evident in some structures, e.g. dimeric copper(II) acetate monohydrate:[90]

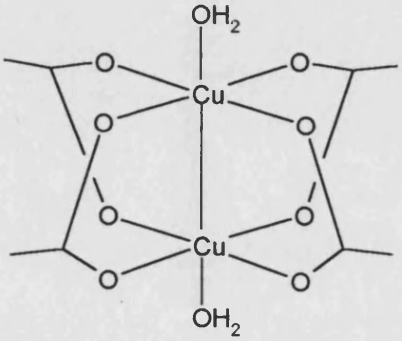

1.8.2. Zinc and Group 12

The elements in this group all have two *s* electrons beyond a completed *d* shells. Removal of the *s* electrons results in divalent compounds, and a +II oxidation state is a characteristic of the group. Valancies of higher than two are not found, because removal of more electrons would destroy the symmetry of the completed *d* shell. Since the *d* shell is complete, and is not available for bonding, the elements in this group show few of the properties associated with typical transition elements. They do not show variable valency, and since they have a d^{10} configuration they cannot produce *d-d* transitions and hence the majority of the complexes formed are white.

Zinc in oxidation state +II readily forms complexes with a number of ligands, adopting coordination numbers 4,5 and 6.

Four coordinate zinc(II) compounds: Promotion of one of the *s* electrons to the 4*p* orbital allows the formation of a σ-bond to, for example, a halide with the coordination sphere being completed by donation into the vacant *p* orbitals by a suitable ligand (e.g. pyridine). This $[Zn(pyridine)_2Cl_2]$ compound exhibits tetrahedral geometry.[90]

Five coordinate zinc(II) compounds: Five coordination is not common in zinc compounds. An example of a trigonal bipyramidal complex is $[Zn(terpyridyl)Cl_2]$.[90] There are examples of five coordinate zinc with less clearly defined geometry.[95,96] The reactions of zinc with *m*-xylenediamine bis(Kemp's triacid imide), H_2XDK, lead to a range of geometries about the zinc, depending on the polarity of the recrystallisation solvent. The ligand contains two carboxylate groups which can act in a monodentate or bidentate manner depending on the nature of the solvent. This observation is consistent with some work carried out previously on the influence of solvent polarity on the mode of chelation of a carboxylate ligand.[97]

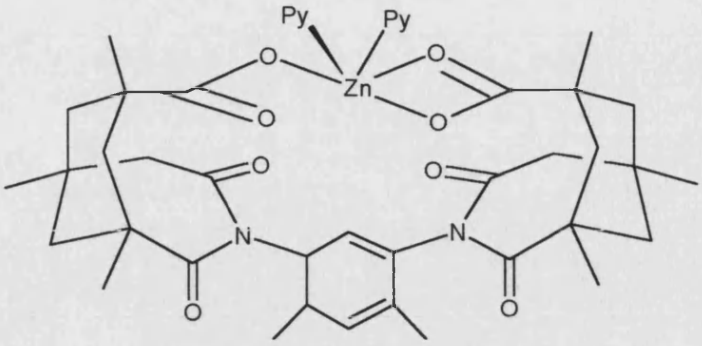

$ZnXDK(Py)_2$

In the above complex the distance between the Zn and the free oxygen is 2.977(8)Å, which could be due to twisting of the triacid groups from their idealised angles. This twisting leaves the carbonyl group further away than the other Zn-O interactions, {2.048(9)Å, 2.39(1)Å, 1.953(7)Å}, a distance which is considered to be too far to be a bond.

Six coordinate zinc(II) compounds: Zinc forms a number of six coordinate octahedral compounds.[96,98-100] The examples quoted are all composed of two bidentate oxygen ligands in the square plane with two water molecules completing the octahedral geometry. The Zn-O bond lengths are all similar, ranging from 2.0 - 2.2Å. It is possible to see cis-trans isomerism in some of these complexes, but such behaviour is outside the scope of this review.

1.9. Metal(II) Compounds of Relevance to Dental Formulations.

1.9.1. Metal(II) phosphate compounds

M(II) phosphates are an important class compounds which are incorporated into dental formulations, with stannous pyrophosphate being the most widely used. As mentioned earlier in this review phosphates are broken down by the action of phosphatase enzymes present in the oral cavity, and tin(II) ions have known anti-bacterial properties. This means that once in the mouth, stannous ions are released over a period of hours providing sustained anti-bacterial activity.

A series of stannous salts of phosphorus oxy-acids have been identified in the literature, including stannous phosphate, stannous dihydrogen phosphate,[101] stannous phosphite[102] and stannous hypophosphite.[103] The amount of spectral data quoted in the literature for tin(II) phosphates is limited, although a number have been structurally characterised.

$Sn_3(PO_4)_2$: The structure of stannous phosphate (Figure 1.1) has been determined,[79] the compound having being synthesised by the reaction of 1M solutions of SnF_2 and H_3PO_4. The structure of this compound consists of alternating layers of Sn^{2+} and $[PO_4]^{3-}$ ions arranged parallel to the *ac* plane. Two large open channels which run parallel to the *b* axis are formed by Sn^{2+} ions arranged in a helical fashion. The open spaces are generally considered to be the result of hemispherical coordination preferred by stannous ions.[78,104,105]

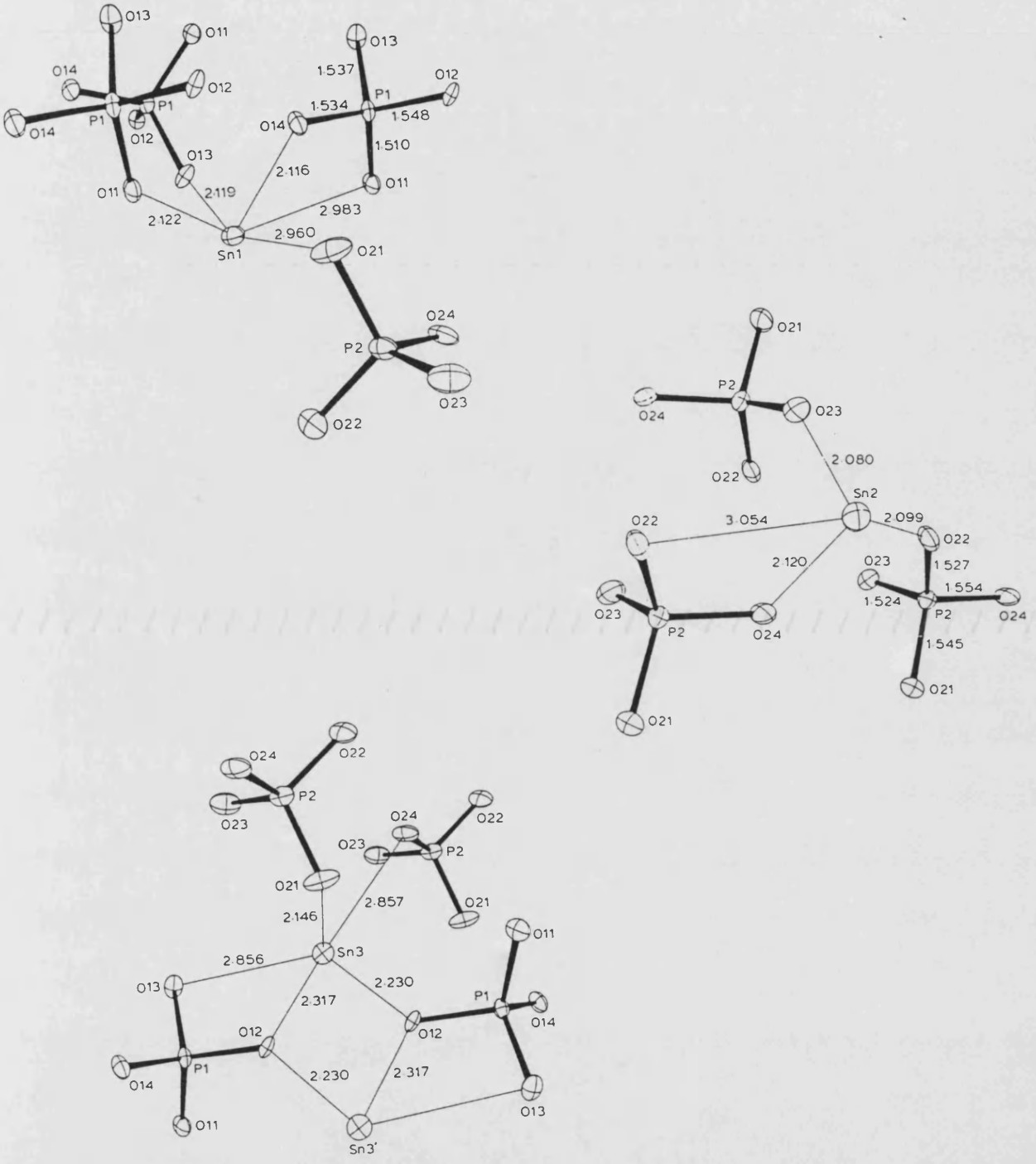

Figure 1.1. The 3 Sn(II) sites in $Sn_3(PO_4)_2$.

$Sn_3(PO_4)_2$ has stannous ions in three environments. Sn(1) is strongly coordinated to three oxygen atoms from three phosphate groups with Sn-O bond lengths of 2.119Å. The coordination around this tin is completed by two weaker Sn-O interactions of 2.971Å. The coordination around Sn(2) is very similar to Sn(1), however there is only one weak Sn-O interaction (3.054Å) not two. Sn(3) has a quite different coordination in that there are three Sn-O interactions (average, 2.88Å) and a very weak interaction at 3.250Å. A salient feature of the coordination around Sn(3) is the presence of an oxygen bridged Sn(3)-O-Sn(3) dimer lying across a centre of symmetry.

$SnHPO_4$ and $SnHPO_3$: The structures of stannous phosphate ($SnHPO_4$) and stannous phosphite ($SnHPO_3$) are quite similar and consist of infinite sheets stacked perpendicular to the *b* axis. The sheets consist of SnO_3 groups fused with PO_4 groups in the phosphate and SnO_3 groups fused with HPO_3 groups in the phosphite. In the phosphate structure there is hydrogen bonding which has the effect of holding the sheets together. In both compounds the oxygen atoms closest to the Sn form a SnO_3 pyramid with Sn at the apex. The average Sn-O bond lengths in both the phosphate and phosphite are 2.27Å and 2.19Å respectively.

$Sn(H_2PO_4)_2$: The structural determination of tin(II) bis(dihydrogenphosphate)[104] revealed that the tin atoms are each coordinated by four oxygen atoms, all lying on one side. Two of the Sn-O bonds are short (2.209Å) and the other two are longer (2.466Å). This leads to a distorted square pyramidal geometry around the tin, with the four oxygens in the square plane and the apex occupied by the stereochemically active lone-pair of electrons from tin. The structure consists of infinite zigzag chains parallel to the *c* axis, and, similar to $SnHPO_4$, there is strong hydrogen bonding between the phosphate groups holding the chains together.

$Sn_3F_3PO_4$: Stannous fluorophosphate is the main product of the reaction of stannous fluoride and hydroxyapatite.[40] This reaction is of particular importance to dental applications in that it is a reaction which occurs at the surface of a tooth, i.e. the enamel. A structural determination of this compound[80] has revealed a distorted trigonal pyramidal geometry around the tin. There are six neighbours around each tin atom: two

fluorine and one oxygen at an average distance of 2.15Å, two other oxygens at 2.54Å and 2.96Å, and one fluorine at 3.22Å. The overall array of this compound can be considered as consisting of phosphate ions bound together through [O-Sn-F-Sn-O] links.

$Sn_2(OH)PO_4$ and $Sn_3O(OH)PO_4$: These compounds are two more of the products of the reaction of stannous fluoride and hydroxyapatite. The structure of $Sn_2(OH)PO_4$ contains as its asymmetric unit two tin atoms, one PO_4 group and one OH group. The overall array is layered, with the layers parallel to the *ab* plane. The layers are held together by weak Sn-O interactions (ca. 3.0Å), and possibly by van der Waals bonds. The coordination around the tin is pyramidal with average Sn-O bond lengths of 2.12Å, and weaker Sn-O interactions of 3.01Å. $Sn_3O(OH)PO_4$ has a structure similar to most of the tin(II) phosphates, in that the coordination around tin is square pyramidal with three Sn-O bonds (2.15Å) and weaker Sn-O interactions.

$Sn_2P_2O_7$: Stannous pyrophosphate is known,[106] although little structural data is available due to the amorphous nature of the compound. Stannous salts of condensed polyphosphoric acids are of great importance in dental applications, especially the pyrophosphate which has been extensively utilised in dental formulations as a source of anti-bacterial stannous ions.

Table 1.3. Bond length data for Sn(II) oxy-phosphorus compounds.

Compound	CN	[Sn(1)-O]/Å	[Sn(2)-O]/Å	[Sn(3)-O]/Å
$Sn_3(PO_4)_2$	3	2.122(7), 2.119(7), 2.116(7)	2.080(7), 2.099(7), 2.120(7)	2.146(7), 2.230(7), 2.317(7)
$SnHPO_3$	3	2.15(1), 2.14(1), 2.22(1)		
$SnHPO_4$	3	2.15(1), 2.29(1), 2.36(1)		
$Sn(H_2PO_4)_2$	4	2.209(2), 2.209(2), 2.466(2), 2.466(2)		
$Sn_2(OH)PO_4$	3	2.080(6), 2.155(6), 2.178(6)	2.105(6), 2.133(6), 2.153(6)	
$Sn_3O(OH)PO_4$	3	2.124(6), 2.136(6), 2.150(6)	2.069(6), 2.172(6), 2.282(6)	2.065(6), 2.158(6), 2.262(6)

Copper(II) phosphate chemistry is interesting because of the structural multiplicity attributed to the Jahn-Teller effect. This distortion leads to a wide variety of frameworks observed in ternary and quaternary phosphates.

[BaCl][$CuPO_4$]: This compound was recently characterised[107] and was shown to exhibit a honeycomb-like open-framework structure. The structure is composed of square planar CuO_4 and tetrahedral PO_4 units connected in an alternating fashion of corner and edge sharing. Each CuO_4 square plane shares one edge with a PO_4 and two corners with two different PO_4 groups. The structure is strengthened by the barium and chloride ions which reside in the framework. The Cu-O bond distances range from 1.981 to 2.076Å.

$Ba_2Cu(PO_4)_2$:[108] The framework of this compound consists of linear chains of $Cu(PO_4)_2$ with Ba^{2+} cations residing between the parallel chains. The chains are composed of an array of Cu^{2+} cations that are doubly bridged by PO_4 anions. Each pair of bridging PO_4 tetrahedra are in a staggered configuration above and below the CuO_4 square plane, resulting in a linear chain with long Cu-Cu separations of 5.13Å. In this compound all Cu-O bond distances are equal, 1.941Å.

Zinc(II) phosphates have been studied in detail over the last few years, with the majority of the compounds exhibiting a layered structure.[109] The other form which a lot of zinc(II) phosphates adopt is a linear polymeric chain.

$Zn[O_2P(OCH_3)_2]_2$ and **$Zn[O_2P(OC_2H_5)_2]_2$**:[110,111] These compounds both form infinite one-dimensional chains of vertex linked ZnO_4 and PO_4 tetrahedra, shielded from each other by the methyl/ethyl groups attached to the phosphate centres. There are no inter-chain bonds, apart from van der Waals type interactions. The Zn-O bond distances range from 1.883 to 1.968Å in the methyl compound, and 1.888 to 1.903Å in the ethyl derivative.

1.9.2. Metal(II) carboxylate compounds

M(II) carboxylates are another important class of compounds for dental applications. The most common of these is zinc citrate trihydrate (ZCT) which is widely utilised in the dental industry. This compound is often used with triclosan or stannous fluoride when incorporated into toothpastes. When used with SnF_2 the most probable reason for the high activity is the formation of stannous citrates *in situ*, which may be stable and active themselves.

Zinc forms two types of carboxylate complexes, $Zn_4O(O_2CR)_6$ or "basic" zinc acetate and $Zn(O_2CR)_2$. In the former case, the molecule itself has a tetrahedral symmetry with a central oxygen atom surrounded tetrahedrally by four zinc atoms.[112] The six acetate groups are attached symmetrically to the six edges of the tetrahedron.

The $Zn(O_2CR)_2$ molecule exists as a dihydrate with chelating acetate groups and two coordinating water molecules completing a distorted octahedral geometry around the zinc atom.[113] A number of zinc(II) carboxylates and their adducts with nitrogen-containing ligands have been reported,[114-117] but further detailed descriptions are outside the scope of this review.

In the case of tin(II) carboxylates, a coordination number of three appears to persist.[118] Tin(II) formate[119] and tin(II) acetate[102] are made by dissolving tin(II) oxide in the requisite carboxylic acid. The tin(II) carboxylates, except tin(II) formate, are fibrous in nature and exhibit low solubility, suggesting a linear polymeric structure (see Figure 1.2) which can break down on sublimation, or upon solution in donor solvents.

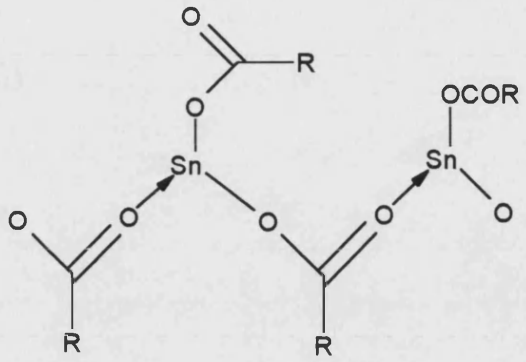

Figure 1.2. General structure of Sn(II) carboxylates.

Both Mössbauer and infrared spectra of tin(II) carboxylates support the above structure, i.e. long chains of pyramidally coordinated tin atoms containing bridging carboxylate groups.[118]

Tin(II) formate differs slightly from the general structure depicted in Figure 1.2 in that it adopts a sheet like structure.

Cu(II) carboxylates have been studied extensively, and a large number of complexes have been structurally characterised.[118,120-125] The structure of Cu(II) acetate monohydrate contains copper ions bridged in pairs by acetate groups to afford essentially centrosymmetric eight-membered rings.[126] The copper-copper distance in this complex is similar to that observed for metallic copper (i.e. 2.55Å).[90] In each of the four bridging acetate groups one of the oxygen atoms is weakly coordinated to a copper atom of another binuclear unit to produce a planar polymeric molecule.

1.10. ^{119m}Sn Mössbauer Spectroscopy

The technique of Mössbauer spectroscopy (or nuclear gamma resonance spectroscopy) has grown steadily in importance since its earliest observations by Rudolph Mössbauer in 1957. The Mössbauer effect is the emission or absorption of γ-rays without loss of energy due to recoil of the nucleus. The theory and basic principles of ^{119m}Sn Mössbauer spectroscopy have been extensively discussed in a number of books[127-129] and only a brief summary of the technique is presented here.

The application of Mössbauer spectroscopy in chemistry arises from the ability to detect slight variations in the energy of interaction between the nucleus and extra-nuclear electrons. The Mössbauer effect should be present in all γ-ray excited state-ground state transitions, but the magnitude is often so small as to be undetectable. Consequently there are a limited number of elements to which the technique can be applied. The major application of Mössbauer spectroscopy is in iron[130] and tin[131-134] chemistry, although the technique can also be used for antimony,[135] tellurium,[136] iodine,[137] xenon,[137] europium,[138] gold,[139] neptunium,[140] nickel,[141] ruthenium,[142] tungsten[143] and iridium.[144] Mössbauer spectroscopy can not be used for the elucidation of the structures of the zinc and copper compounds detailed in this thesis. The technique was quickly established with ^{57}Fe where large resonance effects were observed at room temperature. The conditions for the development of ^{119m}Sn Mössbauer were not as favourable due to the higher γ-ray energy of 23.875keV, which meant low temperatures (liquid nitrogen, 78K) were required to achieve the desired recoil-free resonance. This low temperature increases the recoil-free fraction which is important as it is this fraction which gives rise to the spectrum. In practice this means that ^{119}Sn Mössbauer spectroscopy is limited to samples which are solids or solutions (which would be frozen prior to analysis).

The Mössbauer effect is a nuclear process observed for tin when the source, the metastable ^{119m}Sn isotope, emits a 23.875keV γ-ray and excites a ^{119}Sn nucleus to its first excited state (Figure 1.3). Since γ-rays have precisely defined energies the exciting

radiation is strictly monochromatic. The energy of the emitted γ-rays (E_γ) can be modulated, employing the Doppler effect, by oscillating the radioactive source and applying a controlled velocity. For this reason Mössbauer parameters are expressed in units of mms^{-1}.

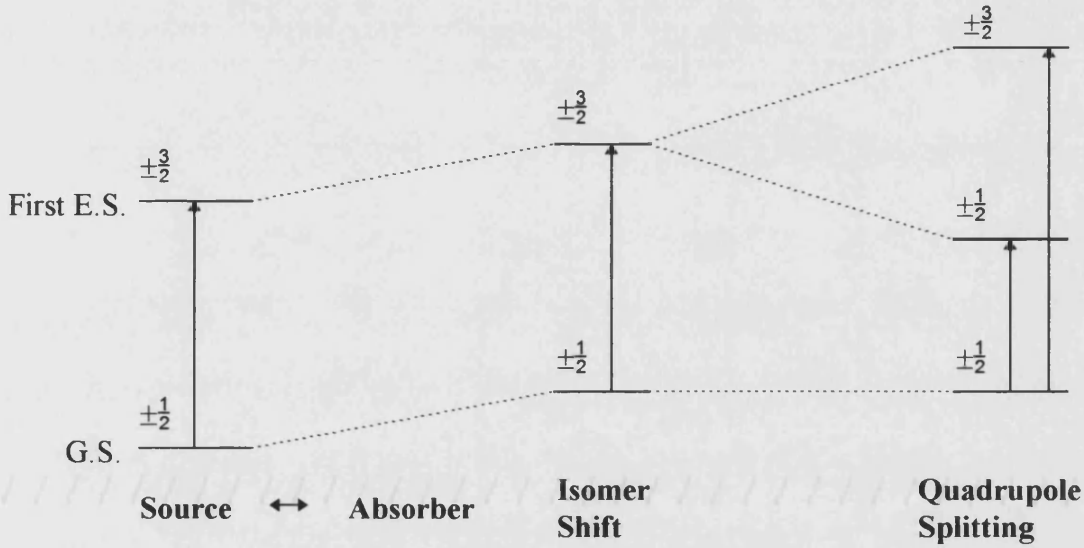

Figure 1.3. Nuclear energy levels, Isomer Shift and Quadrupole Splitting in ^{119m}Sn Mössbauer Spectroscopy.

There are four parameters commonly utilised in Mössbauer spectroscopy which are, isomer shift, quadrupole splitting, line width and intensity.

The isomer shift, IS (δ), depends on the total electron density at the nucleus of the atom relative to the standard material (usually SnO_2). This shift is due to the effect of the electronic environment of the tin atom upon its nuclear energy levels. Since *s*-electron wave functions have their maxima at the nucleus, where *p*, *d* and *f* wave functions are zero, the isomer shift is most sensitive to changes in *s*-electron orbital occupancy. In Sn(II) compounds the electronic configuration is $5s^2$: the *s*-electron density at the nucleus is greater than in the tin atom ($5s^25p^2$), because the screening effect of the 5*p* electrons has gone. This causes a positive isomer shift relative to the standard. In Sn(IV) compounds the two 5*s* electrons have been removed reducing the *s*-

electron density and causing a negative isomer shift relative to the standard. The general range of observed δ values for both oxidation states of tin is:

Tin(IV) $\delta = -0.5$ to $+2.1$

Tin(II) $\delta = +2.5$ to $+5.0$

In the case of Sn^{2+} (and Sn^{4+}) compounds it is usual for δ to decrease with increasing coordination number due to the reduced electron density at the nucleus.

The quadrupole splitting, QS (Δ), arises from an asymmetry in the electron cloud around the nucleus of the sample. Such asymmetry may occur through the presence of lone pairs of electrons, i.e. non-bonding electrons, or through bonding interactions. If the symmetry of the tin nuclei is perfectly spherical, e.g. Bu_4Sn, then there will be a zero electric field gradient and a single line will be observed. If, however, an electric field gradient is generated at the nucleus, the degeneracy of the excited state is lifted and a doublet spectrum will be observed. This field gradient may have one of the two following origins:

i) Non-cubic, or distorted coordination geometries.

ii) Imbalance in the σ-framework of cubic geometries.

The value of the quadrupole splitting in ^{119m}Sn Mössbauer can provide information regarding the overall symmetry of the coordination sphere. In general, the magnitude of Δ is related to the differing electronegativities and coordination geometries of the surrounding ligands. In the case of certain tin(IV) compounds the quadrupole splitting value can give a precise indication as to the coordination number, because definite ranges of Δ exist for particular ligand configurations. In tin(II) compounds however, the presence of the stereochemically active lone pair can produce irregular and unpredictable geometries. This causes difficulty in interpreting the observed differences in the values of Δ obtained, rendering the data less useful in assigning coordination geometries.

In the majority of Sn(II) samples a small percentage of the tin will have been oxidised to Sn(IV) causing a peak to appear on the spectrum at ca. 0.00mms^{-1}, as well as the observed doublet for the Sn(II) portion. The peak areas observed in such stannous samples can be very useful in estimating the percentage of the sample which has been oxidised to Sn(IV). If the area under the peak observed at 0mms^{-1} is ca. 5% of the total area, then it can be said that approximately 5% of the sample has been oxidised during production or storage of the sample. Utilisation of this technique is invaluable when synthesising compounds which have to be tin(II), as if the sample is not prepared in completely oxygen-free conditions the Mössbauer will identify how much of the sample has been oxidised.

As mentioned previously in the Introduction it is only the tin(II) ions which exhibit biological activity and not the higher oxidation state tin(IV) ions. This fact has important implications when considering the use of a stannous compound in a commercial toothpaste. If a high percentage of the stannous ions are being oxidised to stannic then the toothpaste will not offer any anti-bacterial advantage over a placebo toothpaste. It is for this reason that Mössbauer spectroscopy has been applied to the study of toothpastes containing compounds such as $Sn_2P_2O_7$. This study, carried out on a range of stannous compounds in a number of formulations, allowed quantitative analysis of the degree of stannous oxidation to be assessed.

The presence of a tin(IV) impurity in these samples could clearly be observed in the Mössbauer spectra due to differing isomer shifts of the tin(II) and tin(IV) components within the sample. The oxidation of stannous ions when incorporated into a toothpaste is due to interactions with other components of the paste. This phenomenon can be observed using Mössbauer spectroscopy by looking at the reduction in the isomer shift values of the compound when in a toothpaste, compared to the compound alone (Figure 1.4). This technique has assisted with establishing links between stannous stability levels and product formulation and storage conditions.

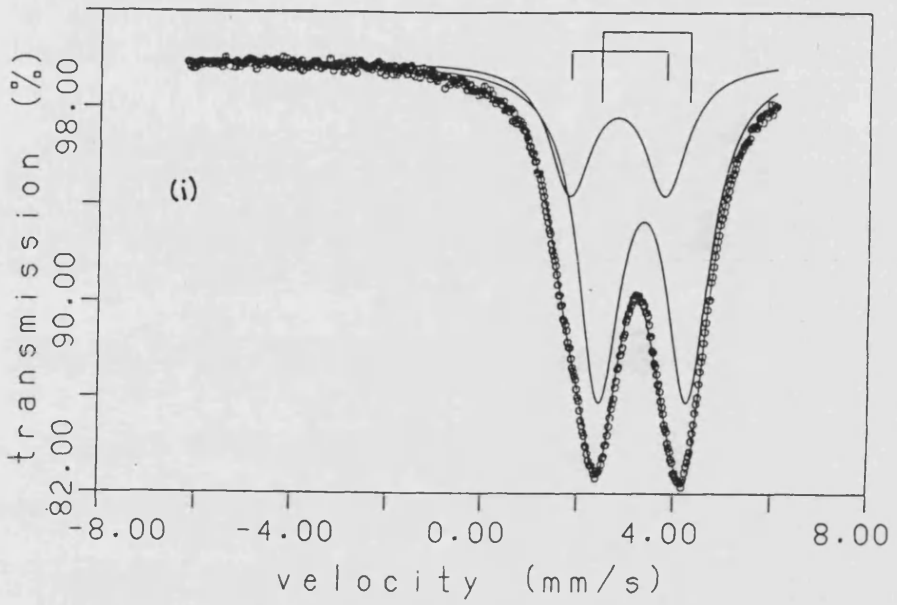

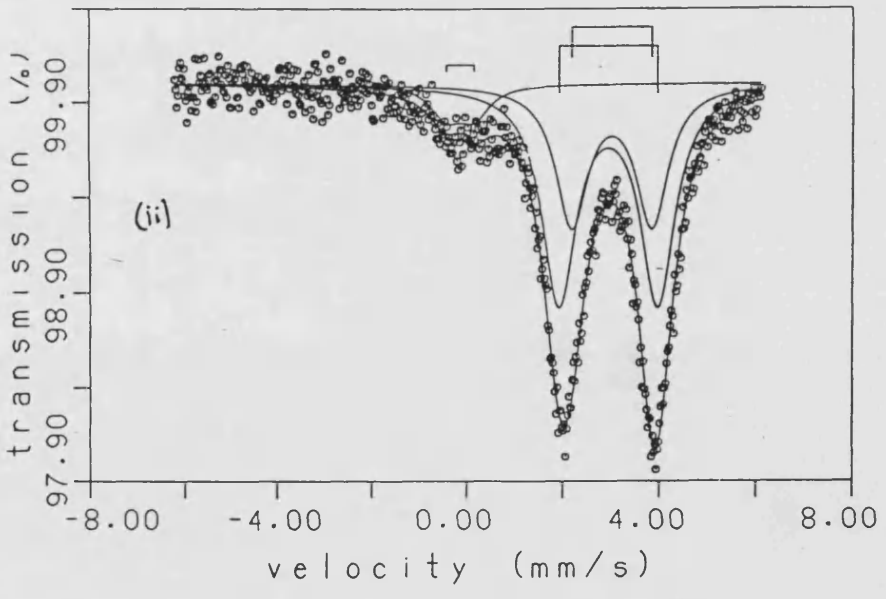

Figure 1.4. The Mössbauer spectra of (i) solid $Sn_2P_2O_7$ and (ii) $Sn_2P_2O_7$ in a toothpaste formulation.

1.11. ^{119}Sn Nuclear Magnetic Resonance

Tin has three naturally occurring isotopes with spin $\frac{1}{2}$, all others having spin = 0. These isotopes are ^{115}Sn (0.35% abundance), ^{117}Sn (7.61% abundance) and ^{119}Sn (8.58% abundance). Most commonly, tin-NMR studies have used the ^{119}Sn isotope because of its higher natural abundance. Compounds containing tin are usually amenable to study by several nuclei, and spectra can afford a substantial amount of information concerning bonding and stereochemistry. Because of the differing abundances of the different NMR nuclei present, spectra in which tin is involved in coupling to other nuclei are readily recognisable. This can be illustrated by looking at the spectra for tetramethyltin[145] (Figure 1.5).

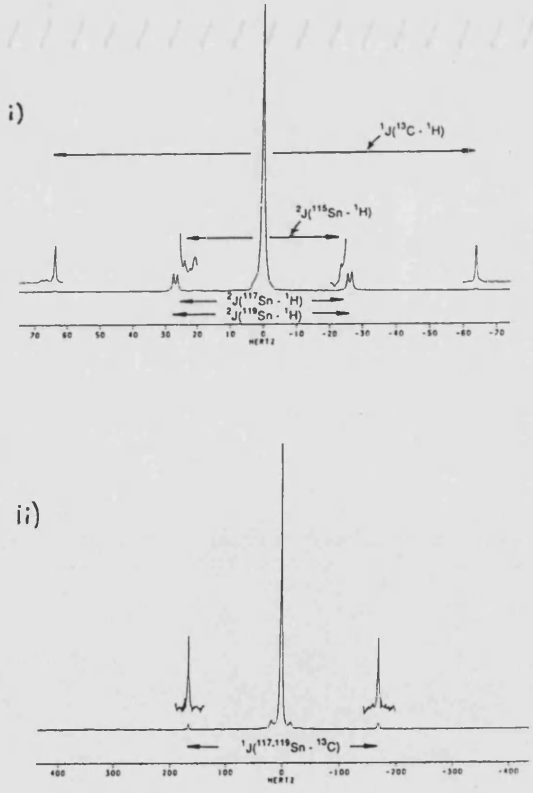

Figure 1.5. (i) ^{1}H NMR and (ii) ^{13}C NMR of Me_4Sn showing coupling.

As can be seen in Figure 1.4. both the ^{1}H and ^{13}C spectra comprise an intense central peak which is flanked on either side by two pairs of satellites due to the two-bond coupling to the ^{117}Sn and ^{119}Sn nuclei. In addition, in the ^{1}H spectrum two much weaker pairs of satellites can also be seen, due to two-bond coupling to ^{115}Sn and one-bond coupling to ^{13}C nuclei. The ^{119}Sn NMR spectrum, which is not shown, comprises thirteen peaks due to coupling to the twelve equivalent hydrogen nuclei. If any groups other than hydrogen were present the spectrum would become very complicated and for this reason ^{119}Sn chemical shifts are normally obtained from broad band decoupled spectra.

Tetramethyltin, with an absolute resonance frequency of (37290665±3) Hz is the universally adopted reference standard for ^{119}Sn chemical shifts. Conventionally, negative chemical shift values are upfield from $Me_4Sn = 0$. Tin chemical shifts span a large range (>4000 ppm), and the precise δ value is affected by a number of parameters. The major factors are the electronegativity of the groups attached to tin, geometric distortions which modify the interbond angles at tin, and the coordination number of the tin.

Due to the large range of δ values, ^{119}Sn NMR is a particularly useful tool for the characterisation of compounds. Unfortunately, the number of tin(II) compounds which have been studied using ^{119}Sn NMR is relatively small. This is probably due, in part, to the relatively low solubilities of many stannous compounds and the low abundance of the spin-active nucleii.

The ^{119}Sn NMR spectra of tin(II) halides in solution in donor solvents consist of single resonances, the chemical shifts of which are markedly solvent, concentration and temperature dependant in most cases.[146] The single peaks observed in these spectra indicate that rapid exchange among the tin species is operative. Thus, the observed shifts represent a time averaged view of the solvated species present. The δ values move downfield (become more positive) in the order $SnF_2 < SnCl_2 < SnBr_2 < SnI_2$. The difference in δ values of $SnCl_2.N(CH_3)_3$ and $SnCl_2$.DMSO is ca. 258ppm.[147] This can be

attributed to changes to the hybridisation, charge distribution and symmetry in the coordination sphere of the tin.

Unfortunately, neither copper nor zinc have NMR active nuclei, which reduces the number of methods available to fully characterise the Zn(II) and Cu(II) compounds synthesised. As Zn(II) is diamagnetic it is possible to obtain ^{1}H and ^{13}C NMR spectra for the zinc complexes, but as Cu(II) is paramagnetic (d^9) no NMR spectra could be obtained. In order to characterise the copper complexes further, ESR spectroscopy would be required.

A selection of chemical shifts of a number of tin(II) compounds can be seen in Table 1.4. (all δ values are relative to tetramethyltin).

Table 1.4. Selected ^{119}Sn NMR data for Sn(II) and Sn(IV) compounds.

COMPOUND	δ (ppm)	REFERENCE
$SnCl_2.N(CH_3)_3$	-111.8	147
$SnCl_2.Py$	-294.0	147
$SnCl_2.DMF$	-324.1	146
$SnCl_2.DMSO$	-369.5	147
$SnBr_2.DMSO$	-319.5	146
$SnBr_2.DMF$	-202.1	146
$SnF_2.DMSO$	-629.0	146
$(Me_5C_5)_2Sn$	-2129	148
$(C_5H_5)_2Sn$	-2199	149
$SnCl_4$	-150	150
$SnBr_4$	-638	150
SnI_4	-1701	150

1.12. Project Aims

Recent research[151] into stannous containing toothpastes has led to a Unilever patent based on a range of compounds which can be grouped together under the "bait-link-bactericide" concept:

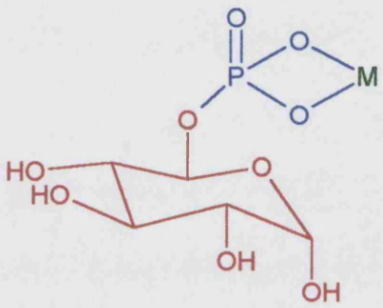

"Bait-link-bactericide"

This concept involves one part of the molecule acting as a "bait" for the bacteria (e.g. a sugar), connected via a link group (e.g. a phosphate) to a bactericidal metal ion (e.g. Sn^{2+}). The Sn(II) derivative has exhibited high anti-bacterial activity *in vitro*. The development of this concept affords the opportunity to synthesise and characterise a range of compounds, varying each of the 3 components, and to then evaluate their anti-bacterial properties. The use of different bactericidal metal ions, i.e. Zn^{2+} and Cu^{2+} needs to be investigated, as from a commercial aspect they are easier to synthesise than the stannous compounds. There are also less problems with stability (i.e. oxidation of the metal ion) once the compounds are formulated into a toothpaste.

An important feature of anti-bacterial agents is to achieve a balance between stability and activity, i.e. a stannous compound which is stable may well not be active. The evaluation of a new compound both in terms of anti-bacterial activity and chemical structure is therefore vital when evaluating this balance. The crystal structure of a compound which has either high, low or no anti-bacterial activity can prove to be important in assessing why the particular level of activity was attained.

It has long been known that using two or more anti-bacterial agents together can lead to synergistic effects in oral health products. For example, triclosan and zinc citrate (ZCT) have been used together in a number of products.[64-66] The investigation into other combinations of anti-bacterial agents is therefore of relevance, e.g. metal triclosan derivatives.

CHAPTER 2

SUGAR PHOSPHATES AND CARBOXYLATES

2. CHAPTER 2 - SUGAR PHOSPHATES AND CARBOXYLATES

2.1. Introduction

The biological importance of metal ions in anti-bacterial formulations has long been known. A problem over the years, however, has been how to deliver the anti-bacterial agent to the oral environment in a stable yet effective form. This problem is especially relevant to stannous anti-bacterial agents due to their poor stability with respect to oxidation. Historically, this problem has been overcome by utilising the chelating properties of other toothpaste ingredients such as sorbitol, which is known to stabilise Sn^{2+} ions.[50]

An improvement to this method of stabilisation would be to use a stannous anti-bacterial agent which is stable in its own right. This is, however, difficult to achieve in practice, because by producing a stannous compound which is too stable to oxidation (i.e. protects the Sn^{2+} ion by chelation) the release of Sn^{2+} ions in the oral environment is prevented. The subsequent decrease in the free stannous ion concentration would lead to a greatly reduced efficacy (effectiveness) of the compound as an anti-bacterial agent.

As mentioned in Chapter 1, the synthesis and subsequent use of zinc(II) and copper(II) compounds is significantly easier due to their greater stability with respect to oxidation. Compounds containing either Zn(II) or Cu(II) must be designed such that when in the oral environment the ions are easily released, to maximise their efficacy.

It is known that Sn(II) α-D-glucose-6-phosphate has shown high efficacy against certain bacteria.[151] In Chapter 1 the concept of "bait-link-bactericide" was presented, with the concept borne from this compound. Glucose, or more specifically glucose-6-phosphate, is a vital component of the glycolytic pathway, which is the way in which bacteria metabolise.[152] Glycolysis is the process by which glucose is anaerobically broken down to yield lactic acid. Glycolysis, an example of catabolism (the metabolic

breakdown of large molecules in living organisms to smaller ones - commonly referred to as anaerobic fermentation), is one process by which organisms can extract chemical energy from various fuels in the absence of molecular oxygen.

All of the compounds detailed in this chapter use glucose as the "bait" because, as glucose is known to be important in biological systems, it should therefore be an effective bait. The other elements of the concept have, however, been changed in an attempt to evaluate their importance. Various "links" have been examined, including carboxylate and ether, to see if any improvement over the phosphate link in α-D-glucose-6-phosphate could be gained. As well as the link, variations in the "bactericide" have been examined, using Zn(II) and Cu(II).

Historically, the carbon atoms in the glucose molecule have been numbered in a certain way (see Figure 2.1.) and this numbering will be adopted throughout this chapter.

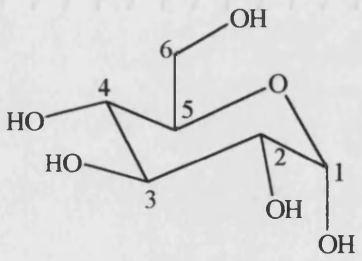

Figure 2.1. Atom labelling scheme in α-D-glucose.

The α notation for the above compound arises from the axial position of the hydroxyl group at C_1. If this hydroxyl group were equatorial, then the compound would be β-G6P. This anomeric form of glucose was not pursued as the stannous derivative has been found to exhibit less activity than the α-form in anti-bacterial tests.[151] It is known that D-glucose can exist as either a chain (with an aldehyde functional group) or ring. Most of the simple sugars that are known, including glucose, exist in the six-membered ring form, and when the hemiacetal is formed the former aldehyde becomes a stereocentre, hence the α and β forms of D-glucose. Interconversion between these two cyclic forms is subject to both acid and base catalysis. Maintaining a neutral solution during all syntheses ensures that the α-G6P starting materials, and subsequent products,

remain in this conformation and hence have a greater possibility of exhibiting high activity.

The synthesis and characterisation of a range of tin(II), zinc(II) and copper(II) sugar compounds for evaluation as anti-bacterial agents is detailed in this chapter. All of the compounds have been characterised using microanalysis, infrared, and, where applicable, NMR (Zn, Sn) and Mössbauer (Sn) spectroscopy. The anti-bacterial testing of the compounds was carried out at Unilever Research Port Sunlight Laboratory (URPSL), and this chapter introduces an assay, the acid inhibition experiment (pH Stat), which has generally been employed to evaluate the activity of potential anti-bacterial agents. The majority of the compounds detailed in this chapter were evaluated using the pH Stat assay, and the results are presented in this chapter.

2.2. Synthesis and Characterisation of M(II) Sugar Phosphates

2.2.1. Synthetic Strategies for the M(II) α-D-glucose phosphates

As mentioned in the Introduction, for an anti-bacterial agent to be active when incorporated into a toothpaste it must be stable. The glucose phosphates were chosen for formulation with metal ions in the hope of producing stable M(II) complexes. The idea was that the metal ions would be stabilised by the phosphate group, and also by the hydroxyl groups of adjacent glucose molecules, by coordination saturation.

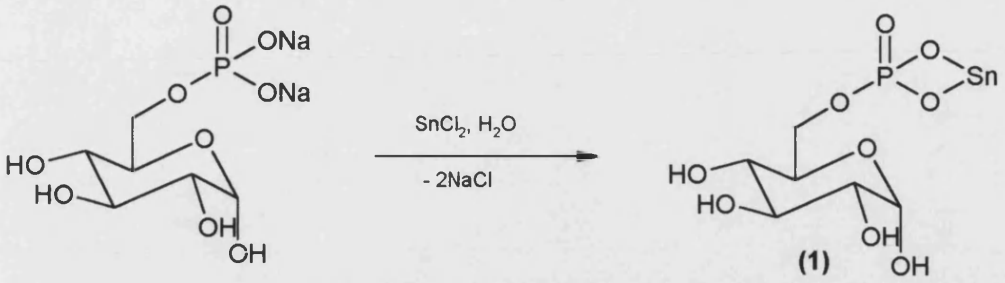

Scheme 2.1. Synthesis of tin(II) glucose-6-phosphate (**1**).

Sn(II)αG6P trihydrate (**1**) was prepared by the reaction of tin(II) chloride with Na_2αG6P in thoroughly degassed water (Scheme 2.1). The product, which was found to be soluble in water, was precipitated from solution by the addition of methanol. Attempted recrystallisations of this compound from common solvents (e.g. MeOH, THF) proved unsuccessful, yielding powder precipitates rather than crystals. The low solubility of the amorphous white solid points to the compound being polymeric, not monomeric as the above scheme suggests.

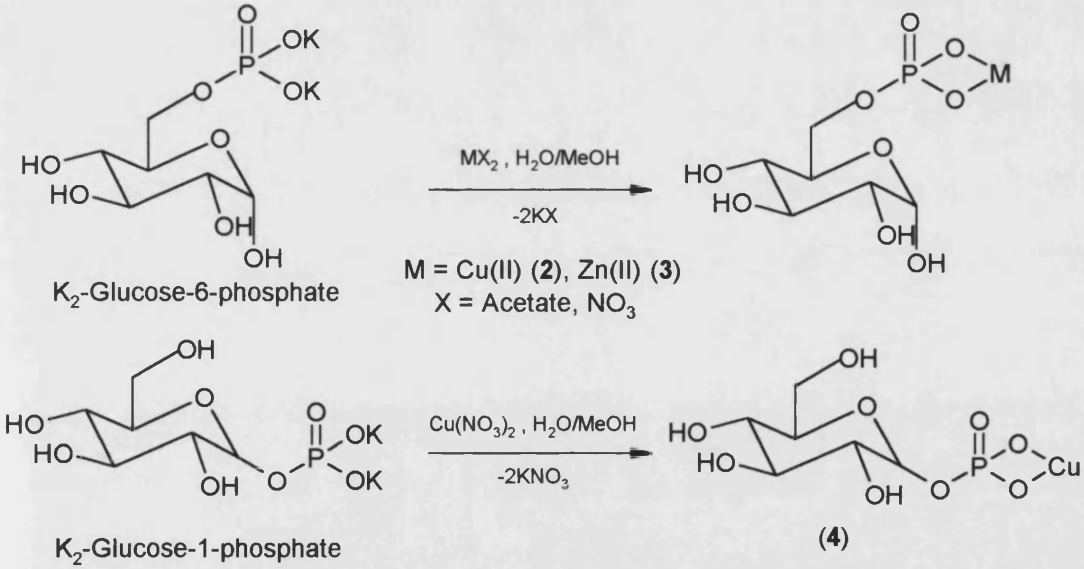

Scheme 2.2. Synthesis of copper and zinc glucose phosphates.

Cu(II)αG6P (**2**), Zn(II)αG6P (**3**) and Cu(II)αG1P (**4**) were prepared using the reactions shown in Scheme 2.2. In all three cases, the products were precipitated from a water/methanol solution upon addition of the MX_2 reagent. The physical properties of

the compounds varied in that Zn(II)αG6P and Cu(II)αG1P were water soluble, whilst Cu(II)αG6P was much less soluble in water. The three products were all insoluble in common recrystallisation solvents which could indicate similar structural features to that of Sn(II)αG6P. The synthesis of Zn(II) α-D-glucose-1-phosphate was also completed, but the product was found to be too hygroscopic to obtain meaningful analytical data.

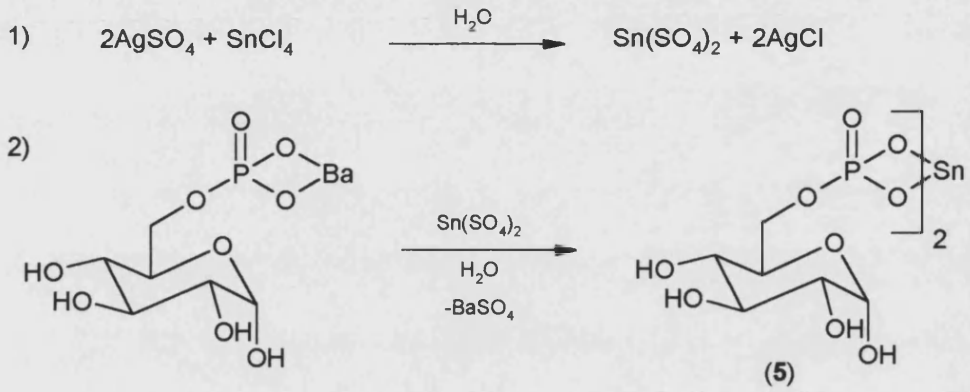

Scheme 2.3. Synthesis of tin(IV) α-D-glulcose-6-phosphate (**5**).

A slightly modified method (Scheme 2.3) using $SnCl_4$ was adopted for the production of Sn(IV)αG6P heptahydrate (**5**). This method involved the *in situ* production of stannic sulphate, with a solid silver salt as the by-product which was removed by filtration. Attempts to isolate the intermediate stannic sulphate proved unsuccessful, which was not unexpected as there is no known structure for tin(IV) sulphate. Once the silver chloride had been filtered, the addition of BaαG6P caused the precipitation of $BaSO_4$, which was filtered to leave the product, Sn(IV)αG6P, in solution. Removal of the water under reduced pressure yielded the product which was found to be a heptahydrate.

The structures of the products of the reaction of metal salts with α-D-glucose phosphates are likely to be more complex than those shown. It is likely that the free hydroxyl groups of the glucose are involved in hydrogen bonding with other glucose molecules and also in chelation to the metal ion. The microanalytical data suggests all of the glucose phosphate compounds produced were hydrated and it is likely that the water molecules are also involved in hydrogen bonding in the complex.

2.2.2. Comparison of infrared spectra for M(II) α-D-glucose phosphates

A comparison of the infrared spectra of compounds **1-5** yields similarities, as one would expect. The most notable similarity was that there was no band observed in the region 1300-1250cm^{-1} due to υ(P=O), though a broad band was observed in the 1200-1000cm^{-1} region due to υ(P-O), suggesting that the P-O bond order is always lower than 2. The implication of this is that the P=O unit is either coordinated to the metal ion or involved in H-bonding to the waters of crystallisation. The exact position of υ(P=O) could give an indication as to extent to which the P=O character has been distorted in the formation of the metal complex, i.e. the lower the value of υ(P=O), the lower the bond order.

In the tin and zinc α-D-glucose phosphate complexes the υ(P=O) appears in roughly the same position (ca. 1110cm^{-1}). This implies a significant reduction in the P=O in all of the complexes, although it is difficult to predict the exact nature of the interactions between the metal ions and the glucose phosphates without crystallographic data. In the two copper α-D-glucose phosphate complexes the υ(P=O) appears at a higher wavenumber (ca. 1150cm^{-1}), which implies there is more double bond character in these compounds.

The reduction of the P=O double bond character in the glucose phosphate complexes can thus be roughly observed using infrared spectroscopy although the results are by no means conclusive proof that the P=O is involved in bonding. Precedent that the P=O is involved in coordination can be found by looking at three glucose phosphate compounds for which crystal structures have been solved: K_2αG1P dihydrate[153]; Ba(II)αG6P heptahydrate[154]; α-D-glucose-6-(sodium hydrogen phosphate).[155] The respective bond-lengths for these compounds are listed in Table 2.1.

The schematic depicted in Figure 2.2. directly corresponds with the bond numbering of the glucose phosphates in Table 2.1. As can be seen from Table 2.1, the bond between the P-O-Glucose is identical (within experimental error) for all three of the

compounds - ca. 1.59Å. The interesting conclusion which can be drawn from Table 2.1 is that there is no evidence of one bond being significantly shorter than any other. It is notable in the third example, NaHαG6P, that the P-O(4) bond is longer than in the other two examples, the reason being that this is a P-OH bond.

Table 2.1. P-O bond lengths for glucose phosphate compounds.

Compound	P-O(1)/Å	P-O(2)/Å	P-O(3)/Å	P-O(4)/Å
K_2αG1P.2H_2O	1.59(3)	1.48(3)	1.52(3)	1.53(3)
BaαG6P.7H_2O	1.61(1)	1.51(1)	1.51(2)	1.53(1)
NaHαG6P	1.58(1)	1.49(1)	1.52(1)	1.59(1)

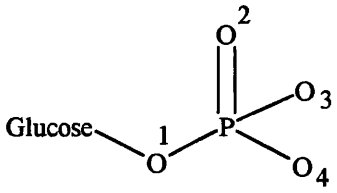

Figure 2.2. Schematic of the phosphate functional group in the glucose phosphate compounds.

It is known that in Ba(II)αG6P there are intermolecular interactions between the plethora of available oxygens and hydrogens, forming a spiral arrangement,[154] with the hydroxyl groups taking part in hydrogen bonding both as acceptors and as donors. The crystal structure of Ba(II)αG6P heptahydrate (Figure 2.3) shows how the metal ions interact with the glucose phosphate, and how the intermolecular hydrogen bonding contributes to the spiral structure.

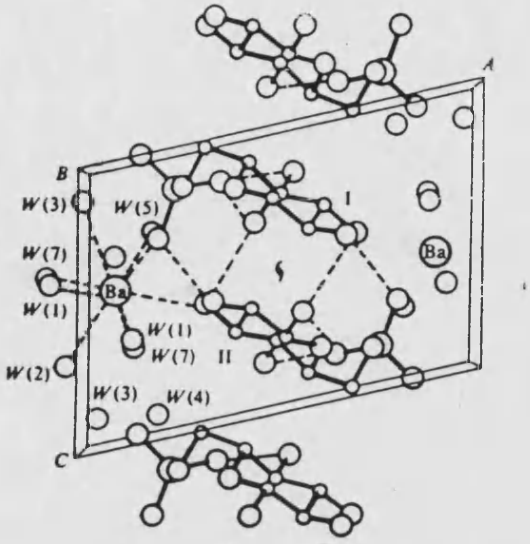

Figure 2.3. Packing arrangement within the Ba(II)αG6P crystal structure.[154]

The molecules (I) and (II) {shown in Figure 2.3}, related by the twofold screw axis, are linked to one another via three hydrogen bonds which arrange the molecules in a spiral fashion around the screw axis. The Ba^{2+} ions and water molecules link adjacent columns of αG6P molecules. The phosphate group exists as a dianion as the compound is a Ba^{2+} salt. As shown in Table 2.1 the three terminal P-O bonds are nearly equal [1.51(1)Å, 1.51(2)Å, 1.53(1)Å] and the double negative charge is distributed between the three oxygen atoms. This gives precedent for a structure in which there is no formal P=O bond, and implies that the phosphate group is involved in bonding as shown in Figure 2.4.

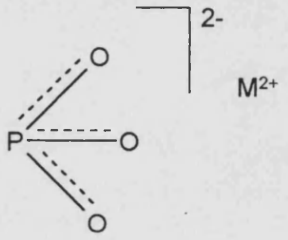

Figure 2.4. Mode of bonding of the phosphate group in Ba(II)αG6P.

The structures of NaHαG6P and K_2αG6P also show a large amount of intermolecular hydrogen bonding as one would expect. The packing arrangement is not

the same as the Ba(II)αG6P, as the spiral structure is not observed in either NaHαG6P or K_2αG6P. The reason for the different packing arrangements can be accounted for by looking at the conformation of the phosphate group with respect to the glucose ring. As shown in Figure 2.5 the phosphate group in the Ba(II)αG6P is in a completely different conformation, with respect to the C_5-C_6 bond, than the phosphate group in the NaHαG6P.

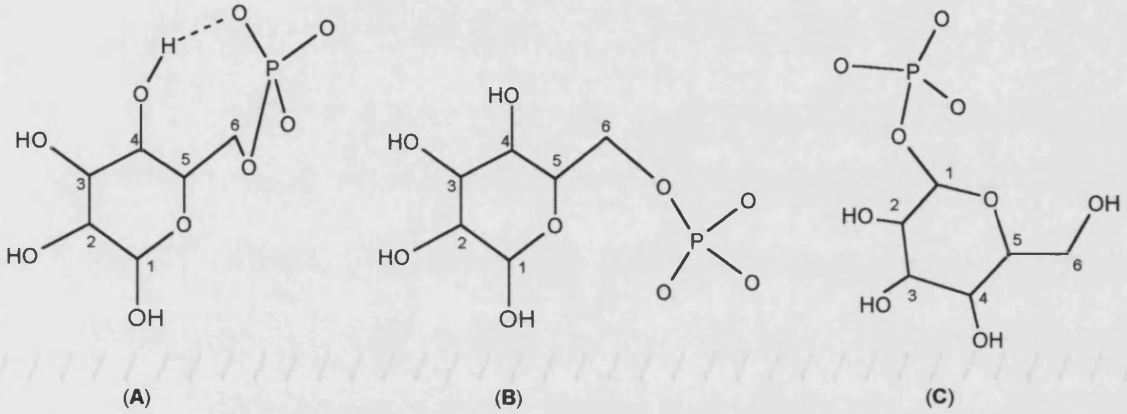

Figure 2.5. Conformation of the phosphate groups in Ba(II)αG6P (**A**), NaHαG6P (**B**) and K_2αG1P (**C**), showing intramolecular hydrogen bonding in (**A**).

As well as the intermolecular H-bonding, Ba(II)αG6P also exhibits a degree of intramolecular hydrogen bonding between one of the phosphate oxygens and a ring hydroxyl group (2.62Å), as depicted in Figure 2.5.[154] As can be seen from this Figure, there is no possibility of intramolecular H-bonding in either of the other two complexes.

The evidence gained from these crystal structures supports the findings of the infrared experiments, carried out on the tin, zinc and copper glucose phosphates, that there is no formal P=O double bond in the glucose phosphate compounds described in this chapter.

2.2.3. Comparison of the NMR and Mössbauer spectra of the M(II) α-D-glucose phosphates

In order that one may interpret the ^{1}H NMR spectra of the glucose phosphate compounds it is important to realise that the spectra are very complicated with a large number of peaks. The reason for the numerous peaks is that in a ring system such as glucose the hydrogen atoms can occupy various positions in space and can therefore couple to other nuclei when in axial or equatorial orientation. The magnitude of the coupling constant is related to the relative orientations of the hydrogen atoms in space. Glucose is similar to cyclohexane in that two chair forms are possible, and the least repulsive interactions will predominate. It has been found that there is a 6 kcalmol^{-1} difference in favour of the α-isomer. In glucose the preferred conformation for the CH_2OH group is equatorial, hence the depiction of the αG6P as in Figure 2.1.

All of the NMR data collected for the glucose phosphates used D_2O as the solvent and, consequently, peaks in the ^{1}H NMR due to the exocyclic hydroxyl groups are not observed due to deuterium exchange.

As with the ^{1}H NMR spectra, the ^{13}C NMR spectra obtained for the sugar phosphates (a selection of which are presented in Table 2.2) are more complex than would be expected from the proposed structures.

Table 2.2. ^{13}C NMR data for glucose phosphates.

Compound	C_1	C_2	C_3	C_4	C_5	C_6
α-D-glucose[156]	92.9	72.5	73.8	70.6	72.3	61.6
αG6P[157]	93.0	72.2	73.3	69.9	71.3	64.8
Sn(II)αG6P (**1**)	96.9	73.5	76.4	74.9	72.2	65.3
Zn(II)αG6P (**3**)	95.7	73.9	74.5	75.1	72.2	63.4

There are only six carbon atoms in each of the compounds, but the ^{13}C spectra typically contain more than 6 peaks. In the spectrum recorded for Sn(II)αG6P (**1**), 12 peaks are evident with two peaks significantly downfield to the others (96.9 and 92.9ppm). These peaks are in the area of the spectrum where one would expect to see ^{13}C chemical shifts for C_1 of a glucose compound. The peak at 96.9ppm has been assigned to the C_1 of Sn(II)αG6P because the other peak has a chemical shift in an identical position to the αG6P (δ =93.0ppm). The reason for the two peaks could be that in solution there is a mixture of species present, i.e. Sn(II)αG6P and αG6P. Of the other peaks present in the spectrum, five correspond directly to the known values of αG6P thus strengthening this hypothesis. Another explanation for the presence of the extra peaks could be that in solution the Sn(II)αG6P exists as a dimer.

Comparison of the Sn(II)αG6P (**1**) and Zn(II)αG6P (**3**) ^{13}C NMR with the data for the αG6P show small but noticeable downfield shifts in the corresponding peak positions where chelation to the tin or zinc is taking place. In Sn(II)αG6P the peaks due to C_1, C_3 and C_4 have shifted downfield (3.9, 3.1 and 5.0ppm respectively) with the other peaks effectively unchanged. These results could indicate that the chelation of the Sn(II) occurs through each of these sites, although that to C_4(OH) is the strongest. The position of the phosphate group in Ba(II)αG6P (shown in Figure 2.5) is such that if Sn(II)αG6P was to adopt a similar structure, then the Sn(II) would be close enough to C_4(OH), and to a lesser degree C_3(OH), to cause chelation. In the absence of crystallographic data it is not possible to say with any conviction whether the apparent downfield shift of the two peaks is due to chelation to the metal ion or hydrogen bonding. The reason for the change of 3.9ppm in the chemical shift due to C_1 is probably due to either intermolecular chelation to the Sn(II), or intermolecular hydrogen bonding. The peak observed for C_6 is much easier to identify as it appears ca. 3-7ppm downfield of the corresponding peak in α-D-glucose, due to the presence of the phosphate group to which it is coupled.

The ^{31}P NMR spectra obtained for the tin and zinc αG6P show a similarity in that there is only one peak in each spectrum indicating a single phosphorus environment in

solution. The chemical shifts, however, vary by ca. 14ppm, with the Sn(II)αG6P (**1**) exhibiting a shift of -9.7ppm, Sn(IV)αG6P (**5**) a shift of -0.1ppm and the Zn(II)αG6P (**3**) a shift of 4.1ppm. Although the chemical shifts are different, the difference is too small to enable any conclusions to be drawn regarding the environment of the phosphate groups and metal ions in the complexes.

The ^{119}Sn NMR data obtained for Sn(II)αG6P and Sn(IV)αG6P are presented in Table 2.3, along with other Sn(II) and Sn(IV) compounds where the tin has a coordination number of 6.

Table 2.3. ^{119}Sn chemical shifts in various compounds.

Compound	Sn oxid. No.	δ(ppm)	Reference
Sn(II)αG6P (**1**)	+2	-681	This work
Sn(IV)αG6P (**5**)	+4	-674	This work
Sn(II)βG6P	+2	-718	151
$Na_2[Sn(OH)_6]$	+4	-592	158
$K_2[Sn(OH)_6]$	+4	-590	158

The ^{119}Sn NMR spectrum of (**1**) shows just one peak (δ= -681ppm) which is evidence of a single tin environment in solution, a result which is consistent with the results of the ^{31}P NMR experiment, i.e. only one phosphorus environment. The spectrum obtained for the Sn(IV)αG6P yielded an unexpected result in that the chemical shift (δ = -674ppm) was almost identical to the result of the Sn(II)αG6P. It is known that chemical shifts of Sn(II) compounds are not necessarily in a different region to those of Sn(IV) compounds, that is, the chemical shifts of $SnSO_4$ and $SnCl_2$ are within the same range as those for the stannic compounds.[159] The results of the NMR experiments thus suggest that in both the tin(II) and tin(IV) αG6P complexes, the coordination sites of the tin are similar. The ^{119}Sn NMR chemical shift is comparable to other compounds (see Table 2.3) where the tin ion (either Sn^{2+} or Sn^{4+}) is surrounded by 6 oxygen atoms.

The results from the ^{31}P and ^{119}Sn NMR obtained for the Sn(II) and the Sn(IV)αG6P indicate that there is only one tin and phosphorus environment in solution. This evidence, together with that obtained by ^{13}C NMR, suggests that the species which is present in solution is likely to be dimeric, and not a mixture of Sn(II)αG6P and αG6P (which would probably lead to more than one ^{31}P chemical shift).

As mentioned in Chapter 1, Mössbauer spectroscopy is a useful tool for analysing Sn(II) compounds as spectra obtained using this technique allow differentiation between Sn(II) and Sn(IV) very quickly and easily. The only problem with using Mössbauer for Sn(II) compounds is that the value of the quadrupole splitting does not yield the same structural information as it does for Sn(IV) compounds because of the presence of the stereochemically active lone pair.

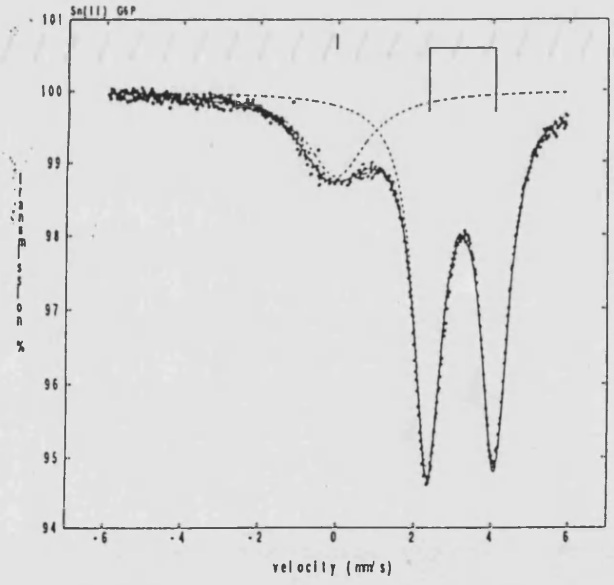

Figure 2.6. ^{119m}Sn Mössbauer spectrum of Sn(II) αG6P (**1**).

From the spectrum depicted in Figure 2.6, it can be concluded that the tin in this compound is indeed in its lower (+II) oxidation state with the isomer shift (δ) of 3.21mms^{-1}, falling within the range of $2.5<\delta<5.0$, indicative of tin(II) compounds.[131,134,135,160] Also evident from the spectrum is the low level of tin(IV) impurity, i.e. the compound is quite pure in terms of its stannous content. The tin(IV) impurity (less than 2% by peak area) is evident in Figure 2.6 as a small peak (not marked

but evident from baseline scatter) at ca. 0mms^{-1}. The main feature of this spectrum is a doublet with a quadrupole splitting (Δ) value of 1.75mms^{-1}, a feature which indicates that the tin atom is in an asymmetrical environment. In this compound the tin atom is surrounded by oxygen atoms and a lone pair of electrons, and changes in the oxygen coordination sphere around the tin probably account for the asymmetrical environment, and subsequent quadrupole splitting. The Δ value obtained for Sn(II)αG6P is typical of compounds containing Sn-O bonds as shown in Table 2.4 which contains the quadrupole splitting values of a range of tin(II) compounds of varying coordination number.

Further information regarding the nature of the compound can be obtained by looking at the linewidths in the spectrum. For Sn(II)αG6P (**1**), the linewidths Γ_1= 1.07mms^{-1} and Γ_2= 0.94mms^{-1} are unequal and could indicate the presence of more than one tin environment in the compound in the solid state. The unequal linewidths could be due to the amorphous (i.e. not ordered) nature of the solid compound, causing subtle local variations in the tin coordination.

Table 2.4. Quadrupole splitting values of various Sn-O compounds

Compound	C.N.	Quadrupole Splitting (mms^{-1})	Reference
SnO	4	1.50	134
$Sn(OCH_3)_2$	4	2.02	160
$Sn(OC_2H_5)_2$	3	1.92	160
$[Sn_3(OH)_4][NO_3]_2$	4	1.85	161
$Sn(O_2CH)_2$	4	1.70	119
Sn(II)αG6P (**1**)	6[a]	1.75	This work

[a] - Estimated CN, based on EXAFS data from Ref 151.

As mentioned previously, the Mössbauer spectrum of Sn(II)αG6P contains a singlet (less than 2% by peak area) with an isomer shift of ca. $0mms^{-1}$, due to a small amount of Sn(IV) impurity. The size of this singlet can be used to monitor the degree of oxidation from Sn(II) to Sn(IV) upon exposure to air. After being exposed to air for 3 months the peak area of the singlet had not altered, indicating that the stannous compound is very air stable. This is a property of stannous anti-bacterial agents which is vital if the agents are to be effective. It is known that Sn(IV) ions exhibit no activity against oral bacteria, and thus a compound in which the Sn(II) ions are stable has a much greater probability of being active. The stability of the compound to air is not the only property which needs evaluating in order to determine if it will be effective as an anti-bacterial agent in a toothpaste. For this reason the Sn(II)αG6P was incorporated into a toothpaste (1% w/w) and incubated at 37°C for 3 months, after which time a Mössbauer experiment was carried out to determine the degree of oxidation which had occurred. The peak area of the singlet (δ= $0.00mms^{-1}$) was found to be ca. 8-10%. This small peak area is good evidence that even after storage the toothpaste would retain its activity, as a high percentage of the sample still contains the tin in its lower oxidation state.

The Mössbauer spectrum for the Sn(IV)αG6P.$7H_2O$ (**5**) has, as expected, a much lower isomer shift (δ= $-0.09mms^{-1}$) than the corresponding Sn(II)αG6P. In the spectrum the peak appears as a broad singlet (Γ= $1.28mms^{-1}$) which probably reflects a narrow doublet, which was not resolved.

Figure 2.7 contains three Mössbauer spectra: (i) Sn(II)αG6P (**1**); (ii) Sn(II)αG6P in a toothpaste after 3 months storage at 37°C; (iii) Sn(IV)αG6P (**5**).

The three spectra clearly show the ease with which one can distinguish between Sn(II) and Sn(IV) compounds using Mössbauer spectroscopy. What is shown in Figure 2.7 is a pure Sn(II) compound, followed by a Sn(II) compound which has been partially oxidised in a toothpaste, and a pure Sn(IV) compound. One can clearly see the peak which is due to the Sn(IV) beginning to appear in spectrum (ii) as the sample oxidises.

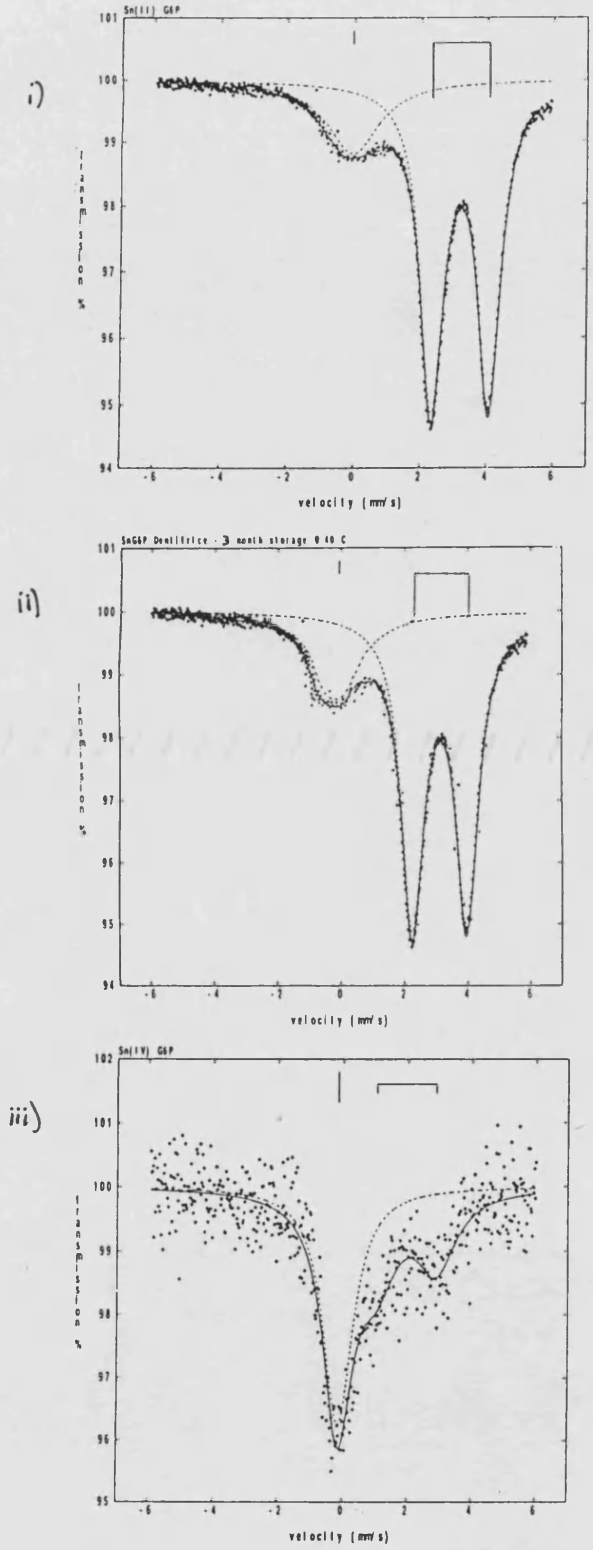

Figure 2.7. ^{119m}Sn Mössbauer spectra of (i) Sn(II)αG6P, (ii) Sn(II)αG6P in a toothpaste after 3 months storage, and (iii) Sn(IV)αG6P.

2.3. Synthesis and Characterisation of M(II) Sugar Carboxylates

The compounds detailed in this section are borne from the "bait-link-bactericide" concept, and, as can be seen from the structures, all contain the same "bait" and "bactericides". This section looks at compounds which have a different "link" group - either a carboxylate [M(II)lactobionates] or an alkoxide group [Sn(II)mannoheptose].

2.3.1. Synthetic Strategies for the M(II) lactobionates

Lactobionic acid (**IV**), which is derived from the oxidation of the glucose unit of lactose, contains both a glucose moiety and a gluconic acid residue. Like the anions of other hydroxycarboxylic acids, the gluconate ion binds calcium ions in aqueous solution.[162] D-Gluconic acid (**V**) is a straight chain form of glucose, and is shown in Figure 2.8.

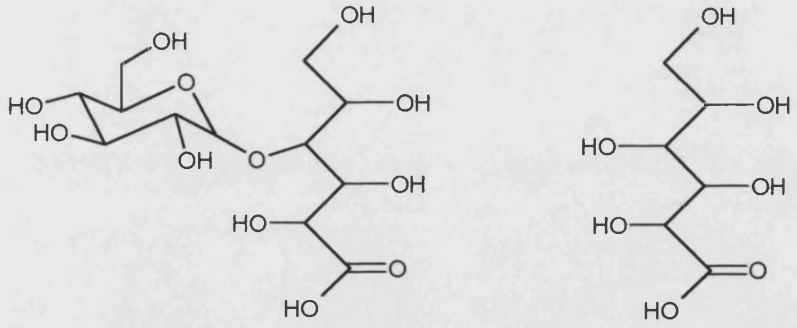

(**IV**) (**V**)

Figure 2.8. Structure of uncoordinated lactobionic acid (**IV**) and D-gluconic acid (**V**).

Tin(II) lactobionate chloride monohydrate (**6**) was prepared by the reaction of lactobionic acid hemi-calcium salt with stannous chloride in degassed water, as shown in Scheme 2.4. The product of the reaction was isolated from solution by the addition of degassed methanol which caused precipitation. The compound was a readily water soluble white solid which, according to microanalytical data, was monohydrated.

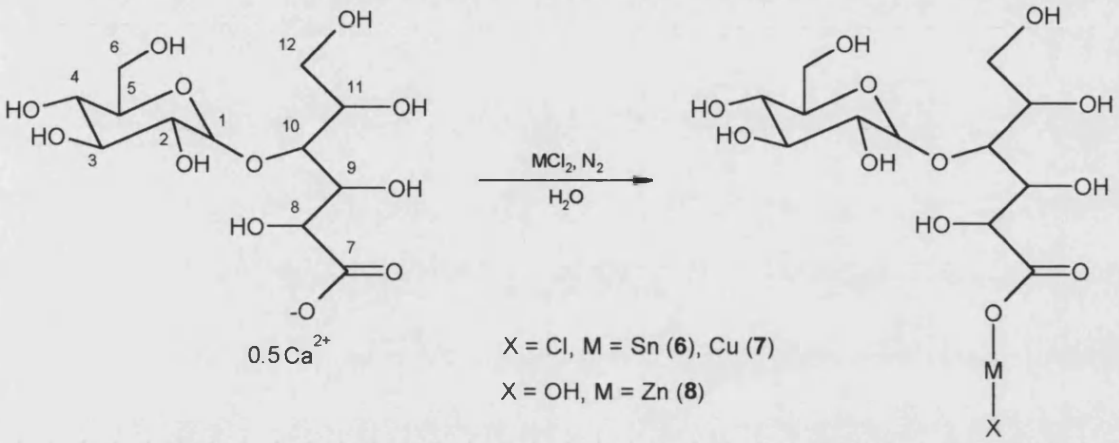

Scheme 2.4. Synthesis of M(II) lactobionates, including atom numbering.

The Cu(II) and Zn(II) lactobionate derivatives (**7** and **8** respectively) were prepared using a similar method to the tin compound, without the need for degassed water. The products of both reactions were isolated from solution by the addition of methanol, which again caused precipitation. The Cu(II) lactobionate was found, from microanalysis, to be trihydrated. The microanalysis obtained for the Zn lactobionate yielded a strange result in that a good fit could not be attained assuming a complex such as that adopted by the Cu and Sn complexes. The results of the microanalysis appeared to be a good fit for a complex where the zinc ion is coordinated to the carboxylate oxygen of the ligand and to a hydroxyl ligand as shown in Scheme 2.4. The proposed structure for the zinc lactobionate complex is discussed in more detail later in this chapter.

All of the compounds **6-8** were found to be water soluble, although attempted recrystallisations from water proved unsuccessful. The complexes were found to be insoluble in all common recrystallisation solvents (e.g. MeOH, THF).

2.3.2. Comparison of infrared spectra for the M(II) lactobionates

The infrared spectra for these compounds are similar in that they each contain a peak at ca. 1600cm^{-1}, due to υ(C=O). This is similar to the observed peak in the spectrum of the hemi-calcium salt, but ca. 130cm^{-1} different to the carbonyl stretch observed for the uncoordinated lactobionic acid. This difference can be attributed to the coordination of the metal ion to the carbonyl group.

Table 2.5. υ(C=O) for a range of M(II) carboxylates.

Compound	Carboxyl bonding	υ(C=O) cm^{-1}	Reference
Lactobionic acid	N/A	1736	This work
Sn(II) lactobionate (**6**)	?	1600	This work
Cu(II) lactobionate (**7**)	?	1605	This work
Zn(II) lactobionate (**8**)	?	1595	This work
$Zn(O_2CCH_3)_2\{SC(NH_2)_2\}_2$	Unidentate	1559	163
$Hg(O_2CCH_3)_2$	Unidentate	1556	164
$Zn(O_2CCH_3)_2(H_2O)_2$	Chelating	1550	165
$Hg(O_2CCH_3)_2(PBu_3)$	Chelating	1575	166
$Zn_4O(O_2CCH_3)_6$	Bridging	1639	165
$\{Cu_2(O_2CCH_3)_4\}2H_2O$	Bridging	1603	167

The infrared spectroscopic data of carboxylic acids (a selection of which is presented in Table 2.5) can reveal information as to the mode of bonding.

It is known that carboxyl groups can adopt any of 4 possible bonding modes,[168] as shown in Figure 2.9. The 4 types of bonding shown are: (I) ionic or uncoordinated, (II) unidentate, (III) bidentate chelating, and (IV) bidentate bridging. Of the four, only II and III need be considered as possibilities for M(II) compounds. The ionic mode of bonding is only applicable to highly electropositive elements such as Na^+ and K^+.[168] The fourth mode of bonding, bidentate bridging, can be discounted based on the

microanalysis results which indicated that only 1:1 metal:ligand complexes were produced.

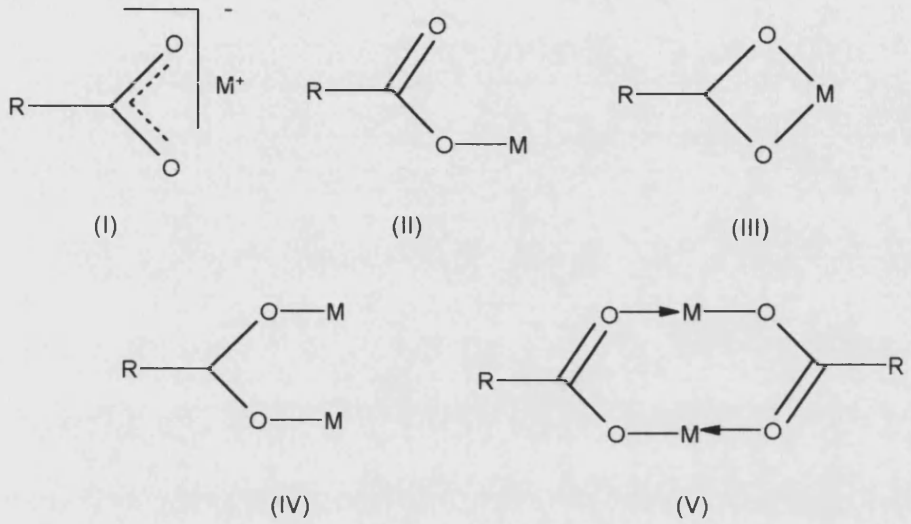

Figure 2.9. Modes of bonding of carboxylates.

Figure 2.9 also shows a fifth possibility for the bonding adopted by the lactobionate complexes, namely a dimer. This type of structure could be adopted by the lactobionates, however it would give rise to the same type of carboxyl bonding as II, (due to hydrogen bonding) and would therefore not affect the infrared stretching frequency.

The other two modes of bonding are quite difficult to differentiate between based on infrared stretching frequencies alone. This difficulty arises due to the occurrence of hydrogen bonding between solvent molecules and the uncoordinated C=O in the unidentate (II) example, which has the effect of lowering the υ(C=O). This lower υ(C=O) would thus appear in a similar position on an infrared spectrum to the υ(C=O) for a bidentate chelating carboxyl group (III) where the effective bond order is between 1 and 2.

The assignment of the mode of bonding of the carboxyl group in the M(II) lactobionates is not possible based solely on the infrared data, and further analyses are thus required.

2.3.3. Comparison of the NMR and Mössbauer spectra of the M(II) lactobionates

In the NMR discussion of the lactobionates the chemical shifts of the carbon atoms in the glucose ring have been omitted as it is known that the glucose portion of the lactobionate complexes is not involved in coordination to the metal ions,[162] and shifts were effectively constant in all the compounds studied.

The ^{1}H NMR and ^{13}C NMR for lactobionic acid (**IV**), and the two diamagnetic M(II) lactobionate complexes (**6** and **8**), both contained a number of peaks close together which were difficult to assign unambiguously. A full assignment of the ^{13}C chemical shifts has been made on the basis of a published ^{1}H-^{1}H coupled two-dimensional ^{1}H-^{13}C chemical shift correlation NMR spectrum.[169] This paper detailed the complete assignment of the ^{13}C chemical shifts of lactobionic acid in D_2O with a high degree of accuracy, due to the confident assignment of the ^{1}H NMR peaks.

Table 2.6. ^{13}C NMR of selected metal complexes with D-gluconic acid and lactobionic acid (all spectra recorded in D_2O).

Compound	C_7	C_8	C_9	C_{10}	C_{11}	C_{12}
Lactobionic acid (**IV**)[169]	180.8	74.8	73.9	83.9	74.1	64.3
Sn(II) lactobionate (**6**)	179.6	75.9	71.9[a]	82.1	72.3[a]	62.5
Zn(II) lactobionate (**8**)	179.3	74.3	71.9[a]	82.2	71.8[a]	62.8
D-Gluconic acid (**V**)[157]	179.8	75.2	72.4	73.8	72.0	63.5
Zn(II) D-gluconate[170]	179.1	74.0	72.1	73.2	71.7	63.5

Note:- [a] Tentative assignments

The tentative assignments of the peaks for the gluconate portion of compounds **6** and **8** were made based on the results of the 2D NMR investigation.

The paper from which the NMR data for the lactobionic acid was taken also detailed the formation of an Fe(III) lactobionate complex.[169] Potentiometric and UV investigations were carried out on a range of different ligand-metal ratios, and the findings were that regardless of the ratio used, only the 1:1 complex was formed. The equilibrium potentiometric profiles of the Fe(III) lactobionate system showed the release of varying numbers of protons from the complex, in addition to the carboxylate proton, depending on the pH at which the experiment was carried out(see Table 2.7).

Table 2.7. Complex formation of iron lactobionates at varying pH.

pH	Number of protons removed	Complex formed
<5.5	2	$[Fe.Lact.]^+$
5.5<pH<7.5	3	[Fe.Lact.]
>7.5	4	$[Fe.Lact.]^-$

The information gained from the potentiometric experiment alone was not sufficient to determine which protons were being removed in addition to the carboxylate proton (which is always removed first). In order to attain this information a series of NMR experiments were run, in alkaline solution, with increasing concentrations of Fe(III). By observing the peak broadening in the ^{13}C NMR spectra it was possible to accurately predict which protons were being removed. From this experiment it is known that the carbons which are most affected in alkaline conditions are C_8, C_9 and C_{11}. This implies that protons are being removed from the hydroxyl groups attached to these three carbons, in addition to the carboxylic proton The paper does not assign which protons are removed in the formation of the iron complexes at lower pH.

Since it is known which protons are removed during complexation, the nature of the bonding in the complex can be alluded to. It is known that at high pH the Fe(III) is chelated to four oxygen atoms of just one lactobionate molecule, and for this to occur the gluconate portion of the molecule must be in a different conformation to that shown

in Figure 2.8. According to the findings of the potentiometric, UV and NMR experiments, the structure is likely to be similar to that shown in Figure 2.10.

The findings of this paper give an indication as to the possible structure of the Sn(II) (**6**) and Cu(II) lactobionate chloride (**7**). Instead of the coordinated water molecule as depicted in the Fe(III) example, in the copper and tin compounds it is possible that a chlorine atom takes this place. This would imply that during the reaction of M(II) chloride with the lactobionic acid, only one of the chloride ions is displaced by the ligand and that chelation occurs in a manner similar to the iron lactobionate.

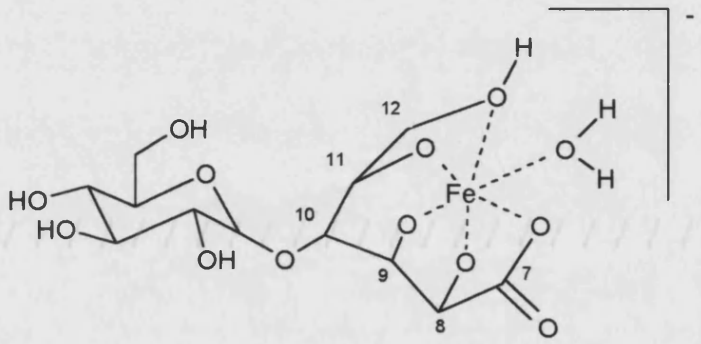

Figure 2.10. Possible coordination environment of Fe(III) in the lactobionate complex in alkaline solution.

It is notable from the structure depicted in Figure 2.10 that the C=O is not involved in chelation to the Fe(III). This implies that the carbonyl group in this compound is adopting a unidentate mode of bonding. Unfortunately, the paper does not report an infrared spectrum of the complex, so it is not possible to see where the υ(C=O) appears for comparison with the M(II) lactobionates.

Figure 2.11 shows representations of the possible M(II) sites within the copper and tin lactobionate complexes. Using a direct correlation to the iron lactobionate reference, the complex one would expect to see would be (**I**). In this example the carboxylic proton and one other have been removed in the complexation of the tin, leaving a neutral complex. This example does not, however, contain any chloride ion, which the microanalysis suggests is present in the complex. Incorporation of a chloride ion into the complex would lead to (**II**), which again is a neutral complex and contains

the proposed O-M-Cl bond. There is little, if any, precedent for O-M-Cl units in the literature which leads to (**III**), which is similar to (**II**) except that the C=O is involved in bonding this time.

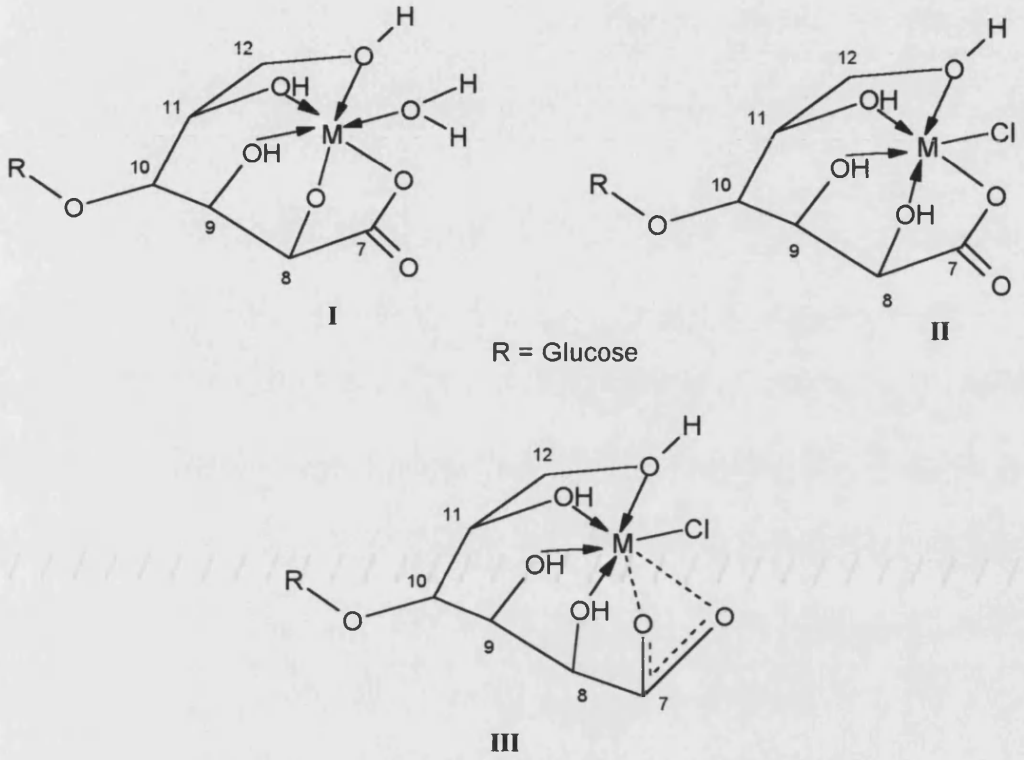

Figure 2.11. Possible coordination sites of the M(II) ion in the lactobionate complex.

The knowledge that the ligand chelates to the metal ion as in the Fe(III) example, i.e. in a 1:1 manner, suggests that steric crowding plays a large part in the formation of the product. Also suggested by the 1:1 complex is that one lactobionate ligand can saturate the metal, without the need for a second ligand, which would give precedent to the presence of the M-Cl bond in the product at the expense of a second, polydentate ligand.

The proposed structure for the zinc lactobionate complex is different to the tin and copper lactobionates in that there is no chloride or waters of crystallisation present. The microanalysis (found: C, 32.2; H, 5.83) is further out when calculating for Zn(II) lactobionate chloride (C, 31.4; H, 4.6) than for Zn(II) hydroxy lactobionate (C, 32.8; H,

5.05). Allowing for two solvent (MeOH) molecules in the calculation takes both carbon and hydrogen very close to the actual results. The ^{1}H and $^{13}C\{^{1}H\}$ NMR spectra, however, do not exhibit any peaks due to methanol, thus discounting this hypothesis.

Based on the information gained from the infrared spectra of the lactobionates, the Fe(III) lactobionate reference and Figure 2.11, it is possible to predict the most likely structure for the M(II) lactobionates. The Zn(II) lactobionate complex is anhydrous which implies there is no chance of the zinc complex adopting structure **II**, as the υ(C=O) for a complex such as this would appear at ca. 1700cm^{-1}. As there is no chloride present in the zinc complex, the most likely structure is **III**, with an OH instead of the Cl. The Sn(II) and Cu(II) lactobionates are both hydrated, which means differentiation between structures **II** and **III** is difficult as the υ(C=O) would appear in similar positions due to chelation to the metal ion in **II**, and intermolecular H-bonding in **III**. Further structural work would be required to confidently assign a structure to either the Sn(II) or Cu(II) lactobionate complexes.

In addition to the synthesis of Zn lactobionate by the method detailed earlier in this chapter (using $ZnCl_2$), zinc(II) acetate was also reacted with the lactobionate ligand:

$$C_{12}H_{21}O_{11}OH + ZnCl_2 \xrightarrow{H_2O} C_{12}H_{21}O_{12}ZnOH + 2HCl$$

$$C_{12}H_{21}O_{11}OH + Zn(OAc)_2 \xrightarrow{H_2O} C_{12}H_{21}O_{12}ZnOH + 2CH_3CO_2H$$

Scheme 2.5. Reaction of lactobionic acid with two different zinc salts yielding the same final product.

The proposed representation for (**8**) as Zn(II) hydroxy lactobionate can be further strengthened by the results of the reactions between lactobionic acid and different zinc(II) salts (Scheme 2.5). The microanalysis for the products of the reactions was similar to that obtained in the original experiment, as was the infrared spectrum. These results imply that the reaction between any zinc salt with lactobionic acid will produce a complex in which the Zn is bonded to the same additional counterion (i.e. OH^-), independent of the reagent used. There is precedent for a complex in which the zinc is bonded to a hydroxyl, as it is known that basic zinc salts are commonplace and stable in

solution. The most common zinc salts in solution being: $[Zn(OH)_4]^{2-}$, $[Zn(OH)_3.H_2O]^-$ and $[Zn(OH)_3(H_2O)_3]^-$.[90]

The Mössbauer spectrum for Sn(II) lactobionate (**6**) exhibits a large doublet with an isomer shift, $\delta = 3.29 mms^{-1}$ and a quadrupole splitting, $\Delta = 1.82 mms^{-1}$. The linewidths ($\Gamma_1 = 1.06 mms^{-1}$, $\Gamma_2 = 0.89 mms^{-1}$) which are unequal possibly due to the amorphous (i.e. not ordered) nature of the solid compound, causing subtle local variations in the tin coordination. The Mössbauer parameters obtained are similar to documented tin(II) carboxylates such as those shown in Table 2.8.

Table 2.8. Mössbauer data for some tin(II) carboxylates.

Compound	δ (mms^{-1})	Δ (mms^{-1})	Reference
$Sn(O_2CH)_2$	3.33	1.70	119
$Sn(O_2CCH_3)_2$	3.31	1.77	171
$Sn(C_2O_4)$	3.35	1.65	131
Sn lactobionate (**6**)	3.29	1.82	This work

Also present in the Mössbauer spectrum was a small singlet with an isomer shift of ca. 0 mms^{-1}, due to a small amount of tin(IV) impurity. The peak area of this singlet was less than 3%, indicating that the compound produced was quite pure in terms of its stannous content. The area of the peak at $\delta = 0.00 mms^{-1}$ can be used as an indication of the purity of the sample, and can also be used to indicate how stable a compound is with respect to oxidation when exposed to air. If an unstable compound is exposed to air then one would expect to see an increase in the peak area of the singlet as the Sn(II) oxidised to Sn(IV). After being exposed to air for 3 months a Mössbauer experiment was re-recorded, with the results showing that the percentage of Sn(IV) in the sample had increased to ca. 5%, a result which indicates that the compound is relatively stable to air. As mentioned previously in this chapter, the stability of the compound within a toothpaste must also be determined. The Sn(II) lactobionate was incorporated into a toothpaste (1% w/w) and stored for 3 months at 37°C, after which time a Mössbauer

experiment was repeated. The spectrum obtained showed that the peak area of the singlet had increased from 5% to 35%, indicating that the Sn(II) ions are not as stable in the toothpaste as in the pure lactobionate complex.

2.3.4. The Synthesis of Sn(II) D-mannoheptose hydrate (9)

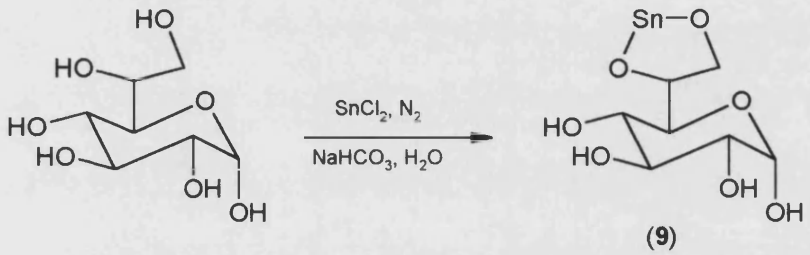

(9)

Scheme 2.6. Reaction scheme for the synthesis of Sn(II) D-mannoheptose monohydrate (**9**).

Tin(II) D-mannoheptose monohydrate (**9**) was prepared by the reaction of D-mannoheptose with stannous chloride, in the presence of a base, in thoroughly degassed water. The product of the reaction was an amorphous white solid, which proved to be insoluble in all common solvents. Due to this insolubility, it was not possible to obtain any NMR data for this compound. The microanalysis and infrared data for this compound suggested that it was synthesised as a monohydrate.

The Mössbauer spectrum of (**9**), ($\delta = 3.12 mms^{-1}$; $\Delta = 2.03 mms^{-1}$; $\Gamma_1 = 0.96 mms^{-1}$ and $\Gamma_2 = 0.84 mms^{-1}$) indicated that the product contained tin in its lower (+II) oxidation state, and that the tin (in the solid state) is in an asymmetric ligand environment. The Mössbauer parameters are typical of Sn(II) alkoxides such as Sn(II) methoxide ($\delta = 2.80 mms^{-1}$, $\Delta = 2.02 mms^{-1}$) and Sn(II) ethoxide ($\delta = 2.85 mms^{-1}$, $\Delta = 1.92 mms^{-1}$).[160] The narrow linewidths suggest that there is only one tin environment. After being exposed to the air for 3 months, another Mössbauer spectrum was recorded, which showed very little increase in the amount of tin(IV) impurity. The inference from the Mössbauer

results was that the compound which had been produced by this reaction was a stable tin(II) complex.

Tin(II) D-mannoheptose has a suspected structure as shown in Scheme 2.6, i.e., that of a tin(II) alkoxide. The stability of the compound to air is thus quite surprising as other tin(II) alkoxides are known to be inherently unstable with respect to oxidation to tin(IV).[119] The stability of the tin(II) in this complex probably comes from the ring formed between the tin and the two oxygen atoms, which is similar to the way in which the tin is bonded in tin(II) sorbitol. Sorbitol is known to stabilise stannous ions,[50] and if the bonding in Sn(II) D-mannoheptose is similar to that in Sn(II) sorbitol this could explain the stability of the stannous mannoheptose complex.

2.4. Anti-bacterial evaluation

All of the divalent metal compounds which have been synthesised, **(1-4, 6-9)**, were evaluated for potential anti-bacterial properties at Unilever Research Port Sunlight Laboratory. The efficacy of the selected compounds was evaluated using a common anti-bacterial assay, the acid-inhibition, or pH Stat, assay.

The method development for analysis of the test compounds using the pH Stat can be found in Appendix A.

2.4.1. The Acid-Inhibition (pH Stat) Assay

The pH stat assay measures the acid-inhibition properties of a particular compound. This property relates to the degree of inhibition of lactic acid production brought about by the disruption of the anaerobic metabolism of glucose by oral bacteria. This process of lactic acid

production is known as glycolysis and occurs through the glycolytic pathway. For the purposes of the pH stat assay the strain of bacteria used was *Streptococcus mutans (S mutans)*, an important organism present in the human oral cavity as a component of dental plaque.

The acid-inhibition assay (pH stat) was carried out using pH-stat automatic titration apparatus. The equipment automatically, and instantaneously, titrates the lactic acid produced during the bacterial metabolism of α-D-glucose with dilute (0.01M) potassium hydroxide to a constant neutral end-point of pH 7.0 (±0.05). The test solutions were constantly agitated with a mechanical stirrer paddle and the temperature maintained at 37°C (±0.5°C) by immersion of the sample vessel in a thermostatically controlled water-jacket. Further information regarding this method can be found in Appendix A.

2.4.2. pH Stat Assay Results

The results obtained from the pH Stat assays are presented in Figures 2.12 and 2.13. As can be seen from the graphs the basic shape of the plots is essentially the same for all the compounds tested. A feature of all the compounds is that the increase in acid-inhibition is not directly proportional to the concentration of the test solution.

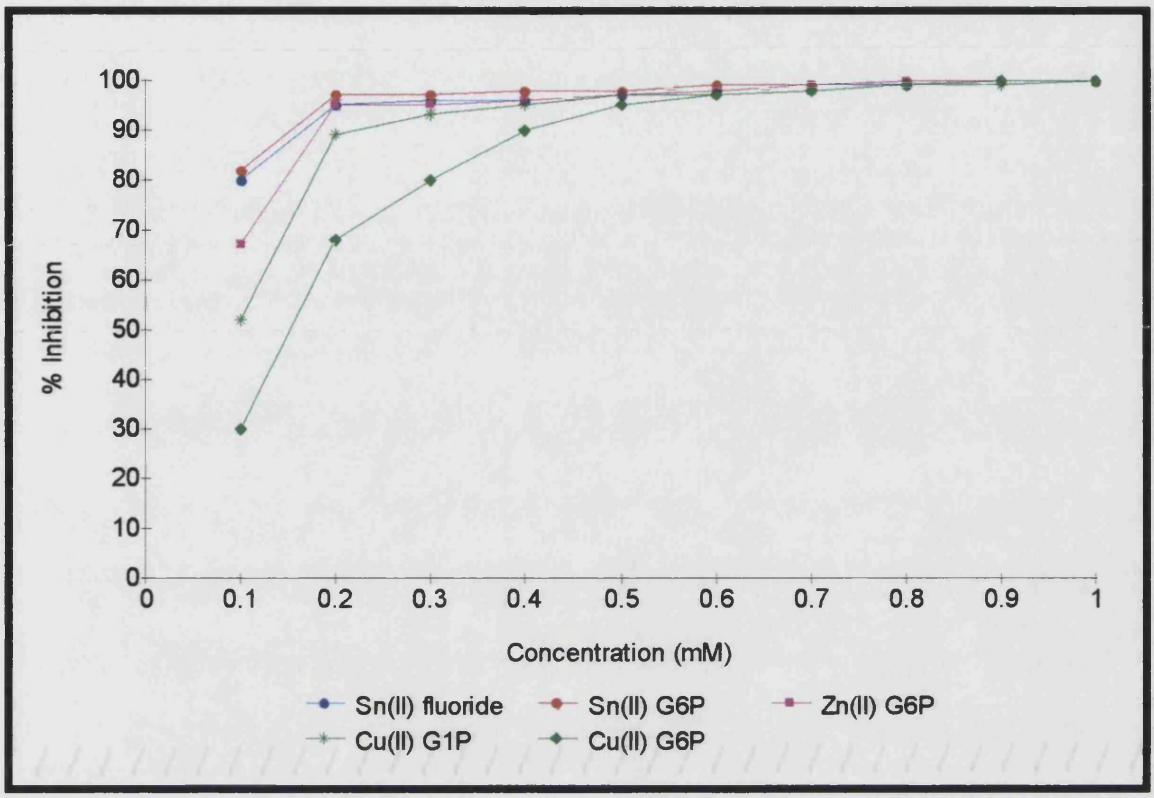

Figure 2.12. Acid-Inhibition of *Streptococcus mutans* by M(II) glucose phosphates, compared to a stannous fluoride control.

The results of the testing on the M(II) glucose phosphates showed that the Sn(II)αG6P, Zn(II)αG6P and Cu(II)αG1P compounds exhibited activity equivalent to that of SnF_2 (the positive control for all of the pH Stat experiments) at a concentration of 0.2mM and greater. At low concentrations (i.e. 0.1mM) the Sn(II)αG6P has significantly higher activity than the other compounds. When the concentration was increased to 0.2mM the activity of the Sn(II)αG6P, Zn(II)αG6P and Cu(II)αG1P became equal, although the Cu(II)αG6P still showed less activity. The inactivity of the Cu(II)αG6P could be due to its partial insolubility in water, which affects the availability/release of the Cu(II) ions and thus decreases the biological activity. The Cu(II)αG6P sample was dissolved in a solution of dilute HCl (pH 5), and neutralised with KOH prior to running the experiment. It was hoped that the acid would cause

decomposition of the complex to metal halide and free ligand, thereby creating synergism between the two components.

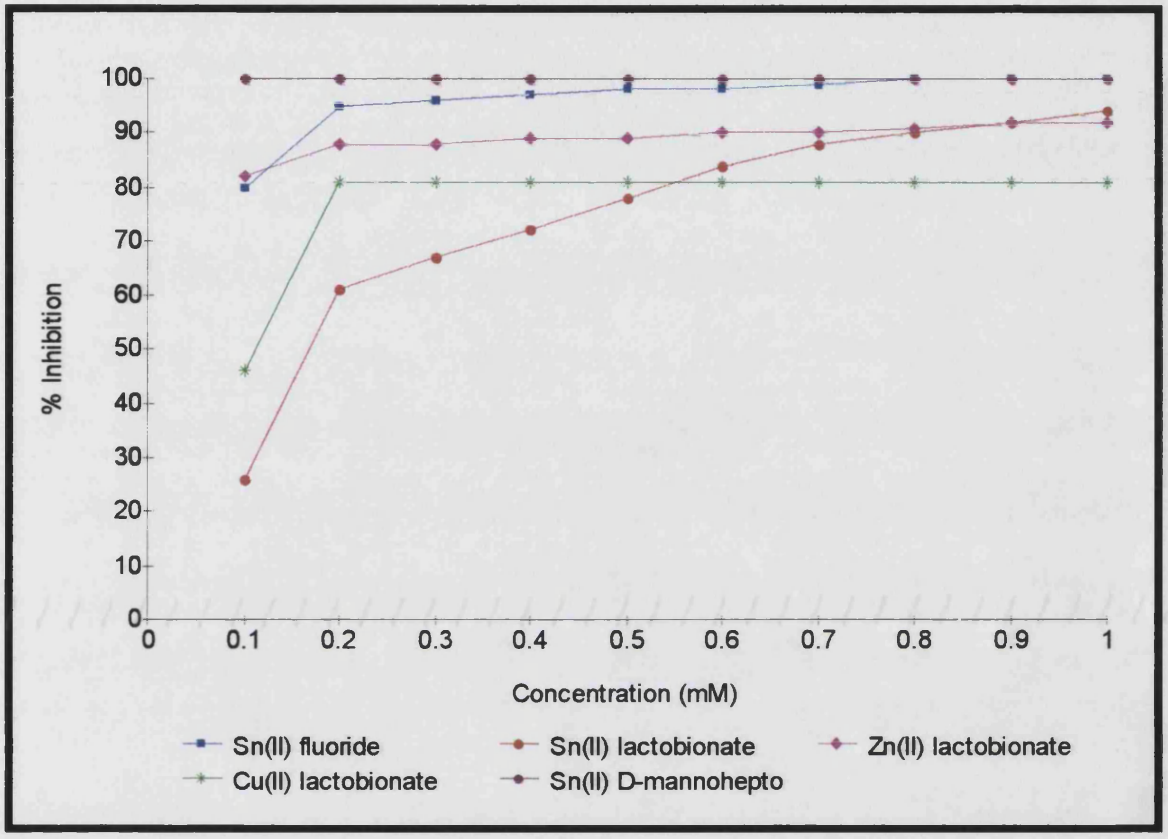

Figure 2.13. Acid-Inhibition of *Streptococcus mutans* by M(II) carboxylates, compared to a stannous fluoride control.

As can be seen in Figure 2.13 the results for the series of M(II) lactobionates are disappointing as none of the compounds achieved acid-inhibition results near to those of the stannous fluoride control. Even at a concentration of 1mM the anti-bacterial activity was poor. The nature of the bactericide (M) appears to be unimportant, as all three M(II) lactobionates gave poor results. As mentioned in the earlier discussion (Section 2.3.1) the structure of the lactobionates is such that the metal ion is probably chelated by a number of oxygen atoms. In the case of the stannous lactobionate this chelation is important as it appears to stabilise the Sn(II) ions thus preventing oxidation to the inactive Sn(IV) ions {on standing for three months the amount of Sn(IV) impurity had only risen by ca. 3%}. The problem with stabilising the stannous ion too much is that

although the tin remains in its lower oxidation state, the stannous ions are not released when the compound is in an aqueous environment. The consequence of this is a reduction in the number of free Sn(II) ions, which are the bactericidal ions, and a subsequent reduction in the anti-bacterial activity of the complex. Since the results for the zinc and copper lactobionates are similarly poor, it would appear that the Zn(II) and Cu(II) ions are also not released when the compound is in an aqueous environment.

The Sn(II) D-mannoheptose on the other hand achieved 100% inhibition at all test concentrations, a result which indicates that even at low concentrations this compound effectively destroys all bacteria. The assay results could, however, be slightly misleading, as due to its insolubility in water the compound was dissolved in dilute acid prior to testing. The pH was neutralised prior to running the experiment so the effect of the acid should have been negligible. A control was run to investigate the effect, if any, of the addition of the acid prior to the assay. The control consisted of decreasing the pH of water to ca. 3 and then neutralising this with KOH before running the assay. The results of the control indicated that the acid had no effect on the % inhibition values obtained. The low solubility of this compound is probably due to the Sn(II) being too tightly bound to the D-mannoheptose, probably in a polymeric arrangement. The addition of the dilute acid probably caused the breakdown of the polymeric structure thereby releasing Sn(II) ions into solution. This could be construed as a false result since the anti-bacterial agent has been tested as its constituent parts, i.e. a free metal ion and a ligand, and not as a whole. However, since the pH of plaque can be as low as 3.5 the assay does mimic the conditions to which the anti-bacterial agent would be exposed if it was used in a dental product.

All of the anti-bacterial evaluations detailed in this chapter have been carried out on the "neat" compounds. This is an important first step towards deciding which, if any, compounds will exhibit anti-bacterial activity in a dental application. In the case of the stannous compounds, one way to further evaluate potential activity is to observe what effect a toothpaste would have on the stability of the stannous active agent. This was achieved by adding the compounds to placebo toothpastes (i.e. pastes with no anti-bacterial agent) and then analysing the paste using Mössbauer spectroscopy to measure

the level of tin(II) relative to tin(IV). The pastes were then stored at 37°C for 3 months before being analysed.

Sn(II)αG6P in the solid state contains about 2% Sn(IV). After 3 months in a basic dentifrice (containing no fluoride or anti-bacterial agents) the amount of Sn(IV) increased to about 8-10% (Figure 2.14). When incorporated into a fluoride containing dentifrice (0.32% NaF) the amount of Sn(IV) was also about 10%. These results indicate a high level of stability of stannous glucose-6-phosphate both in the solid state and in toothpastes.

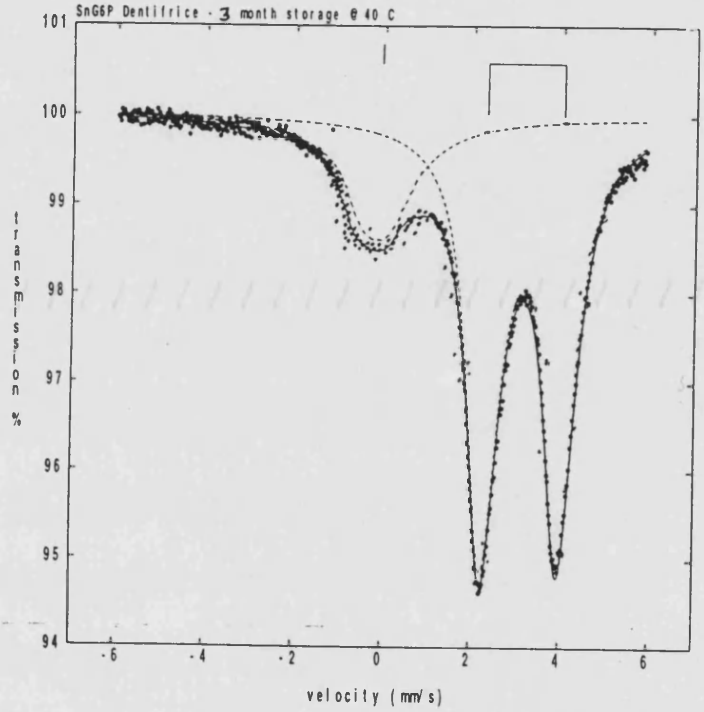

Figure 2.14. Mössbauer spectrum of toothpaste containing Sn(II)αG6P showing the extent of oxidation to Sn(IV) after 3 months.

Sn lactobionate in the solid state contains <5% Sn(IV). After storage for three months in a toothpaste the level of Sn(IV) impurity had risen to ca. 35%. This indicates poor stability of the stannous lactobionate, and this reduced level of Sn(II) will have a dramatic effect on the anti-bacterial properties of the paste.

The importance of this storage experiment is highlighted by the above two compounds because, for a compound to be used in a toothpaste, it must be stable with respect to the other ingredients in the paste. It is evident from the results of the Sn(II)

lactobionate that interactions with components of the toothpaste are causing significant oxidation of the tin. This is not the case for the Sn(II)αG6P making this compound a much more viable potential anti-bacterial agent.

The results obtained during the anti-bacterial evaluation of the compounds in this chapter have shed light on which "bait-link-bactericide" combination offers the highest level of anti-bacterial activity. Replacement of the phosphate link with a gluconate link has the effect of dramatically reducing the anti-bacterial activity regardless of the bactericide used. However the use of an ether type link group, as in Sn(II) D-mannoheptose, appears to offer a much higher level of activity than the phosphate link. This is an important result as Sn(II)αG6P has been patented and is therefore a potential new anti-bacterial agent, and to produce a compound which exceeds the *in vitro* activity of Sn(II)αG6P is extremely encouraging.

D-mannoheptose is, however, expensive (ca. £40/g) and therefore the stannous derivative is probably not a viable commercial compound. The positive results for Sn(II) D-mannoheptose suggests that other, less expensive, compounds with similar ether "link" groups could exhibit anti-bacterial activity.

2.5. Experimental

2.5.1. Synthesis of Sn(II) α-D-glucose-6-phosphate trihydrate (1)

Di-sodium α-D-glucose-6-phosphate (1.00g, 3.3mmol) was added to degassed water (40ml) with stirring. Once dissolved, a solution of tin(II) chloride (0.62g, 3.3mmol) was added and the solution stirred for 1 hour. After this time, degassed methanol (40ml) was added causing the formation of a precipitate. This white solid was filtered rapidly, washed with water and methanol, and dried *in vacuo*, yielding the title product (0.94g, 77%).

Analysis, found (calc. for $C_6H_{17}O_{12}PSn$): C, 16.4 (16.7); H, 3.52 (3.94).

Selected infrared: 3310cm^{-1} υ(H-O-H); 1630cm^{-1} δ(H-O-H); 1109cm^{-1}, 1074cm^{-1} and 1008cm^{-1} υ(P=O) and υ(P-O).

^{1}H NMR (D_2O): 5.08ppm (*d*, 1H, J_{1-2}=3.4Hz) H_1; 4.52 (*d*, 2H, J_{6-5}=7.9Hz) H_6; 4.05 (*m*, 1H) H_5; 3.57 (*dd*, 1H, J_{2-3}=9.5, J_{2-1}=3.4Hz) H_2; 3.36 (*dd*, 1H, J_{3-4}=8.2, J_{3-2}=9.5Hz) H_3; 3.10 (*dd*, 1H, J_{4-5}=9.6, J_{4-3}=8.2Hz) H_4.

^{13}C{^{1}H} NMR (D_2O): 96.9ppm (C_1); 76.4 (C_3), 74.9 (C_4), 73.5(C_2), 72.2 (C_5), 65.3 (*d*, $^2J_{P-C}$=5.5Hz) C_6.

^{31}P{^{1}H} NMR (D_2O): -9.7ppm.

^{119}Sn{^{1}H} NMR (D_2O): -681ppm.

^{119M}Sn Mössbauer: δ=3.21mms^{-1}, Δ=1.75mms^{-1}, Γ_1=1.07mms^{-1}, Γ_2=0.94mms^{-1}.

2.5.2. Synthesis of Cu(II) α-D-glucose-6-phosphate dihydrate (2)

Di-potassium α-D-glucose-6-phosphate (0.50g, 1.50mmol) was added to water/methanol (50ml) with stirring and gentle heating. Once dissolved, copper nitrate (0.36g, 1.50mmol) was added, as a solution, causing a precipitate to be formed. The precipitate was filtered, washed with water and dried *in vacuo* yielding the title product (0.34g, 60%) as an amorphous blue powder.

Analysis, found (calc. for $C_6H_{15}CuO_{11}P$): C, 19.5 (19.1); H, 4.3 (4.5).

Selected infrared: 3300cm^{-1} υ(H-O-H); 1635cm^{-1} δ(H-O-H); 1147cm^{-1}, 1100cm^{-1} and 1082cm^{-1} υ(P=O) and υ(P-O).

2.5.3. Synthesis of Zn(II) α-D-glucose-6-phosphate dihydrate (3)

Di-potassium α-D-glucose-6-phosphate (0.56g, 1.51mmol) was added to water/methanol (40ml) with stirring. Once dissolved, a solution of zinc acetate (0.33g, 1.51mmol) was added causing the precipitation of the title product, which was filtered and washed before being dried *in vacuo*. Yield (0.42g, 78%).

Analysis, found (calc. for $C_6H_{15}O_{11}PZn$): C, 19.9 (20.0); H, 3.90 (4.20).

Selected infrared data: 3320cm^{-1} υ(H-O-H); 1605cm^{-1} δ(H-O-H); 1105cm^{-1}, 1087cm^{-1} and 1016cm^{-1} υ(P=O) and υ(P-O).

^{1}H NMR (D_2O): 5.05ppm (*d*, 1H, $J_{1\text{-}2}$=3.6Hz) H_1; 4.46 (*d*, 2H, $J_{6\text{-}5}$=7.9Hz) H_6; 3.90 (*m*, 1H) H_5; 3.50 (*dd*, 1H, $J_{2\text{-}3}$=9.7, $J_{2\text{-}1}$=3.6Hz) H_2; 3.34 (*dd*, 1H, $J_{3\text{-}4}$=7.9, $J_{3\text{-}2}$=9.7Hz) H_3; 3.09 (*dd*, 1H, $J_{4\text{-}5}$=9.7, $J_{4\text{-}3}$=7.9Hz) H_4.

^{13}C{^{1}H} NMR (D_2O): 95.7ppm (C_1); 75.1 (C_4), 74.5 (C_3), 73.9 (C_2), 72.2 (C_5),

68.9 (*d*, $^{2}J_{P-C}$=7.0Hz) C_6.

$^{31}P\{^{1}H\}$ NMR (D_2O): 4.05ppm.

2.5.4. Synthesis of Cu(II) α-D-glucose-1-phosphate trihydrate (4)

Di-potassium α-D-glucose-1-phosphate (0.50g, 1.50mmol) was added to water/methanol (50ml) with stirring and gentle heating. Once dissolved, copper nitrate (0.36g, 1.50mmol) was added, as a solution, causing a precipitate to be formed. The precipitate was filtered, washed with water and dried *in vacuo* yielding the title product (0.34g, 60%) as an amorphous blue powder.

Analysis, found (calc. for $C_6H_{17}CuO_{12}P$): C, 17.1 (19.1); H, 4.3 (4.5).

Selected infrared: 3290cm^{-1} υ(H-O-H); 1640cm^{-1} δ(H-O-H); 1151cm^{-1}, 1100cm^{-1} and 1080cm^{-1} υ(P=O) and υ(P-O).

2.5.5. Synthesis of Sn(IV) α-D-glucose-6-phosphate heptahydrate (5)

To a round bottomed flask containing water (40ml) was added silver sulphate (1.5g, 3.68mmol) and tin(IV) chloride pentahydrate (0.64g, 1.84mmol) with stirring and gentle heating. The mixture was allowed to stir for 2 hours, to allow precipitation of the by-product, silver chloride, which was filtered to leave tin(IV) sulphate in solution. To this solution was then added barium α-D-glucose-6-phosphate hydrate (1.45g, 3.68mmol) and the reaction stirred and heated. After 2 hours the precipitated barium sulphate was filtered to leave Sn(IV) α-D-glucose-6-phosphate in solution. Removal of the solvent afforded the title compound as a pale yellow oil, yield (1.59g, 68%).

Analysis, found (calc. for $C_{12}H_{36}O_{16}P_2Sn$): C, 19.0 (18.9); H, 4.95 (4.73).

Selected infrared: 3300cm^{-1} υ(H-O-H); 1620cm^{-1} δ(H-O-H); 1115cm^{-1}, 1080cm^{-1} and 1028cm^{-1} υ(P=O) and υ(P-O).

^{1}H NMR (D_2O): 5.02ppm (*d*, 1H, J_{1-2}=3.9Hz) H_1; 4.47 (*d*, 2H, J_{6-5}=7.9Hz) H_6; 3.90 (*m*, 1H) H_5; 3.52 (*dd*, 1H, J_{2-3}=9.8, J_{2-1}=3.9Hz) H_2; 3.34 (*dd*, 1H, J_{3-4}=9.5, J_{3-2}=9.8Hz) H_3; 3.07 (*dd*, 1H, J_{4-5}=7.9, J_{4-3}=9.5Hz) H_4.

^{13}C{^{1}H} NMR (D_2O): 95.6ppm (C_1); 76.2 (C_3), 75.0 (C_4), 73.7 (C_2), 72.2 (C_5), 64.7 (*d*, $^{2}J_{P-C}$=5.5Hz) C_6.

^{31}P{^{1}H} NMR (D_2O): 0.12ppm.

^{119}Sn{^{1}H} NMR (D_2O): -674ppm.

^{119M}Sn Mössbauer: δ=-0.09mms^{-1}, Δ=0.00mms^{-1}, Γ=1.28mms^{-1}.

2.5.6. Synthesis of Sn(II) lactobionate chloride monohydrate (6)

Lactobionic acid hemi-calcium salt (3.98g, 10.55mmol) was added to degassed water (30ml) with stirring. Once dissolved, a solution of stannous chloride (1g, 5.27mmol) was added. After 2 hours of stirring and gentle heating, degassed methanol was added in order to precipitate the product, which was filtered, washed with water and methanol, before being dried *in vacuo* to yield the title compound (2.05g, 74%).

Analysis, found (calc. for $C_{12}H_{23}ClO_{13}Sn$): C, 26.7 (27.2); H, 4.33 (4.37).

Selected infrared: 3340cm^{-1} υ(H-O-H); 1600cm^{-1} υ(C=O); 1076-915cm^{-1} υ(C-O-C).

^{1}H NMR (D_2O): 4.40ppm (*d*, 1H, J_{1-2}=7.6Hz) H_1; 4.15 (*d*, 1H, J_{8-9}=3.3Hz) H_8; 4.04 (*dd*, 1H, J_{9-10}=3.8Hz, J_{9-8}=3.2Hz) H_9; 3.84 (*dd*, 1H, J_{10-11}=10.6Hz, J_{10-9}=3.8Hz) H_{10}; 3.75 (*d*, 2H, J_{12-11}=9.1Hz) H_{12}; 3.71 (*dd*, 1H, J_{4-5}=11.3Hz, J_{4-3}=3.3Hz) H_4; 3.68 (*d*, 2H,

$J_{6\text{-}5}$=9.0Hz) H_6; 3.60 (*m*, 1H) H_{11}; 3.51 (*m*, 1H) H_5; 3.48 (*dd*, 1H, $J_{3\text{-}4}$=3.3Hz, $J_{3\text{-}2}$=9.7Hz) H_3; 3.40 (*dd*, 1H, $J_{2\text{-}3}$=9.8Hz, $J_{2\text{-}1}$=7.6Hz) H_2.

$^{13}C\{^1H\}$ NMR (D_2O): 179.6ppm (C_7); 104.2 (C_1); 82.1 (C_{10}); 76.2 (C_5); 75.9 (C_8); 74.7 (C_3); 73.3 (C_2); 72.3 (C_{11}); 71.9 (C_9); 69.4 (C_4); 62.5 (C_{12}); 61.6 (C_6).

$^{119}Sn\{^1H\}$ NMR (D_2O): -520ppm.

^{119M}Sn Mössbauer: δ=3.29mms^{-1}, Δ=1.82mms^{-1}, Γ_1=1.06mms^{-1}, Γ_2=0.89mms^{-1}.

2.5.7. Synthesis of Cu(II) lactobionate chloride trihydrate (7)

Lactobionic acid hemi-calcium salt (5g, 13.25mmol) was added to water (40ml). Once dissolved, a solution of copper(II) chloride (2.26g, 13.25mmol) was added with stirring. After 1 hour of stirring methanol was added to precipitate the product. The blue precipitate was filtered, washed with water and methanol, and then dried *in vacuo* to yield the title product (4.9g, 73%).

Analysis, found (calc. for $C_{12}H_{27}ClCuO_{15}$): C, 27.7 (28.2); H, 5.54 (5.34).

Selected infrared: 3400cm^{-1} υ(H-O-H); 1605cm^{-1} υ(C=O); 1070-920cm^{-1} υ(C-O-C).

2.5.8. Synthesis of Zn(II) hydroxy lactobionate (8)

Lactobionic acid hemi-calcium salt (2g, 5.30mmol) was added to water (40ml). Once dissolved, a solution of zinc chloride (0.36g, 2.65mmol) was added with stirring. The reaction was heated gently, with stirring, for 1 hour. After this time, methanol was added to cause precipitation of the product. A fine suspension was produced which was

filtered, washed with water and methanol, before being dried *in vacuo* to yield the title product (0.79g, 68%) as a sticky solid.

Analysis, found (calc. for $C_{12}H_{22}O_{13}Zn$): C, 32.2 (32.8); H, 5.83 (5.05).

Selected infrared: 3300cm^{-1} υ(O-H); 1595cm^{-1} υ(C=O); 1070-920cm^{-1} υ(C-O-C).

^{1}H NMR (D_2O): 4.42ppm (*d*, 1H, J_{1-2}=7.6Hz) H_1; 4.18 (*d*, 1H, J_{8-9}=3.1Hz) H_8; 4.09 (*dd*, 1H, J_{9-10}=3.6Hz, J_{9-8}=3.1Hz) H_9; 3.85 (*dd*, 1H, J_{10-11}=10.4Hz, J_{10-9}=3.6Hz) H_{10}; 3.76 (*d*, 2H, J_{12-11}=9.1Hz) H_{12}; 3.70 (*dd*, 1H, J_{4-5}=11.9Hz, J_{4-3}=3.1Hz) H_4; 3.62 (*d*, 2H, J_{6-5}=8.5Hz) H_6; 3.60 (*m*, 1H) H_{11}; 3.58 (*m*, 1H) H_5; 3.50 (*dd*, 1H, J_{3-4}=3.3Hz, J_{3-2}=9.8Hz) H_3; 3.40 (*dd*, 1H, J_{2-3}=9.8Hz, J_{2-1}=7.6Hz) H_2.

^{13}C{^{1}H} NMR (D_2O): 179.3ppm (C_7); 104.3 (C_1); 82.2 (C_{10}); 76.3 (C_5); 74.3 (C_8); 73.3 (C_3); 72.3 (C_2); 71.9 (C_9); 71.8 (C_{11}); 69.5 (C_4); 62.8 (C_{12}); 61.8 (C_6).

2.5.9. Synthesis of Sn(II) D-mannoheptose hydrate (9)

D-mannoheptose (0.10g, 0.48mmol) was added to degassed water (20ml). Once dissolved, a solution of stannous chloride (0.09g, 0.48mmol) was added with stirring. A precipitate was formed immediately upon addition of the tin(II) chloride. The solvent was removed *in vacuo* yielding a white powder containing both tin(II) D-mannoheptose and the by-product, sodium chloride. The sodium chloride was removed by the addition of a small amount of degassed water. Yield (0.10g, 61%).

Analysis, found (calc. for $C_7H_{14}O_8Sn$): C, 24.8 (24.3); H, 4.09 (5.14).

Selected infrared data: 3360cm^{-1} υ(H-O-H); 1634cm^{-1} δ(H-O-H); 1308 and 1260cm^{-1} υ(C-O).

^{119m}Sn Mössbauer: δ=3.12mms^{-1}, Δ=2.03mms^{-1}, Γ_1=0.96mms^{-1}, Γ_2=0.84mms^{-1}.

2.6. Conclusions

The research carried out in this chapter has been based on work begun earlier, which led to the discovery of the "bait-link-bactericide" concept for which Unilever have a patent. This chapter introduces the first of the anti-bacterial evaluations which were used during this thesis to test the new compounds.

The "bait-link-bactericide" concept was borne from the biological activity of Sn(II)αG6P. From this compound work was carried out to synthesise the Sn(IV) derivative in the hope that this compound would be easier to crystallise than the Sn(II). Unfortunately extensive recrystallisations from various solvents proved unsuccessful in producing any suitable crystals for x-ray diffraction studies. The Zn(II) and Cu(II) derivatives of αG6P were also synthesised and found to exhibit variable anti-bacterial activity. In the absence of structural information the reason for this variance can only be speculated upon, but one possibility could be the extent to which the metal ion is bound by the ligand. The Cu(II)αG6P was much less soluble than the Zn(II)αG6P which could indicate a greater degree of inter-molecular bonding in the complex, which would in turn reduce the anti-bacterial activity.

The next group of compounds which were evaluated were the M(II) lactobionates which were an extension on the "bait-link-bactericide" concept where the link group was changed to a carboxylate group. The results obtained from the Sn(II), Zn(II) and Cu(II) lactobionates were disappointing as they exhibited very low anti-bacterial activity. The reason for this was shown to be the chelating effect of the gluconate group on the metal ion. This had the effect of binding the metal ion too tightly and thus making them unavailable to exhibit their activity. Another reason for the lack of activity could be that the bacteria do not attempt to metabolise the lactobionates in the same way as the αG6P, which is used by bacteria in their normal metabolism.

The "bait-link-bactericide" concept appeared to work well for the next compound to be evaluated, Sn(II) D-mannoheptose. This compound has an alkoxide group acting

as the link group and the results obtained were very promising as they were better than for Sn(II)αG6P. The disadvantages to using Sn(II) D-mannoheptose are the lack of solubility and cost. If this compound was to be used commercially cost may not be a problem, as due to its high efficacy it could potentially be used at a low level.

The commercial use of Sn(II) αG6P and Sn(II) D-mannoheptose is possible due to the stability of the compounds, with respect to oxidation of the Sn(II) to the inactive Sn(IV), both in air and in a toothpaste.

Another compound which was evaluated in the study was M(II)αG1P which although only slightly different to the αG6P was found to have significantly lower activity. This could be due to the high selectivity of bacteria, i.e. they are not able to metabolise αG1P.

The results presented in this chapter suggest that the activity of compounds which fit the "bait-link-bactericide" concept is due to their ability to be metabolised by bacteria. The one compound which is known to be metabolised, i.e. the αG6P, showed high activity while, with the exception of the Sn(II) D-mannoheptose, none of the others exhibited any real activity. It is not known whether bacteria metabolise the mannoheptose or not, but the findings of this work would suggest it is possible.

CHAPTER 3

TRICLOSAN AND RELATED COMPOUNDS

3. CHAPTER 3 - TRICLOSAN AND RELATED COMPOUNDS

3.1 Introduction

As mentioned in Chapter 1, for an anti-bacterial agent to be incorporated into a toothpaste it must have good oral substantivity/retention, good chemical stability, be non-toxic, and exhibit a broad spectrum of activity. A compound which is known to exhibit these properties is 2,4,4′-trichloro-2′-hydroxy diphenyl ether, more commonly known as triclosan (**I**).[53-57]

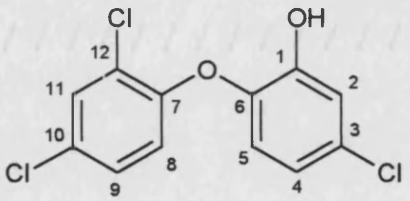

Triclosan (**I**)

Figure 3.1. Triclosan, including atom numbering.

A major drawback to the use of triclosan as an anti-bacterial agent has been its limited solubility (1ppm in water at 20°C). In light of this deficiency, a lot of work has focused on increasing the solubility so as to improve the efficacy of triclosan. This work has led to a patent[172] on a derivative of triclosan, triclosan phosphate (**10**), which has been found to be much more soluble in water. It is believed that when **10** is used in a dental formulation, that the compound is enzymatically degraded to generate molecular triclosan, yielding a more active product.

The knowledge that triclosan phosphate offers improved water solubility and increased anti-bacterial efficacy has led us to examine a range of compounds which may offer even greater biological activity - the M(II) triclosan phosphates.

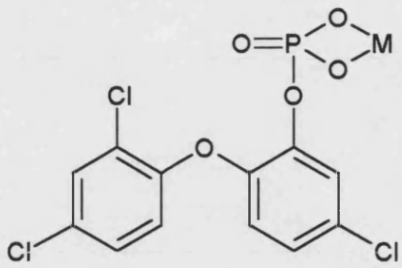

Figure 3.2. M(II) triclosan phosphate (M = Sn, Zn or Cu.)

It was hoped that this type of compound would exhibit increased anti-bacterial activity due to a synergistic effect produced by combining the known activity of triclosan with the bactericidal metal ions.

During the synthesis of triclosan phosphate[172] an interesting side product is produced, triclosan phosphate diester (**11**), a compound for which it appears no anti-bacterial evaluations have been carried out.

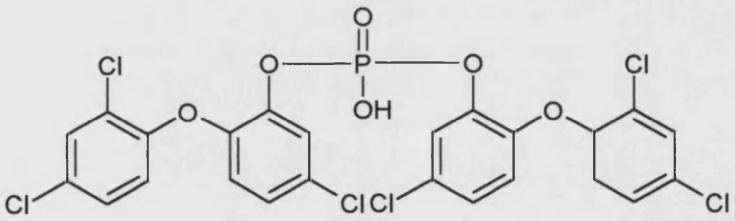

Figure 3.3. The proposed formula for the diester of triclosan phosphate (**11**).

The exact structure (i.e. extent of oligomerisation through H-bonds) for the triclosan phosphate diester is not known as no X-ray crystallisation work has been carried out, and the above representation is only a possible structure. The diester is likely to have one OH group through which it may be possible to attach a metal ion. As can be seen from the formula above the diester contains two triclosan molecules, whereas triclosan phosphate has only one. The advantage of using the diester could thus be in the delivery of more anti-bacterial triclosan in a dental formulation. As with the triclosan phosphate it was hoped that by attaching a bactericidal metal ion to the hydroxyl group a synergistic effect would be observed, leading to increased biological activity.

The synthesis and characterisation of triclosan phosphate, M(II) triclosan phosphates and the diester of triclosan phosphate for evaluation as anti-bacterial agents is detailed in this chapter.

3.2. Synthesis and Characterisation of M(II) Triclosan Phosphates

3.2.1. Synthetic strategies for the M(II) triclosan phosphates

The compounds detailed in this chapter are all based on triclosan phosphate, the synthesis of which is quite straightforward using triclosan as a starting material.

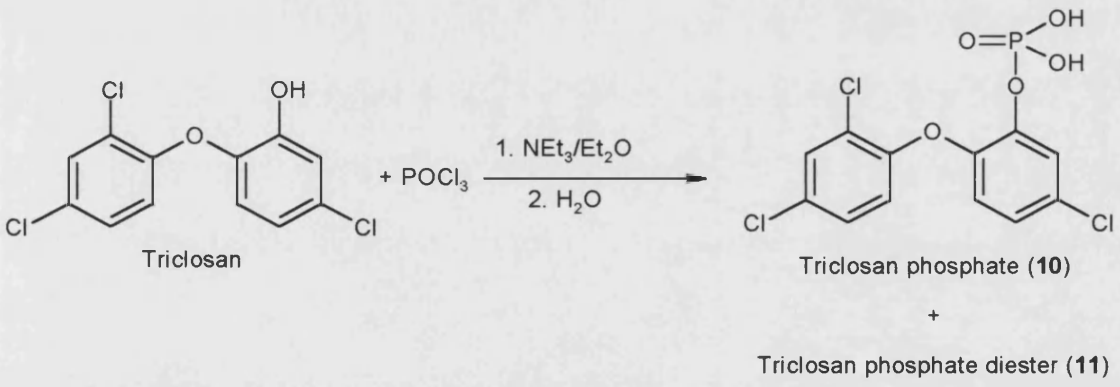

Triclosan

Triclosan phosphate (**10**)

+

Triclosan phosphate diester (**11**)

Scheme 3.1. Synthesis of triclosan phosphate (**10**), and triclosan phosphate diester (**11**).

This synthesis is taken from the patent for triclosan phosphate,[172] and yields triclosan phosphate in good yield by crystallisation/precipitation from dichloromethane over ca. 10 days. The white solid which was produced after this time was found, according to the microanalysis data, to be monohydrated. Recrystallisation of triclosan phosphate from common organic solvents was unsuccessful, but a recrystallisation from

pyridine yielded large crystals from which a crystal structure was determined (see Section 3.2.3).

As mentioned previously, during the synthesis of triclosan phosphate an interesting by-product, triclosan phosphate diester (**11**), is obtained (Figure 3.3). This compound was purified by recrystallisation from ethyl acetate, and was found to be dihydrated according to the microanalysis data. Although the product was purified using ethyl acetate, recrystallisations using this and other solvents were unsuccessful in producing crystals of a suitable quality for X-ray characterisation.

The pure triclosan phosphate was then used as the starting material in the synthesis of Sn(II), Zn(II) and Cu(II) triclosan phosphate.

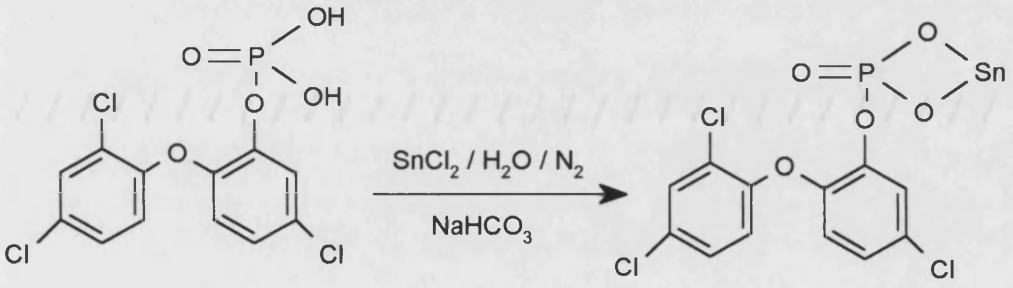

Triclosan phosphate Sn(II) triclosan phosphate (**12**)

Scheme 3.2. Synthesis of Sn(II) triclosan phosphate (**12**).

Tin(II) triclosan phosphate (**12**), was prepared by the reaction of triclosan phosphate with a solution of tin(II) chloride in thoroughly degassed alkaline water (Scheme 3.2). The product precipitated from the alkaline solution immediately upon addition of the stannous chloride, yielding the title compound as a white solid, which the microanalysis suggested was anhydrous. In Scheme 3.2 a general representation of the structure of Sn(II) triclosan phosphate is shown, as the solid product is likely to be polymeric. The poor solubility in common solvents is consistent with this hypothesis.

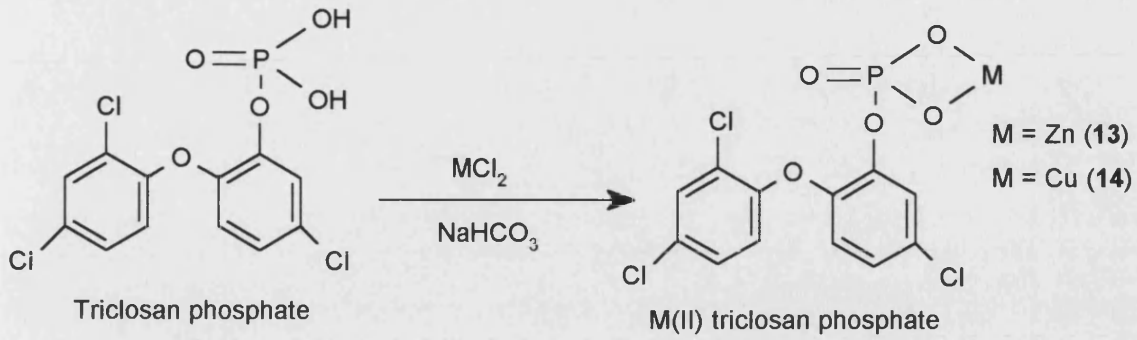

Triclosan phosphate M(II) triclosan phosphate

Scheme 3.3. Synthesis of Zn(II) and Cu(II) triclosan phosphate.

Zn(II) triclosan phosphate (**13**) and Cu(II) triclosan phosphate (**14**), were prepared by the reaction of triclosan phosphate with two moles of base and solutions of zinc(II) chloride/copper(II) chloride, in water. In each case the product readily precipitated from solution upon addition of the MCl_2 giving good yields of the title compounds as amorphous powders. The microanalytical data suggested that the zinc compound was formed as a dihydrate, with the copper compound forming as a monohydrate. Like the Sn(II) triclosan phosphate, both the Zn(II) and Cu(II) triclosan phosphate were found to be insoluble in all common recrystallisation solvents (methanol, THF, toluene, etc.) and as a consequence no crystals were obtained for structural work.

As mentioned in the introduction to Chapter 3, compounds such as the M(II) triclosan phosphate diester were to be synthesised to observe if any increased anti-bacterial activity was attained due to synergism. Unfortunately attempts to produce metal derivatives of the diester proved unsuccessful, probably due to steric hindrance, and as a result this avenue of research was not pursued any further.

3.2.2. Comparison of infrared, NMR and Mössbauer spectra for triclosan and related compounds

The infrared spectra of all the compounds detailed in this chapter were as expected very similar, both to one another, and to triclosan. All of the hydrated compounds exhibited the characteristic stretching band (ca. 3300cm^{-1}) and bend (1610cm^{-1}) for water. The spectrum obtained for Sn(II) triclosan phosphate did not contain any peaks due to water, which, as with the microanalysis data, suggested that the complex was anhydrous. The spectra obtained for all of the compounds contained a large number of peaks due to C-O, P-O, and C-Cl stretches.

The ^{1}H NMR spectra for triclosan phosphate, triclosan phosphate diester, Sn(II) triclosan phosphate and Zn(II) triclosan phosphate were all very similar, with 6 peaks in the aromatic ($\delta \sim 7$ppm) region of the spectrum. The coupling constants for all of the spectra were also very similar, [2.1<J<2.5Hz] and [8.5<J<8.9Hz]. These coupling constants arise from various interactions with protons which are *ortho*, *meta* or *para* to one another, and fall within the following ranges, independent of the substituents:[131,173]

$J_{H\text{-}H}$(*ortho*) = 7.0 to 9.2Hz.

$J_{H\text{-}H}$(*meta*) = 1.1 to 3.1Hz.

$J_{H\text{-}H}$(*para*) = 0.0 to 0.7Hz.

There are no $J_{H\text{-}H}$(*para*) quoted in the discussion or experimental, even though there will undoubtedly be para-coupling, as the NMR spectrometer (270MHz) did not allow the resolution of such small coupling constants.

As with the ^{1}H NMR, the ^{13}C{^{1}H} NMR spectra for the triclosan phosphates were found to be very similar. Each spectrum contained 3 peaks which were downfield (by ca. 10-20ppm) of the other 9 peaks. These 3 peaks were easily assigned as the signals due to the 3 [C-O]. Of the other 9 peaks, three were readily assigned to the 3 [C-

Cl] using a 135 DEPT. $^{13}C\{^1H\}$ spectrum. The other six carbon signals (all C-H bonds) were difficult to assign unambiguously, even with the use of NMR tables. As one would expect from the structure of the triclosan phosphates, the $^{13}C\{^1H\}$ NMR spectra for this series did not yield much useful information, and was used as a means of identification and a guide as to how pure the samples were.

The $^{31}P\{^1H\}$ NMR spectra yielded more information as to the solution state structures of the triclosan phosphates. The spectrum for Sn(II) triclosan phosphate (**12**) contained 4 peaks ranging from -12.1 to -21.6ppm. This indicates the presence of four slightly different phosphorus environments in the solution state, none of which are due to the triclosan phosphate starting material (δ = -3.7ppm). The inference from this result is that there are probably subtle local variations in the phosphorus environments in Sn(II) triclosan phosphate in solution. Unfortunately in the absence of any crystallographic data it is difficult to say what the different phosphorus environments are. It is possible, drawing on the knowledge that the compound is insoluble, to propose that the Sn(II) triclosan phosphate is polymeric. If the compound was polymeric this could account for the changes in the local environments of the phosphate groups. The spectrum obtained for the Zn(II) triclosan phosphate was different in that it contained only one peak with a chemical shift of -6.1ppm, a value which is close to the chemical shift observed in the starting material (δ = -3.7ppm).

Unfortunately due to low solubility of **12** no $^{119}Sn\{^1H\}$ NMR was obtained, a spectrum which would have possibly contained 4 peaks for differing Sn(II) environments as well.

In an attempt to discover more about the Sn(II) triclosan phosphate, a Mössbauer experiment was carried out yielding the spectrum depicted in Figure 3.4. This Mössbauer spectrum clearly shows that this compound contains tin is in its lower (+II) oxidation state with the isomer shift (δ) of 3.08mms^{-1}, falling well within the range of $2.5<\delta<5.0$, indicative of Sn(II) compounds.[134,135] It is also clear from the spectrum that there is very little Sn(IV) impurity as there is only a small peak at $\delta<2.2$mms^{-1} indicating Sn(IV) impurity. The doublet in this spectrum exhibits a quadrupole splitting (Δ) value

of 1.83mms^{-1}, which indicates that the Sn(II) is in an asymmetric environment in the solid state. It is believed that the tin in this compound is surrounded by oxygen atoms, and changes in the oxygen coordination sphere around the tin probably account for the asymmetric environment and, subsequent quadrupole splitting. The Δ value for Sn(II) triclosan phosphate is typical of compounds where the tin is surrounded by oxygen atoms, examples of which can be found in Table 2.4 in the previous chapter. The equal linewidths (Γ_1,Γ_2 = 0.81mms^{-1}) obtained for **12** indicate the presence of just one tin environment in the solid state.

Figures 3.4, 3.5 and 3.6 show three different Mössbauer spectra of the same compound, but with varying degrees of oxidation of the Sn(II):

Figure 3.4. - Sn(II) triclosan phosphate (**12**).

Figure 3.5. - **12** after 2 weeks exposure to air.

Figure 3.6. - **12** in a toothpaste after 3 months storage at 37°C.

As can be seen in Figure 3.5., a peak is now evident at ca. 0mms^{-1}, which is due to Sn(IV), indicating that the compound is unstable in air with respect to oxidation to Sn(IV). This is not a promising finding for a compound which is to potentially be used as an anti-bacterial agent in toothpastes, as for this application the compound must be oxidatively stable. An experiment was carried out to see how stable the compound is when incorporated into a toothpaste. The Sn(II) triclosan phosphate was added to a toothpaste formulation (1% w/w) and incubated for 3 months at 37°C, after which time a Mössbauer experiment was run (Figure 3.6) to determine the extent of oxidation to tin(IV). The results were, unsurprisingly, very poor, with the spectrum being dominated by a peak with an isomer shift of ca. 0mms^{-1} (ca. 80% by peak area) indicating that Sn(II) triclosan phosphate is not a viable compound for any dental formulations.

Figures 3.4, 3.5 and 3.6 clearly show how unstable the Sn(II) triclosan phosphate is to both air, and the free water content of a toothpaste.

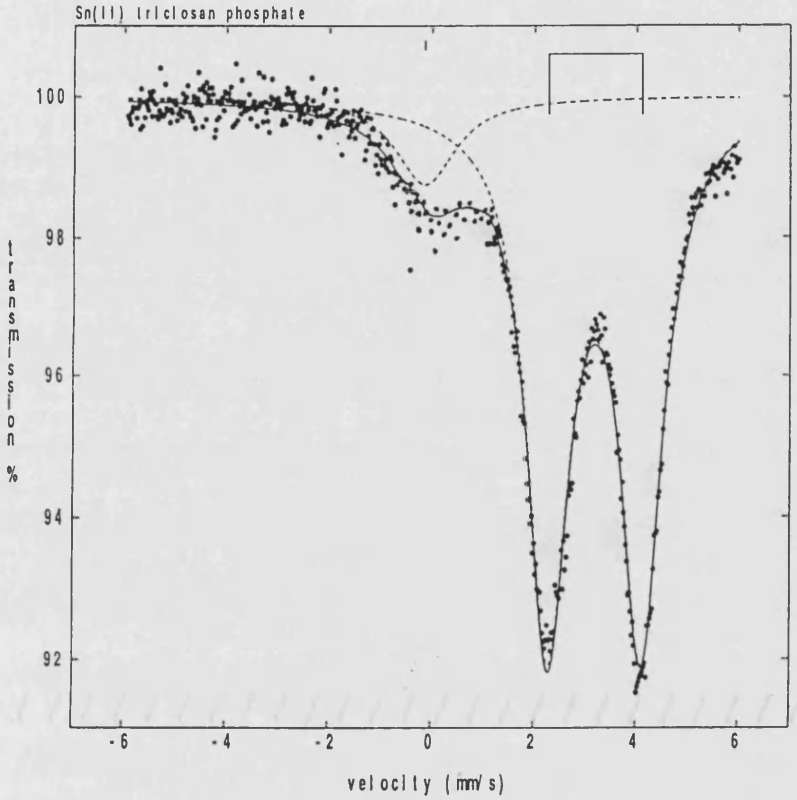

Figure 3.4. ^{119m}Sn Mössbauer spectra of Sn(II) triclosan phosphate (**12**)

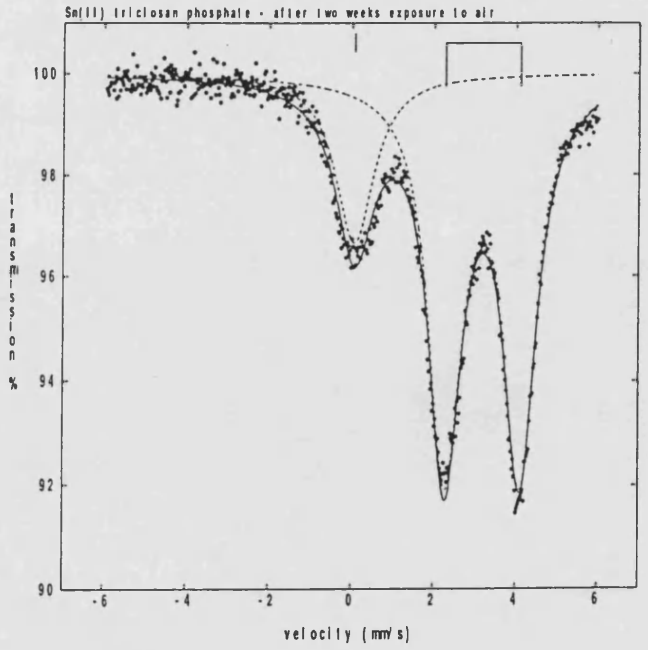

Figure 3.5. **12** after two weeks exposure to air.

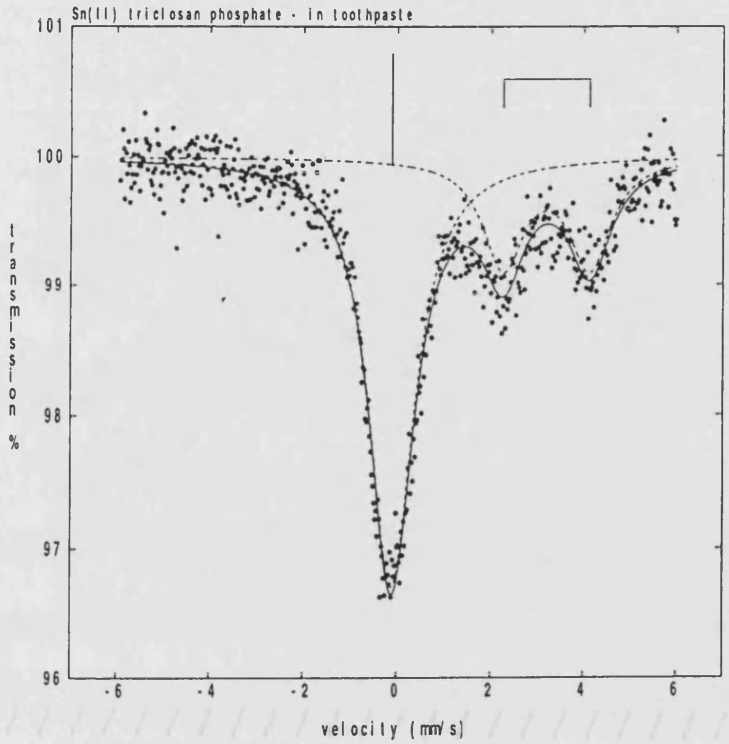

Figure 3.6. **12** after 3 months in a toothpaste.

3.2.3. Structural Determination of pyridinium triclosan phosphate

Triclosan phosphate was recrystallised from pyridine, yielding a crystal of the pyridinium salt, of approximate dimensions 0.3 x 0.3 x 0.3mm which was used for data collection. Selected structural data are included in the discussion, with the crystal data and additional supplementary structural data included in Appendix B.

Table 3.1. [P-O] bond lengths and angles in pyridinium triclosan phosphate.

Bond	Length / Å	Bond	Angle / °
P(1)-O(3)	1.487(5)	O(3)-P(1)-O(2)	116.2(3)
P(1)-O(2)	1.500(5)	O(3)-P(1)-O(1)	109.5(3)
P(1)-O(1)	1.524(5)	O(2)-P(1)-O(1)	113.4(3)
P(1)-O(4)	1.626(5)	O(3)-P(1)-O(4)	107.8(3)
		O(2)-P(1)-O(4)	102.9(3)
		O(1)-P(1)-O(4)	106.2(3)

Note: esd's are shown in parentheses.

The compound for which the crystal structure was obtained is pyridinium 2,4,4′-trichloro-2′-phosphate-diphenyl ether. Of the two pyridine molecules which are included in the crystal structure, one is hydrogen bonded to a hydroxyl group of the phosphate group while the other is present in the lattice structure. As can be seen from Figure 3.7, in this crystal the molecule exists as a dimer with the bonding occurring through a P-OH of one molecule with P-O of the other molecule. It is not possible to ascertain whether the P-O bonds in the molecules are ionic bonds or P=O double bonds.

As there are two pyridine molecules present in the crystal structure, one would expect both of the pyridines to be positively charged, to act as counter ions to two $P\text{-}O^-$ bonds. However it appears that only one of the pyridine molecules is charged, suggesting that only one of the P-O bonds is charged. The remaining P-OH is involved

in hydrogen bonding to the other triclosan phosphate molecule rather than protonating the second pyridine.

This arrangement creates a planar centrosymmetric 8 membered ring between the two triclosan-2′-phosphate molecules.

As can be seen from Table 3.1, there are two bonds which are shorter than the others [P(1)-O(3) = 1.487(5)Å, and P(1)-O(2) = 1.500(5)Å]. The bond lengths are very close to each other, indicating similar bonds. If the bonds are the same then it is not possible to have a P=O in the structure, as this would exceed the maximum valency of the phosphorus. It would, however, be possible to have a structure in which the double bond and single negative charge were shared between the two [P-O] bonds. This would account for the two approximately equal bond lengths in the pyridinium triclosan phosphate structure. The bonds are both longer than usual P=O bonds,[174-176] which strengthens the notion that neither are formally double bonds. The bond lengths are close to those observed in bis(cyclohexylammonium) 4-nitrophenyl phosphate dihydrate, which contains a RPO_3^{2-} group and has three [P-O] bond lengths of 1.498(5), 1.495(5) and 1.498(5)Å.[177]

Also notable from Table 3.1 is that one bond is significantly longer than the others [P(1)-O(4) = 1.626(5)]. This is the P-O-Aryl bond and the length is comparable to, although slightly longer than, other P-O-Aryl bond distances for example, 4-carbethoxyanalinium bis-*p*-nitrophenylphosphate 1.60(1),[174] and triphenyl phosphate 1.613(3).[176] The other [P-O] bond length in triclosan phosphate is 1.524(5)Å and is assigned to the P-OH bond in the structure. The length of a P-OH bond can vary considerably, for example in 2-amino-ethanol phosphate [P-OH = 1.557(5)Å],[178] in dibenzyl phosphoric acid [P-OH = 1.545(4)Å][179] and in N-methyldopamine 4-*O*-dihydrogenphosphate [P-OH(1) = 1.546(4) and P-OH(2) = 1.517(5)Å].[180]

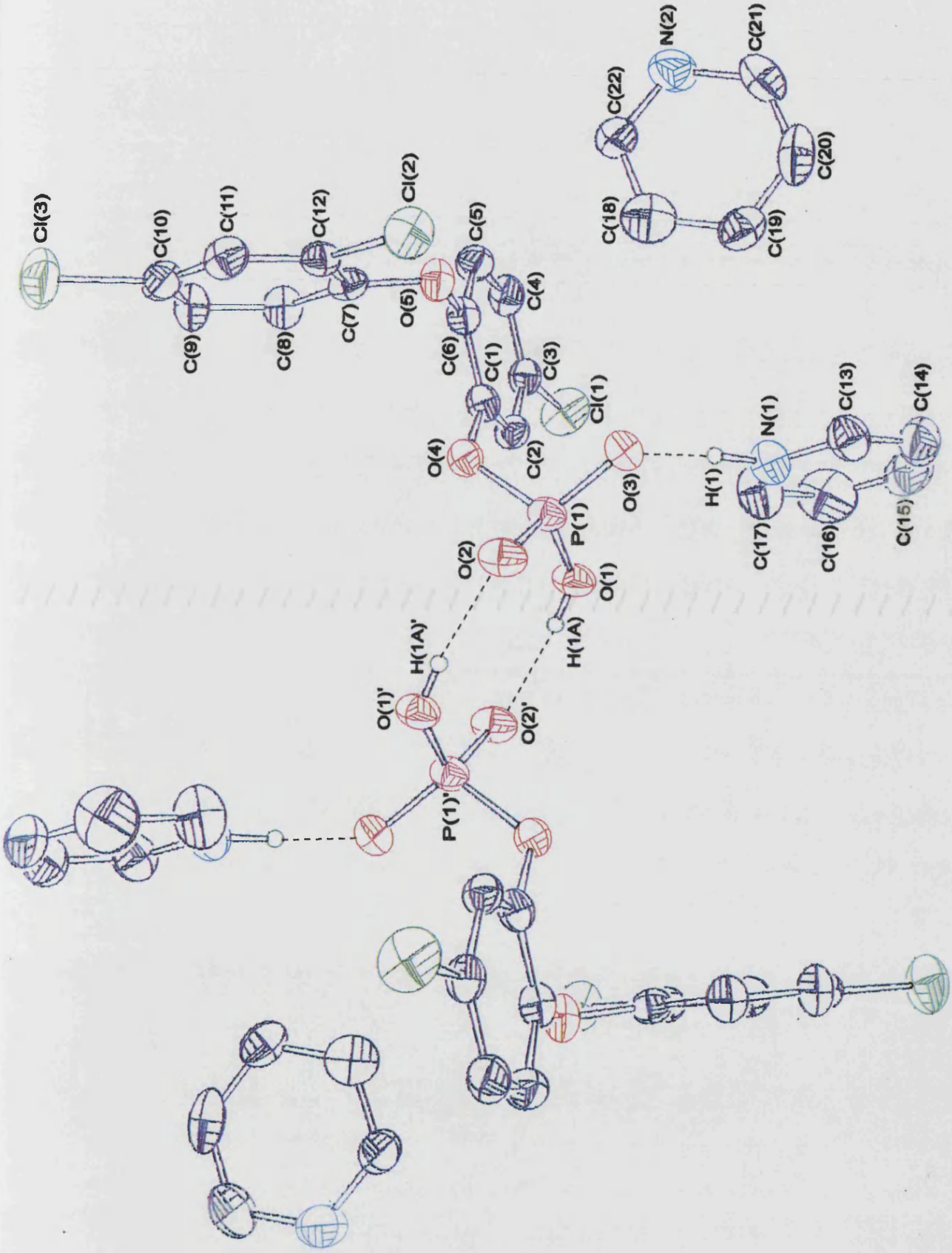

Figure 3.7. The asymmetric unit of pyridinium triclosan-2′-phosphate.

Table 3.2. [O-P-O] bond angles in selected phenyl phosphates.

Compound	[O-P-O]bond angle/°		Reference
	Low	High	
Pyridinium triclosan phosphate	102.9(3)	116.2(3)	This work
Triphenyl phosphate	96.6(5)	119.1(6)	174
4-Carbethoxyanalinium bis-*p*-nitrophenylphosphate	97.8(1)	120.1(2)	176
N-methyldopamine 4-*O*-dihydrogenphosphate	96.7(2)	116.4(3)	180

Table 3.2 shows that the phosphate tetrahedron in pyridinium triclosan phosphate is less distorted than in many other phosphates, as indicated by the 6 [O-P-O] bond angles all falling within a relatively narrow range [102.9 (3) to 116.2 (3)°].

The largest of the O-P-O bond angles in pyridinium triclosan phosphate [116.2 (3)°] is between the two oxygens which are involved in hydrogen bonding [O(3)-P(1)-O(2)]. The magnitude of this angle can be accounted for by the large electronic repulsion which is in effect between two short P-O bonds with a higher electron density than other P-O bonds in the structure. This large bond angle is common in other compounds with short P-O bonds, for example, adenosine-5'-phosphate [118.2 (4)°],[181] calcium 1-naphthyl phosphate trihydrate [116.8 (4)°][182] and dibenzyl phosphoric acid [117.2 (2)°].[179] As mentioned previously there is another P-O bond which is quite short [P(1)-O(1) = 1.524(5)Å] which is the P-OH bond. Based on the reasons just presented, it is not surprising that the bond angle formed between this P-OH and one of the short P-O bonds is also larger than the others [113.4 (3)°].

The smallest/narrowest of the bond angles in pyridinium triclosan phosphate is 102.9 (3)°. This angle is formed between [O(2)-P(1)-O(4)], which involves the P-O-Aryl bond [1.626 (5)Å] and one of the short P-O bonds. The reason for this narrow bond angle is obviously that there is much less electronic repulsion between these two bonds.

The other bond angle which needs to be addressed in relation to the phosphate group is the [C(6)-O(5)-C(7) = 118.2(5)°]. As can be seen from the structure, pyridinium triclosan phosphate is a bis-diphenyl ether, where two phenyl rings are connected by an oxygen atom. It is known that there are four possible conformers of diphenyl ether as shown in Figure 3.8.

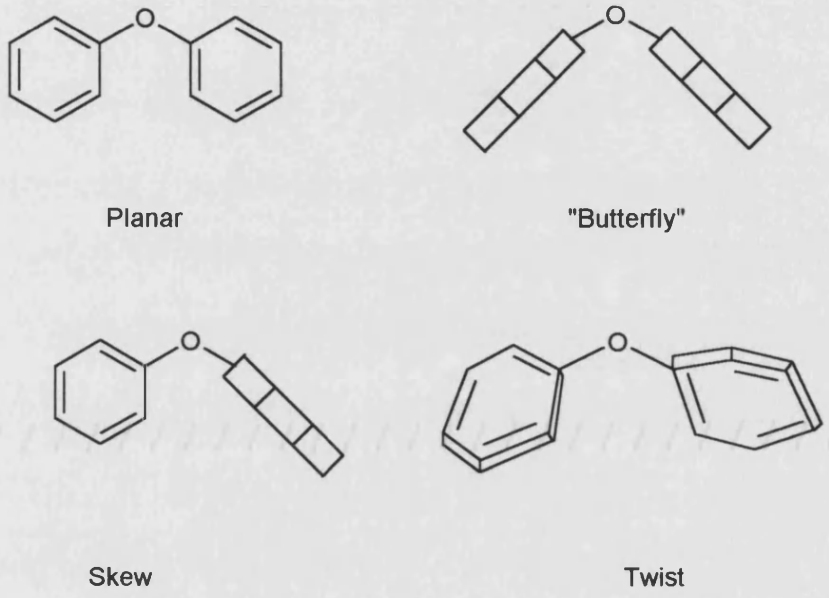

Figure 3.8. Possible conformers of diphenyl ether.[183]

The asymmetric unit of triclosan phosphate shows that the molecule has a skew conformation between the phenyl rings. All [C-C] bond distances and angles in pyridinium triclosan phosphate (see Appendix B) are normal for a diphenyl ether.[183] The oxygen atom situated between the phenyl rings is 118.2 (5)°. This angle does not deviate markedly from the values observed in bis(2,4-dichlorophenyl) ether,[183] 120.6 (6)°, and bis(3,4-dichlorophenyl) ether,[184] 119.6 (3)°. The number, and positions, of chlorine atoms on the phenyl ring does not cause much of a deviation from the 120° angle, regardless of the conformation of the two phenyl rings relative to each other.[183] The paper from which this observation was made examines the structural and conformational properties of 11 polychlorinated diphenyl ethers (PCDE's). The C-O-C bond angles of the PCDE's ranged from 116.2 - 120.6°.

In pyridinium triclosan phosphate, the [O(5)-C(6)] and [O(5)-C(7)] bond lengths are, as expected, very similar [1.384(8) and 1.369(8)Å] and are approximately the same as those observed in bis(2,4-dichlorophenyl) ether, where both [C-O] bonds are 1.376(8)Å. The [C-Cl] bond lengths in the PCDE's ranged from 1.698(6) to 1.748(6) Å, the values obtained for the 3 [C-Cl] bonds in pyridinium triclosan phosphate [1.740(7), 1.730(7) and 1.728(7)Å] are thus not surprising.

3.3. Anti-bacterial evaluation

The principal anti-bacterial assay used to evaluate the compounds detailed in this chapter, the Biofilm Assay, was developed by Unilever in response to the need for a rapid and simple method to predict differences in anti-bacterial activity between various toothpastes and mouthwashes. It is especially useful in industry in helping to screen products prior to advancing to clinical trials. The method was slightly modified to allow testing of compounds in solution rather than in toothpastes. The pH stat assay (detailed in chapter 2) was also used but to a lesser degree (i.e. only for triclosan phosphate). The method adopted for the biofilm assay can be found in Appendix A.

3.3.1. pH Stat Assay Results

As mentioned in Chapter 2, for a compound to be tested it must be water soluble. Of all the compounds synthesised in this chapter, only the triclosan phosphate was found to be water soluble and as such this was the only compound to be tested using this method. The results of this assay are presented in Figure 3.9 along with the SnF_2 control and Sn(II)αG6P.

The results from the pH stat assay are encouraging since they show that triclosan phosphate alone is a potent anti-bacterial agent. It therefore follows that if a water soluble M(II) derivative (i.e. an M(II) compound which will potentially breakdown to yield triclosan phosphate and a metal ion in solution) can be synthesised, the compound will be a powerful anti-bacterial agent. The reason why this kind of compound could show increased activity is that there could be synergism between the two active components.

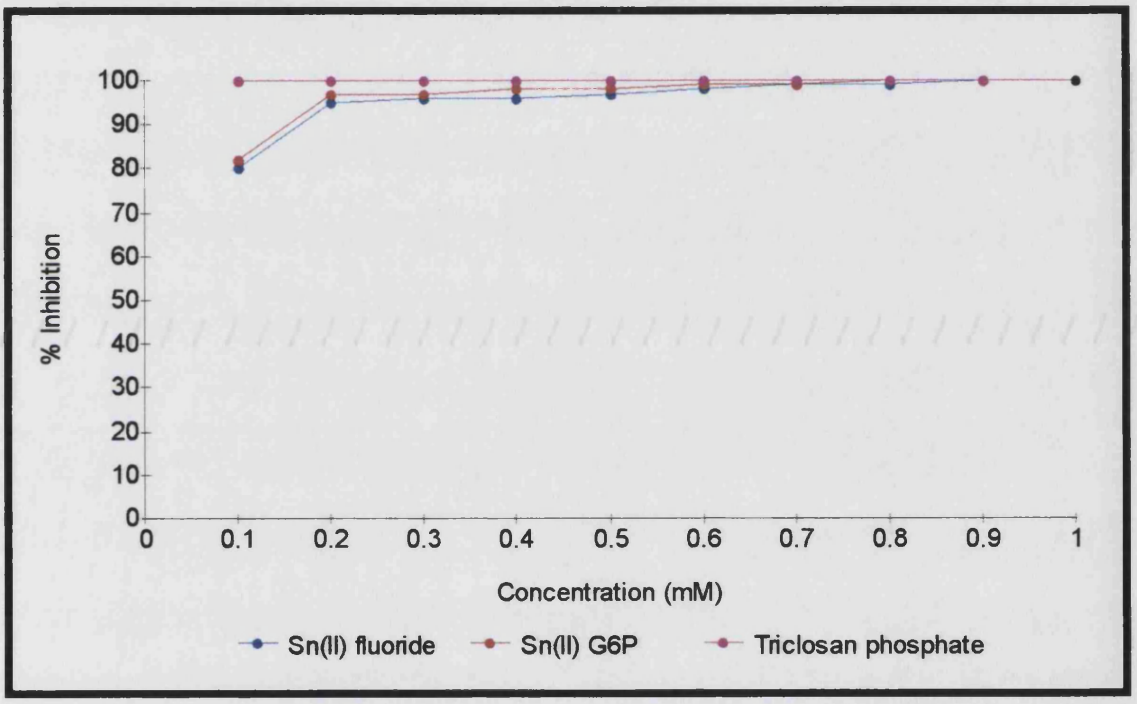

Figure 3.9. Acid-Inhibition of *Streptococcus mutans* by triclosan phosphate, compared to Sn(II)αG6P and a stannous fluoride control.

3.3.2. The Biofilm Assay

The assay involves preparing biofilms (a biofilm is a film of bacteria which is grown onto a sample plate over a period of a few days) in a 96-well microtitre plate which is then

exposed to the various test compounds for one minute before being filled with BHI (Brain Heart Infusion - a growth medium for the bacteria) broth and topped with mineral oil. The plate is then placed in a plate reader which reads the optical density (OD) of the wells every 15 minutes for up to 23 hours at a time (the plate being kept at 37°C the whole time). The optical density increases as the number of bacteria increases, and when an OD of 0.5 is obtained the experiment is considered to be finished. The time taken to reach this OD is therefore a measure of how many bacteria are present after being exposed to the respective treatments. An average of seven wells is then taken to give a mean time. It is therefore a long mean time which indicates an effective treatment. The results from the biofilm experiment are represented graphically in this section.

3.3.3. Biofilm Assay Results

As well as being a more effective method of predicting the anti-bacterial properties of a new compound, the biofilm assay also has the advantage of allowing the testing of compounds which are too insoluble to be tested using the pH stat (which requires test solutions in neutral aqueous solution). The reason being that it was possible to use dimethylsulphoxide (DMSO) as a solvent in the biofilm assay to dissolve the compounds, and run DMSO controls to determine the extent to which the bacteria are affected by the solvent alone. The results of the DMSO controls were subtracted from the test results to give an indication as to the biological activity of the compound alone. All of the tests were carried out using either *Enterobacter cloacae (E. cloacae)* or *Staphylococcus saprophyticus (S. saprophyticus)* bacteria. For the purpose of this experiment the compounds were dissolved in DMSO, with the exception of the water soluble triclosan phosphate.

The concentrations of the compounds tested were, with the exception of the Zn(II) triclosan phosphate (**13**), close to the concentration of triclosan which is typically used in dental formulations, i.e. ca. 0.3% w/w. Compounds **10** and **11** were assayed at a

concentration of 0.4% w/w, compound **14** at 0.5% w/w, compound **13** at 0.9% w/w and compound **12** at a concentration of 6000ppm Sn^{2+} (to allow comparison with the 6000ppm SnF_2 control, equivalent to 1%w/w in a toothpaste formulation). The reason for using Cu(II) triclosan phosphate at 0.5% while using Zn(II) triclosan phosphate at 0.9% was that in commercial products the maximum amount of copper permitted is significantly lower than zinc. The actual concentrations used in the assay were not too important, as the biofilm assay is only a preliminary guide as to whether a particular compound shows *in vitro* biological activity. A more comprehensive biological assay would have to be run to determine the concentration at which the compounds exhibit maximum activity, and this was outside the scope of this work.

Analysis of the results from the biofilm assays shows that it is difficult to correlate data from different batches of bacteria (the assays being performed 4-5 months apart). This is why stannous fluoride (used as a positive control at a concentration of 6000 ppm Sn^{2+}) was evaluated in both assay 1 and assay 2, to allow some degree of correlation to be made between the two. As mentioned previously the exact concentration of the test sample is not too important, and the results presented in Figures 3.10, 3.11 and 3.12 clearly show that some of the compounds tested were anti-bacterial.

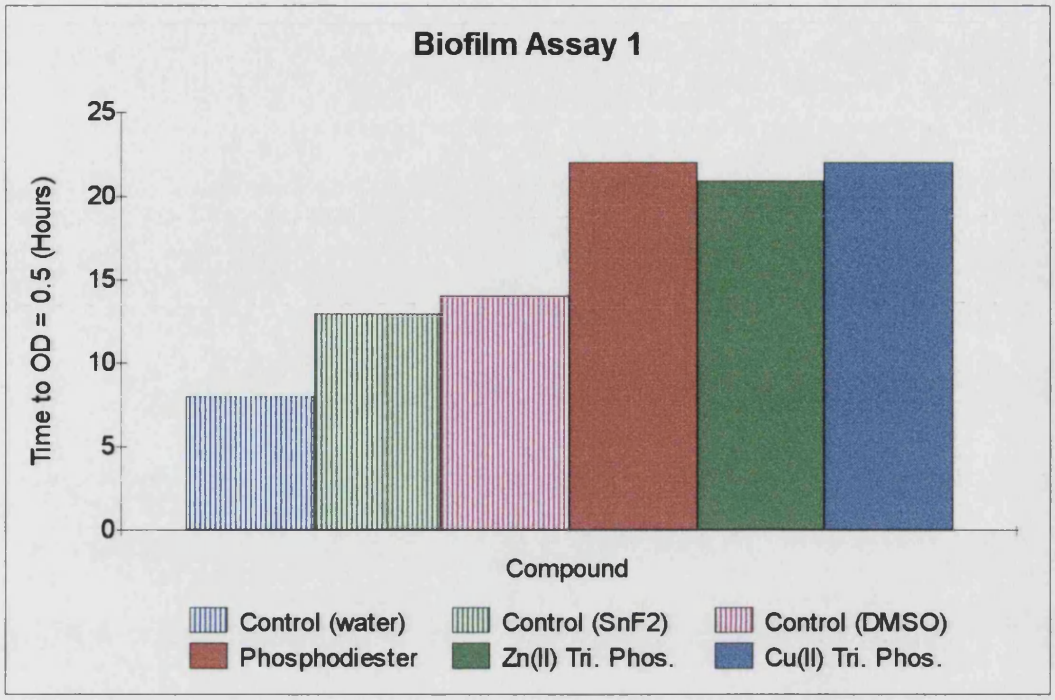

Figure 3.10. Results from Biofilm Assay 1 (bacteria used *E cloacae*).

As can be seen from the results for Assay 1, the bacteria took over eight hours to regrow (to the extent where the OD reaches 0.5) in the water control. As the control value should be around four hours, this result suggests that the bacteria used for the experiment were not as active as usual. The results for the wells containing the DMSO controls were also nearly double in the first assay which supports the hypothesis that the bacteria were not as active, and explains the long regrowth times observed for the wells containing the test samples. The results obtained for Cu(II) triclosan phosphate (**14**) and the phosphodiester of triclosan (**11**) in Assay 1 were significantly longer than the other compounds in the assay. One reason for this could be that compounds **11** and **14** are much more active than the others and that all of the bacteria in the wells exposed to these compounds are destroyed in which case the OD will never reach 0.5 during the assay. This hypothesis seems reasonable although one would expect that the Zn(II) triclosan phosphate (**13**) result would be comparable. It is possible that in solution basic zinc salts could be forming [e.g. $Zn(OH)_3(H_2O)]^-$, which would probably not exhibit anti-bacterial activity as the zinc would not be accessible through lack of solubility.

The DMSO alone kills a large number of bacteria as can be seen from the results where the time taken to reach the specified OD is almost double what is seen in the water control. The results do show however that the DMSO does not kill all the bacteria, which means that a measure of the efficacy of the test compounds can be made.

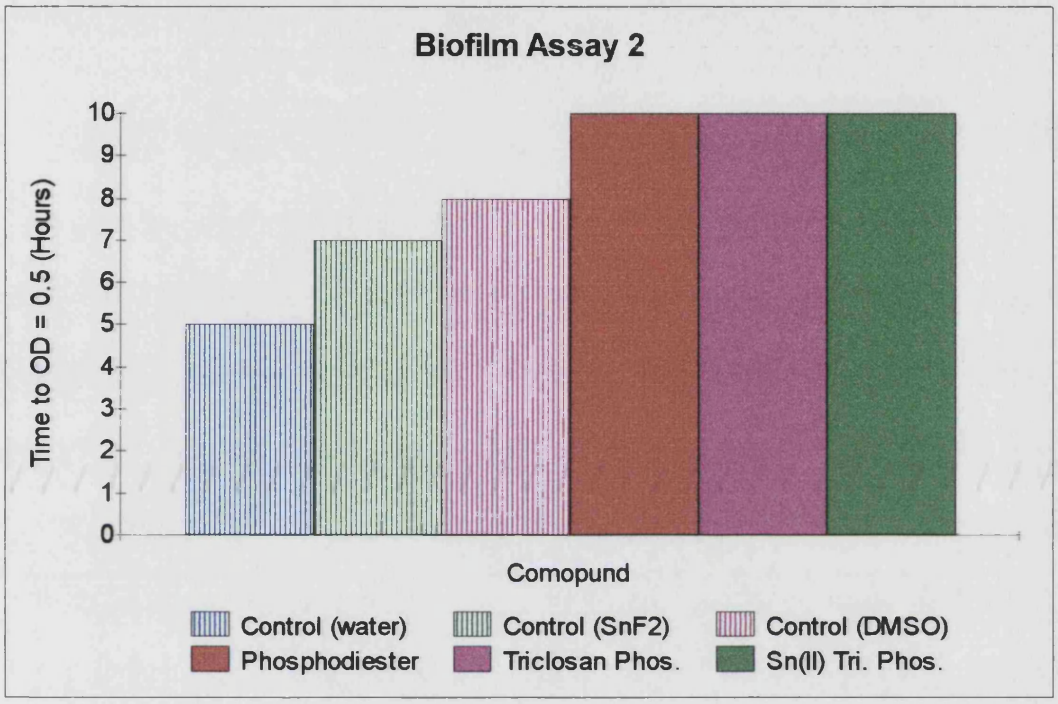

Figure 3.11. Results from Biofilm Assay 2 (bacteria used *E cloacae*).

In Assay 2, both the phosphodiester of triclosan and the Sn(II) triclosan phosphate were dissolved in DMSO/H_2O the results indicating moderate anti-bacterial activity. The result for the phosphodiester of triclosan from this assay was unexpected when compared to the results from Assay 1 (Figure 3.10), where it appeared that all of the bacteria had been killed. However it can be seen from the results that the three test compounds exhibit anti-bacterial activity greater than the DMSO alone. This was encouraging as even against the more active bacteria, the compounds tested showed a degree of efficacy.

The results obtained for the triclosan phosphate were encouraging since this compound was dissolved in water alone for this test. The time taken for the OD to reach 0.5 was nearly 10 hours which was the best of all the results from the second assay.

It is evident from both Assays 1 and 2 that all five of the test compounds exhibit activity over and above that of the SnF_2 control. These are encouraging *in vitro* assay results, and indicate that the incorporation of the test compounds into dental formulations may result in promising *in vivo* assay results.

A third experiment was carried out, this time using three concentrations of triclosan phosphate in water, and also a mixture of triclosan phosphate with sodium lauryl sulphate (SLS) to see if there were any synergistic effects obtained from using the two agents together. It is known that when SLS is used with triclosan that there is an increase in the biological activity.[185] Sodium lauryl sulphate is used as standard in most toothpaste formulations as a detergent, and is known to be anti-bacterial.[185-189]

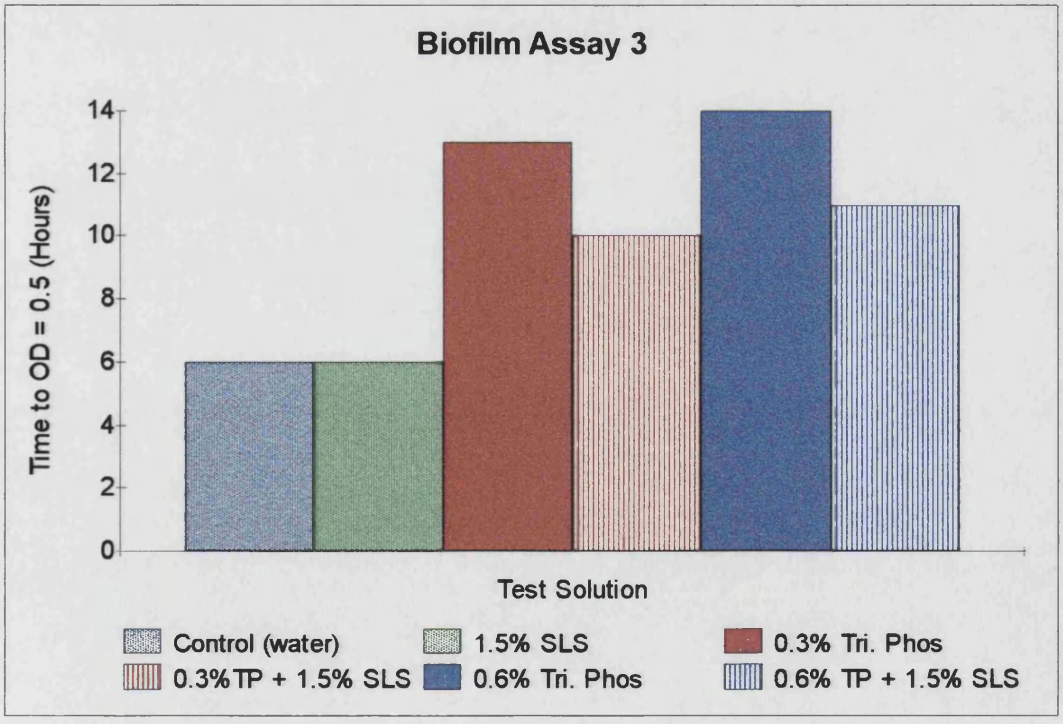

Figure 3.12. Results from Biofilm Assay 3 (Bacteria used - *S. saprophyticus*).

The results from Assay 3 (Figure 3.12) were encouraging in that they confirmed that triclosan phosphate is indeed a potent anti-bacterial agent. The reason for using the SLS was to see if there were any synergistic effects between the two agents. The results showed that there is no synergism. It is known that the *S. saprophyticus* is more resistant to SLS than is *E. cloacae* which is why it was chosen for this experiment to see if the triclosan phosphate would disrupt/attack the bacteria and the SLS would then be able to attack the vulnerable bacteria. Triclosan phosphate appears to be more active against the *S. saprophyticus* than the *E. cloacae*. Although the triclosan phosphate is effective against *S. saprophyticus*, it is evident from the results presented in Figure 3.12 that the mixtures of triclosan phosphate and SLS are at best as, or usually less, effective than the triclosan phosphate alone. This implies there is no synergism between triclosan phosphate and SLS, which there is with triclosan and SLS.[185]

Triclosan phosphate has been patented by Proctor and Gamble, so it is not possible to use the compound in its original form. It is possible however to use modified triclosan phosphate molecules such as the M(II) triclosan phosphates and the diester of triclosan phosphate.

From the biofilm assay results obtained it is notable that the Sn(II) triclosan phosphate offers no improved anti-bacterial activity over that of triclosan phosphate. This result could be due to instability of the compound with respect to oxidation, apparent from the results of the Mössbauer experiments. The Zn(II) and Cu(II) triclosan phosphates on the other hand exhibit much greater anti-bacterial activity than triclosan phosphate, indicating a possible synergistic effect between the triclosan and the bactericidal metal ions. Since the assays were carried out in DMSO it is difficult to say for certain whether it is the compound itself which is active, or whether the solvent has the effect of breaking the molecule down to triclosan phosphate and Zn(II)/Cu(II) ions. It is therefore evident that further work must be done to ascertain why there is increased anti-bacterial activity, before any further biological testing is carried out on the active compounds.

The patent which covers the use of triclosan phosphate in dental formulations does not cover the use of the diester. The preliminary *in vitro* assay results obtained were therefore encouraging as they showed the diester to be more active than triclosan phosphate, which is perhaps not surprising as the diester has two molecules of triclosan compared to one molecule from triclosan phosphate. The increased activity of the diester over the triclosan monophosphate suggests that further work with the diester is needed, in terms of producing M(II) derivatives. Also, the M(II) diester is less likely to be polymeric (i.e. insoluble) as less "sterically open" oxygen available for intermolecular coordination. If this is possible, the compounds produced should exhibit very good *in vitro* anti-bacterial assay results due to synergism between the bactericidal metal ions and the diester. Further work in this area could thus be focused on metal derivatives of the diester. It may be possible, if feasible from a steric viewpoint, to try to replace the last OH group with another molecule of triclosan, thus producing a triester of triclosan phosphate. A molecule such as this would theoretically give even better anti-bacterial results as it would contain three molecules of triclosan.

In conclusion, the results obtained from the pH stat and the biofilm assays show that triclosan phosphate is a very active compound, and that if an M(II) derivative could be made more water soluble that an even more active compound could possibly be produced. The diester of triclosan phosphate is a compound which should definitely be pursued further, especially the possibility of a metal derivative as this should present a compound which has very high anti-bacterial activity.

3.4. Experimental

3.4.1. Synthesis of triclosan phosphate monohydrate (10)

To a 3-litre, 3-necked round-bottomed flask fitted with a mechanical stirrer was added triclosan [(50g, 173mmol) IrgacareMP, HX533 from Ciba-Geigy]. Phosphoryl chloride (60.8g, 396mmol) was added and mechanical stirring begun. Once the triclosan had dissolved, the vessel was immersed in an ice-water bath and the solution stirred for a further 10 minutes. Triethylamine (19.2g, 190mmol) was then introduced dropwise via an addition funnel over a period of 30 minutes. The resulting viscous mixture was stirred for an additional 2 hours at 0°C, and for a further 30 minutes at room temperature.

Diethyl ether (500ml) was introduced to the flask with stirring, resulting in a granular suspension. The flask was again cooled to 0°C before the addition of water (500ml) in a dropwise manner over a period of ca. 1 hour. The dropping rate for the first 100ml was 1 drop every 2 seconds. The resulting amber biphasic system was stirred at 0°C for 2 hours, then at ambient temperature overnight. Diethyl ether (500ml) was again added to the mixture with stirring.

The entire contents of the flask was then transferred to a separating funnel, where the lower, aqueous phase, was drained off and extracted with 2x500ml portions of ether. The original ether phase from the reaction mixture was then recombined with these two subsequent ether extracts. The acidic aqueous phase was then discarded.

The ether solution, containing primarily triclosan monophosphate and a phosphodiester by-product, was extracted with 4x1 litre portions of 1M NaOH. The combined NaOH extracts were back extracted with 2x500ml portions of ether. These ether extracts were added to the original ether solution. The NaOH solution (containing the pure triclosan monophosphate) was acidified with concentrated HCl to pH 1.0±0.2, and then extracted with 3x500ml portions ether. The combined extracts were dried over

$MgSO_4$, filtered, and concentrated to an oil *in vacuo*. The oil was triturated with dichloromethane (1 litre) which induced crystallisation/precipitation. The resulting white solid was filtered using a Büchner funnel, and dried *in vacuo* for 48 hours, yielding the title product (20g).

Analysis, found (calc. for$C_{12}H_8Cl_3O_5P$): C, 38.3 (39.0); H, 2.17 (2.18).

Selected infrared data: 3400cm^{-1} υ(H-O-H); 1610cm^{-1} δ(H-O-H); 1278cm^{-1} υ(P=O); 1188cm^{-1} υ(P-O); 1126-1059cm^{-1} (C-O); 780-690cm^{-1} υ(C-Cl).

^{1}H NMR (d_6-Acetone): 7.58ppm (*d*, 1H, $J_{2\text{-}4}$=2.4Hz)H_2; 7.56 (*d*, 1H, $J_{11\text{-}9}$=2.6Hz)H_{11}; 7.35 (*dd*, 1H, $J_{9\text{-}8}$=8.8Hz, $J_{9\text{-}11}$=2.6Hz)H_9; 7.22 (*dd*, 1H, $J_{4\text{-}5}$=8.8Hz, $J_{4\text{-}2}$=2.4Hz)H_4; 7.01(*d*, 1H, $J_{5\text{-}4}$=8.8Hz)H_5; 6.98(*d*, 1H, $J_{8\text{-}9}$=8.8Hz)H_8; 5.18(*s*, 2H)2xP-O*H*.

^{13}C{^{1}H} NMR (d_6-Acetone): 152.4ppm (C_7), 146.9 (C_6, $^2J_{P\text{-}C}$=5.5Hz), 143.7 (C_1, $^2J_{P\text{-}C}$=5.4Hz), 130.9 (C_{10}), 129.6 (C_3), 126.3 (C_{12}), 130.8, 129.3, 126.2, 122.9, 121.8, 121.6 (C_2, C_4, C_5, C_8, C_9, C_{11} - all C-H).
^{31}P{^{1}H} NMR (d_6-Acetone): -3.7ppm.

3.4.1.2. Data for the crystals of pyridinium triclosan-2′-phosphate.

^{1}H NMR (d_6-DMSO): 8.60ppm (*d*, 2H, J=4.3Hz)pyridineH; 7.83 (*m*, 1H)pyridineH; 7.74 (*d*, 1H, $J_{2\text{-}4}$=2.7Hz)H_2; 7.56 (*d*, 1H, $J_{11\text{-}9}$=2.4Hz)H_{11}; 7.43 (*m*, 2H)pyridineH; 7.38 (*dd*, 1H, $J_{9\text{-}11}$=2.4, $J_{9\text{-}8}$=8.9Hz)H_9; 7.18 (*d*, 1H, $J_{8\text{-}9}$=8.9Hz)H_8; 7.00 (*dd*, 1H, $J_{4\text{-}5}$=8.9, $J_{4\text{-}2}$=2.7Hz)H_4; 6.90 (*d*, 1H, $J_{5\text{-}4}$=8.9Hz)H_5.

^{13}C{^{1}H} NMR (d_6-DMSO): 155.8ppm (C_7), 148.9 (C_6), 143.7 (C_1), 128.9 (C_{10}), 127.9 (C_3), 125.8 (C_{12}), 127.4, 128.7, 125.6, 124.5, 121.5, 120.6 (C_2, C_4, C_5, C_8, C_9, C_{11} - all C-H).

^{31}P{^{1}H} NMR (d_6-DMSO): -5.9ppm.

3.4.1.3. Synthesis of triclosan phosphate diester dihydrate (11)

This compound is a by-product of the synthesis of triclosan phosphate, as detailed in section 3.5.1. It was isolated from the ether portion of the solvent extraction (in which the aqueous portion contained the triclosan monophosphate) by removal of the solvent using a rotary evaporator.

Analysis, found (calc. for $C_{24}H_{16}Cl_6O_8P$): C, 42.7 (42.6); H, 2.33 (2.39).

Selected infrared data: 3330cm^{-1} υ(H-O-H); 1640cm^{-1} δ(H-O-H); 1265cm^{-1} υ(P=O); 1230, 1204cm^{-1} υ(P-O-Aryl); 1120-1000cm^{-1} υ(C-O); 780-690cm^{-1} υ(C-Cl).

^{1}H NMR (d_6-Acetone): 7.83ppm (*d*, 1H, $J_{2\text{-}4}$=2.4Hz)H_2; 7.45 (*d*, 1H, $J_{11\text{-}9}$=2.1Hz)H_{11}; 7.15 (*dd*, 1H, $J_{4\text{-}2}$=2.4, $J_{4\text{-}5}$=8.8Hz)H_4; 6.97 (*d*, 1H, $J_{8\text{-}9}$=8.5Hz)H_8; 6.79(*dd*, 1H, $J_{9\text{-}8}$=8.5, $J_{9\text{-}11}$=2.1Hz)H_9; 6.75(*d*, 1H, $J_{5\text{-}4}$=8.5Hz)H_5.

^{13}C{^{1}H} NMR (d_6-Acetone): 153.3ppm (C_7), 146.5 (C_6), 145.2 (C_1), 129.8 (C_3), 129.3 (C_{10}), 125.4 (C_{12}), 130.9, 128.5, 124.7, 122.4, 121.9, 121.0 (C_2, C_4, C_5, C_8, C_9, C_{11} - all C-H).

^{31}P{^{1}H} NMR (d_6-Acetone): -8.4ppm and -13.8ppm (major peak - ca. 80%).

3.4.2. Synthesis of Sn(II) triclosan phosphate (12)

Triclosan phosphate (0.3g, 0.81mmol) was added to thoroughly degassed water (30ml) with stirring. Once dissolved, a solution of stannous chloride (0.15g, 0.81mmol) in H_2O (10ml) was added causing a precipitate. This precipitate was filtered rapidly, washed with water and ethanol before being dried in vacuo to yield the title compound (0.32g, 80%).

Analysis, found (calc. for $C_{12}H_6Cl_3O_5PSn$): C, 29.2 (29.6); H, 1.18 (1.24).

Selected infrared data: 1296cm^{-1} υ(P=O); 1230, 1200cm^{-1} υ(P-O-Aryl); 1160-1048cm^{-1} υ(C-O); 780-690cm^{-1} υ(C-Cl).

^{1}H NMR (d_6-DMSO): 7.66ppm (*d*, 1H, $J_{2\text{-}4}$=2.4Hz)H_2; 7.59 (*d*, 1H, $J_{11\text{-}9}$=2.4Hz)H_{11}; 7.30 (*dd*, 1H, $J_{9\text{-}11}$=2.4, $J_{9\text{-}8}$=8.5Hz)H_9; 7.11 (*d*, 1H, $J_{8\text{-}9}$=8.5Hz)H_8; 6.88(*dd*, 1H, $J_{4\text{-}5}$=8.8, $J_{4\text{-}2}$=2.4Hz)H_4; 6.71(*d*, 1H, $J_{5\text{-}4}$=8.8Hz)H_5.

^{13}C{^{1}H} NMR (d_6-DMSO): 151.6ppm (C_7), 149.9 (C_6), 141.3 (C_1), 130.0 (C_3), 128.5 (C_{10}), 124.6 (C_{12}), 130.2, 129.9, 123.3, 122.9, 121.5, 119.7 (C_2, C_4, C_5, C_8, C_9, C_{11} - all C-H).

^{31}P{^{1}H} NMR (d_6-DMSO): -12.1, -12.9, -16.8, -21.7ppm.

^{119m}Sn Mössbauer: δ=3.08mms^{-1}, Δ=1.83mms^{-1}, Γ_1=0.81mms^{-1}, Γ_2=0.81mms^{-1}.

3.4.3. Synthesis of Zn(II) triclosan phosphate dihydrate (13)

Triclosan phosphate (0.15g, 0.40mmol) and sodium hydrogen carbonate (0.07g, 0.81mmol) were added to water (40ml) with stirring. Once dissolved, a solution of zinc chloride (0.06g, 0.40mmol) was added causing a precipitate to be formed which was filtered and dried *in vacuo*. This yielded the title product (0.14g, 75%) as a white powder.

Analysis, found (calc. for $C_{12}H_{10}Cl_3O_7PZn$): C, 30.4 (30.7); H, 2.08 (2.14).

Selected infrared data: 3300cm^{-1} υ(H-O-H); 1630cm^{-1} δ(H-O-H); 1280cm^{-1} υ(P=O); 1230, 1200cm^{-1} υ(P-O-Aryl); 1160-1020cm^{-1} υ(C-O); 780-690cm^{-1} υ(C-Cl).

^{1}H NMR (d_6-DMSO): 7.69ppm (*d*, 1H, $J_{2\text{-}4}$=2.4Hz)H_2; 7.61(*d*, 1H, $J_{11\text{-}9}$=2.5Hz)H_{11}; 7.33 (*dd*, 1H, $J_{9\text{-}11}$=2.5, $J_{9\text{-}8}$=8.5Hz)H_9; 7.14 (*d*, 1H, $J_{8\text{-}9}$=8.5Hz)H_8; 6.93(*dd*, 1H, $J_{4\text{-}5}$=8.8, $J_{4\text{-}2}$=2.4Hz)H_4; 6.75(*d*, 1H, $J_{5\text{-}4}$=8.8Hz)H_5.

^{13}C{^{1}H} NMR (d_6-DMSO): 151.4ppm (C_7), 145.0 (C_6), 144.2 (C_1, $^2J_{P\text{-}C}$=3.7Hz), 128.7 (C_3), 128.3 (C_{10}), 124.5 (C_{12}), 129.9, 127.8, 123.9, 121.6, 121.1, 120.5 (C_2, C_4, C_5, C_8, C_9, C_{11} - all C-H).

^{31}P{^{1}H} NMR (d_6-DMSO): -6.1ppm.

3.4.4. Synthesis of copper(II) triclosan phosphate monohydrate (14)

Triclosan phosphate (0.15g, 0.40mmol) and sodium hydrogen carbonate (0.07g, 0.81mmol) were added to water (40ml) with stirring. Once dissolved, copper nitrate (0.09g, 0.40mmol) was added causing the formation of a precipitate, which was filtered and dried *in vacuo*. This yielded the title product (0.15g, 80%) as a blue powder.

Analysis, found (calc. for $C_{12}H_8Cl_3O_6PCu$): C, 31.7 (32.1); H, 1.74 (1.79).

Selected infrared data: 3320cm^{-1} υ(H-O-H); 1625cm^{-1} δ(H-O-H); 1285cm^{-1} υ(P=O); 1235, 1200cm^{-1} υ(P-O-Aryl); 1150-1010cm^{-1} υ(C-O); 780-690cm^{-1} υ(C-Cl).

3.5. Conclusions

The research carried out in this chapter has led to the production of a number of new compounds, all of which are based on triclosan. In addition to the new M(II) compounds which were produced, the crystal structure of pyridinium triclosan phosphate was solved.

The basis of this chapter, as mentioned previously, was triclosan, a phenolic compound with known anti-bacterial activity. The precise reason for the activity of triclosan is not known hence the interest in the compounds synthesised in this chapter. It was hoped that the combination of triclosan (in the form of triclosan phosphate) and bactericidal metal ions would work in a synergistic manner giving enhanced anti-bacterial activity. It was not possible to use the triclosan directly in combination with the metal ion as there was no way of forming a stable system. For this reason the triclosan was first converted into triclosan monophosphate which afforded a stable complex when reacted with Sn(II), Zn(II) and Cu(II).

Recrystallisation of the triclosan monophosphate from pyridine yielded a bis-pyridine solvate with an interesting crystal structure in which one of the two pyridine molecules was found to be hydrogen bonded to the phosphate group. The pyridinium group was found to be present in the lattice and non hydrogen bonded. The acidity of the two hydroxyl groups are different, and this will explain why, along with steric factors, there is only one hydrogen bonded pyridine molecule. Another factor which could explain the uncoordinated pyridine molecule is the high boiling point of pyridine which makes it difficult to remove all residual solvent from the crystal lattice.

During the synthesis of triclosan phosphate a second compound was isolated, the diester of triclosan phosphate, which has yet to be fully investigated. This compound offers the potential of producing metal derivatives with enhanced anti-bacterial activity. Another compound which merits further investigation as to its synthesis is the triester of triclosan phosphate which could potentially offer a greater delivery of triclosan than

either the mono- or di- ester. The drawback to this compound would be that there is no way of producing a metal derivative.

The anti-bacterial testing of the compounds synthesised in this chapter yielded some interesting findings as to the source of the activity of triclosan, and other compounds.

The results obtained showed that the Sn(II) triclosan phosphate exhibited an identical level of activity to the triclosan monophosphate alone. This suggested that the compound was being broken down to its constituent parts i.e. Sn(II) and triclosan monophosphate, and subsequently the Sn(II) was being oxidised into Sn(IV) and thereby losing its biological activity. This theory is strengthened by the results obtained for the Zn(II) and Cu(II) triclosan phosphates which both exhibited a much higher (at least double) activity then the triclosan phosphate alone. The Cu(II) triclosan phosphate gave results of more than double those obtained for the Zn(II). The reason for this increased activity could be that Cu(II) ions are known to have a higher efficacy than Zn(II) ions although the copper was used at a lower concentration during the assay to minimise this.

The Sn(II) triclosan phosphate is not commercially viable as the results of the Mössbauer show that the Sn(II) is rapidly oxidised to Sn(IV) when formulated in a toothpaste, and is thus rendered biologically inactive. Triclosan phosphate alone has the potential to be used in toothpastes due to its high level of activity. The Zn(II) and Cu(II) triclosan phosphates and the phosphodiester of triclosan are all potentially commercially viable as they have high levels of activity, along with increased stability compared to the Sn(II) triclosan phosphate.

CHAPTER 4

MALTOL AND RELATED COMPOUNDS

4. CHAPTER 4 - MALTOL AND RELATED COMPOUNDS

4.1 Introduction

There has recently been both biological and medicinal interest in compounds which have both ketone and hydroxyl functional groups adjacent to one another,[190] and which exhibit anti-bacterial properties. Two compounds which fit into this category are 2-hydroxy-2,4,6-cycloheptatrien-1-one, commonly known as tropolone (II), and 6-isopropyltropolone (III), commonly called hinokitiol.

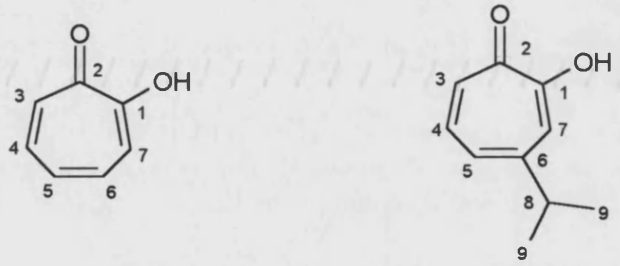

(II) (III)

Figure 4.1. Tropolone (II) and Hinokitiol (III), including atom numbering.[191]

Tropolone is a representative of the non-benzenoid aromatic compounds, and has been studied in depth over the last thirty to forty years. The functional groups of tropolone allow complexation of a number of different metal ions (M^{2+}, M^{3+} and M^{4+}). Hinokitiol is isolated from the wood of the *Chamacyparis taiwanesis* tree, and since its discovery in 1936[192] it has been reported to exhibit anti-microbial effects,[190] and also to stimulate plant growth.

Bis(tropolonato)copper(II)[193] is one example of many M(II) tropolone complexes which have been reported.[194] As the name suggests, Cu(II) tropolone incorporates two univalent ligands, with the Cu atom adopting four-coordinate square planar geometry. The Cu-O bonds are equivalent, 1.913(3) and 1.915(3)Å respectively, and the angle O-

Cu-O is 83.8°. The delocalised negative charge and the formation of a five-membered chelate ring probably contributes to the effectiveness of this compound in forming complexes with metal ions. The tropolonate ligands show significant deviations from planarity in this complex (an angle of 5.6° between the plane of the tropolone ring and that formed by the O-Cu-O bonds), whereas the uncoordinated ligand is planar to within 0.021Å.[195] This deviation from planarity has a significant influence on the properties of the complex, as it is not stabilised by stacking interactions as is the case with tropolone.

There are a number of M^{3+} (bis and tris)[196,197] and M^{4+} (bis, tris and tetra)[198,199] tropolone complexes which have been structurally characterised, but these are outside the scope of this review.

Another important class of compounds which contain the same functional groups as tropolone and hinokitiol are the pyranones and pyridinones. An example of a compound which belongs to this group is 3-hydroxy-2-methyl-4H-pyran-4-one (**VIII**), commonly called maltol.

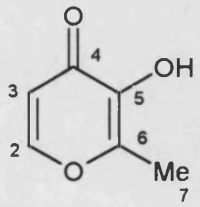

Figure 4.2. Maltol (**VIII**), including atom numbering.

Maltol, a naturally occurring pyranone, is a water soluble, non-toxic food additive, much used in the baking industry.[200] When deprotonated it forms an anionic system capable of acting as a chelating, bidentate, O,O′ ligand as shown in Figure 4.3. Because this ligand can confer water solubility on its metal complexes, even when the complexes are uncharged, there have been many reports on the use of this ligand in biological studies.[201-203]

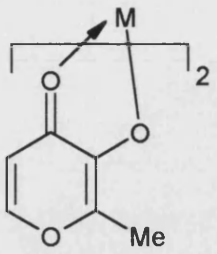

Figure 4.3. M(II) maltolate.

As can be seen from Figure 4.3, maltol forms a bis complex with M^{2+} ions such as Ru(II)[204]. It follows therefore that with M^{3+} maltol will form tris complexes, and this is indeed the case, e.g., $Al(maltol)_3$[201] and $Fe(maltol)_3$.[202,205] These types of compounds have many uses, for example, $Al(maltol)_3$ has been used in recent work on Alzheimer's disease,[201] $Fe(maltol)_3$ has been shown to have potential use as a treatment for iron-deficiency anaemia[202] and $V^{IV}(O)(maltol)_2$ has been tested as an insulin mimetic.[203]

The structure of $Ru(maltol)_2(cod)$ has been solved[204] and shows similarities with the tropolonate complexes. The Ru-O bond lengths are typically 2.098 and 2.126Å. The bite angle of the two donor oxygens from the ligand at the Ru is 79.5°, which is slightly smaller than that for bis(tropolonato)copper(II) (83.8°). This small separation between the oxygen donor atoms, similar to that observed in tropolone, illustrates why the two ligands form similar complexes i.e., five-membered chelate rings. The formation of stable MO_2C_2 rings is also an important factor in the above examples.

The synthesis and characterisation of copper and zinc derivatives of maltol, ethyl maltol and hinokitiol is detailed in this chapter. The evaluation of the maltol and ethyl maltol compounds for anti-bacterial activity using the biofilm assay is also detailed.

4.2. Synthesis and Characterisation of M(II) Maltolate and M(II) Hinokitiol

4.2.1. Synthetic strategies for M(II) Maltolate and M(II) Hinokitiol

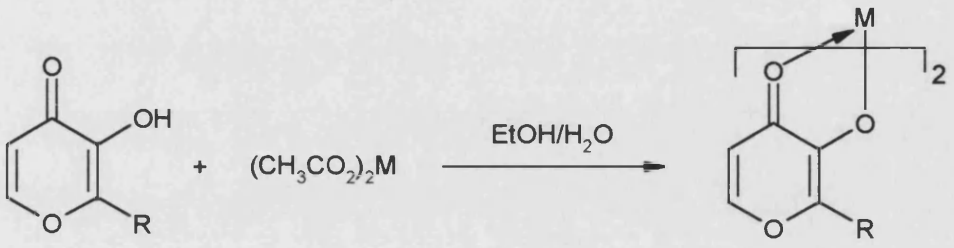

M = Zn, R = Me (**15**)
M = Cu, R = Me (**16**)
M = Zn, R = Et (**17**)
M = Cu, R = Et (**18**)

Scheme 4.1. Synthesis of M(II) maltolate and M(II) ethyl maltolate.

Zn(II) maltolate (**15**) was prepared by the reaction, in aqueous ethanol, of maltol with a solution of Zn(II) acetate. After refluxing for 2 hours the solution had turned pale yellow in colour with no precipitation evident. This solution was allowed to stand until precipitation or crystallisation began. After 1 week there was a large number of colourless crystalline needles present in the solution which, upon analysis, were found to be Zn(II) maltolate. The microanalytical data for **15** indicated that the complex formed was a dihydrate. The crystals formed were of a very good quality and size and were submitted for X-ray analysis. The results from the X-ray structural data obtained are presented both in Section 4.2.3 and in Appendix C.

Cu(II) maltolate (**16**) was prepared as shown in Scheme 4.1, and as with the zinc complex was allowed to stand in order to crystallise from the solution. After standing for 1 week a green/blue solid precipitated from the solution and, after drying, the

microanalysis showed this solid to be anhydrous Cu(II) maltolate. Attempted recrystallisations, for the purpose of X-ray studies, from all common solvents proved unsuccessful.

Zn(II) ethyl maltolate (**17**) was prepared in the same way as the zinc(II) maltolate (Scheme 4.1), the only difference being that the eventual product precipitated from solution after 48 hours as an amorphous solid, not in a crystalline form. As with the Zn(II) maltolate, microanalysis on Zn(II) ethyl maltolate showed the complex to be dihydrated even after extensive drying. Recrystallisation work with the Zn(II) ethyl maltolate did not yield any crystals, which, considering the only difference between maltol and ethyl maltol is an extra CH_2 group, was quite surprising.

Cu(II) ethyl maltolate (**18**) was prepared in the same way as copper(II) maltolate (Scheme 4.1), with the method again yielding a green/blue solid which after drying was also found to be anhydrous. Recrystallisation for the purpose of growing crystals for X-ray analysis of this complex again proved unsuccessful from all common solvents.

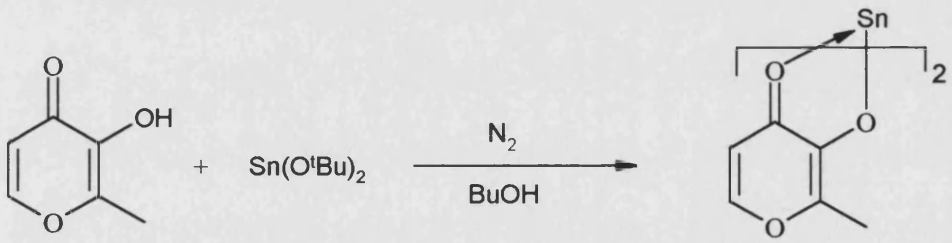

Scheme 4.2. Attempted synthesis of Sn(II) maltolate.

As shown in Scheme 4.2, maltol was reacted with a solution of Sn(II) butoxide under an inert nitrogen atmosphere, a reaction which should have produced Sn(II) maltolate. The mixture was then refluxed for 2 hours before being allowed to stand to crystallise. Analysis of the product by Mössbauer showed that the sample had oxidised to Sn(IV), and for this reason no other data (e.g. IR or NMR) were collected. The Mössbauer spectrum exhibited just one large singlet at δ=0.00mms^{-1} indicating a Sn(IV) sample. As it is known that only Sn(II) compounds exhibit anti-bacterial activity this spectra was never interpreted any further, nor were any other analyses, other than

microanalysis, carried out. After standing for a number of months the Sn(IV) compound was found to have crystallised out of solution, yielding crystals of a suitable quality to enable the crystal structure to be determined. Unfortunately due to the small number of crystals produced no other analyses could be carried out on the crystals, which is why no other information is given in the experimental section (compound number **21**).

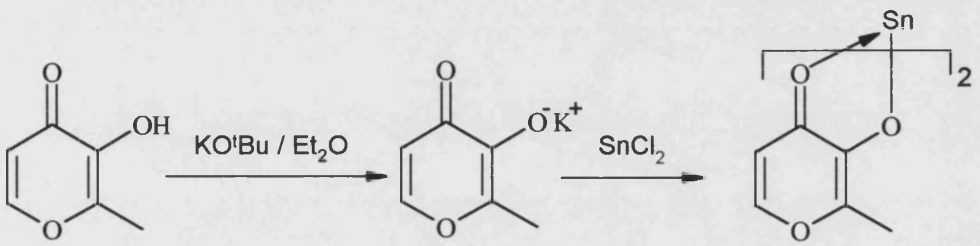

Scheme 4.3. Attempted synthesis of Sn(II) maltolate.

The synthesis of Sn(II) maltolate (Scheme 4.3) was also attempted using a recently reported method[204] for the synthesis of Ru(II) maltolate. This method details the production of the potassium salt of maltol by reaction with ^{t}BuOK in ether. The salt was then reacted with $RuCl_2$ to yield the Ru(II) maltolate. This method was adapted for the attempted synthesis of Sn(II) maltolate, using $SnCl_2$ instead of $RuCl_2$. The solution produced by this method (which should contain Sn(II) maltolate) was allowed to stand for 1 week after which time there was still no solid product. Removal of the solvent *in vacuo* yielded a white solid which was recrystallised from a number of common solvents, but unfortunately did not yield any crystals - a white solid was produced each time. A Mössbauer spectrum was recorded on the sample produced, and analysis of this spectrum showed that the sample had oxidised to Sn(IV). As with the previous attempt to produce a sample of Sn(II)maltolate, the Mössbauer spectrum was never interpreted fully as the fact that the sample had oxidised was enough information.

Another method which was looked at was to use Sn(II) acetate in a similar way to how the Zn(II) and Cu(II) maltolate were synthesised. This was unsuccessful, presumably due to the limited solubility of Sn(II) acetate.

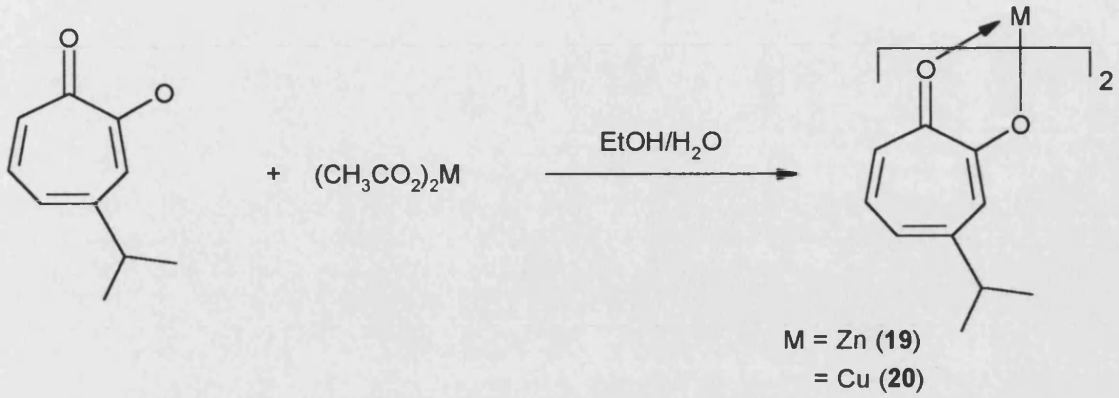

Scheme 4.4. Synthesis of M(II) hinokitiol.

As can be seen in Scheme 4.4, the synthesis of Zn(II) and Cu(II) hinokitiol is much the same as that employed for the maltol and ethyl maltolate reactions. The Zn(II) hinokitiol complex (**19**) differed from the other zinc complexes detailed in this chapter in that it was found, by microanalysis, to be anhydrous. The yellow solid which precipitated from solution after 4 days was recrystallised from toluene and other common solvents, but unfortunately this yielded only yellow solids, and not crystals for X-ray work.

Cu(II) hinokitiol (**20**) was synthesised using the method detailed in Scheme 4.4, but yielded a different result in that after 1 week a large number of blue plate-like crystals had formed in the solution. Microanalysis of these crystals showed the complex to be anhydrous. The crystals were of sufficient quality to enable an X-ray structure to be obtained, the results of which are shown both in Section 4.2.4 and Appendix D.

4.2.2. Comparison of infrared and NMR spectra for M(II) maltolate, M(II) ethyl maltolate and M(II) hinokitiol

The infrared spectra of the compounds detailed in this chapter are relatively similar, as one would expect. The υ(C=O) band which appears at ca. 1650cm^{-1} in all of the starting materials is shifted to a lower wavenumber by between 36-53cm^{-1} in the

M(II) complexes. The bands at 1610 and 1550cm^{-1}, which probably arise from mixed υ(C=C) and υ(C=O) modes,[206] are also shifted to lower wavenumbers on coordination. Also evident from the spectra of the hydrated complexes is a peak at ca. 1600cm^{-1} due to waters of crystallisation (a weak broad band is also present at ca. 3300cm^{-1} due to the water). These findings are consistent with the infrared data quoted for a number of M(II) maltolates,[207] Al(malt)$_3$,[201] Re(O)Br(malt)$_2$,[208] and also In(III) tropolonate[209] and catecholato complexes.[210] The results collected from the infrared experiments are good evidence for the formation of M(II) maltol/hinokitiol/ethyl maltol complexes by removal of the hydroxyl proton, and chelation by the carbonyl oxygen. Further evidence for this bonding can be seen in the crystal structures of Zn(II) maltolate (Section 4.2.3) and Cu(II) hinokitiol (Section 4.2.4).

^{1}H NMR spectra were recorded for Zn(II) maltolate and Zn(II) ethyl maltolate, and the peaks which appeared in the spectra were relatively simple to assign to the protons of the complexes. In Zn(II) maltolate the three methyl protons (C_7 - see Figure 4.2) gave a singlet at δ = 2.32ppm, a peak which integrated well for 3H. There was also two doublets at δ = 6.52, 8.09 ppm, both of which integrated for 1H, and were assigned to the protons in the five and six positions respectively (see Figure 4.2). There was no peak in the spectrum in the region where hydroxyl protons appear which supports the findings of the infrared experiments, i.e. that the hydroxyl group is involved in bonding to the metal ion.

The ^{13}C{^{1}H} NMR spectrum of maltol has been assigned,[211] and this data is presented in Table 4.1 along with Pd(II) maltolate,[206] Zn(II) maltolate and Zn(II) ethyl maltolate (note - the chemical shift for the -CH_2- of the ethyl group has been omitted for clarity).

The results quoted in Table 4.1 show that on complexation with a metal ion, three of the carbon atoms of maltol exhibited a notable downfield shift of the order of 10-15ppm. This downfield shift is similar in magnitude to that observed in the complexation of catechol (2-hydroxy phenol) with osmium.[212] It is a common phenomena for the chemical shifts of the carbons attached to O-donor atoms to move

downfield in a complex compared to the free ligand. This accounts for the changes in the shifts of C_3 and C_4, but not for C_2 (the reason for which is less clear).

Table 4.1. ^{13}C NMR data for maltol and M(II) maltolate complexes

Compound	Chemical Shift (ppm)					
	C_2	C_3	C_4	C_5	C_6	C_7
Maltol[206]	144.1	142.8	172.1	113.2	154.4	13.8
Pd(II) maltolate[206]	159.7	155.5	185.4	111.5	151.7	14.1
Zn(II) maltolate (**15**)	151.7	153.8	177.7	109.0	150.1	14.8
Zn(II) ethyl maltolate (**17**)	152.5	154.1	176.2	108.4	151.2	15.4

4.2.3. Structure Determination of Zn(II) Maltolate Dihydrate (15)

Zn(II) maltolate dihydrate was recrystallised from aqueous ethanol, yielding a crystal of approximate dimensions 0.3 x 0.3 x 0.3mm which was used for data collection. Selected structural data are included in the discussion, with the crystal data and additional supplementary structural data included in Appendix C.

The asymmetric unit, $C_{12}H_{15}O_{8.5}Zn$, consists of one half of an octahedral zinc complex $Zn(C_6H_5O_3)_2(H_2O)_2$, where the central metal atom is seated on an inversion centre at 0, 0, 0.5. The remaining portion of the asymmetric unit consists of one half of a square pyramidal zinc complex $Zn(C_6H_5O_3)_2(H_2O)$, where the metal and the oxygen in the ligated water molecule, O4, are seated on a 2 fold rotation axis at x, -0.25, 0.5, and one full water molecule of crystallisation, on a general lattice position.

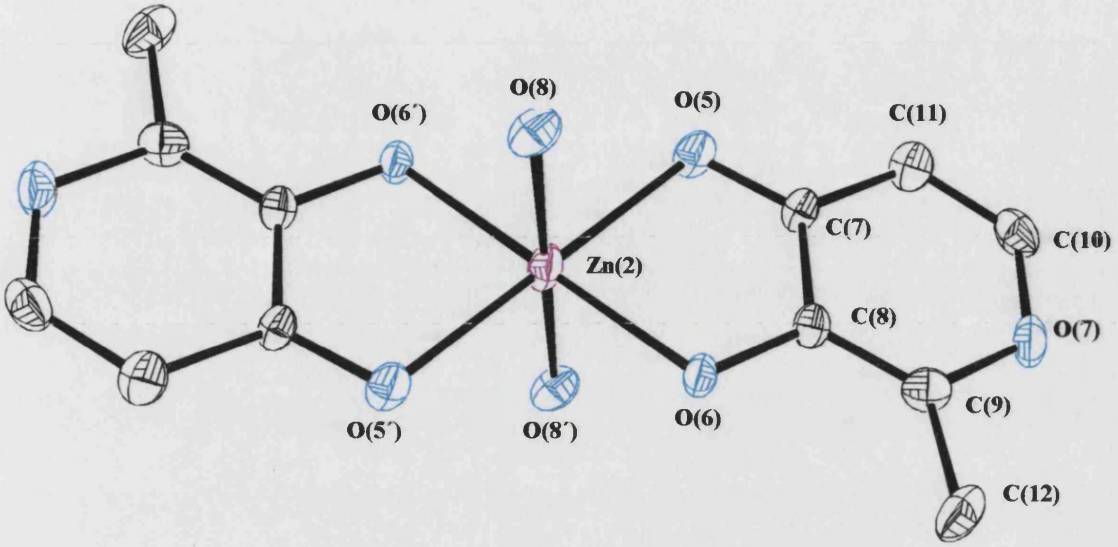

Figure 4.4. Octahedrally coordinated zinc in Zn(II) maltolate.

The discussion on the structure of Zn(II) maltolate will be in three parts with the octahedral zinc molecule discussed first, then the square pyramidal zinc followed by a discussion on the supramolecular array of the structure, which consists of an unusual "triple-layer extended sandwich" type structure.

The octahedral zinc site in Zn(II) maltolate exhibits a structure where the two maltolate ligands are to be found in equatorial positions, with the two water ligands occupying axial positions. It is also noteworthy that the octahedron is distorted, a feature which is seen in other octahedral maltol complexes such as, diphenyltin bis(maltolate)[213] and dichlorotin bis(maltolate).[213]

The fact that the two water ligands are *trans* to one another is not common in diaquabis(L_2) Zn(II) complexes (L = any bidentate ligand). In all of the following examples the water ligands are always found occupying *cis* positions: diaqua bis(methoxyacetato) Zn(II),[117] diaqua bis(glycollato) Zn(II)[214] and diaqua bis(DL-lactato) Zn(II) hydrate.[99]

Table 4.2. Metal-oxygen bond lengths in selected maltol complexes.

Compound	[M-O(1)]/Å	[M-O(2)]/Å	[M-O(3)]/Å[a]	Ref.
Zn(II) maltolate[b]	2.034(3)	2.072(3)	2.261(4)	This work
Zn(II) maltolate[c]	2.012(3)	2.078(3)	2.008(5)	This work
Cd(II) maltolate	2.237(8)	2.312(9)		215
Cl_2Sn(IV) maltolate	2.050(7)	2.135(7)		216

[a] [M-O(3)] is a metal-water bond [b] octahedral site [c] square pyramidal site

The [Zn-O(maltol)] bond lengths in the Zn(II) maltolate complex are typical of other [Zn-O] bond lengths in complexes where the zinc ion is complexed by oxygen atoms, where the average bond length falls within the range 2.00 - 2.26Å.[99,217,218] In the above table the [M-O(3)] bond refers to the M-OH_2 bonds within the two zinc sites in Zn(II) maltolate.

Table 4.2 shows that the [Zn-O] bond lengths in the octahedral and square pyramidal site of Zn(II) maltolate are similar, due to the chelation being much more symmetrical than in the other reported cases. Another interesting feature which can be seen in Table 4.2. are the metal to water bond lengths. The [Zn-O] water bonds in the octahedral site are significantly longer than in the sq. pyramidal site, as one would expect, due to the stronger and hence shorter bonds in the 5 coordinate site.

The Zn-water bonds [Zn(2)-O(8) and Zn(2)-O(8′)] are 2.261Å, which are longer than those observed in the earlier examples of diaqua compounds, where the water ligands are *cis* (Zn-O bond lengths are ca. 2.05Å) which is possibly as a result of their role in the lattice construction via hydrogen bonding. The reason for the large difference in Zn-OH_2 bond lengths in the octahedral and square pyramidal Zn(II) sites is dealt with in the discussion on the supramolecular array of Zn(II) maltolate.

Table 4.3. Exocyclic [C-O] bond lengths in selected maltol complexes.

Compound	[C-O(1)]/Å	[C-O(2)]/Å	Bite angle/°
Zn(II) maltolate[a]	1.336(6)	1.270(6)	82.0(1)
Zn(II) maltolate[b]	1.330(5)	1.261(6)	82.1(1)
Cd(II) maltolate	1.309(14)	1.242(13)	74.2(3)
Cl_2Sn(IV) maltolate	1.344(12)	1.277(10)	79.2(3)

[a] octahedral site [b] square pyramidal site

As can be seen in Table 4.3 the exocyclic [C-O] bond lengths in the maltolate ligands in the octahedrally coordinated zinc site are typical of those seen in a number of other maltolate complexes. In all of the examples cited there is one bond which is significantly shorter, this being the keto oxygen, than the other one, namely the hydroxy oxygen. This observation is consistent with the [M-O] bond lengths (Table 4.2) where the longer of the two bonds is due to the formation of a dative bond with the ketone function, the shorter bond being due to the formation of a covalent bond with the hydroxyl oxygen.

In all maltolate complexes, an interesting feature to look at is the bite angle which is formed between the ligand and the metal ion. The bite angle (which relates to the separation between donor atoms and can be seen in Figure 4.5) of maltolate ligands probably contributes to the effectiveness of these ligands in forming complexes with metals. The bite angles for maltolate complexes generally fall° within the range of 74°-82°, as can be seen in Table 4.3 (which shows a small selection of the large number of maltolate systems studied). Coupled with the bite angle is the non-bonded distance between the two oxygen atoms, which usually falls around 2.5Å,[219] but can be as low as 2.38Å.[220] The value of the non-bonded distance in the free ligand is approximately 2.75Å.[220] In the octahedral zinc site in Zn(II) maltolate the non-bonded distance is 2.69Å. Considering the bite angle of the Zn(II) maltolate is wider than that observed in other maltolate complexes this is not surprising. Another possible reason for the larger bite angle observed in the octahedral zinc site is the fact that the maltol ligand is involved

in hydrogen bonding. The bite angle of 82° is larger than in any other maltol systems which were examined (11 compounds).[198,202,204,205,208,213,215,216,221,222]

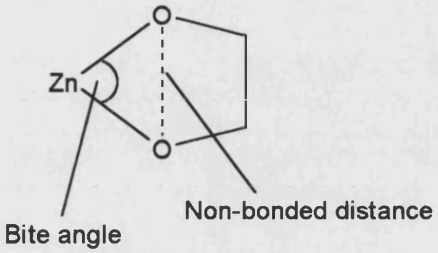

Figure 4.5. Schematic of bite angle and non-bonded distance in maltolate complexes.

A least squares plane calculation was carried out on the octahedral zinc site, focusing on the following atoms: Zn(2), O(5), O(6), C(7) and C(8). It was found that the metal ion was displaced by 0.044Å from the plane of the ligand, this portion of the molecule thus being considered essentially planar. This deviation of the metal ion is similar to that observed in another metal:maltolate system, e.g., Fe(III) maltolate, where the deviation of the metal ion from the ligand plane was 0.049Å.[223]

As mentioned earlier, there are two distinct zinc coordination sites in the Zn(II) maltolate complex, the second one being a square pyramidal site.

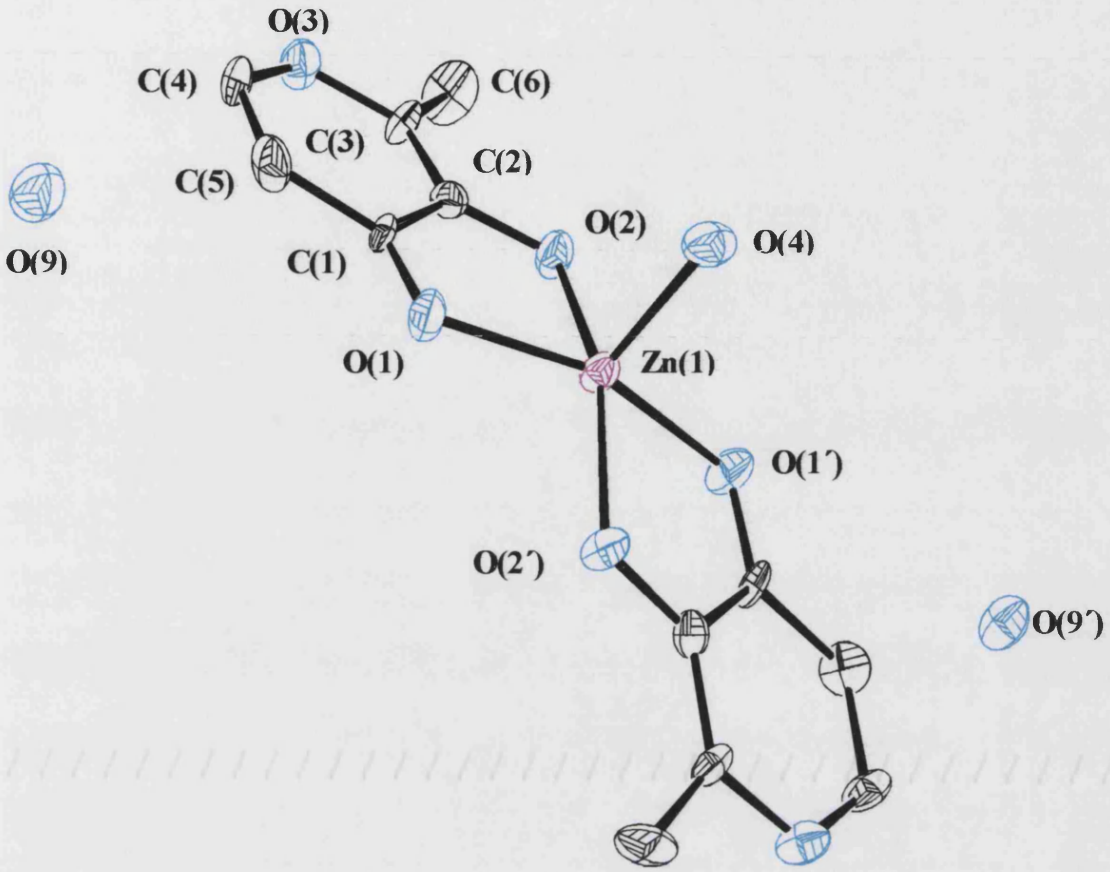

Figure 4.6. Square pyramidally coordinated zinc in Zn(II) maltolate

Most pentacoordinated zinc complexes have a tendency to form trigonal bipyramidal[224,225] or distorted trigonal bipyramidal[226] structures, with very few examples of square pyramidal coordination. One such example of square pyramidal coordination can be found in $[Zn_2L_2][ClO_4]_2$ - where L = 2-{bis[2-(2-pyridyl)ethyl]aminomethyl} phenolate.[227] In this example the geometry is actually very slightly distorted from perfect square pyramidal. As can be seen in Figures 4.6 and 4.7, Zn(II) maltolate has a distorted square pyramidal geometry and is explained in more detail later in the discussion (the supramolecular array of the complex).

The angle formed {between the planes formed by O(1), O(2), Zn(1) and O(1′), O(2′), Zn(1)} between the two maltolate ligands in the square pyramidal zinc complex is 154°, a feature which can more clearly be seen in the supramolecular array (Figure 4.7),

where the square pyramidal zinc complexes (shown in red) are slightly "bent" at the zinc atom.

The bond lengths and angles in the square pyramidal zinc site are slightly different than those observed in the octahedral zinc site. The [C-O] bonds from the chelating maltol ligands in the sq. pyramidal and octahedral sites are the same within experimental error (see Table 4.3) which is to be expected as the mode of chelation is the same. The [C-C] bond lengths are also very similar to the octahedral zinc site with a value of 1.436(7)Å for the two carbons involved in the five membered ring with the zinc [C(1)-C(2)], being the same as the corresponding bond in the octahedral zinc site.

The [Zn-O] bond lengths to the maltol ligands are also very similar with a bond range of 2.01-2.08Å (c.f. 2.03-2.07Å for the octahedral site - see Table 4.2). The bond between the zinc ion and the coordinated water ligand is however notably shorter in the square pyramidal site [Zn(1)-O(4), 2.008(5)Å] compared to the other zinc site where the bond lengths to the water ligands are 2.261(4)Å. This shorter bond length is more typical of other Zn-OH_2 bonds. The longer Zn-OH_2 bond lengths in the octahedral zinc site probably arise due to steric factors, whereby the H_2O ligands on the central zinc must move away from the metal to allow the square pyramidal zinc units to hydrogen bond.

The bite angle in the square pyramidal zinc site is, as expected, very similar to the bite angle in the octahedral zinc site with a value of 82.1(1)° compared to 82.0(1)°. Considering the maltol ligands always coordinate in an equatorial manner in the Zn(II) maltolate structures this is unsurprising. The non-bonded distance is obviously also very similar to that observed in the octahedral site. A least squares plane calculation was also carried out on the square pyramidal zinc site, revealing that the plane formed by the five membered ring [C(1), C(2), O(2), Zn(1), O(1)] is much closer to planarity than the octahedral zinc, with the zinc atom only displaced by 0.015Å.

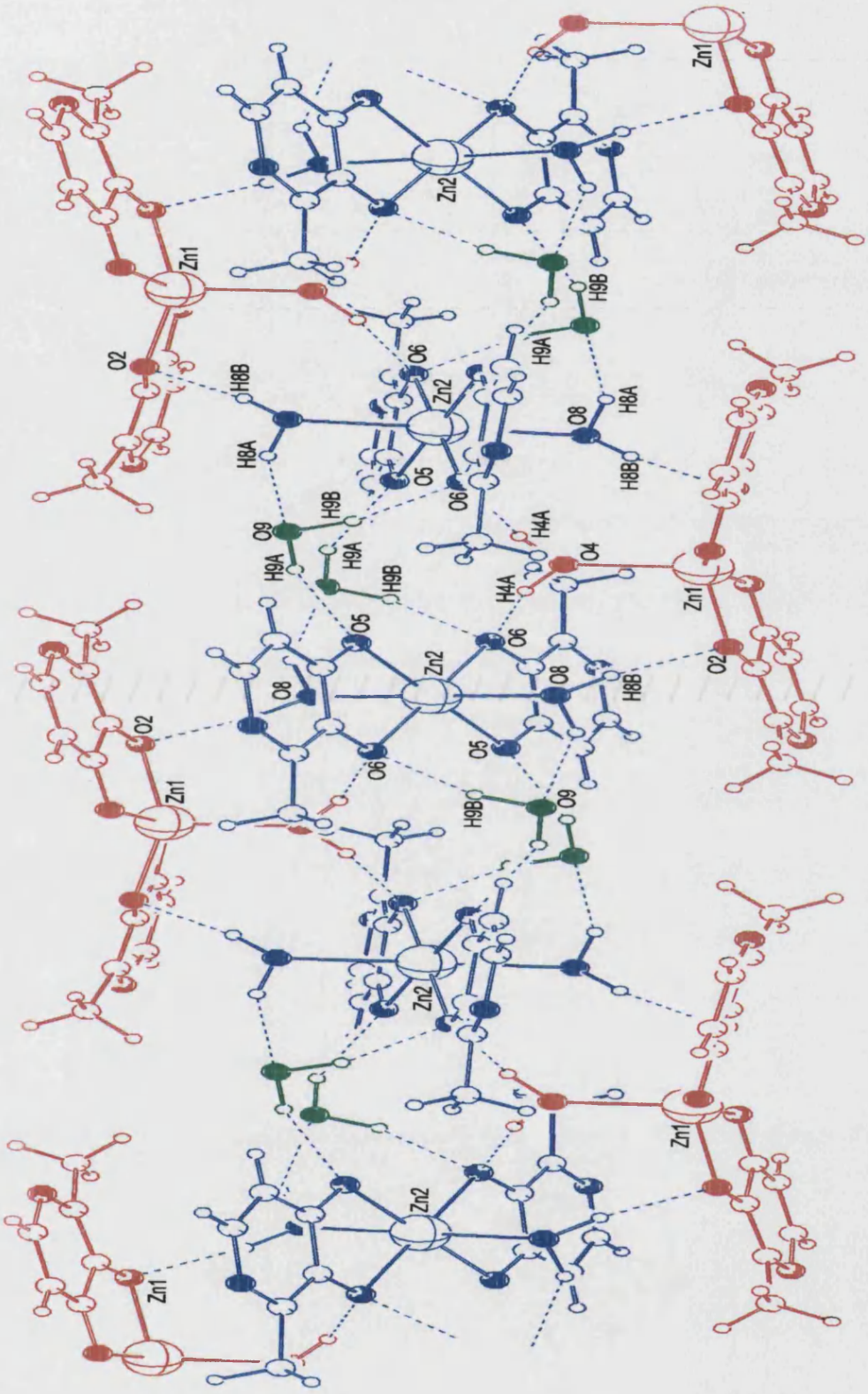

Figure 4.7. Hydrogen bonding interactions in the supramolecular array of **15**.

As mentioned previously in the discussion, the two distinct Zn(II) maltolate structures form the unusual "triple-layer extended sandwich" type structure shown in Figure 4.7, with the square pyramidal zinc sites positioned above and below a row of octahedral zinc sites. Also present in the lattice are interstitial water molecules which, through hydrogen bonding, play an important part in the overall lattice structure.

Square pyramidal zinc coordination in the same lattice structure as octahedrally coordinated zinc is not common. Extensive literature searching in this area failed to turn up any examples of compounds containing both square pyramidal and octahedral zinc sites. Compounds which contain two distinct zinc sites are known although not common. An example of a compound with two zinc sites is μ_3-hydroxo-tri-μ-(2-chlorobenzoato)dizinc(II) dihydrate.[228] The geometries observed at the zinc atoms are distorted octahedral and distorted trigonal bipyramidal. Similar to the bonding seen in Zn(II) maltolate, the five coordinate zinc atom has just one water ligand which is in an axial position and the six coordinate zinc has two water ligands which are both in axial positions. The respective bond lengths are listed in Table 4.4.

Table 4.4. [Zn-OH_2] bond lengths

Compound	[Zn-OH] 5CN Zn	[Zn-OH(1)] 6CN Zn	[Zn-OH(2)] 6CN Zn
Zn(II) maltolate (**15**)	2.008(5)	2.072(3)	2.261(3)
μ_3-hydroxo-tri-μ-(2-chlorobenzoato)dizinc(II) dihydrate	1.986(8)	2.101(8)	2.266(9)

As can be seen from Figure 4.7, the supramolecular array of the Zn(II) maltolate is complex with several hydrogen bonding interactions contributing to the overall packing of the complex. Examination of the supramolecular array of this structure reveals the formation of linear 'sandwich' polymers parallel to the *b* axis. The sandwich 'filling' is composed of the octahedral zinc species and the lattice water molecules. The

sandwich 'bread' meanwhile consists of the square pyramidal zinc moieties which hydrogen bond as can be seen in Figure 4.7.

The octahedral zinc moieties (i.e., the sandwich filling) do not all have the same orientation in the supramolecular array, as every other octahedron has the square plane containing the maltolate ligands approximately parallel to the 'bread' of the sandwich (the square pyramidal zinc). The other zinc octahedra are at approximately 45° to the bread of the sandwich. The reason for this orientation is presumably to accommodate the interstitial water molecules, and add to the stability of the lattice. This orientation seems to allow the square pyramidal zinc moieties to align themselves in such a way as to have the coordinated water ligand oriented towards the middle of the sandwich. If the octahedral zinc molecules were not aligned in this way this would probably not be possible. The coordinated water from the square pyramidal zinc site is involved exclusively in hydrogen bonding with the coordinating oxygens of the maltol ligands, and never with the ring oxygen atom.

The square pyramidal zinc moieties are not planar, as mentioned in the earlier discussion, and this deviation from planarity can clearly be seen in the supramolecular array. The reason for the 'bending' of the square pyramidal zinc is presumably to allow the lattice to adopt the lowest energy arrangement. Also evident form the supramolecular array of the Zn(II) maltolate complex is that the zinc atoms at the centres of the octahedra are all approximately co-linear along the *b* axis. It appears therefore that in the formation of the lattice, it is the maltolate ligands which have to orient themselves rather than the whole octahedron moving to allow the observed packing.

4.2.4. Structural Determination of Cu(II) Hinokitiol (20)

Before discussing the structure of Cu(II) hinokitiol, it is necessary to discuss the "pseudo-aromaticity" of hinokitiol. Figure 4.8 shows two representations of hinokitiol, and forms the basis for the discussion.

Figure 4.8. Partial π-electron delocalisation in hinokitiol(III).

The π-electron system in hinokitiol is partially delocalised.[229] The formal double bonds in the ring, C(1)-C(7), C(6)-C(5) and C(4)-C(3), have lengths of 1.367, 1.355 and 1.364Å respectively, compared to 1.335Å for a C=C double bond. The formal single bonds, C(7)-C(6), C(5)-C(4) and C(3)-C(2), have lengths of 1.422, 1.413 and 1.413Å respectively, which are shorter than the average length of a C-C single bond. The C(1)-C(2) bond (1.469Å) is significantly longer than the other carbon-carbon bonds and is also slightly longer than the C-C single bond length. The C=O bond length in hinokitiol (1.261Å) and the C-O bond length (1.349Å) are both significantly shorter than average carbon-oxygen bonds because of their involvement in the partial π-electron delocalisation, leading to the delocalised structure shown in Figure 4.8.

Cu(II) hinokitiol was recrystallised from aqueous ethanol, yielding a crystal of approximate dimensions 0.3 x 0.3 x 0.5mm which was used for data collection. Selected structural data are included in the discussion, with the crystal data and additional supplementary structural data included in Appendix D.

The Cu(II) hinokitiol complex has the molecular formula ($C_{20}H_{22}CuO_4$), and the asymmetric unit is presented in figure 4.8.

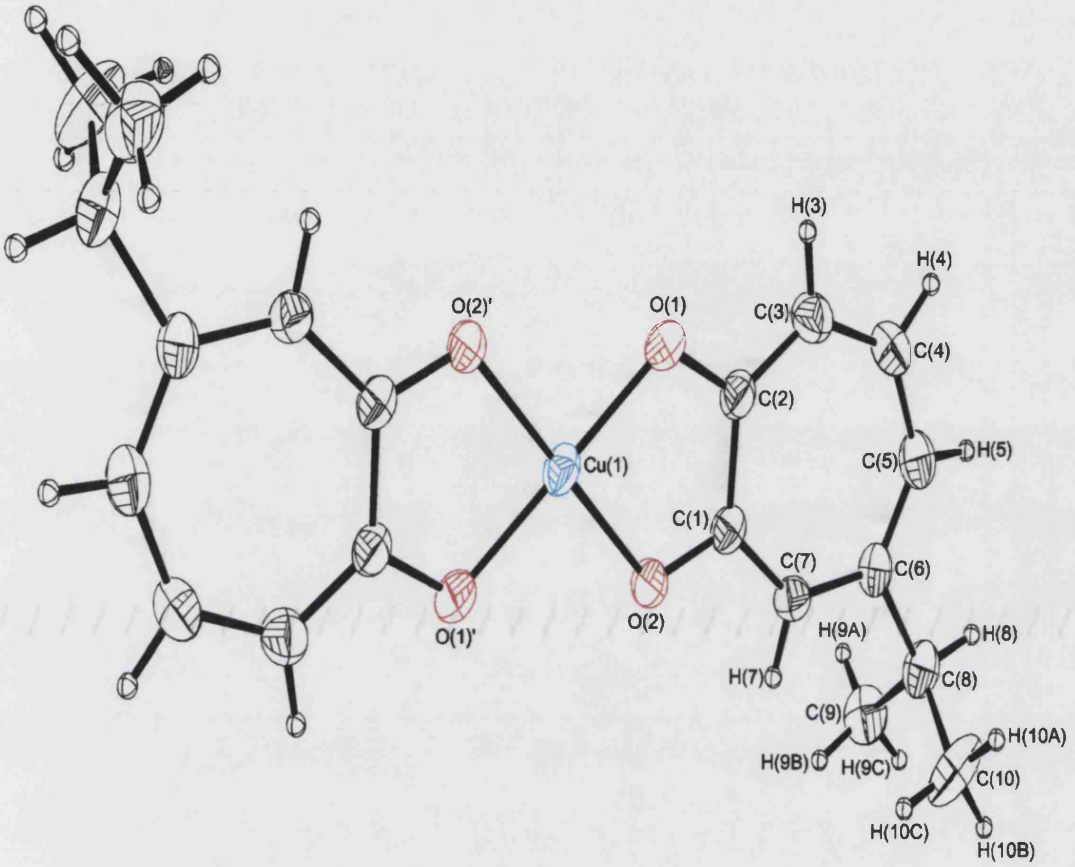

Figure 4.9. Asymmetric unit, and labelling scheme, in Cu(II) hinokitiol (**20**).

The asymmetric unit in this structure (Figure 4.9) comprises of one half of a molecule, the remaining portion being generated via an inversion centre at 0, 0, 0 on which the copper is sited, coordinated to two hinokitiol ligands. The Cu(II) in this molecule is four coordinate, and in a square planar environment. The [Cu-O] bonds are equivalent, 1.900(2) and 1.904(3)Å for Cu-O(2) and Cu-O(1), respectively, and the [O(1)-Cu-O(2)] bond angle is 83.8(1)°. The Cu-O bond lengths are in agreement with other Cu(II) complexes, e.g., Cu(II) erythritol [Cu-O = 1.912(4) and 1.922(4)Å],[86] and a Cu(II) nitroxyl-β-keto ester [Cu-O = 1.901(4) and 1.921(4)].[93]

Table 4.5. [C-O] bond lengths in some metal tropolonates.

Compound	[C-O(1)] / Å	[C-O(2)] / Å	[C(1)-C(2)] / Å	Reference
Mn(III)(trop)$_3$	1.30(1)[a]	1.29(1)[a]	1.46(2)[a]	197
Me_2Sn(IV)(trop)$_2$	1.30(1)[a]	1.27(1)[a]	1.47(1)[a]	198
Cu(II)(trop)$_2$	1.302(5)	1.286(5)	1.463(6)	193
Cu(II)(hinokitiol)$_2$	1.296(3)	1.293(3)	1.464(6)	This work

Note: [a] - Average bond distance of the non-equivalent ligands.

Both of the C-O bond lengths in Cu(II) hinokitiol compare well with those found in a number of other metal tropolonates, i.e. 1.27-1.30Å. The C-O bond length appears to be independent of the either the metal ion or the number of tropolonate ligands, as can be seen in Table 4.5. Upon coordination to the Cu(II) the C-O bond lengths become equal [1.293(5) and 1.296(3)Å], indicating a similar bond order in both. As mentioned previously, it is believed that both of the oxygen atoms of hinokitiol are involved in the partial π-electron delocalisation. It is therefore not surprising that the two C-O bonds are of a similar length in Cu(II) hinokitiol.

The bond lengths of the C-C bonds in the hinokitiol ring are approximately equal (ca. 1.38Å) with one notable exception. The C(1)-C(2) bond is significantly longer than the others (see Table 4.5) indicating that it is not involved to the same extent in the π-electron delocalisation of the tropolonate system. The value of 1.464(6)Å observed for the C(1)-C(2) bond in Cu(II) hinokitiol is close to that expected for a C(sp^2)-C(sp^2) single bond. This is a common feature of the tropolonates as can be seen from Table 4.6. These observed bond lengths are in agreement with the earlier discussion relating to the "pseudo-aromatic" nature of the hinokitiol molecule.

Table 4.6. 'Bite' angles in selected metal tropolonates.

Compound	'Bite' angles / °			Reference
	ligand #1	ligand #2	ligand #3	
In(III)(4-isopropyl trop)$_3$	74.9(1)	75.1(1)	75.1(1)	209
Mn(III)(trop)$_3$	77.8(6)	79.1(6)	80.7(6)	197
Cu(II)(trop)$_2$	83.8(1)	83.8(1)		193
Cu(II)(hinokitiol)$_2$	83.8(1)	83.8(1)		This work

The small 'bite' angle (separation between donor atoms) of the tropolonate ligands probably contributes to the effectiveness of the ligands in forming complexes with metal ions (see Table 4.6). The non-bonded distance between the two oxygen donor atoms in Cu(II) hinokitiol is 2.54Å, which is comparable to that observed in the Cu(II) tropolonate (2.56Å).[193]

The hinokitiol ligand in the Cu(II) hinokitiol complex deviates only slightly from planarity as shown in Table 4.7. Also shown in Table 4.7 are the deviations from planarity of the carbon atoms in the ring of the uncoordinated ligand.

Table 4.7. Deviations of atoms (in Å) from the least-squares planes through the seven membered ring C(1)-C(7) in hinokitiol and **20**.

Atom	Hinokitiol[a]	Cu(II) hinokitiol (**20**)[b]
C(1)	-0.019	-0.005
C(2)	-0.011	0.006
C(3)	0.021	-0.019
C(4)	0.004	-0.014
C(5)	-0.025	0.008
C(6)	0.007	0.014
C(7)	0.022	0.001
O(1)	-0.036	0.029
O(2)	-0.004	-0.017
Cu(1)		-0.005

Note - [a] Equation of plane : $14.531x + 2.556y + 5.319z = 7.402$.[229]
[b] Equation of plane : $0.071x + 0.647y - 0.759z = -0.005$.

4.2.5. Structural Determination of Tris(maltolato)monohydroxotin(IV) .3.5H_2O(21)

Tris(maltolato)monohydroxotin(IV).3.5H_2O was formed during the attempted synthesis of Sn(II) maltolate, yielding a crystal of approximate dimensions 0.25 x 0.2 x 0.2mm which was used for data collection. Selected structural data are included in the discussion, with the crystal data and additional supplementary structural data included in Appendix E. The refinement of the structure was completed without including the hydroxyl proton bound to O(10) or the water hydrogens, as attempts to locate these protons did not meet with success.

As mentioned above, the complex produced was hydrated and an analysis of the supramolecular array (Figure 4.11) reveals a complex network of hydrogen bonds which will be discussed later in this section. The title compound ($C_{18}H_{16}O_{10}Sn.3.5H_2O$) can be seen in Figure 4.10 - where the water molecules have been omitted for clarity.

As can be seen in Figure 4.10 the Sn(IV) is seven coordinate in tris(maltolato)monohydroxotin(IV). The coordination sphere around the tin atom is composed of seven oxygen atoms, six from the maltol ligands and one from the hydroxyl group. This arrangement of ligands gives the tin an approximate pentagonal bipyramidal geometry

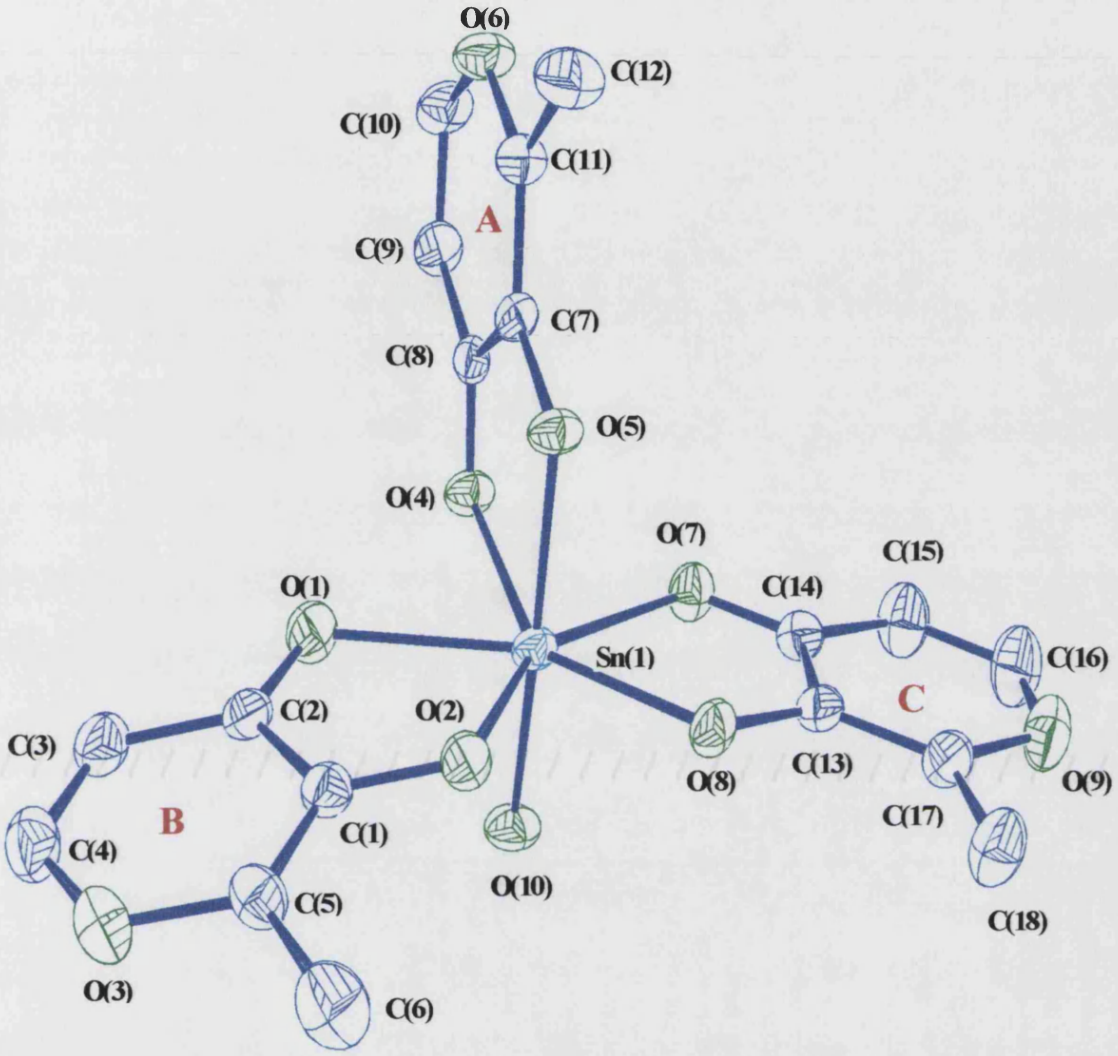

Figure 4.10 . The asymmetric unit of tris(maltolato)monohydroxotin(IV) (**21**).

Although not obvious from the asymmetric unit shown in Figure 4.10, one of the maltolate ligands is coordinated in such a way as to occupy both an axial and an equatorial position (ligand A). The other axial position is occupied by the hydroxyl group, with the other four equatorial positions being occupied by the two remaining maltolate ligands (ligands B and C).

Table 4.8. [Sn-O] bond lengths in tris(maltolato)monohydroxotin(IV) (**21**).

[Sn-O] Bond	Bond Length / Å
Sn-O(1)	2.280(3)
Sn-O(2)	2.096(3)
Sn-O(4)	2.219(3)
Sn-O(5)	2.053(3)
Sn-O(7)	2.268(3)
Sn-O(8)	2.089(3)
Sn-O(10)	1.975(3)

From the figures quoted in Table 4.8 it is evident that there are three bonds which are longer than the others, namely those to oxygens 1,4 and 7. The reason for this is that the oxygens in question are the [C=O] oxygens from the maltol ligands. The other three [Sn-O] bonds which involve [C-O] maltolato oxygens are almost identical in length, while the remaining bond [Sn-OH] is, as one would expect, much shorter at 1.975Å indicating strong complexation of the hydroxyl ligand to the metal ion.

The [Sn-O] bonds in the title compound are similar to those observed in a number of other Sn(IV) complexes of maltol and tropolone, as can be seen from the data in Table 4.9.

Table 4.9. Average [Sn-O] bonds in a range of tin(IV) complexes of maltol and tropolone.

Compound	Average [Sn-O]/Å	Average Bite angle/°	Average [O-O] distance/Å
Tris(maltolato)monohydroxotin(IV) (**21**)	2.14	74.9	2.58
Tris(tropolonato)monohydroxotin(IV)[230]	2.12	71.6	2.54
Dimethyltin Bis(tropolonate)[198]	2.17	72.8	2.55
Diphenyltin Bis(maltolate)[213]	2.17	76.1	2.60
Dichlorotin Bis(tropolonate)[216]	2.09	79.2	2.64
Dichlorotin Bis(maltolate)[216]	2.07	78.7	2.63

The data presented in the above table shows that the title compound is typical of a number of other complexes in which a Sn(IV) atom is surrounded by oxygen atoms from either tropolonate or maltolate ligands. The bite angles (which have previously been discussed in this chapter) all fall within the expected range for maltol complexes of any metals. Coupled with the bite angle is the non-bonded distance between the two oxygens of the maltol ligand which as can be seen form the above Table is a relatively consistent figure of between 2.55-2.64Å.

As mentioned previously the coordination polyhedron around the tin atom closely resembles a pentagonal bipyramid with five maltol oxygens constituting the pentagon, while the other maltol oxygen and the hydroxyl group occupy the axial positions. The angle of 173.6(1)° between the O(10)-Sn-O(5) reflects the slight deviation from a perfect pentagonal bipyramid. The angles of the atoms in the equatorial plane subtended at the tin centre, however, lie within a narrow range of 69.0(1)-75.0(1)° (see Table 4.10).

Table 4.10. O-Sn-O bond angles in tris(maltolato)monohydroxotin(IV) .3.5H_2O (**21**).

O-Sn-O	Bond angle / °	O-Sn-O	Bond angle / °
O(10)-Sn-O(1)	86.3(1)	O(4)-Sn-O(5)	77.3(1)
O(10)-Sn-O(2)	94.8(1)	O(5)-Sn-O(8)	89.3(1)
O(10)-Sn-O(4)	96.5(1)	O(5)-Sn-O(2)	90.8(1)
O(10)-Sn-O(7)	86.1(1)	O(5)-Sn-O(1)	92.5(1)
O(10)-Sn-O(8)	95.0(1)	O(5)-Sn-O(7)	90.5(1)
O(4)-Sn-O(1)	69.0(1)	O(10)-Sn-O(5)	173.6(1)
O(4)-Sn-O(7)	70.2(1)	O(8)-Sn-O(1)	148.6(1)
O(2)-Sn-O(8)	75.0(1)	O(2)-Sn-O(7)	148.9(1)
O(1)-Sn-O(2)	73.6(1)	O(2)-Sn-O(4)	140.0(1)
O(7)-Sn-O(8)	74.0(1)	O(8)-Sn-O(4)	141.4(1)

One of the interesting bond angles in the above table is the one formed between O(10)-Sn-O(4). This angle of 96.5° confirms that one of the oxygen atoms from the maltol ligand which spans both an axial and an equatorial position, does actually complete the slightly distorted pentagonal bipyramidal arrangement around the tin. Another interesting feature is that this is not the only bond formed between the axial hydroxyl group and the equatorial ligands which is over 90°. The average bond angle of the five formed between the axial hydroxyl and the equatorial oxygens is slightly greater than 90°, the actual figure being 91.7°. This is presumably due to repulsion from, or steric factors due to, the hydroxyl group, as this has a very short [Sn-O] bond length of 1.975(3)Å.

Table 4.11. Contact distances [Å] for possible hydrogen bonds in (**21**).

O-O	Contact distance/Å	O-O	Contact distance/Å
O(1)-O(12)	3.013(5)	O(10)-O(14)	2.781(5)
O(1)-O(13)	3.160(9)	O(10)-O(13)	2.751(8)
O(4)-O(12)	3.086(5)	O(11)-O(12)	2.771(5)
O(7)-O(14)	2.957(5)	O(12)-O(13)	2.993(10)
O(10)-O(13)	2.627(8)	O(11)-O(14)	2.834(5)

The lattice structure of the title compound is very complex with a number of hydrogen bonding interactions present. As mentioned earlier in this discussion the hydrogen atoms of the water molecules were not able to be located, despite dogged attempts. The oxygens were located and the hydrogen bonds which are formed with the maltol oxygens are detailed in Figure 4.11.

It is interesting to note that one of the two chelating oxygens of each maltol ligand is not involved in any hydrogen bonding. This is consistent throughout the lattice. The oxygen which is not involved in the hydrogen bonding is always the [C-O-Sn] rather than the [C=O-Sn]. The oxygen from the carbonyl is involved in two hydrogen bonding interactions throughout the lattice. An overview of the lattice yields an almost helical arrangement of the four molecules in the centre of the lattice with additional stabilisation from the molecules running parallel to the helix. This pattern is repeated throughout the complex as a whole.

O(10) - the hydroxyl ligand - has a hydrogen bonding interaction with the water molecule indicated by O(13), which also forms a hydrogen bond with the oxygen [O(1)] of the maltol ligand. This water molecule also forms a hydrogen bond with O(12) which in turn hydrogen bonds with the C=O of another maltol ligand. This hydrogen bonding network forms bridges between molecules, and is an important factor in determining the overall helical arrangement of the complex.

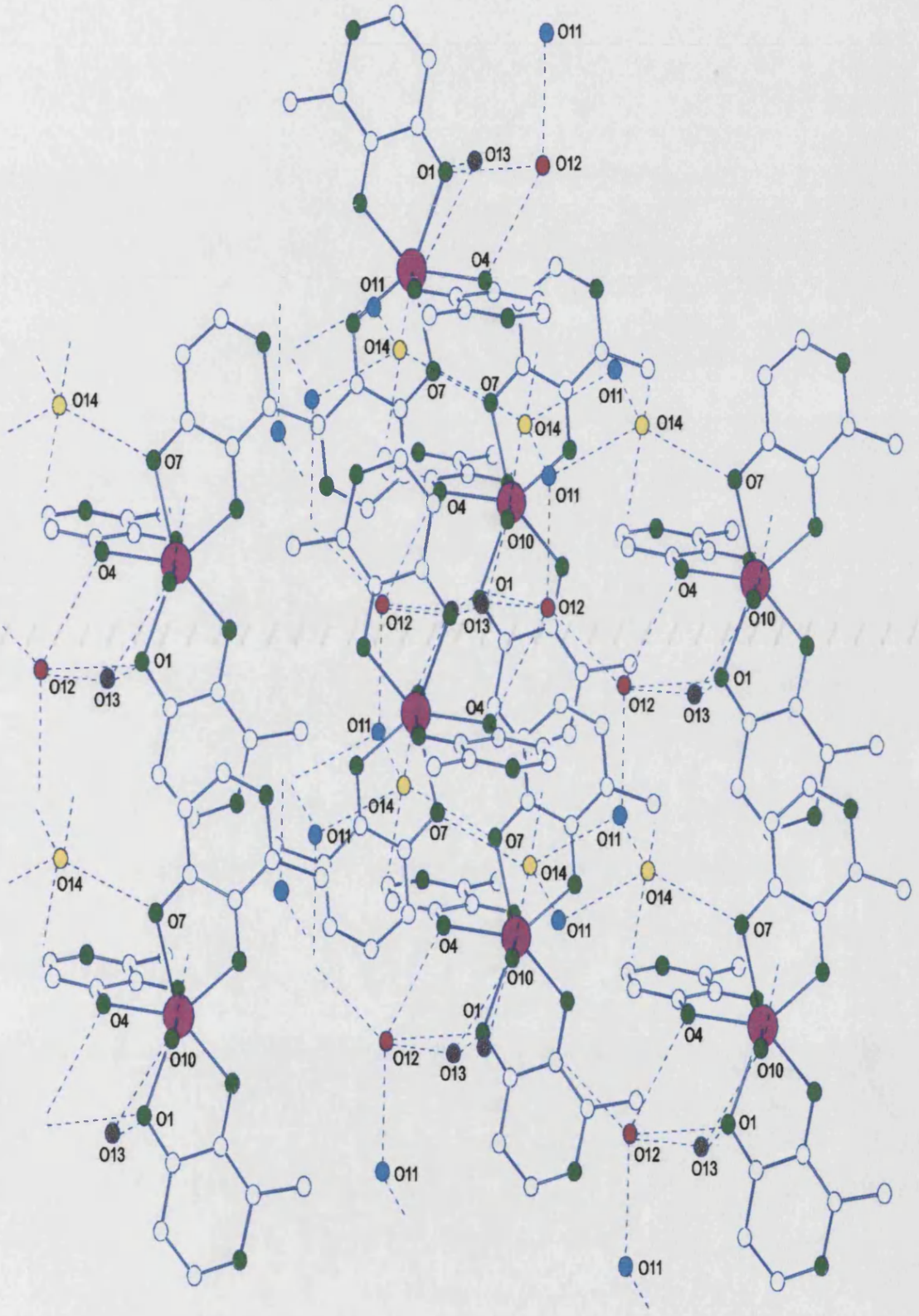

Figure 4.11. Lattice structure of tris(maltolato)monohydroxotin(IV) (**21**).

4.3. Anti-bacterial evaluation

4.3.1. Biofilm Assay Results

The biofilm assay which was utilised for the anti-bacterial evaluation of the compounds in Chapter 4 was slightly different to those mentioned in previous chapters, in that some of the compounds were incorporated into toothpastes for the assay. The copper samples were used at a concentration of 8mM and the zinc samples at 35mM in Signal toothpaste. In the previous chapter, the biofilms were exposed to the test samples for 1 minute before being washed. During the testing of the Cu(II) and Zn(II) compounds, the biofilms were exposed to the toothpastes containing the compounds for 15 seconds (the standard exposure time for *in vitro* testing of toothpastes).

Due to some unforeseen problems during the assays which were carried out at Unilever it was not possible to obtain results for all of the compounds which were tested. The results which are missing pertain to the hinokitiol samples. This is not however too great a problem as the activity of hinokitiol and Cu(II) hinokitiol have previously been determined,[231] and proved to be less active than the Cu(II) maltolate and Cu(II) ethyl maltolate, although the actual results have not been disclosed.

The results for the Cu(II) maltolate/ethyl maltolate and Zn(II) maltolate/ethyl maltolate are presented in this Section.

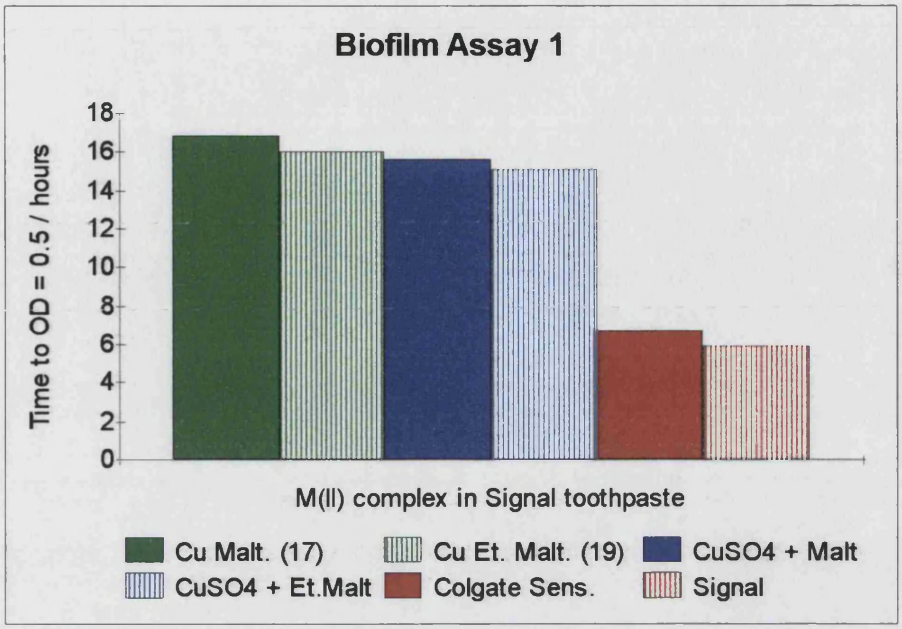

Figure 4.12. Activity of Cu(II) maltolate/ethyl maltolate and mixtures of $CuSO_4$ and maltol/ethyl maltol in Signal toothpaste on *Strep. warneri* biofilm.

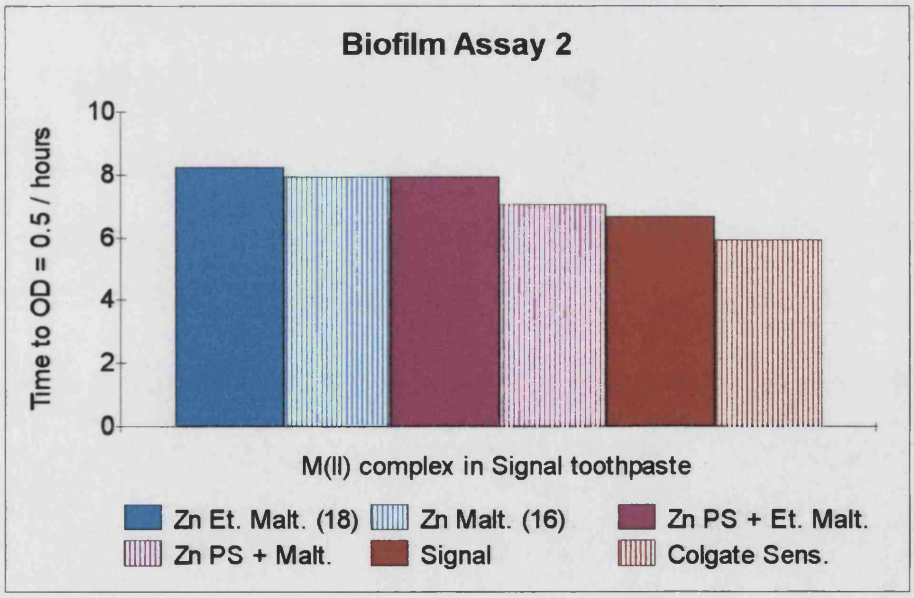

Figure 4.13. Activity of Zn(II) maltol/ethyl maltolate and mixtures of Zn phenyl sulphate (Zn PS) and maltol/ethyl maltol in signal toothpaste on *Strep. warneri* biofilm.

Figure 4.12 shows the results for Cu(II) maltolate and Cu(II) ethyl maltolate where the samples were mixed into Signal toothpaste prior to testing. The copper samples were incorporated at a concentration of 8mM (the standard concentrations at which copper is used in a commercial toothpaste - Cuprident™, Biosystems Inc., Cincinnati, Ohio). Also run in this experiment were mixtures of copper sulphate with maltol and ethyl maltol. The reason for assaying the mixtures was to see if the activity of Cu(II) maltolate and Cu(II) ethyl maltolate was due to the compound, or merely due to the presence of the bactericidal metal ions. The samples were evaluated against Signal toothpaste and also Colgate Sensations toothpaste. The results obtained clearly show that there is very little difference between the copper compounds and the mixtures, indicating that the activity is most likely due to the bactericidal metal ions and not the copper compounds. This is not unexpected as it is known that Cu^{2+} ions are biologically active, and it would appear that it is not how the copper ions are delivered to the bacteria which is important, as long as the ions are available (i.e. not too highly complexed).

The results obtained for the Zn(II) maltolate and Zn(II) ethyl maltolate (Figure 4.13) were unexpected, as zinc compounds generally give good results when tested against bacteria (e.g. zinc citrate, which is widely used in a range of commercial toothpastes).[232-234] A possible reason for the lack of activity displayed by the Zn(II) maltolate and Zn(II) ethyl maltolate can be found by looking at the crystal structure obtained for the Zn(II) maltolate. In this structure it can easily be seen (Figure 4.7) that the zinc ions are tightly held within a matrix of maltolato and water ligands. The reason for the lack of activity can thus be attributed to the non-availability of the Zn^{2+} ions in these compounds. In water-soluble compounds such as zinc citrate, the Zn^{2+} ions are more readily available when in solution, and this is where the activity of zinc citrate presumably comes from. Some evidence for the mode of action of zinc can be found in research carried out by a number of authors.[235,236] Zinc may reduce bacterial colonisation and subsequent plaque maturation by modifying the cell surface properties of individual plaque bacteria. Some evidence suggests the zinc may act directly by altering cell proteins,[235] or indirectly by inhibiting protease-induced adhesion.[236]

Unfortunately there is no crystal structure available for the Cu(II) maltolate or Cu(II) ethyl maltolate and comparisons are thus difficult. It is possible however to use the structure of Cu(II) hinokitiol as a guide to what the structure of the copper compounds would be, allowing comparison to the zinc compounds. In the anhydrous Cu(II) hinokitiol, the Cu(II) ions are more accessible than the zinc ions in Zn(II) maltolate and, as mentioned previously, this availability of metal ions seems to be an important factor in the activity of a M(II) compound in a toothpaste. Both Cu(II) maltolate and Cu(II) ethyl maltolate were found, by microanalysis, to be anhydrous, and would thus be expected to be similar in structure to the Cu(II) hinokitiol.

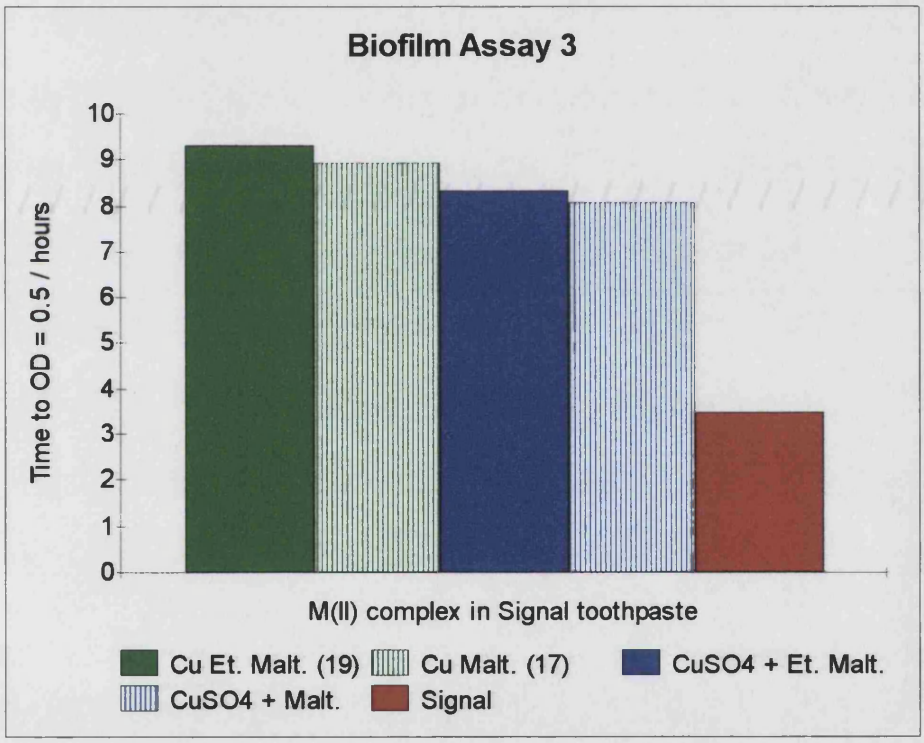

Figure 4.14. Activity of Cu(II) maltolate/ethyl maltolate and mixtures of $CuSO_4$ and maltol/ethyl maltol in Signal toothpaste on *E. cloacae* biofilm.

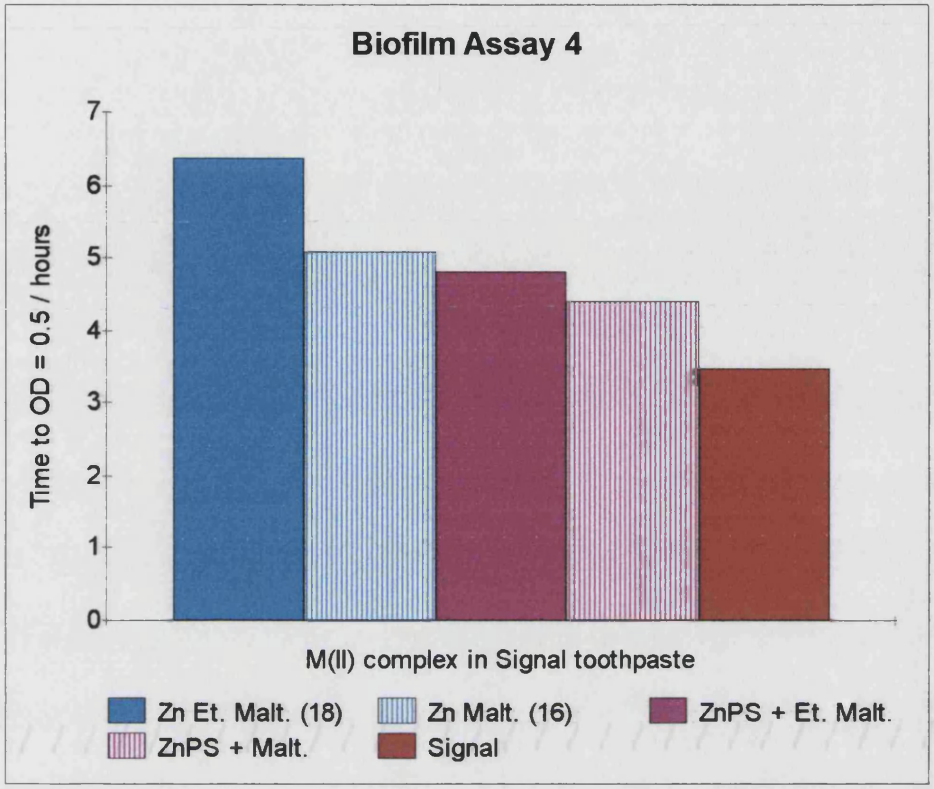

Figure 4.15. Activity of Zn(II) maltol/ethyl maltolate and mixtures of Zn phenyl sulphate (Zn PS) and maltol/ethyl maltol in Signal toothpaste on *E. cloacae* biofilm.

Figures 4.14 and 4.15 contain the same compounds and mixtures as those in Figures 4.12 and 4.13, with the difference being the type of bacterium used in the assay. What this assay shows is that it is very important to select the right bacterium for an assay so that the results obtained are as meaningful as possible. *E. cloacae* is obviously a more resistant bacterium than is *S. warneri*, as shown by the fact that the time taken for the bacteria to regrow is almost halved when using *E. cloacae*. What is encouraging from this assay is that the results are in agreement with those obtained from the assay using *S. warneri*, in that the copper compounds are again much more active.

4.4. Experimental

Maltol and ethyl maltol were purchased from Sigma Chemicals, and the hinokitiol sample was provided by Unilever.

4.4.1. Synthesis of Zn(II) Maltolate Dihydrate (15)

Maltol (1.27g, 10.0mmol) was dissolved in aqueous ethanol (50:50, 50ml) with stirring. Once dissolved, a solution of zinc acetate (1.09g, 5.0mmol) was added and the stirring continued. After stirring for 2 hours the solution was gently refluxed for 2 hours, causing a slight yellowing of the solution. This solution was allowed to stand for 1 week after which time the product crystallised from solution as colourless needle shaped crystals.

Analysis, found (calc. for $C_{12}H_{14}O_8Zn$): C, 40.0 (40.9); H, 4.13 (4.58).

Selected infrared data: 3400cm^{-1} υ(H-O-H); 1614cm^{-1} & 1577cm^{-1} υ(C=O); 1510cm^{-1} υ(C=C); 1277-1201cm^{-1} υ(C-O).

^{1}H NMR (d_6-DMSO): 8.09ppm(*d*, 1H, $J_{5\text{-}6}$=5.1Hz)H_5; 6.52(*d*, 1H, $J_{6\text{-}5}$=5.1Hz)H_6; 2.32(*s*, 3H)H_7.

^{13}C{^{1}H} NMR (d_6-DMSO): 177.7ppm (C_4), 153.8, 151.7 (C_2, C_3), 150.1 (C_6), 109.0 (C_5), 14.8 (C_7).

4.4.2. Synthesis of Cu(II) Maltolate (16)

Maltol (0.50g, 4.0mmol) was dissolved in aqueous ethanol (50:50, 50ml) with stirring. Once dissolved, a solution of copper acetate (0.39g, 2.0mmol) was added and the stirring continued. After stirring and gentle heating for 2 hours, the green/blue solution was allowed to stand for 1 week after which time the product precipitated from solution as a green/blue solid.

Analysis, found (calc. for $C_{12}H_{10}O_6Cu$): C, 45.5 (46.0); H, 3.07 (3.22).

Selected infrared data: 1606cm^{-1} & 1572cm^{-1} υ(C=O); 1508cm^{-1} υ(C=C); 1290-1202cm^{-1} υ(C-O).

4.4.3. Synthesis of Zn(II) Ethyl Maltolate Dihydrate (17)

Ethyl maltol (2.00g, 14.3mmol) was dissolved in aqueous ethanol (50:50, 50ml) with stirring. Once dissolved, a solution of zinc acetate (1.57g, 7.2mmol) was added and the stirring continued. After stirring for 2 hours the solution was gently refluxed for 2 hours, causing a slight yellowing of the solution. This solution was allowed to stand for 1 week after which time the product precipitated from solution as a slightly off white solid.

Analysis, found (calc. for $C_{14}H_{18}O_8Zn$): C, 44.2 (44.3); H, 4.79 (4.79).

Selected infrared data: 3380cm^{-1} υ(H-O-H); 1610cm^{-1} & 1582cm^{-1} υ(C=O); 1271-1196cm^{-1} υ(C-O).

^{1}H NMR (d_6-DMSO): 8.17ppm(*d*, 1H, $J_{5\text{-}6}$=5.2Hz)H_5; 6.60(*d*, 1H, $J_{6\text{-}5}$=5.2Hz)H_6; 2.90(*q*, 2H, $J_{7\text{-}8}$=7.5Hz)H_7, 1.25(*t*, 3H, $J_{8\text{-}7}$=7.5Hz)H_8.

$^{13}C\{^1H\}$ NMR (d_6-DMSO): 176.2ppm (C_4), 154.1, 152.5 (C_2, C_3), 151.2 (C_6), 108.4 (C_5), 29.5 (C_8), 15.4 (C_7).

4.4.4. Synthesis of Cu(II) Ethyl Maltolate (18)

Ethyl maltol (2.00g, 14.3mmol) was dissolved in aqueous ethanol (50:50, 50ml) with stirring. Once dissolved, a solution of copper acetate (1.43g, 7.2mmol) was added and the stirring continued. After stirring and gentle heating for 2 hours, the green/blue solution was allowed to stand for 1 week after which time the product precipitated from solution as a green/blue solid.

Analysis, found (calc. for $C_{14}H_{14}O_6Cu$): C, 48.7 (49.2); H, 4.06 (4.14).

Selected infrared data: 1612cm^{-1} & 1578cm^{-1} υ(C=O); 1514cm^{-1} υ(C=C); 1295-1210cm^{-1} υ(C-O).

4.4.5. Synthesis of Zn(II) Hinokitiol (19)

Hinokitiol (0.20g, 1.22mol) was dissolved in aqueous ethanol (50:50, 50ml) with stirring. Once dissolved, a solution of zinc acetate (0.13g, 0.61mmol) was added and the stirring continued. After stirring and gentle heating for 2 hours, the solution was allowed to stand for 1 week after which time the product precipitated from solution as a yellow solid. This solid was then recrystallised from toluene, yielding an off white solid.

Analysis, found (calc. for $C_{20}H_{22}O_4Zn$): C, 61.3 (60.9); H, 5.67 (5.63).

Selected infrared data: 1597cm^{-1} & 1576cm^{-1} υ(C=O); 1504cm^{-1} υ(C=C); 1280-1240cm^{-1} υ(C-O).

^{1}H NMR (d_6-DMSO): 7.36ppm(*dd*, 1H, J=11.0, 10.1Hz)H_4; 7.18(*s*, 1H)H_7; 7.07(*d*, 1H, J=11.0Hz)H_5; 6.86(*d*, 1H, J=10.1Hz)H_3; 2.85(*m*, 1H)H_8; 1.21(*d*, 6H, J=6.8Hz)H_9.

^{13}C{^{1}H} NMR (d_6-DMSO): 178.2 and 177.7ppm (C_1, C_2), 159.1 (C_6), 137.7 (C_3), 123.6, 123.4, 122.3 (C_7, C_5, C_4), 39.1 (C_8), 23.7 (C_9).

4.4.6. Synthesis of Cu(II) Hinokitiol (20)

Hinokitiol (0.30g, 1.83mmol) was dissolved in aqueous ethanol (50:50, 50ml) with stirring. Once dissolved, a solution of copper acetate (0.19g, 0.95mmol) was added and the stirring continued. After stirring and gentle heating for 2 hours, the green/blue solution was allowed to stand for 1 week after which time the product crystallised from solution as green/blue plate-like crystals.

Analysis, found (calc. for $C_{20}H_{22}O_4Cu$): C, 61.6 (61.6); H, 5.64 (5.69).

Selected infrared data: 1600cm^{-1} & 1574cm^{-1} υ(C=O); 1512cm^{-1} υ(C=C); 1286-1228cm^{-1} υ(C-O).

4.4.7. Synthesis of Tris(maltolato)monohydroxotin(IV).3.5H_2O (21)

As mentioned in the discussion earlier in this chapter this compound was produced via the oxidation of the product of the reaction of Sn(II) butoxide and maltol in an equimolar ratio. This reaction yielded ca. 20mg of a colourless crystalline solid which was then analysed using microanalysis and later by X-ray crystallography.

Analysis, found (calc. for $C_{18}H_{16}O_{10}Sn.3.5H_2O$): C, 37.3 (37.7); H, 3.98 (4.01).

4.5. Conclusions

The structure of Zn(II) maltolate has been determined and was found to be composed of two distinct zinc sites (one square pyramidal and one octahedral) within the same crystal which, as mentioned in the discussion, is very rare.

A further interesting observation which can be made from the structure is the importance of the availability of the metal ion in determining the biological activity of the complex. The lattice arrangement of Zn(II) maltolate is such that the zinc ions are tightly bound and, as such, are not able to exert their anti-bacterial effect. If, on the other hand, one looks at the Cu(II) hinokitiol it is clear that the Cu(II) ion is much more readily available and this is a possible explanation for the greatly enhanced anti-bacterial activity of this complex. By inference, it can be postulated that the high anti-bacterial activity of Cu(II) maltolate and Cu(II) ethyl maltolate is also due to the availability of the metal ion.

These results are strengthened by comparison with the other complexes/mixtures which were assayed in this chapter. It can be clearly seen that a mixture of M(II) and the starting material (i.e., maltol, ethyl maltolate or hinokitiol) gave a very similar anti-bacterial activity to that of the complex. The reason for the consistently slightly higher anti-bacterial activity of the complexes over the mixtures is presumably due to the prolonged bioavailability of the M(II) ions in the complexes. In mixtures the M(II) ion will probably react very quickly with either other components of toothpaste, or with substances present in the oral cavity. The use of the complexes avoids this problem and also overcomes an inherent problem of using M(II) compounds in toothpastes - their taste, as both maltol and hinokitiol are able to mask the unacceptable taste of M(II) ions (especially true of the metallic taste of zinc).

The results obtained in this chapter clearly demonstrate a potential new family of compounds which could be used in the oral care industry. There are numerous compounds with a carbonyl group adjacent to a hydroxyl group which have the potential of being used in a similar manner to that outlined in this chapter, i.e., to stabilise and

increase the bioavailability of metal ions in oral care applications. The big advantage that some of these compounds have is that they are synthetic and as such are likely to be cheaper and more commercially available than the natural products that the compounds are based on/derived from.

The use of Cu(II) in toothpastes is not common (only one toothpaste containing copper is known to the author). There are many reasons for this e.g. taste and toxicity. The compounds detailed in this chapter all have the advantage of masking the taste of the copper. The use of a complex which delivers copper more effectively and increases its bioavailability, leads to a lower usage concentration of copper which is more beneficial from a toxicological viewpoint. As previously stated, the types of compounds detailed in this chapter offer cheap and effective ways of overcoming the problems normally associated with the use of metal ions.

In the oral care industry, Zn(II) is much more widely used than Cu(II), and is highly patented. The Zn(II) complexes detailed in this chapter, whilst being less effective than the Cu(II), still exhibit an anti-bacterial effect and (as they are standard organic reagents) may well be free from patent cover.

As a result of the work carried out in this chapter, Unilever have been able to file an Oral Care patent on the use of metal maltolates and similar compounds.

The use of Sn(II) is widespread in the oral care industry and a method of effectively stabilising these ions is still being sought. The work presented in this chapter offers no immediate solution to this problem, but suggests that since these types of compounds are so effective for copper and zinc that this technology could be applied to Sn(II).

APPENDICES

APPENDIX A - Experimental procedures for pH Stat and Biofilm assays

1. pH Stat assay

The bacteria used for the test were *Streptococcus mutans*, a suitable suspension of which was prepared and cultivated as follows:-

A swab of *Streptococcus mutans* was taken from a pure culture and placed in a bottle containing 20ml brain/heart infusion (BHI) broth. Two such bottles were prepared and these were then incubated in a CO_2 incubator at 37°C for 5-6 hours. After the period of incubation, the broths containing the cells were each carefully poured into 500ml BHI broth contained in 1000ml conical flasks. 20ml sterile 20% (w/v)α-D-glucose was also added to both of the flasks. The two flasks were then placed in an orbital incubator (at 37°C) overnight at 80-100rpm. The following morning, the broths were poured into four 250ml sorval bottles and balanced to the nearest gram using millipore water. The bottles were then centrifuged at 10,000 rpm (in a rotor) at 4°C for 20 minutes. After centrifuging, the waste media was poured into a beaker containing `Virkon'. In the bottom of each sorval bottle was an off-white pellet of cells. To this pellet was added 30ml 0.135mM KCl solution. The pellet of cells was then carefully suspended in the KCl using a cotton swab (this was done to ensure that there were no lumps of cells). The four suspensions were then combined into two sorval bottles and re-centrifuged as before.

All supernatant fluid from the centrifuged bottles was discarded into the `Virkon'. The cells were then re-suspended in 30ml 0.135mM KCl and then combined into one sorval bottle and centrifuged again. The supernatant was discarded and the cells re-suspended with a cotton swab in 5ml 0.135mM KCl. The suspension was then poured into a 30ml sterilin flask and made up to 10ml with KCl yielding a milky-white suspension of viable cells. The flask was then stored in ice and shaken frequently during the course of the experiment.

Each of the compounds under investigation were tested over a range of concentrations (0.1mM - 1.0mM). Each test solution was of 5ml total volume and consisted

of the following five components, each of which was carefully added with an automatic pipette:-

(i) 4.00ml 0.135mM KCl.

(ii) 0.50ml *Streptococcus mutans* cell suspension.

(iii) 0.10ml 20% sterile glucose solution.

(iv) 0.30ml millipore water.

(v) 0.10ml test solution.

1.1. Experimental method for determination of % acid-inhibition

The KCl solution (4.00ml), *S. mutans* cell suspension (0.50ml) and the millipore water (0.40ml) were placed in a titration vessel, and the vessel immersed in the water-jacket. No test solution was added to the flask in order to obtain a background control value. The mechanical stirrer and pH-stat were engaged and the volume of KOH added was noted at two minute intervals. After ten minutes, 0.10ml glucose solution was added, and the volume of glucose added was noted. The pH began to fall as the glucose was metabolised by the *S. mutans*, prompting the addition of KOH to maintain the pH at 7.0. After two minutes the final volume of KOH added was recorded.

X = (vol.KOH @ 10min.) - (vol.KOH @ 8min.)

Y = (vol.KOH @ 12min.) - (vol.KOH @ 10min.)

The control value could then be calculated by subtracting X from Y.

The above procedure was repeated with the addition of the test solutions (0.10ml) together with millipore water (0.30ml). In order to compensate for the fifty-fold dilution of the test solution when it is made up to 5.0ml, the original stock solution must be 50mM.

Upon addition of the glucose, the pH tends to fall much less rapidly due to the inhibitory effect of the compounds being tested.

The % acid-inhibition can be determined using the following equation:

$$\% \text{ acid inhibition} = 100 - 100\ [\ (Y_{sample} - X_{sample}) / (Y_{control} - X_{control})]$$

For convenience, the results are represented graphically as % inhibition *vs.* concentration of compound.

2. Biofilm assay

2.1. Preparation of *E. cloacae*-coated microtitre plates

A subculture of *E. cloacae* was added to Brain Heart Infusion (BHI) broth, and incubated overnight at 37°C. The BHI with *E. cloacae* was then transferred to 10ml sterile centrifuge tubes and spun for 5 minutes at 6000 rpm. The supernatant was safely discarded and 5ml of sterile phosphate buffered saline (PBS) added to each tube. The bacteria were resuspended using a whirlmixer, and the tubes recentrifuged. This procedure was repeated three times to thoroughly wash the bacteria. The bacteria were then resuspended in PBS in 150ml sterilins to produce an optical density (OD) of 0.2 relative to a PBS blank.

The 96-well plates on which the biofilms were coated were Corning, code 25860-96. Firstly, the wells from row A, No. 7-12 were covered with a strip of plate sealer to eliminate the possibility of splashing *E. cloacae* into these wells during the biofilm preparation stages. These wells form the "no biofilm" control wells. Aliquots of 190µl of *E. cloacae* in PBS (OD 0.2) were then added to all the remaining wells of the plate. Row A, No.1-6 become "no treatment" wells, leaving the remaining 12 columns (B-H,

No. 1-12) for treatment with samples, each in replicates of seven. The lids were then replaced on the plates which were labelled with the name of the bacterium, the date and the name of the user. The plates were then centrifuged to cause sedimentation of the bacteria (i.e. the biofilm).

The *E. cloacae*/PBS was shaken from the wells into a 1 litre beaker containing around 500ml Virkon. The plate was then patted firmly down a couple of times onto a piece of absorbent paper before adding 200µl of sterile 20% glycerol in distilled water to all the biofilm wells. The plates were then stacked in 3`s or 4`s and taped together, before being placed in a freezer until required.

The Staphylococcus plates were prepared in a similar manner, except that the plates were used on the same day they were made.

2.2. Preparation of test samples and subsequent treatment of biofilms

A known weight of each compound to be tested was dissolved in a solvent (the compounds described in this report were all soluble in either water or a dimethylsulphoxide/water mixture). If the compound to be tested was a Sn(II), Zn(II) or Cu(II) compound then the weight of sample used had to be sufficient to provide ca. 6000ppm of the metal ion. In the testing of both triclosan phosphate and the phosphodiester of triclosan, the concentration of compound was ca. 0.4% w/w.

Experimental samples were added to the biofilm wells for a certain exposure time - for the purpose of this experiment the time was 1 minute. To facilitate this, all samples being tested were first prepared and then added to a separate clean 96-well plate in a slight excess (e.g. 210µl) according to a known plate plan. A strip of plate sealer was then placed on the plate to prevent any contamination from other test samples. Pieces of the plate sealer were then removed when necessary to allow the exposure of the biofilm to the test solution.

The first compound to be tested was then added to the biofilm and left for 1 minute (this compound will usually be in wells B1-H1). After 1 minute the sample was then removed by shaking the plate firmly over a beaker of Virkon, patting down on absorbent paper and filling the wells with sterile distilled water from a wash bottle. Typically 3-4 washes were needed.

The second test compound (in wells B2-H2) was then added to the biofilm plate and left for 1 minute, tipped out and washed as before. This procedure was repeated for the remaining test solutions.

After the whole plate had been treated it was washed again and patted down. 200µl of BHI broth and 80µl of sterile mineral oil were then added to each of the wells. The plate was then placed in a plate reader, such as the Dynatech Dias. This enables the optical densities of all the wells to be read over a period of up to 23 hours, whilst being incubated at 37°C. The optical density (at 630nm) of the wells is then read every 15 minutes. The Dynatech has a kinetic program which determines the mean times for the wells to reach a certain OD (e.g. 0.3).

APPENDIX B - Data for crystal structure of pyridinium triclosan phosphate

A crystal of approximate dimensions 0.3 x 0.3 x 0.3 mm was used for data collection.

Crystal data: $C_{22}H_{18}Cl_3N_2O_5P$, $M = 527.70$, Triclinic, $a = 9.615(3)$, $b = 10.272(3)$, $c = 13.480(3)$ Å, $\alpha = 94.50(2)$, $\beta = 95.63(3)$, $\gamma = 115.18(3)^\circ$, $U = 1188.3(6)$ Å^3, space group P-1(No.2), $Z = 2$, $D_c = 1.475 gcm^{-3}$, μ(Mo-K_α) = $0.490 mm^{-1}$, $F(000) = 540$. Crystallographic measurements were made at 293(2) K on a CAD4 automatic four-circle diffractometer in the range $2.21<\theta<23.93^\circ$. Data (3967 reflections) were corrected for Lorentz and polarisation and not for absorption.

In the final least squares cycles all atoms were allowed to vibrate anisotropically. Hydrogen atoms were included at calculated positions where relevant, except for H1 (attached to N1) and H1A (attached to O1). These latter hydrogens were located and refined at a fixed distance of 0.8Å from the relevant parent atoms.

The solution of the structure (SHELX86)[1] and refinement (SHELX93)[2] converged to a conventional [i.e. based on 1573 with $Fo>4\sigma(Fo)$] $R1 = 0.0480$ and $wR2 = 0.1044$. Goodness of fit = 0.948. The max. and min. residual densities were 0.429 and -0.240 eÅ^{-3} respectively. The asymmetric unit along with the labelling scheme used was produced using ORTEX.[3] Final fractional atomic co-ordinates and isotropic thermal parameters, bond distances and angles and anisotropic temperature factors are given in Tables B1 - B4.

Table B1. Atomic coordinates (x 10^4) and equivalent isotropic displacement parameters ($Å^2$ x 10^3) for **10** U(eq) is defined as one third of the trace of the orthogonalized Uij tensor.

Atom	x	y	z	U(eq)
P(1)	4479(2)	1399(2)	9196(2)	49(1)
Cl(1)	7543(3)	2111(3)	5731(2)	91(1)
Cl(2)	-945(3)	874(3)	8012(2)	77(1)
Cl(3)	-3918(3)	-4738(3)	6450(2)	102(1)
N(1)	7344(8)	5096(8)	9126(5)	66(2)
N(2)	2683(11)	4433(11)	7758(7)	101(3)
O(1)	6085(6)	1434(6)	9295(4)	61(2)
O(2)	3503(6)	582(6)	9944(4)	62(1)
O(3)	4631(6)	2893(5)	9137(4)	63(1)
O(4)	3549(5)	416(5)	8128(4)	52(1)
O(5)	1464(5)	927(5)	6895(4)	57(1)
C(1)	3959(8)	925(7)	7244(5)	48(2)
C(2)	5381(8)	1177(7)	6953(6)	50(2)
C(3)	5697(8)	1665(8)	6049(6)	52(2)
C(4)	4619(10)	1822(9)	5385(6)	64(2)
C(5)	3170(9)	1513(8)	5655(6)	59(2)
C(6)	2849(8)	1083(8)	6587(6)	53(2)
C(7)	271(7)	-438(8)	6790(5)	48(2)
C(8)	242(9)	-1636(8)	6235(6)	57(2)
C(9)	-1039(9)	-2968(9)	6146(7)	65(2)
C(10)	-2298(9)	-3080(9)	6587(6)	63(2)
C(11)	-2273(8)	-1909(10)	7159(6)	59(2)
C(12)	-1014(8)	-598(8)	7253(5)	48(2)
C(13)	7597(11)	6398(11)	9509(7)	73(2)
C(14)	8933(17)	7541(12)	9502(8)	96(3)
C(15)	10093(14)	7348(16)	9102(11)	116(5)
C(16)	9809(13)	5968(18)	8695(12)	121(4)
C(17)	8430(12)	4853(12)	8725(9)	94(3)
C(18)	3595(10)	5747(12)	8316(7)	72(2)
C(19)	3704(10)	6940(11)	7897(10)	85(3)
C(20)	3008(13)	6891(11)	6977(10)	84(3)
C(21)	2108(12)	5590(12)	6437(7)	84(3)
C(22)	1923(11)	4384(10)	6834(7)	73(2)

Table B2. Bond lengths [A] and angles [°] for **10**.

P(1)-O(3)	1.488(5)	O(1)-P(1)-O(4)	106.2(3)
P(1)-O(2)	1.500(5)	C(13)-N(1)-C(17)	121.3(8)
P(1)-O(1)	1.522(5)	C(18)-N(2)-C(22)	119.2(9)
P(1)-O(4)	1.626(5)	C(1)-O(4)-P(1)	120.3(4)
Cl(1)-C(3)	1.741(7)	C(6)-O(5)-C(7)	118.2(5)
Cl(2)-C(12)	1.731(7)	O(4)-C(1)-C(2)	122.4(6)
Cl(3)-C(10)	1.731(8)	O(4)-C(1)-C(6)	117.9(6)
N(1)-C(13)	1.31(1)	C(2)-C(1)-C(6)	119.5(6)
N(1)-C(17)	1.33(1)	C(3)-C(2)-C(1)	118.9(7)
N(2)-C(18)	1.36(1)	C(2)-C(3)-C(4)	122.5(6)
N(2)-C(22)	1.37(1)	C(2)-C(3)-Cl(1)	118.6(6)
O(4)-C(1)	1.365(8)	C(4)-C(3)-Cl(1)	118.9(6)
O(5)-C(6)	1.382(8)	C(5)-C(4)-C(3)	118.7(7)
O(5)-C(7)	1.367(8)	C(4)-C(5)-C(6)	119.7(7)
C(1)-C(2)	1.381(9)	O(5)-C(6)-C(5)	119.4(7)
C(1)-C(6)	1.39(1)	O(5)-C(6)-C(1)	120.0(6)
C(2)-C(3)	1.37(1)	C(5)-C(6)-C(1)	120.5(7)
C(3)-C(4)	1.37(1)	O(5)-C(7)-C(12)	116.9(6)
C(4)-C(5)	1.38(1)	O(5)-C(7)-C(8)	124.5(6)
C(5)-C(6)	1.38(1)	C(12)-C(7)-C(8)	118.6(7)
C(7)-C(12)	1.392(9)	C(7)-C(8)-C(9)	120.4(7)
C(7)-C(8)	1.38(1)	C(10)-C(9)-C(8)	119.5(8)
C(8)-C(9)	1.38(1)	C(9)-C(10)-C(11)	120.7(7)
C(9)-C(10)	1.37(1)	C(9)-C(10)-Cl(3)	119.5(7)
C(10)-C(11)	1.37(1)	C(11)-C(10)-Cl(3)	119.8(6)
C(11)-C(12)	1.36(1)	C(12)-C(11)-C(10)	119.9(7)
C(13)-C(14)	1.32(2)	C(11)-C(12)-C(7)	120.8(7)
C(14)-C(15)	1.36(2)	C(11)-C(12)-Cl(2)	120.1(6)
C(15)-C(16)	1.38(2)	C(7)-C(12)-Cl(2)	119.0(6)
C(16)-C(17)	1.34(2)	N(1)-C(13)-C(14)	122.0(1)
C(18)-C(19)	1.36(1)	C(13)-C(14)-C(15)	119.0(1)
C(19)-C(20)	1.34(1)	C(16)-C(15)-C(14)	118.5(1)
C(20)-C(21)	1.34(1)	C(17)-C(16)-C(15)	119.6(1)
C(21)-C(22)	1.34(1)	N(1)-C(17)-C(16)	119.5(1)
		C(19)-C(18)-N(2)	116.7(9)
O(3)-P(1)-O(2)	116.3(3)	C(18)-C(19)-C(20)	123.9(9)
O(3)-P(1)-O(1)	109.2(3)	C(19)-C(20)-C(21)	118.8(9)
O(2)-P(1)-O(1)	113.6(3)	C(22)-C(21)-C(20)	119.4(1)
O(3)-P(1)-O(4)	107.8(3)	C(21)-C(22)-N(2)	121.9(9)
O(2)-P(1)-O(4)	103.0(3)		

Table B3. Anisotropic displacement parameters ($Å^2$ x 10^3) for **10**. The anisotropic displacement factor exponent takes the form: $-2\ pi^2\ [\ h^2\ a^*\ 2\ U11 + ... + 2\ h\ k\ a^*\ b^*\ U12\ ]$

Atom	U11	U22	U33	U23	U13	U12
P(1)	49(1)	53(1)	51(1)	17(1)	13(1)	24(1)
Cl(1)	60(1)	126(2)	85(2)	23(2)	37(1)	31(1)
Cl(2)	72(1)	85(2)	82(2)	-5(1)	18(1)	42(1)
Cl(3)	67(2)	73(2)	131(2)	11(2)	13(2)	-3(1)
N(1)	64(4)	63(5)	72(5)	15(4)	24(4)	24(4)
N(2)	106(6)	106(7)	95(7)	21(6)	12(6)	51(6)
O(1)	48(3)	67(4)	77(4)	31(3)	14(3)	29(3)
O(2)	61(3)	80(4)	57(3)	28(3)	24(3)	36(3)
O(3)	69(3)	49(3)	71(4)	11(3)	7(3)	26(3)
O(4)	46(3)	50(3)	54(3)	15(2)	13(2)	13(2)
O(5)	46(3)	48(3)	74(4)	-3(2)	13(2)	19(2)
C(1)	47(4)	43(4)	54(5)	11(3)	17(4)	15(3)
C(2)	41(4)	53(4)	53(5)	9(4)	7(3)	16(3)
C(3)	44(4)	49(4)	58(5)	4(4)	12(4)	16(3)
C(4)	68(5)	58(5)	49(5)	14(4)	16(4)	10(4)
C(5)	59(5)	62(5)	51(5)	14(4)	6(4)	22(4)
C(6)	50(4)	46(4)	61(5)	5(4)	12(4)	18(3)
C(7)	39(4)	60(5)	49(4)	10(4)	4(3)	25(4)
C(8)	58(5)	59(5)	57(5)	2(4)	20(4)	25(4)
C(9)	60(5)	49(5)	74(6)	-4(4)	12(4)	12(4)
C(10)	51(5)	65(5)	59(5)	15(4)	0(4)	14(4)
C(11)	45(4)	73(6)	58(5)	17(4)	15(4)	20(4)
C(12)	49(4)	53(5)	48(4)	7(3)	6(3)	29(4)
C(13)	84(6)	65(6)	73(6)	11(5)	22(5)	32(5)
C(14)	129(10)	68(7)	67(7)	-1(5)	-6(7)	25(8)
C(15)	74(8)	94(9)	123(11)	44(8)	-18(7)	-15(7)
C(16)	67(7)	141(12)	166(13)	50(10)	46(7)	44(8)
C(17)	81(7)	83(7)	125(9)	5(6)	37(6)	40(6)
C(18)	61(5)	89(7)	66(6)	-3(6)	1(4)	38(5)
C(19)	61(6)	62(6)	110(9)	-28(6)	21(6)	11(5)
C(20)	100(7)	63(6)	105(9)	16(6)	29(7)	47(6)
C(21)	116(8)	85(7)	62(6)	8(6)	0(5)	57(6)
C(22)	76(6)	67(6)	73(6)	-1(5)	-9(5)	34(5)

Table B4. Hydrogen coordinates (x 10^4) and isotropic displacement parameters ($Å^2$ x 10^3) for **10**.

Atom	x	y	z	U(eq)
H(1A)	6295(105)	894(98)	9541(70)	73
H(3A)	6284(103)	4251(97)	9102(61)	76
H(2)	6110(8)	1017(7)	7366(6)	60
H(4)	4857(10)	2131(9)	4767(6)	77
H(5)	2415(9)	1593(8)	5212(6)	71
H(8)	1087(9)	-1549(8)	5917(6)	69
H(9)	-1041(9)	-3782(9)	5789(7)	79
H(11)	-3115(8)	-2008(10)	7484(6)	71
H(13)	6815(11)	6526(11)	9794(7)	88
H(14)	9080(17)	8462(12)	9765(8)	116
H(15)	11053(14)	8130(16)	9104(11)	139
H(16)	10571(13)	5813(18)	8401(12)	145
H(17)	8236(12)	3916(12)	8465(9)	112
H(18)	4117(10)	5822(12)	8952(7)	86
H(19)	4297(10)	7846(11)	8273(10)	102
H(20)	3146(13)	7742(11)	6715(10)	100
H(21)	1618(12)	5529(12)	5793(7)	101
H(22)	1258(11)	3487(10)	6471(7)	88

References

1. G. M. Sheldrick, *Acta Cryst.*,1990, **A46**, 467.
2. G. M. Sheldrick, SHELXL, a computer program for crystal structure refinement, University of Göttingen, 1993.
3. P. McArdle, *J. Appl. Cryst.*, 1994, **27**, 438.

APPENDIX C - Data for crystal structure of Zn(II)maltolate

A crystal of approximate dimensions 0.3 x 0.3 x 0.3 mm was used for data collection.

Crystal data: $C_{12}H_{15}O_{8.5}Zn$, M=360.1, Orthorhombic, a = 13.107(2), b = 13.389(2), c =16.149(2)Å, U = 2834.0(7) Å^3, space group *P*bna, Z = 8, D_c = 1.690gcm^{-3}, μ(Mo-K_α) = 1.774mm^{-1}, F(000) = 1480. Crystallographic measurements were made at 293(2) K on a CAD4 automatic four-circle diffractometer in the range $2.00<\theta<23.94°$. Data (4439 reflections) were corrected for Lorentz and polarisation but not absorption.

The molecular formula above refers to the asymmetric unit, which consists of one half of an octahedral zinc complex (with the central metal atom seated on an inversion centre at 0, 0, 0.5), one half of a square pyramidal zinc complex (where the metal and the oxygen in the ligated water molecule, O4, are seated on a 2 fold rotation axis at x, -0.25, 0.5) and one full water molecule of recrystallisation.

In the final least squares cycles all atoms were allowed to vibrate anisotropically. Hydrogen atoms were included at calculated positions where relevant except for the water hydrogens, which were refined at a fixed distance of 0.98Å from the relevant parent oxygen atoms.

The solution of the structure (SHELX86)[1] and refinement (SHELX93)[2] converged to a conventional [i.e. based on 1287F^2 data with $Fo>4\sigma(Fo)$] R1=0.0400 and wR2=0.0710. Goodness of fit = 1.050. The max. and min. residual densities were 0.322 and -0.412 eÅ-3 respectively. The asymmetric unit, along with the labelling scheme used was produced using ORTEX.[3] Final fractional atomic co-ordinates and isotropic thermal parameters, bond distances and angles and anisotropic temperature factors are given in tables C1 - C4.

Table C1. Atomic coordinates (x 10^4) and equivalent isotropic displacement parameters ($Å^2$ x 10^3) for **15**. U(eq) is defined as one third of the trace of the orthogonalized Uij tensor.

Atom	x	y	z	U(eq)
Zn(1)	2949(1)	-2500	5000	30(1)
O(1)	3236(3)	-2244(2)	3752(2)	40(1)
O(2)	3257(2)	-1031(2)	5077(2)	35(1)
O(3)	3797(3)	692(2)	3421(2)	43(1)
O(4)	1417(3)	-2500	5000	54(1)
C(1)	3398(4)	-1325(4)	3641(3)	31(1)
C(2)	3438(4)	-650(3)	4331(3)	28(1)
C(3)	3668(4)	318(4)	4209(3)	35(1)
C(4)	3713(4)	75(4)	2771(3)	39(1)
C(5)	3533(4)	-886(4)	2840(3)	38(1)
C(6)	3821(5)	1096(4)	4851(4)	56(2)
Zn(2)	0	0	5000	33(1)
O(5)	652(3)	953(2)	4139(2)	38(1)
O(6)	454(3)	-1048(2)	4167(2)	30(1)
O(7)	1265(3)	-601(3)	2060(2)	40(1)
O(8)	1503(3)	-63(3)	5686(2)	41(1)
O(9)	1425(4)	2982(3)	4071(3)	58(1)
C(7)	873(4)	471(3)	3485(3)	28(1)
C(8)	777(4)	-597(3)	3477(3)	27(1)
C(9)	990(4)	-1105(4)	2770(3)	34(1)
C(10)	1367(5)	378(5)	2067(3)	43(1)
C(11)	1201(4)	940(4)	2742(3)	35(1)
C(12)	957(5)	-2192(4)	2655(3)	47(1)

Table C2. Bond lengths [Å] and angles [°] for **15**.

Zn(1)-O(4)	2.008(5)	C(4)-O(3)-C(3)	119.3(4)
Zn(1)-O(2)#1	2.012(3)	O(1)-C(1)-C(5)	123.4(5)
Zn(1)-O(2)	2.012(3)	O(1)-C(1)-C(2)	120.6(4)
Zn(1)-O(1)	2.078(3)	C(5)-C(1)-C(2)	116.0(4)
Zn(1)-O(1)#1	2.078(3)	O(2)-C(2)-C(3)	122.8(4)
O(1)-C(1)	1.261(6)	O(2)-C(2)-C(1)	117.1(4)
O(2)-C(2)	1.330(5)	C(3)-C(2)-C(1)	120.1(4)
O(3)-C(4)	1.342(6)	C(2)-C(3)-O(3)	120.9(4)
O(3)-C(3)	1.378(6)	C(2)-C(3)-C(6)	127.2(4)
C(1)-C(5)	1.432(7)	O(3)-C(3)-C(6)	111.9(4)
C(1)-C(2)	1.436(7)	C(5)-C(4)-O(3)	123.5(5)
C(2)-C(3)	1.345(7)	C(4)-C(5)-C(1)	120.1(5)
C(3)-C(6)	1.483(7)	O(6)-Zn(2)-O(6)#2	180.0
C(4)-C(5)	1.313(7)	O(6)-Zn(2)-O(5)	82.0(1)
Zn(2)-O(6)	2.034(3)	O(6)#2-Zn(2)-O(5)	98.0(1)
Zn(2)-O(6)#2	2.034(3)	O(6)-Zn(2)-O(5)#2	98.0(1)
Zn(2)-O(5)	2.072(3)	O(6)#2-Zn(2)-O(5)#2	82.0(1)
Zn(2)-O(5)#2	2.072(3)	O(5)-Zn(2)-O(5)#2	180.0
Zn(2)-O(8)#2	2.261(4)	O(6)-Zn(2)-O(8)#2	87.5(1)
Zn(2)-O(8)	2.261(4)	O(6)#2-Zn(2)-O(8)#2	92.5(1)
O(5)-C(7)	1.270(6)	O(5)-Zn(2)-O(8)#2	90.4(1)
O(6)-C(8)	1.336(6)	O(5)#2-Zn(2)-O(8)#2	89.6(1)
O(7)-C(10)	1.317(7)	O(6)-Zn(2)-O(8)	92.5(1)
O(7)-C(9)	1.378(6)	O(6)#2-Zn(2)-O(8)	87.5(1)
C(7)-C(11)	1.420(7)	O(5)-Zn(2)-O(8)	89.6(1)
C(7)-C(8)	1.436(6)	O(5)#2-Zn(2)-O(8)	90.4(1)
C(8)-C(9)	1.359(7)	O(8)#2-Zn(2)-O(8)	180.0
C(9)-C(12)	1.467(7)	C(7)-O(5)-Zn(2)	109.8(3)
C(10)-C(11)	1.343(7)	C(8)-O(6)-Zn(2)	109.4(3)
		C(10)-O(7)-C(9)	120.4(4)
O(4)-Zn(1)-O(2)#1	101.59(9)	O(5)-C(7)-C(11)	123.1(4)
O(4)-Zn(1)-O(2)	101.59(9)	O(5)-C(7)-C(8)	119.6(4)
O(2)#1-Zn(1)-O(2)	156.8(2)	C(11)-C(7)-C(8)	117.3(5)
O(4)-Zn(1)-O(1)	100.4(1)	O(6)-C(8)-C(9)	122.6(4)
O(2)#1-Zn(1)-O(1)	93.7(1)	O(6)-C(8)-C(7)	118.1(4)
O(2)-Zn(1)-O(1)	82.1(1)	C(9)-C(8)-C(7)	119.2(5)
O(4)-Zn(1)-O(1)#1	100.4(1)	C(8)-C(9)-O(7)	120.5(4)
O(2)#1-Zn(1)-O(1)#1	82.1(1)	C(8)-C(9)-C(12)	126.6(5)
O(2)-Zn(1)-O(1)#1	93.7(1)	O(7)-C(9)-C(12)	112.8(4)
O(1)-Zn(1)-O(1)#1	159.2(2)	O(7)-C(10)-C(11)	123.2(5)
C(1)-O(1)-Zn(1)	109.2(3)	C(10)-C(11)-C(7)	119.2(5)
C(2)-O(2)-Zn(1)	110.7(3)		

Symmetry transformations used to generate equivalent atoms:

#1 x,-y-1/2,-z+1

#2 -x,-y,-z+1

Table C3. Anisotropic displacement parameters ($Å^2$ x 10^3) for **15**. The anisotropic displacement factor exponent takes the form: $-2\ pi^2\ [\ h^2\ a^*\ 2\ U11 + ... + 2\ h\ k\ a^*\ b^*\ U12\ ]$.

Atom	U11	U22	U33	U23	U13	U12
Zn(1)	41(1)	21(1)	28(1)	3(1)	0	0
O(1)	63(2)	27(2)	30(2)	-1(1)	7(2)	-1(2)
O(2)	55(2)	25(1)	26(2)	1(2)	4(2)	-4(1)
O(3)	55(2)	32(2)	41(2)	10(2)	4(2)	-3(2)
O(4)	31(3)	40(3)	91(4)	35(4)	0	0
C(1)	32(3)	31(3)	29(3)	4(2)	3(2)	4(2)
C(2)	35(3)	27(3)	21(2)	2(2)	1(2)	-1(2)
C(3)	41(3)	29(3)	34(3)	5(2)	2(2)	-4(2)
C(4)	45(3)	45(3)	26(3)	8(2)	6(2)	-3(3)
C(5)	45(3)	42(3)	26(3)	1(2)	8(3)	3(3)
C(6)	87(4)	31(3)	49(4)	1(3)	0(3)	-21(3)
Zn(2)	56(1)	24(1)	20(1)	0(1)	9(1)	4(1)
O(5)	62(2)	21(2)	29(2)	0(2)	8(2)	2(2)
O(6)	42(2)	22(2)	25(2)	3(1)	7(2)	5(2)
O(7)	48(2)	47(2)	23(2)	-5(2)	8(2)	-2(2)
O(8)	50(2)	39(2)	34(2)	-4(2)	-1(2)	7(2)
O(9)	76(3)	35(2)	63(3)	-8(2)	8(2)	-2(2)
C(7)	31(3)	26(2)	26(2)	1(2)	2(2)	3(2)
C(8)	32(3)	27(2)	22(2)	3(2)	-3(2)	0(2)
C(9)	39(3)	34(3)	28(3)	-6(2)	-1(2)	5(2)
C(10)	43(3)	51(4)	34(3)	11(3)	9(3)	-3(3)
C(11)	43(3)	31(3)	32(3)	8(2)	7(2)	2(2)
C(12)	55(3)	41(3)	46(3)	-16(2)	5(3)	3(3)

Table C4. Hydrogen coordinates (x 10^4) and isotropic displacement parameters ($Å^2$ x 10^3) for **15**.

Atom	x	y	z	U(eq)
H(4A)	967(36)	-2023(35)	4807(35)	66(19)
H(4)	3785(4)	342(4)	2242(3)	47
H(5)	3494(4)	-1282(4)	2368(3)	45
H(6A)	3287(19)	1584(17)	4811(17)	84
H(6B)	4469(15)	1414(21)	4767(16)	84
H(6C)	3805(32)	793(6)	5389(4)	84
H(8A)	1678(46)	607(22)	5599(40)	80(24)
H(8B)	2046(36)	-449(34)	5443(37)	70(20)
H(9A)	1382(52)	2288(25)	4192(50)	109(31)
H(9B)	704(30)	3187(49)	4001(51)	108(30)
H(10)	1563(5)	695(5)	1580(3)	51
H(11)	1299(4)	1627(4)	2724(3)	42
H(12A)	1611(9)	-2423(5)	2467(21)	71
H(12B)	447(19)	-2356(4)	2250(16)	71
H(12C)	791(26)	-2508(4)	3171(6)	71

References

1. G. M. Sheldrick, *Acta Cryst.*, 1990, **A46**, 467.
2. G. M. Sheldrick, SHELXL, a computer program for crystal structure refinement, University of Göttingen, 1993.
3. P. McArdle, *J. Appl. Cryst.*, 1994, **27**, 438.

APPENDIX D - Data for crystal structure of Cu(II)hinokitiol

A crystal of approximate dimensions 0.3 x 0.3 x 0.5 mm was used for data collection.

Crystal data: $C_{20}H_{22}CuO_4$, $M = 389.92$, Monoclinic, $a = 9.254(2)$, $b = 9.997(2)$, $c = 11.124(3)$Å, $\beta = 113.86(2)°$, $U = 941.2(4)$ Å^3, space group $P21/c$, $Z = 2$, $D_c = 1.376 gcm^{-3}$, $\mu(Mo\text{-}K_\alpha) = 1.180 mm^{-1}$, $F(000) = 406$. Crystallographic measurements were made at 293(2) K on a CAD4 automatic four-circle diffractometer in the range $2.40<\theta<23.92°$. Data (1685 reflections) were corrected for Lorentz, polarization and 10% decay of the crystal in the X-ray beam. An absorption correction was not applied.

The asymmetric unit in this structure comprises of one half of a molecule, the remaining portion being generated via an inversion centre at 0 0 0 on which the copper is sited.

In the final least squares cycles all atoms were allowed to vibrate anisotropically. Hydrogen atoms were included at calculated positions where relevant except for H3, H4, H5 and H7 which were easily located in the penultimate difference Fourier map, and refined at a distance of 0.93Å from the carbon atoms to which they are attached.

The solution of the structure (SHELX86)[1] and refinement (SHELX93)[2] converged to a conventional [i.e. based on 887 F^2 data with $Fo>4\sigma(Fo)$] $R1 = 0.0430$ and $wR2 = 0.0704$. Goodness of fit = 1.059. The max. and min. residual densities were 0.227 and -0.225 eÅ^{-3} respectively. The asymmetric unit, along with the labelling scheme used was produced using ORTEX.[3] Final fractional atomic co-ordinates and isotropic thermal parameters, bond distances and angles and anisotropic temperature factors are given in Tables D1 - D4.

Table D1. Atomic coordinates (x 10^4) and equivalent isotropic displacement parameters ($Å^2$ x 10^3) for **20**. U(eq) is defined as one third of the trace of the orthogonalized Uij tensor.

Atom	x	y	z	U(eq)
Cu(1)	0	0	0	47(1)
O(1)	109(3)	1422(3)	1173(3)	60(1)
O(2)	2237(3)	4(4)	901(2)	51(1)
C(1)	2763(5)	902(5)	1817(4)	43(1)
C(2)	1537(5)	1728(5)	1962(4)	46(1)
C(3)	1791(6)	2775(5)	2838(5)	57(1)
C(4)	3190(6)	3256(5)	3782(5)	59(1)
C(5)	4733(6)	2841(5)	4119(5)	57(1)
C(6)	5292(5)	1835(5)	3584(4)	47(1)
C(7)	4388(5)	999(5)	2561(4)	46(1)
C(8)	7077(5)	1589(5)	4180(4)	61(1)
C(9)	7799(5)	1703(6)	3177(5)	73(2)
C(10)	7479(6)	258(7)	4898(6)	97(2)

Table D2. Bond lengths [Å] and angles [°] for **20**.

Cu(1)-O(2)	1.900(2)
Cu(1)-O(2)#1	1.900(2)
Cu(1)-O(1)#1	1.904(3)
Cu(1)-O(1)	1.904(3)
O(1)-C(2)	1.293(5)
O(2)-C(1)	1.296(5)
C(1)-C(7)	1.396(5)
C(1)-C(2)	1.464(6)
C(2)-C(3)	1.384(6)
C(3)-C(4)	1.382(7)
C(4)-C(5)	1.386(7)
C(5)-C(6)	1.372(6)
C(6)-C(7)	1.386(6)
C(6)-C(8)	1.531(6)
C(8)-C(10)	1.518(8)
C(8)-C(9)	1.520(6)
O(2)-Cu(1)-O(2)#1	180.0
O(2)-Cu(1)-O(1)#1	96.2(1)
O(2)#1-Cu(1)-O(1)#1	83.8(1)
O(2)-Cu(1)-O(1)	83.8(1)
O(2)#1-Cu(1)-O(1)	96.1(1)
O(1)#1-Cu(1)-O(1)	180.0
C(2)-O(1)-Cu(1)	113.5(3)
C(1)-O(2)-Cu(1)	113.5(3)
O(2)-C(1)-C(7)	119.1(4)
O(2)-C(1)-C(2)	114.6(3)
C(7)-C(1)-C(2)	126.3(4)
O(1)-C(2)-C(3)	119.6(4)
O(1)-C(2)-C(1)	114.6(4)
C(3)-C(2)-C(1)	125.9(4)
C(4)-C(3)-C(2)	129.7(5)
C(3)-C(4)-C(5)	130.3(5)
C(6)-C(5)-C(4)	129.1(4)
C(5)-C(6)-C(7)	126.2(4)
C(5)-C(6)-C(8)	117.4(4)
C(7)-C(6)-C(8)	116.5(4)
C(6)-C(7)-C(1)	132.5(4)
C(10)-C(8)-C(9)	111.4(5)
C(10)-C(8)-C(6)	111.1(4)
C(9)-C(8)-C(6)	112.8(4)

Symmetry transformations used to generate equivalent atoms:

#1 -x,-y,-z

Table D3. Anisotropic displacement parameters ($Å^2$ x 10^3) for **20**. The anisotropic displacement factor exponent takes the form: $-2\ pi^2\ [\ h^2\ a^*\ 2\ U11 + ... + 2\ h\ k\ a^*\ b^*\ U12\ ]$

Atom	U11	U22	U33	U23	U13	U12
Cu(1)	30(1)	58(1)	47(1)	0(1)	9(1)	-1(1)
O(1)	34(2)	76(2)	62(2)	-10(2)	10(1)	9(2)
O(2)	33(1)	57(2)	56(2)	-14(2)	11(1)	-1(2)
C(1)	35(2)	51(3)	42(2)	4(2)	13(2)	0(2)
C(2)	39(2)	56(3)	41(2)	2(2)	14(2)	3(2)
C(3)	54(3)	63(3)	60(3)	-5(3)	29(3)	3(3)
C(4)	66(3)	55(3)	61(3)	-12(3)	31(3)	-6(3)
C(5)	59(3)	59(3)	52(3)	-10(3)	21(2)	-15(3)
C(6)	45(2)	53(3)	42(2)	0(2)	16(2)	-11(2)
C(7)	40(2)	47(3)	50(3)	1(2)	18(2)	3(2)
C(8)	41(2)	74(4)	56(3)	-3(3)	8(2)	-12(2)
C(9)	48(3)	89(4)	84(4)	-5(3)	29(3)	-15(3)
C(10)	52(3)	123(7)	96(4)	54(5)	8(3)	9(4)

Table D4. Hydrogen coordinates (x 10^4) and isotropic displacement parameters ($Å^2$ x 10^3) for **20**.

Atom	x	y	z	U(eq)
H(3)	877(34)	3188(35)	2797(35)	38(11)
H(4)	3091(56)	3977(37)	4265(41)	69(15)
H(5)	5466(39)	3404(35)	4742(33)	48(12)
H(7)	4970(40)	385(32)	2314(33)	40(12)
H(8)	7557(5)	2289(5)	4838(4)	73
H(9A)	7441(35)	2513(20)	2681(25)	109
H(9B)	7482(37)	949(20)	2592(24)	109
H(9C)	8930(5)	1719(39)	3622(6)	109
H(10A)	7069(44)	240(18)	5565(28)	146
H(10B)	8605(6)	148(21)	5298(36)	146
H(10C)	7016(43)	-456(8)	4285(9)	146

References

1. G. M. Sheldrick, *Acta Cryst.*, 1990, **A46**, 467.
2. G. M. Sheldrick, SHELXL, a computer program for crystal structure refinement, University of Göttingen, 1993.
3. P. McArdle, *J. Appl. Cryst.*, 1994, **27**, 438.

APPENDIX E - Data for crystal structure of Tris(maltolato)monohydroxotin(IV).3.5H_2O

A crystal of approximate dimensions 0.25 x 0.2 x 0.2 mm was used for data collection.

Crystal data: $C_{18}H_{16}O_{10}Sn.3.5(H_20)$, M = 574.05, Triclinic, a = 9.363(1), b = 9.468(2), c = 13.780(2)Å, α = 103.22(2), β = 96.08(1), γ = 108.41(1)°, U = 1107.2(3)Å^3, space group P-1(No.2), Z = 2, D_c = 1.722gcm^{-3}, μ(Mo-K_α) = 1.223mm^{-1}, F(000) = 578. Crystallographic measurements were made at 293(2) K on a CAD4 automatic four-circle diffractometer in the range 2.33<θ<23.92°. Data (3706 reflections) were corrected for Lorentz and polarization but not for absorption.

In the final least squares cycles all atoms were allowed to vibrate anisotropically. Hydrogen atoms were included at calculated positions where relevant on carbon atoms. Dogged attempts to locate the hydroxyl proton (bound to O10) or the water hydrogens, sadly, did not meet with success. Hence, these hydrogens were not included in the refinement.

One of the water molecules (O12) was seen to be disordered in a 50:50 ratio with it's symmetry related partner by the *1-x, 1-y, -z* transformation. This oxygen refined with a site-occupancy factor of 0.5.

Examination of the supramolecular array revealed a complex network of hydrogen bonding. Contacts are summarised in Table E5.

The solution of the structure (SHELX86)[1] and refinement (SHELX93)[2] converged to a conventional [i.e. based on 3210 F^2 data with $Fo>4\sigma(Fo)$] $R1$ = 0.0441 and $wR2$ = 0.1096. Goodness of fit = 1.299. The max. and min. residual densities were 1.103 and -1.293 eÅ^{-3} respectively. The asymmetric unit, along with the labelling scheme used was produced using ORTEX.[3] Final fractional atomic co-ordinates and isotropic thermal parameters, bond distances and angles and anisotropic temperature factors are given in Tables E1 - E4.

Table E1. Atomic coordinates (x 10^4) and equivalent isotropic displacement parameters ($Å^2$ x 10^3) for **21**. U(eq) is defined as one third of the trace of the orthogonalized Uij tensor.

Atom	x	y	z	U(eq)
Sn(1)	1136(1)	3142(1)	2308(1)	32(1)
O(1)	2553(4)	5584(4)	2293(2)	49(1)
O(2)	490(3)	4661(3)	3382(2)	40(1)
O(3)	1004(4)	8709(4)	3928(2)	52(1)
O(4)	3068(3)	3123(3)	1507(2)	39(1)
O(5)	2769(3)	3102(4)	3411(2)	37(1)
O(6)	6605(4)	3095(4)	3430(3)	54(1)
O(7)	794(4)	677(3)	1444(2)	45(1)
O(8)	-561(3)	1710(3)	2876(2)	40(1)
O(9)	-2524(4)	-2390(4)	2309(3)	61(1)
O(10)	-289(4)	3130(4)	1140(2)	48(1)
C(1)	985(5)	6133(5)	3387(3)	38(1)
C(2)	2109(5)	6611(5)	2795(3)	39(1)
C(3)	2632(5)	8199(5)	2812(4)	51(1)
C(4)	2060(6)	9158(5)	3365(4)	55(1)
C(5)	450(5)	7180(5)	3939(3)	43(1)
C(6)	-713(7)	6879(6)	4585(4)	60(1)
C(7)	4083(4)	3111(4)	3120(3)	33(1)
C(8)	4211(4)	3128(4)	2091(3)	33(1)
C(9)	5611(5)	3121(5)	1793(4)	46(1)
C(10)	6737(5)	3107(6)	2472(4)	53(1)
C(11)	5291(5)	3108(5)	3759(3)	42(1)
C(12)	5352(6)	3119(7)	4842(4)	59(1)
C(13)	-1003(5)	204(5)	2458(3)	38(1)
C(14)	-274(5)	-329(5)	1678(3)	41(1)
C(15)	-759(7)	-1947(6)	1223(4)	62(1)
C(16)	-1852(7)	-2884(6)	1561(5)	69(2)
C(17)	-2119(5)	-838(5)	2754(4)	47(1)
C(18)	-2970(6)	-480(7)	3553(4)	65(1)
O(11)	5054(4)	8995(4)	1014(3)	66(1)
O(12)	4159(5)	5795(5)	521(3)	73(1)
O(13)	811(10)	5317(10)	128(7)	75(2)
O(14)	2606(4)	-403(4)	3(3)	55(1)

Table E2. Bond lengths [Å] and angles [°] for **21**.

Sn(1)-O(10)	1.975(3)	O(4)-Sn(1)-O(7)	70.2(1)
Sn(1)-O(5)	2.053(3)	O(10)-Sn(1)-O(1)	86.3(1)
Sn(1)-O(8)	2.089(3)	O(5)-Sn(1)-O(1)	92.5(1)
Sn(1)-O(2)	2.096(3)	O(8)-Sn(1)-O(1)	148.6(1)
Sn(1)-O(4)	2.219(3)	O(2)-Sn(1)-O(1)	73.6(1)
Sn(1)-O(7)	2.268(3)	O(4)-Sn(1)-O(1)	69.0(1)
Sn(1)-O(1)	2.280(3)	O(7)-Sn(1)-O(1)	137.3(1)
O(1)-C(2)	1.266(5)	C(2)-O(1)-Sn(1)	112.8(3)
O(2)-C(1)	1.321(5)	C(1)-O(2)-Sn(1)	116.7(3)
O(3)-C(4)	1.345(6)	C(4)-O(3)-C(5)	119.8(4)
O(3)-C(5)	1.380(5)	C(8)-O(4)-Sn(1)	111.4(2)
O(4)-C(8)	1.268(5)	C(7)-O(5)-Sn(1)	114.7(2)
O(5)-C(7)	1.332(5)	C(10)-O(6)-C(11)	120.4(3)
O(6)-C(10)	1.342(6)	C(14)-O(7)-Sn(1)	112.9(3)
O(6)-C(11)	1.358(5)	C(13)-O(8)-Sn(1)	117.3(3)
O(7)-C(14)	1.273(5)	C(16)-O(9)-C(17)	119.8(4)
O(8)-C(13)	1.318(5)	O(2)-C(1)-C(5)	121.8(4)
O(9)-C(16)	1.334(7)	O(2)-C(1)-C(2)	118.0(4)
O(9)-C(17)	1.366(6)	C(5)-C(1)-C(2)	120.3(4)
C(1)-C(5)	1.364(6)	O(1)-C(2)-C(3)	125.5(4)
C(1)-C(2)	1.424(6)	O(1)-C(2)-C(1)	117.3(4)
C(2)-C(3)	1.420(6)	C(3)-C(2)-C(1)	117.2(4)
C(3)-C(4)	1.331(7)	C(4)-C(3)-C(2)	119.5(4)
C(5)-C(6)	1.478(7)	C(3)-C(4)-O(3)	123.3(4)
C(7)-C(11)	1.359(6)	C(1)-C(5)-O(3)	119.9(4)
C(7)-C(8)	1.439(5)	C(1)-C(5)-C(6)	127.2(4)
C(8)-C(9)	1.416(6)	O(3)-C(5)-C(6)	112.9(4)
C(9)-C(10)	1.338(8)	O(5)-C(7)-C(11)	122.3(4)
C(11)-C(12)	1.484(6)	O(5)-C(7)-C(8)	118.1(3)
C(13)-C(17)	1.362(6)	C(11)-C(7)-C(8)	119.5(4)
C(13)-C(14)	1.414(6)	O(4)-C(8)-C(9)	124.2(4)
C(14)-C(15)	1.417(7)	O(4)-C(8)-C(7)	118.4(3)
C(15)-C(16)	1.329(8)	C(9)-C(8)-C(7)	117.3(4)
C(17)-C(18)	1.465(7)	C(10)-C(9)-C(8)	119.1(4)
O(13)-O(13)#1	1.42(2)	C(9)-C(10)-O(6)	123.0(4)
		O(6)-C(11)-C(7)	120.6(4)
O(10)-Sn(1)-O(5)	173.6(1)	O(6)-C(11)-C(12)	113.3(4)
O(10)-Sn(1)-O(8)	95.0(1)	C(7)-C(11)-C(12)	126.2(4)
O(5)-Sn(1)-O(8)	89.3(1)	O(8)-C(13)-C(17)	122.4(4)
O(10)-Sn(1)-O(2)	94.8(1)	O(8)-C(13)-C(14)	118.0(4)
O(5)-Sn(1)-O(2)	90.8(1)	C(17)-C(13)-C(14)	119.6(4)
O(8)-Sn(1)-O(2)	75.0(1)	O(7)-C(14)-C(13)	117.7(4)
O(10)-Sn(1)-O(4)	96.5(1)	O(7)-C(14)-C(15)	124.3(4)
O(5)-Sn(1)-O(4)	77.3(1)	C(13)-C(14)-C(15)	118.0(4)
O(8)-Sn(1)-O(4)	141.4(1)	C(16)-C(15)-C(14)	118.5(5)
O(2)-Sn(1)-O(4)	140.0(1)	C(15)-C(16)-O(9)	123.8(5)
O(10)-Sn(1)-O(7)	86.1(1)	C(13)-C(17)-O(9)	120.3(4)

O(5)-Sn(1)-O(7)	90.5(1)	C(13)-C(17)-C(18)	126.4(5)
O(8)-Sn(1)-O(7)	74.0(1)	O(9)-C(17)-C(18)	113.3(4)
O(2)-Sn(1)-O(7)	148.9(1)		

Symmetry transformations used to generate equivalent atoms:

#1 -x,-y+1,-z

Table E3. Anisotropic displacement parameters ($Å^2$ x 10^3) for **21**. The anisotropic displacement factor exponent takes the form: $-2\ pi^2\ [\ h^2\ a^*\ 2\ U11 + ... + 2\ h\ k\ a^*\ b^*\ U12\ ]$.

Atom	U11	U22	U33	U23	U13	U12
Sn(1)	25(1)	43(1)	35(1)	15(1)	10(1)	14(1)
O(1)	42(2)	51(2)	60(2)	22(2)	24(2)	15(1)
O(2)	38(2)	42(2)	47(2)	18(1)	20(1)	17(1)
O(3)	67(2)	42(2)	52(2)	15(1)	10(2)	23(2)
O(4)	31(2)	57(2)	38(1)	19(1)	13(1)	19(1)
O(5)	28(1)	58(2)	33(1)	19(1)	10(1)	20(1)
O(6)	33(2)	73(2)	64(2)	23(2)	7(2)	28(2)
O(7)	45(2)	42(2)	48(2)	12(1)	21(1)	15(1)
O(8)	34(2)	41(2)	48(2)	15(1)	20(1)	12(1)
O(9)	56(2)	46(2)	67(2)	19(2)	11(2)	-1(2)
O(10)	40(2)	68(2)	42(2)	23(2)	1(1)	24(2)
C(1)	35(2)	41(2)	37(2)	14(2)	4(2)	12(2)
C(2)	29(2)	43(2)	44(2)	15(2)	4(2)	10(2)
C(3)	41(3)	53(3)	59(3)	27(2)	10(2)	10(2)
C(4)	61(3)	43(2)	57(3)	21(2)	2(2)	11(2)
C(5)	50(3)	43(2)	39(2)	13(2)	6(2)	21(2)
C(6)	78(4)	62(3)	53(3)	16(2)	27(3)	35(3)
C(7)	26(2)	35(2)	39(2)	12(2)	9(2)	10(2)
C(8)	30(2)	28(2)	45(2)	13(2)	12(2)	10(2)
C(9)	37(2)	52(3)	56(3)	18(2)	21(2)	20(2)
C(10)	30(2)	69(3)	67(3)	20(2)	19(2)	22(2)
C(11)	35(2)	44(2)	47(2)	13(2)	2(2)	16(2)
C(12)	54(3)	78(3)	51(3)	24(2)	3(2)	30(3)
C(13)	29(2)	42(2)	41(2)	15(2)	0(2)	11(2)
C(14)	36(2)	44(2)	44(2)	14(2)	8(2)	16(2)
C(15)	73(4)	47(3)	61(3)	7(2)	23(3)	15(3)
C(16)	77(4)	43(3)	73(4)	7(2)	18(3)	5(3)
C(17)	36(2)	55(3)	51(3)	23(2)	7(2)	12(2)
C(18)	52(3)	71(3)	74(3)	32(3)	27(3)	13(3)
O(11)	63(2)	71(2)	69(2)	29(2)	12(2)	24(2)
O(12)	82(3)	70(2)	75(2)	33(2)	30(2)	24(2)
O(13)	86(5)	75(5)	82(5)	47(4)	16(5)	34(4)
O(14)	40(2)	63(2)	59(2)	11(2)	10(2)	16(2)

Table E4. Hydrogen coordinates (x 10^4) and isotropic displacement parameters ($Å^2$ x 10^3) for **21**.

Atom	x	y	z	U(eq)
H(3)	3369(5)	8565(5)	2440(4)	61
H(4)	2407(6)	10192(5)	3361(4)	66
H(6A)	-1694(11)	6238(38)	4166(5)	91
H(6B)	-771(33)	7844(7)	4955(23)	91
H(6C)	-429(24)	6360(41)	5054(20)	91
H(9)	5746(5)	3126(5)	1135(4)	55
H(10A)	7653(5)	3106(6)	2270(4)	64
H(12A)	6180(29)	4019(25)	5259(5)	88
H(12B)	5514(46)	2202(23)	4934(7)	88
H(12C)	4402(18)	3143(47)	5033(9)	88
H(15)	-323(7)	-2345(6)	700(4)	75
H(16)	-2166(7)	-3945(6)	1259(5)	83
H(18A)	-2298(14)	-116(47)	4204(5)	97
H(18B)	-3808(30)	-1397(13)	3529(21)	97
H(18C)	-3361(42)	309(36)	3450(19)	97

Table E5. Contact distances [Å] for possible hydrogen bonds in **21**.

O1 - O12	3.013(5)
O1 - O13	3.160(9)
O4 - O12	3.086(5)
O7 - O14	2.957(5)
O10 - O13	2.751(8)
O11 - O12	2.771(5)
O12 - O13	2.993(10)
O10 - O13#1	2.627(8)
O13 - O13#1	1.416(17)
O10 - O14#2	2.781(5)
O11 - O14#3	2.834(5)
O11 - O14#4	2.864(5)
O12 - O12#4	2.792(9)

Symmetry transformations used to generate equivalent atoms:

#1 -x,1-y,-z

#2 -x,-y,-z

#3 x,1+y,z

#4 1-x,1-y,-z

References

1. G. M. Sheldrick, *Acta Cryst.*, 1990, **A46**, 467.
2. G. M. Sheldrick, SHELXL, a computer program for crystal structure refinement, University of Göttingen, 1993.
3. P. McArdle, *J. Appl. Cryst.*, 1994, **27**, 438.

APPENDIX F - Experimental procedures

Instrumentation

Infrared Spectra:

The infrared spectra were obtained as finely ground mulls in anhydrous spectroscopic grade liquid paraffin. The mull was sandwiched between windows made of potassium bromide, KBr, to produce a thin film. The spectrometer used for the measurements was a Nicolet 510P Fourier transform device together with computerised data-handling capabilities. The Fourier transform spectra were obtained from 16-64 scans (dependant on sample strength) over the frequency range 4000-400cm^{-1} with a medium slit-width and a peak resolution of 4.0cm^{-1}. The lower limit of the spectra recorded using KBr discs is approximately 410cm^{-1} when the KBr itself begins to absorb the radiation.

Microanalytical data:

The microanalytical data was obtained using a Carlo-Erba microanalyser. Typically, the furnace temperature was set to 500°C. Wherever possible, the results are the mean of duplicated measurements. The measurements were reference against acetanilide, PhNHC(O)CH$_3$ (Ph = C$_6$H$_5$).

Nuclear Magnetic Resonance:

The majority of the ^{1}H and ^{13}C{^{1}H} data were obtained on a JEOL JNM-GX-270FT 270MHz Fourier transform spectrometer at ambient temperature. Occasionally, ^{1}H data was obtained on a JEOL 400MHz spectrometer in order to enhance spectral resolution. ^{31}P{^{1}H} and ^{119}Sn{^{1}H} spectra were all recorded using the high field (400MHz) JEOL spectrometer.

REFERENCES

REFERENCES

1. I. D. Mandel, *Journal American Dental Association.*, 1995, **126**, 573.
2. T. Roseberry, Dental Science and Dental Art (Ed. S. M. Gordon), Lea and Febiger (Philadelphia), 1938.
3. H. A. Schenkein, J. C. Gunsolley, T. E. Koertge, J. G. Schenkein and J. G. Tew, *Journal American Dental Association.*, 1995, **126**, 1107.
4. K. J. Rose and C. M. Carey, *Journal American Dental Association.*, 1995, **126**, 1402.
5. J. Olsson, Per-Olof Glantz and B. Krasse, *Scand. J. Dent. Res.*, 1976, **84**, 240.
6. R. J. Gibbons and J. van Houte, *J. Periodontol.*, 1973, **44**, 347.
7. B. Köhler, D. Birkhed and S. Olsson, *Caries Res.*, 1995, **29**, 402.
8. D. R. Radford and J. R. Radford, *J. Dent.*, 1993, **21**, 87.
9. J. M. Wood and P. Critchley, *Arch. Oral Biol.*, 1966, **11**, 1039.
10. R. J. Gibbons and M. Nygaard, *Arch. Oral Biol.*, 1968, **13**, 1249.
11. G. H. Petersson and D. Bratthall, *Eur. J. Oral Sci.*, 1996, **104**, 436.
12. J. T. Chan and S. H. Koh, *Caries Res.*, 1996, **30**, 88.
13. M. C. Kiritsy, S. M. Levy, J. J. Warren, N. Guha-Chowdhury, J. R. Heilman and T. Marshall, *Journal American Dental Association.*, 1996, **127**, 895.
14. J. L. Dzink, S. S. Socransky and A. D. Haffajee, *J. Clin. Periodontol.*, 1988, **15**, 316.
15. W. E. C. Moore, L. H. Moore, R. R. Ranney, R. M. Smibert, J. A. Burmeister and H. A. Schenkein, *J. Clin. Periodontol.*, 1991, **18**, 729.
16. J. J. Kamma, M. Nakou and F. A. Manti, *J. Periodontol.*, 1994, **65**, 1073.
17. A. D. Haffajee, S. S. Socransky, C. Smith and S. Dibart, *J. Clin. Periodontol.*, 1991, **18**, 744.
18. I. D. Mandel and A. Gaffar, *J. Clin. Periodontol.*, 1986, **13**, 249.
19. B. L. Philstrom, B. McHugh and T. H. Oliphant, *J. Clin. Periodontol.*, 1983, **10**, 524.

20. J. M. Albandar, L. J. Brown, J. A. Brunelle and H. Löe, *J. Periodontol.*, 1996, **67**, 953.
21. J. M. Albanar, L. J. Brown and H. Löe, *J. Periodontol.*, 1996, **67**, 960.
22. L. J. Brown, J. M. Albanar, J. A. Brunelle and H. Löe, *J. Periodontol.*, 1996, **67**, 968.
23. J. Hørmand and A. Frandson, *J. Clin. Periodontol.*, 1979, **6**, 407.
24. J. M. Albandar, *J. Periodontol.*, 1991, **62**, 370.
25. P. N. Baer, *J. Periodontol.*, 1971, **42**, 516.
26. N. Tinanoff and D. B. Weeks, *Pediatric Dentistry*, 1979, **1**, 199.
27. B. B. Beiswanger, P. M. Doyle, R. D. Jackson, M. E. Mallatt, M. S. Mau, B. W. Bollmer, M. M. Crisanti, C. B. Guay, A. C. Lanzalaco, M. F. Lucacovic, S. Majeti and L. K. McClanachan, *J. Clin. Dentistry*, 1995, **6**, 46
28. M. A. Perlich, L. A. Bacca, B. W. Bollmer, A. C. Lanzalaco, L. K. McClanaghan, L. K. Sewak, B. B. Beiswanger, W. A. Eichold, J. R. Hull, R. D. Jackson and M. S. Mau, *J. Clin. Dentistry*, 1995, **6**, 54.
29. B. Svatun and G. Rölla, 'Tooth Surface Interactions and Preventive Dentistry', IRL Press Ltd. (London), 1981, 33.
30. B. Svatun and A. Attramadal, *Acta Odontol. Scand.*, 1978, **36**, 211.
31. R. L. Zameck and N. Tinanoff, *Arch. Oral Biol.*, 1987, **32**, 807.
32. A. Gross and N. Tinanoff, *J. Dent. Res.*, 1977, **56**, 1179.
33. V. C. C. Beazley, P. Thrane and G. Rölla, *Scand. J. Dent. Res.*, 1980, **88**, 193.
34. R. J. Shern and K. M. Couet, *J. Dent. Res.*, 1979, **58**, 1830.
35. K. Skjörland, P. Gjermo and G. Rölla, *Scand. J. Dent. Res.*, 1978, **86**, 103.
36. M. Addy, *J. Clin. Periodontol.*, 1986, **13**, 957.
37. N. Tinanoff, *J. Clin. Dentistry*, 1995, **6**, 37.
38. D. A. Camosci and N. Tinanoff, *J. Dent. Res.*, 1984, **63**, 1121.
39. N. Tinanoff, J. M. Brady and A. Gross, *Caries Res.*, 1976, **10**, 415.
40. T. H. Jordan, S. H. Y. Wei, S. H. Bromberger and J. C. King, *Arch. Oral Biol.*, 1971, **16**, 241.

41. D. J. Krutchkoff, T. H. Jordan, S. H. Y. Wei and W. D. Nordquist, *Arch. Oral Biol.*, 1972, **17**, 923.
42. H. J. Keene, I. L. Shklair and G. J. Mickel, *J. Dent. Res.*, 1977, **56**, 21.
43. D. J. White, *J. Clin. Dentistry*, 1995, **6**, 29.
44. R. Mengel, E. Wissing, A. Schmitz-Habben and L. Florés-de-Jacoby, *J. Clin. Periodontol.*, 1996, **23**, 372.
45. A. Zimmerman, L. Florés-de-Jacoby and P. Pan, *J. Clin. Periodontol.*, 1993, **20**, 346.
46. P. Dowell and M. Addy, *J. Periodont. Res.*, 1984, **19**, 530.
47. A. Attramadal and B. Svatun, *Acta Odontol. Scand.*, 1980, **38**, 349.
48. R. Shern, K. W. Swing and J. J. Crawford, *J. Oral. Med.*, 1970, **25**, 93.
49. J. M. Tanzer, A. M. Slee, B. Kamay and E. R. Scheer, *Antimicrob. Agents Chemother.*, 1979, **15**, 408.
50. H. G. Langer, *US Patent*, 1966, 3 227 707.
51. C. H. Cuhonen, *US Patent*, 1990, 4 961 924.
52. P. C. Waterfield, *European Patent*, 1992, 0 514 966.
53. T. E. Furia and A. G. Schenkel, *Soap Chem. Specialties*, 1968, **44**, 47.
54. C. A. Saxton, B. Svatun and A. M. Lloyd, *Scand. J. Dent. Res.*, 1988, **96**, 212.
55. J. Lindhe, B. Rosling, S. S. Socransky and A. R. Volpe, *J. Clin. Periodontol.*, 1993, **20**, 327.
56. C. A. Saxton, R. M. Lane and F. J. G. van der Ouderaa, *J. Clin. Periodontol.*, 1987, **14**, 144.
57. N. Nabi, C. Mukerjee, R. Schmid and A. Gaffar, *Am. J. Dent.*, 1989, **2**, 197.
58. D. M. Francis, *International Patent*, 1993, WO 93/18741.
59. G. Harrap, J. S. Best and C. A. Saxton, *J. Periodont. Res.*, 1983, **18**, 634.
60. C. A. Saxton, *J. Periodontol.*, 1986, **57**, 555.
61. C. A. Saxton and D. Cummins, *J. Dent. Res.*, 1989, **68**, 971.
62. J. S. van der Hoeven, D. Cummins, M. J. M. Schaeken and F. J. G. van der Ouderaa, *Caries Res.*, 1993, **27**, 298.

63. C. A. Saxton, G. J. Harrap and A. M. Lloyd, *J. Clin. Periodontol.*, 1986, **13**, 301.

64. M. J. M. Schaeken, J. S. van der Hoeven, C. A. Saxton and D. Cummins, *J. Clin. Periodontol.*, 1994, **21**, 360.

65. M. J. M. Schaeken, J. S. van der Hoeven, C. A. Saxton and D. Cummins, *J. Clin. Periodontol.*, 1996, **23**, 465.

66. V. Kjærheim, A. Skaare, P. Barkvoll and G. Rölla, *Eur. J. Oral Sci.*, 1996, **104**, 529.

67. I. Hargittai, J. Tremmel, E. Vadja, A. A. Ischenko, A. A. Ivanov, L. S. Ivashkevich and V. P. Spirindonov, *J. Mol. Struct.*, 1977, **42**, 147.

68. T. Fjeldberg, P. B. Hitchcock, M. F. Lappert, S. J. Smith and A. J. Thorne, *J. Chem. Soc., Chem. Comm.*, 1985, 939.

69. T. Fjelberg, A. Haalnad, B. E. R. Schilling, M. F. Lappert and A. J. Thorne, *J. Chem. Soc., Dalton Trans.*, 1976, 1551.

70. D. E. Goldberg, D. H. Harris, M. F. Lappert and K. M. Thomas, *J. Chem. Soc., Chem. Comm.*, 1976, 261.

71. J. D. Donaldson and D. C. Puxley, *Acta Cryst.*, 1972, **B28**, 864.

72. R. C. McDonald and K. Eriks, *Inorg. Chem.*, 1980, **19**, 1237.

73. W. J. Moore and L. Pauling, *J. Am. Chem. Soc.*, 1941, **63**, 1392.

74. J. E. Anderson, S. M. Sawtelle, J. S. Thompson, S. A. Kretchmar Nguyen and J. Calabrese, *Inorg. Chem.*, 1992, **31**, 2778.

75. C. Geneys, S. Vilminot and L. Cot, *Acta Cryst.*, 1976, **B32**, 3199.

76. R. E. Rundle and D. H. Olsen, *Inorg. Chem.*, 1964, **3**, 596.

77. J. Andersson, *Acta Chemica Scandinavica.*, 1975, **A29**, 956.

78. T. H. Jordan, B. Dickens, L. W. Schroeder and W. E. Brown, *Inorg. Chem.*, 1980, **19**, 2551.

79. M. Mathew, L. W. Schroeder and T. H. Jordan, *Acta Cryst.*, 1977, **B33**, 1812.

80. A. F. Berndt, *J. Dent. Res.*, 1972, **51**, 53.

81. B. Kemenar and D. Grdenic, *J. Inorg. Nucl. Chem.*,1962, **24**, 1039.

82. W. Tremel and R. Hoffman, *Inorg. Chem.*, 1987, **26**, 118.

83. R. E. Rundle, *Acta Cryst.*, 1948, **1**, 180.

84. A. G. Filby, R. Howie and W. Moser, *J. Chem. Soc., Dalton Trans.*, 1978, 1997.

85. J. E. Berg, A. M. Pilotti, A. C. Söderholm and B. Karlsson, *Acta Cryst.*, 1978, **B34**, 3071.

86. P. Klüfers and J. Schuhmacher, *Angew. Chem. Int. Ed. Eng.*, 1994, **33**, 1742.

87. W. Burchard, N. Habermann, P. Klüfers, B. Seger and U. Wilhelm, *Angew. Chem. Int. Ed. Eng.*, 1994, **33**, 885.

88. A. El-Jammel, P. L. Howell, M. A. Turner, N. Li and D. M. Templeton, *J. Med. Chem.*, 1994, **34**, 461.

89. R. Fuchs, N. Habermann and P. Klüfers, *Angew. Chem. Int. Ed. Eng.*, 1993, **32**, 852.

90. J. D. Lee, *Concise Inorganic Chemistry*, Van Nostrand Reinhold (UK), 1977.

91. I. Robertson and R. M. Truter, *J. Chem. Soc. A*, 1967, 303.

92. O. Carugo, *Polyhedron*, 1990, **9**, 2061.

93. A. Grand, P. Rey and R. Subra, *Inorg. Chem.*, 1983, **22**, 391.

94. L. P. Battaglia, A. Bonamartini Corradi, G. Marcotrigiano, L. Menabue and G. C. Pellacani, *Inorg. Chem.*, 1981, **20**, 1075.

95. T. Tanase, J. W. Yun and S. J. Lippard, *Inorg. Chem.*, 1995, **34**, 4220.

96. M. F. Mahon, K. C. Molloy and P. Wright, *Unpublished Results*, 1997.

97. J. A. Connolly, J. H. Kim, M. Banaszcyk, M. Drouin and J. Chin, *Inorg. Chem.*, 1995, **34**, 1094.

98. A. Briabanti, M. A. Pellinghelli, A. Tiripicchio and M. Tiripicchio Camellini, *Acta Cryst.*, 1971, **B27**, 1240.

99. K. D. Singh, S. C. Jain, T. D. Sakore and A. B. Biswas, *Acta Cryst.*, 1975, **B31**, 990.

100. R. P. Adams, H. C. Allen, U. Rychlewska and D. J. Hodgson, *Inorg. Chim. Acta*, 1986, **119**, 67.

101. K. Jablcynski and W. Weickowski, *Z. Anorg. Allg. Chem.*, 1926, **152**, 207.

102. J. D. Donaldson, W. Moser and W. B. Simpson, *J. Chem. Soc.*, 1964, 323.

103. D. A. Everest, *J. Chem. Soc.*, 1951, 2903.

104. R. Herak, B. Prelesnik and M. Curic, *J. Chem. Soc., Dalton Trans.*, 1978, 566.

105. T. H. Jordan, L.W. Schroeder, B. Dickens and W. E. Brown, *Inorg. Chem.*, 1976, **15**, 1810.

106. R. E. Mesmer and R. R. Irani, *J. Inorg. Nucl. Chem.*, 1966, **28**, 493.

107. K. M. S. Etheredge and S. Hwu, *Inorg. Chem.*, 1995, **34**, 3123.

108. K. M. S. Etheredge and S. Hwu, *Inorg. Chem.*, 1996, **35**, 1474.

109. G. Huan, A. J. Jacobson, J. W. Johnson and E. W. Corcoran, Jr., *Chem. Mater.*, 1990, **2**, 91.

110. W. T. A. Harrison, T. M. Nenoff, T. E. Gier and G. D. Stucky, *J. Mat. Chem.*, 1994, **4**, 1111.

111. W. T. A. Harrison, T. M. Nenoff, T. E. Gier and G. D. Stucky, *Inorg. Chem.*, 1992, **31**, 5395.

112. H. Koyama and Y. Saito, *Bull. Chem. Soc. Jpn.*, 1954, **27**, 113.

113. J. N. van Niekerk, F.R. L. Schoening and J. H. Talbot, *Acta Cryst.*,1953, **6**, 720.

114. R. Hara and G. H. Cady, *J. Am. Chem. Soc.*, 1954, **76**, 4285.

115. S. Inoue, M. Kobayashi and T. Tozuka, *J. Organomet. Chem.*, 1974, **81**, 17.

116. G. Rudolph and M. C. Henry, *Inorg. Chem.*, 1965, **4**, 1076.

117. K. Prout, A. Edwards, V. Mtetwa, J. Murray, J. F. Saunders and F. J. C. Rossotti, *Inorg. Chem.*, 1997, **36**, 2820.

118. R. C. Mehrotra and R. Bohra, *Metal Carboxylates*, Academic Press, New York, 1983.

119. P. G. Harrison and E. W. Thornton, *J. Chem. Soc., Dalton Trans.*, 1978, 1274.

120. M. McCann, J. F. Cronin, M. Devereux and G. Ferguson, *Polyhedron*, 1995,**14**, 2379.

121. N. Ueyama, Y. Yamada, J. Takeda, T. Okamura, W. Mori and A. Nakamura, *J. Chem. Soc., Chem. Comm.*, 1996, 1377.

122. T. Hökelek, H. Gündüz and H. Necefoglu, *Acta Cryst.*, 1996, **C52**, 2470.

123. J. Cano, G. Munno, J. L. Sanz, R. Ruiz, J. Faus, F. Lloret, M. Julve and A. Caneschi, *J. Chem. Soc., Dalton Trans.*, 1997, 1915.

124. E. Escrivà, J. Server-Carriò, L. Lezama, J. Folgado, J. L. Pizarro, R. Ballesteros and B. Abarca, *J. Chem. Soc., Dalton Trans.*, 1997, 2033.

125. E. B. Gonzalez, E. Farkas, A. A. Soudi, T. Tan, A. I. Yanovsky and K. B. Nolan, *J. Chem. Soc., Dalton Trans.*, 1997, 2377.

126. P. de Meester, S. R. Fletcher and A. C. Skapski, *J. Chem. Soc., Dalton Trans.*, 1973, 2575.

127. N.N. Greenwood and T.C. Gibb, *Mössbauer Spectroscopy*, Chapman and Hall, London, 1971.

128. T.C. Gibb, *Principles of Mössbauer Spectroscopy*, Chapman and Hall, London, 1976.

129. G. M. Bancroft, *Mössbauer Spectroscopy*, McGraw-Hill, London, 1973.

130. W. van den Berg, L. Boot, H. Joosen, J. G. M. van der Linden, W. P. Bosman, J. M. M. Smits, R. de Gelder, P. T. Beurskens, J. Heck and A. W. Gal, *Inorg. Chem.*, 1997, **36**, 1821.

131. J. Lees and P. A. Flinn, *Physics Letters*, 1965, **19**, 186.

132. J. D. Donaldson, R. Oteng and B. J. Senior, *J. Chem. Soc., Chem. Comm.*, 1965, **24**, 618.

133. J. D. Donaldson and B. J. Senior, *J. Chem. Soc.(A)*, 1969, 2358.

134. M. Cordey-Hayes, *J. Inorg. Nucl. Chem.*, 1964, **26**, 915.

135. G. Alonzo, N. Bertazzi and F. Maggio, *Polyhedron*, 1996, **15**, 4269.

136. C.H.W. Jones and R.D. Sharma, *Organometallics*, 1986, **5**, 1195.

137. T. Birchall, R.D. Myers, H. De Waard and G.J. Schrobilgen, *Inorg. Chem.*, 1982, **21**, 1069.

138. U. Ernet, R. Müllmann, B. D. Mosel, H. Eckert, R. Pöttgen and G. Kotzyba, *J. Mat. Chem.*, 1997, **7**, 255.

139. A. Albinati, J. Eckert, P. Hoffman, H. Rüegger and L.M. Venanzi, *Inorg. Chem.*, 1993, **32**, 2377.

140. M. Bickel, G. Adrian, B. Kanellakopulos, H. Haffner, G. Geggus and H. Appel, *Inorg. Chim. Acta*, 1987, **140**, 101.

141. Z. Hu, N.J. Spangler, M.E. Anderson, J. Xia, P.W. Ludden, P.A. Lindahl and E. Münck, *J. Am. Chem. Soc.*, 1996, **118**, 4, 830.

142. Y. Kobayashi, T. Okada, K. Asai, M. Katada, H. Sano and F. Ambe, *Inorg. Chem.*, 1992, **31**, 4570.

143. G. M. Wang, S. J. Campbell, A. Calka and W. A. Kaczmarek, *J. Mat. Sci.*, 1997, **32**, 1461.

144. A. Vértes, M. Gál, F.E. Wagner, F. Tuczek and P. Gütlich, *Inorg. Chem.*, 1993, **32**, 4478.

145. P. G. Harrison, ed., *Chemistry of Tin*, Blackie, London, 1989.

146. H. Mimi Yeh and R. A. Geanangel, *Inorg. Chim. Acta*, 1981, **52**, 113.

147. C. Chun Hsu and R. A. Geanangel, *Inorg. Chem.*,1980, **19**, 110.

148. P. Jutzi and B. Hielscher, *Organometallics*, 1986, **5**, 1201.

149. *NMR and the Periodic Table (Eds R. K. Harris and B. E. Mann)*, 1978, 351.

150. Wrackmeyer

151. P. R. Deacon, PhD Thesis, University of Bath, 1994.

152. Y. Iwami and T. Yamada, *Arch. Oral Biol.*, 1980, **25**, 163.

153. C. A. Beevers and G. H. Maconochie, *Acta Cryst.*, 1965, **18**, 232.

154. S. K. Katti, T. P. Seshadri and M. A. Viswamitra, *Acta Cryst.*, 1982, **B38**, 1136.

155. T. Lis, *Carbohydrate Res.*, 1985, **135**, 187.

156. W. Voelter, E. Breitmaier and G. Jung, *Angew. Chem.*, 1971, **83**, 1011.

157. K. Bock and C. Pedersen, *Adv. Carbohydr. Chem.*, 1983, **41**, 27.

158. J. J. Burke and P. C. Lauterbur, *J. Am. Chem. Soc.*, 1961, **83**, 326.

159. J. W. Emsley, J. Feeny and L. H. Sutcliffe, *High Resolution Nuclear Magnetic Resonance Spectroscopy Vol. 2*, Pergamon Press, London, 1966.

160. R. Gsell and M. Zeldin, *J. Inorg. Nucl. Chem.*, 1975, **37**, 1133.

161. J. D. Donaldson, S. M. Grimes, S. R. Johnston and I. Abrahams, *J. Chem. Soc., Dalton Trans.*, 1995, 2273.

162. W. J. Cook and C. E. Bugg, *Acta Cryst.*,1973, **B29**, 215.

163. N. F. Curtis, *J. Chem. Soc. (A)*, 1968, 1579.

164. A. J. Downs, E. A. V. Ebsworth and H. J. Emeleus, *J. Chem. Soc.*, 1962, 1254.

165. K. Nakamoto, Y. Morimoto and A. E. Martell, *J. Am. Chem. Soc.*, 1961, **83**, 4528.

166. P. J. Roberts, G. Ferguson, R. G. Goel, W. O. Ogini and R. J. Restivo, *J. Chem. Soc., Dalton Trans.*, 1978, 253.

167. J. N. van Niekerk and F. R. L. Schoening, *Acta Cryst.*, 1953, **6**, 227.

168. R. C. Mehrotra and R. Bohra, *Metal Carboxylates*, Academic Press, London, 1983.

169. G. M. Escandar, A. C. Olivieri, M. Gonzlaez-Sierra and L. F. Sala, *J. Chem. Soc., Dalton Trans.*, 1994, 1189.

170. G. M. Escandar, M. G. Sierra, J. M. S. Peregrin, G. Labadié, M. Santoro, A. A. Frutos and L. F. Sala, *Polyhedron*, 1994, **13**, 909.

171. J. D. Donaldson and A. Jelen, *J. Chem. Soc. (A)*, 1968, 1448.

172. D. M. Francis, *International Patent*, 1995, WO 93/18741.

173. J. B. Leane and R. E. Richards, *Trans. Faraday Soc.*, 1959, **55**, 707.

174. G. W. Svetich and C. N. Caughlan, *Acta Cryst.*, 1965, **19**, 645.

175. M. ul-Haque and C. N. Caughlan, *Acta Cryst.*, 1970, **B26**, 1528.

176. J. Pletcher, M. Sax and C. S. Yoo, *Acta Cryst.*, 1972, **B28**, 378.

177. P. G. Jones, G. M. Sheldrick, A. Kirby and K. W. Y. Abell, *Acta Cryst.*, 1984, **C40**, 550.

178. J. Kraut, *Acta Cryst.*, 1961, **14**, 1146.

179. J. D. Dunitz and J. S. Rollett, *Acta Cryst.*, 1956, **9**, 327.

180. S. Ianelli and M. Nardelli, *Acta Cryst.*, 1995, **C51**, 1338.

181. J. Kraut and L. H. Jensen, *Acta Cryst.*, 1963, **16**, 79.

182. C. Li and C. N. Caughlan, *Acta Cryst.*, 1965, **19**, 637.

183. K. Rissanen, J. Valkonen and L. Virrki, *Acta Cryst.*, 1988, **C44**, 1644.

184. P. Singh and J. D. McKinney, *Acta Cryst.*, 1980, **B36**, 210.

185. W. G. Wade and M. Addy, *J. Periodontol.*, 1992, **63**, 280.

186. J. Moran, M. Addy and R. Newcombe, *J. Clin. Periodontol.*, 1988, **15**, 193.

187. J. Moran, M. Addy and W. G. Wade, *J. Dent.*, 1988, **16**, 27.

188. M. Addy, L. Willis and J. M. Moran, *J. Clin. Periodontol.*, 1983, **10**, 89.

189. P. Ramberg, Y. Furuichi, D. Sherl, A. R. Volpe, N. Nabi, A. Gaffer and J. Lindhe, *J. Clin. Periodontol.*, 1995, **22**, 442.

190. H. Erdtmann and J. Gripenberg, *Nature*, 1948, **161**, 719.

191. H. Oshishi, H. Tsujibo, M. Inoue and Y. Inamori, *Acta Cryst.*, 1994, **C50**, 587.

192. T. Nozoe, *Bull. Chem. Soc. Jpn.*, 1936, **11**, 295.

193. J. Berg, A. Pilotti, A. Söderholm and B. Karlsson, *Acta Cryst.*, 1978, **B34**, 3071.

194. R. J. Irving, M. L. Post and D. C. Povey, *J. Chem. Soc., Dalton Trans.*, 1973, 697.

195. H. Shimanouchi and Y. Sasada, *Acta Cryst.*, 1973, **B29**, 81.

196. W. P. Griffith, C. A. Pumphrey and A. C. Skapski, *Polyhedron*, 1987, **6**, 891.

197. A. Avdeef, J. A. Costamagna and J. P. Fackler, Jr., *Inorg. Chem.*, 1974, **13**, 1854.

198. T. P. Lockhart and F. Davidson, *Organometallics*, 1987, **6**, 2471.

199. A. R. Davis and F. W. B. Einstein, *Inorg. Chem.*, 1974, **13**, 1880.

200. L. F. Cavalieri, *Chem. Rev.*, 1947, **41**, 525.

201. M. M. Finnegan, S. J. Rettig and C. Orvig, *J. Am. Chem. Soc.*, 1986, **108**, 5033.

202. M. T. Ahmet, C. S. Frampton and J. Silver, *J. Chem. Soc., Dalton Trans.*, 1988, 1159.

203. P. Caravan, L. Gelmini, N. Glover, F. G. Herring, H. Li, J. H. McNeill, S. J. Rettig, I. A. Setyawati, E. Shuter, Y. Sun, A. S. Tracey, V. G. Yuen and C. Orvig, *J. Am. Chem. Soc.*, 1995, **117**, 12759.

204. M. D. Fryzuk, M. J. Jonker and S. J. Rettig, *J. Chem. Soc., Chem. Comm.*, 1997, 377.

205. B. F. Anderson, D. A. Buckingham, G. B. Robertson and J. Webb, *Acta Cryst.*, 1983, **C39**, 723.

206. S. J. Greaves and W. P. Griffith, *Polyhedron*, 1988, **7**, 1973.

207. H. Morita, S. Shimomura and S. Kawaguchi, *Bull. Chem. Soc. Jpn.*, 1976, **49**, 2461.

208. H. Luo, S. J. Rettig and C. Orvig, *Inorg. Chem.*, 1993, **32**, 4491.

209. I. Abrahams, N. Choi, K. Hendrick, H. Joyce, R. W. Matthews, M. McPartlin, F. Brady and S. L. Waters, *Polyhedron*, 1994, **13**, 513.

210. W. P. Griffith, C. A. Pumphrey and T. A. Rainey, *J. Chem. Soc., Dalton Trans.*, 1986, 1125.

211. C. A. Kingsbury, M. Cliffton and J. H. Looker, *J. Org. Chem.*, 1976, **41**, 2777.

212. A. J. Nielson and W. P. Griffith, *J. Chem. Soc., Dalton Trans.*, 1978, 1501.

213. S. Bhattacharya, N. Seth, V. D. Gupta, H. Nöth, K. Polborn, M. Thomann and H. Schwenk, *Chem. Ber.*, 1994, **127**, 1895.

214. A. J. Fischinger and L. E. Webb, *J. Chem. Soc., Chem. Comm.*, 1969, 407.

215. T. A. Annan, C. Peppe and D. G. Tuck, *Can. J. Chem.*, 1990, **68**, 1598.

216. C. I. F. Denekamp, D. F. Evans, A. M. Z. Slawin, D. J. Williams, C. Y. Wong and J. D. Woollins, *J. Chem. Soc., Dalton Trans.*, 1992, 2375.

217. C. M. Gramaccioli, *Acta Cryst.*, 1966, **21**, 600.

218. G. J. Palenik, *Acta Cryst.*, 1964, **17**, 696.

219. M. M. Finnegan, S. J. Rettig and C. Orvig, *J. Am. Chem. Soc.*, 1986, **108**, 5033.

220. C. Orvig, S. J. Rettig and J. Trotter, *Can. J. Chem.*, 1987, **65**, 590.

221. G. Capper, L. C. Carter, D. L. Davies, J. Fawcett and D. R. Russell, *J. Chem. Soc., Dalton Trans.*,1996, 1399.

222. C. M. Archer, J. R. Dilworth, P. Jobanputra, M. E. Harman, M. B. Hursthouse and A. Karaulov, *Polyhedron*, 1991, **10**, 1539.

223. B. F. Anderson, D. A. Buckingham, G. B. Robertson and J. Webb, *Acta Cryst.*, 1983, **C39**, 723.

224. T. Tanase, J. W. Yun and S. J. Lippard, *Inorg. Chem.*, 1996, **35**, 3585.

225. T. Tanase, J. W. Yun and S. J. Lippard, *Inorg. Chem.*, 1995, **34**, 4220.

226. A. Abufarag and H. Vahrenkamp, *Inorg. Chem.*, 1995, **34**, 2207.

227. H. Adams, N. A. Bailey, D. E. Fenton and Q-Y. He, *J. Chem. Soc., Dalton Trans.*, 1996, 2857.

228. Y. Nakacho, T. Misawa, T. Fujiwara, A. Wakahara and K. Tomita, *Bull. Chem. Soc. Jpn.*, 1976, **49**, 595.

229. J. E. Derry and T. A. Hamor, *J. Chem. Soc., Perkin Trans. 2*, 1972, 694.

230. J. J. Park, D. M. Collins and J. L. Hoard, *J. Am. Chem. Soc.*, 1970, **92**, 3636.

231. J. Creeth and J. Simmons, *Unpublished Results*, 1997.

232. C. A. Saxton, B. Svatun and A. M. Lloyd, *Scand. J. Dent. Res.*, 1988, **96**, 212.

233. M. J. M. Schaeken, J. S. van der Hoeven, C. A. Saxton and D. Cummins, *J. Clin. Periodontol.*, 1994, **21**, 360.

234. V. Kjærheim, A. Skaare, P. Barkvoll and G. Rolla, *Eur. J. Oral Sci.*, 1996, **104**, 529.

235. J. Li and R. P. Ellen, *J. Dent. Res.*, 1990, **69**, abstract number 257.

236. C. L. Jones, K. W. Stephan, J. A. Ritchie, E. Huntingdon, C. A. Saxton and F. J. van der Oudera, *Caries Res.*, 1988, **22**, 84.